



University of Naples Federico II

Rising groundwater levels in the Neapolitan area and its impacts on civil engineering structures, agricultural soils and archaeological sites

PhD Thesis in
Earth Sciences, Environment and Resources

Tutor
Vincenzo Allocca

PhD Candidate
Silvio Coda

Co-Tutors
Pantaleone De Vita
Domenico Calcaterra
Diego di Martire

May, 2021



Department of Earth Sciences, Environment and Resources

To my parents

Index

Rising groundwater levels in the Neapolitan area and its impacts on civil engineering structures, agricultural soils and archaeological sites

Abstract	1
1 Introduction	4
2 Casalnuovo di Napoli and Volla municipalities case study	7
<i>Phenomenon description and evaluation of its effects in terms of groundwater flooding, ground deformation, hydrochemical variation and socioeconomic consequences.</i>	
2.1 Groundwater rebound and flooding in the Naples' periurban area (Italy).....	13
2.2 Coupled ground uplift and groundwater rebound in the Metropolitan City of Naples (southern Italy).....	49
2.3 Variation of groundwater contamination related to groundwater rebound in the eastern plain of Naples	71
2.4 Integrating hydrogeological and economic analyses of groundwater flooding in urban areas: the Naples metropolitan area case study	80
3 Lufrano and Acerra well-fields	103
<i>Ground deformation induced by groundwater level rising in the core of groundwater rebound</i>	
Uplift evidences related to the recession of groundwater abstraction in a pyroclastic-alluvial aquifer of southern Italy	105
4 Cumae archaeological site	125
<i>A hydrogeological, hydrochemical and isotopic survey in an archaeological site affected by groundwater flooding</i>	
Natural and Anthropogenic Groundwater Contamination in a Coastal Volcanic-Sedimentary Aquifer: The Case of the Archaeological Site of Cumae (Phlegraean Fields, Southern Italy)	127

5 Groundwater Flooding Susceptibility assessment.....	160
<i>The first application of machine learning techniques for the implementation of a groundwater flooding susceptibility assessment methodology</i>	
A novel methodology for Groundwater Flooding Susceptibility assessment through Machine Learning techniques in a mixed-land use aquifer.....	163
6 Conclusions and prospects for research.....	198
7 Scientific production	203
References.....	206

Abstract

The rise of groundwater levels (GWLr) is a worldwide phenomenon with several consequences for urban and rural environment, cultural heritage and human health. In this thesis the phenomenon and its effects are analysed in two sectors of the Metropolitan City of Naples (southern Italy). These areas are the central sector of the eastern plain of Naples and the Cumae archaeological site in the western coastal sector of Phlegraean Fields. The triggering mechanism of GWLr is attributed to anthropogenic and natural causes, as the groundwater rebound (GR) process and the relative sea level rise due to volcano-tectonic subsidence of coastal areas.

In the eastern plain of Naples, the interruption of pumping for public and private purposes occurred in 1990, leading to a progressive increase of piezometric levels with values up to 16.54 m. Since the end of 2000s, episodes of groundwater flooding (GF) have been registered on underground structures and agricultural soils. The historical piezometric levels and a comprehensive conceptual model of the aquifer have been reconstructed, as well as a first inventory of GF episodes and the hydrogeological controlling factors of GF occurrence have been detected. The economic consequences of GF have been analysed for an experimental building of study area, in which a sharp increment of expenditures has been registered. These costs include technical and legal support, construction and maintenance of GF mitigation measures and electricity consumption.

Others GWLr-induced phenomena have been recognised, as ground vertical deformation and variations of the groundwater contamination. A relationship between GWLr and ground uplift emerges from the coupled analysis of piezometric and interferometric data, referred to the 1989-2013 period. The ground deformation occurs in response to the recovery of pore-pressure in the aquifer system, reaching an uplift magnitude up to 40-50 mm. In the 1989-2017 period, the piezometric levels and the concentrations of some natural contaminants in groundwater (Fe, Mn, fluorides) show opposite trends, conversely the same rising trend has been observed with nitrates. These different responses to piezometric rise are related to the lack of mobilization of deep fluids due to the interruption of pumping and to the reduction of the surficial contaminants' time travel caused by a shorter thickness of the vadose zone.

In the western sector of Phlegraean Fields, the naturally triggered GWLr has caused GF in the Cumae archaeological site for the last decade, threatening safeguard and conservation of the archaeological heritage. From an integrated hydrogeological, hydrochemical and isotopic survey, a considerable contamination of groundwater resulted, due to the presence of rising highly mineralized fluids, mobilized during pumping periods, and others anthropogenic sources of contamination.

Lastly, a novel methodology for groundwater flooding susceptibility (GFS) assessment has been developed by using machine learning techniques and tested in the eastern plain of Naples. Points of GF occurrence have been connected to environmental predisposing factors through Spatial Distribution Models' algorithms to estimate the most prone areas' distribution. Ensemble Models have been carried out to reduce the uncertainty associated with each algorithm and increase its reliability. Mapping of GFS has been realized by dividing occurrence probability values into five classes of susceptibility. Results show an optimal correspondence between GF points' location and the highest classes (93% of GF points falls into high and very high classes).

The results of this research provide new knowledge on the GWLr phenomenon that has impacted a large territory of the Metropolitan City of Naples. The methodological approach used can be exported in others hydrogeological contexts to characterize GWLr and its impacts. In addition, the implemented GFS methodology represents a new tool to assist local government authorities, planners and water decision-makers in addressing the problems deriving from GF, and a first step for the evaluation of GF risk as required by Italian and European legislation.

1

Introduction

The phenomenon of rise of groundwater levels (GWLr) represents a current issue of Urban Hydrogeology, particularly in the context of climate changes and in order to make cities more resilient and safety to every kind of geo-risk. This phenomenon is widely diffused at global scale and it can generate several dangerous and damaging consequences for urban and rural environment, cultural heritage and human health.

This thesis, included in the PhD program in Earth Sciences, Environment and Resources of University of Naples Federico II, presents the results of a thorough study about GWLr and its effects in the Metropolitan City of Naples (southern Italy). In this area, GWLr has been originated by the groundwater rebound phenomenon and other types of natural triggering mechanism. The first was strictly connected with the sharp reduction of groundwater abstraction from some drinking water well-fields, occurred at the end of 1980s, leading to a progressive piezometric level recovery. The main effect is groundwater flooding (GF) of civil engineering structures, agricultural soils and archaeological sites. As further consequences, ground deformations and hydrochemical variations of groundwater have been registered.

The natural triggering cause of GWLr is related to subsidence in coastal areas, caused by volcano-tectonic deformation. This process has led to relative increase of sea level and migration of groundwater discharge zone, causing upstream lifting of piezometric levels. Therefore, this study has been conducted by using hydrogeological, hydrochemical, remote sensing and machine learning methodologies, to investigate GWLr and its impacts.

During the PhD course, in the period November 2017 – March 2021, the outcomes of the different aspects of the main issue have been presented to Italian and international conferences and published in scientific journals. Part of the scientific production has been selected and reorganized for the writing of this thesis. In each chapter the content of a scientific paper or conference proceeding is reported, homogenizing their formatting and avoiding as much information redundancy as possible.

The thesis is structured as follow. Chapters are divided for study area and topic. In Chapter 2, GWLr and its effects in a central sector of the easter plain of Naples,

corresponding to Casalnuovo di Napoli and Volla municipalities, are described. In particular, Chapter 2.1 is focused on GWLr and GF. These phenomena are framed at global scale, reporting and comparing several case studies divided for triggering mechanism. Causes and dynamics of piezometric rise and, the hydrogeological, hydrographic and structural factors controlling GF are explained. Chapter 2.2 deals with ground uplift related to GWLr, detected comparing piezometric and interferometric data. In Chapter 2.3, variations of groundwater hydrochemical characteristics, associated to GWLr, are explained. In Chapter 2.4, a socioeconomic analysis of GF in the northern sector of study area is reported. In Chapter 3, ground vertical displacement and GWLr are analysed in the Lufrano and Acerra well-fields areas, considered as the core of groundwater rebound. Chapter 4 is focused on the Cumae archaeological site (Phlegraean Fields), affected by GF. A hydrogeological, hydrochemical and isotopic characterization has been carried out to evaluate natural and anthropogenic contamination of groundwater, which can threaten conservation of the archaeological heritage. In Chapter 6, a novel methodology for GF susceptibility assessment is proposed, based on GF inventory, hydrogeological factors and land use, and employed through Machine Learning techniques. A summary of the main results and future prospects for research are reported in Chapter 6. Lastly, the whole scientific production is listed in Chapters 7.

2

Casalnuovo di Napoli and Volla municipalities case study

2.1 Groundwater rebound and flooding in the Naples' periurban area (Italy)

Abstract.....	13
1. Introduction.....	14
2. GWLr and GF: an overview	16
3. Description of the study area.....	18
3.1 Geology and geomorphology	18
3.2 Hydrography and hydrogeology	20
3.3 Groundwater use and land use changes	23
4. Data and methodologies	24
4.1 Hydro-stratigraphic data.....	24
4.2 Hydrogeological data and drainage network density	26
4.3 Flood monitoring.....	26
5. Results.....	28
5.1 2D hydro-stratigraphic model and groundwater flow pattern	28
5.2 GR characterization.....	31
5.3 GF features.....	35

6. Discussion	39
7. Conclusions	43
Supplementary Material.....	45

2.2 Coupled ground uplift and groundwater rebound in the Metropolitan City of Naples (southern Italy)

Abstract.....	49
1. Introduction.....	51
2. Further geological information about the study area	53
3. Data and methodologies	54
3.1 Hydrogeological data.....	54
3.2 DInSAR data.....	58
4. Results	60
4.1 Groundwater rebound assessment	60
4.2 Satellite-based deformation maps.....	63
5. Discussion.....	65
6. Conclusions	68

2.3 Variation of groundwater contamination related to groundwater rebound in the eastern plain of Naples

Extended Abstract.....	71
1. Data and methodologies	73
1.1 Piezometric data	74
1.2 Hydrochemical data	74
2. Results.....	75

2.1	Piezometric levels variation	75
2.2	Variation of contamination	76
3.	Discussion and conclusions	78

2.4 Integrating hydrogeological and economic analyses of groundwater flooding in an urban aquifer: the plain of Naples (Italy) as a case study

Abstract.....	80
1. Introduction.....	82
2. Data description and methods	84
2.1 Study area	84
2.2 Hydrogeological data.....	86
2.3 Economic data	89
2.4 Methodology	92
2.4.1 <i>A theoretical dynamic analysis of groundwater</i>	92
2.4.2 <i>The defensive expenditure analysis</i>	94
3. Results.....	95
3.1 Water table dynamics when the pumping regime changes	95
3.2 A conservative estimate of the economic costs of groundwater flooding	97
4. Discussion and conclusions	100

List of Figures and Tables

Section 2.1

Figure 2.1 - **a)** Geological map of the Campanian Plain; **b)** Hydrogeological map of the eastern plain of Naples; **c)** Geomorphological setting of study area, and **d)** Hydrogeological setting of the study area.

Figure 2.2 - **a), b)** and **c)** Land use change at basin and locale scale; **d)** Demographic growth for Naples Metropolitan area and study area; **e)** and **f)** Macro and micro-network drainage system reconstructed for the 1943 (at 1:25000 scale) and 2015 years.

Figure 2.3 - Field schede for flooded buildings and agricultural soils.

Figure 2.4 - 2D hydro-stratigrafic model.

Figure 2.5 - Groundwater flow pattern of the deep and shallow aquifer, for the period **(a and d)** November 2013, **(b and e)** March 2015, and piezometric head variations between these measurement periods **(c and f)**. **(g)** SMMO' monthly rainfall.

Figure 2.6 - Hydrodynamic scenarios in the period 1924-2015, in terms of **(a)** piezometric heads (m a.s.l.), **(b)** depth of water table (m b.g.l.) and **(c)** piezometric profiles (m a.s.l.).

Figure 2.7 - **a)** Box plots of piezometric levels (m a. and b. s.l.) in the study area; **b)** Piezometric levels (m a. and b. s.l.) and withdrawals (m³/s) in Lufrano, Acerra and Ponticelli well fields; **c)** SMMO' annual rainfall.

Figure 2.8 - Maps of the groundwater depth (m b.g.l.) in the deep **(a, d and e)** and in the shallow aquifer **(b and c)**, and spatio-temporal distribution of GF episodes in the period November 2013-March 2015.

Figure 2.9 - Anthropogenic and natural factors controlling GF. **a)** Impacted buildings with depth of the flooded underground structures; **b)** Local condition of artesian aquifer; **c)** Drainage density modification of network system from 1943 to 2015 (Figs. 2.2e and 2.2f) and current maintenance state with occlusion of channels.

Figure 2.10 - Damages on buildings and agricultural soils.

Figure 2.11 - Piezometric head variations in the period November 2013 – March 2015 for the deep semi-confined aquifer **(a and c)** and the shallow one **(b)**, and spatio-temporal distribution of GF in the northern **(b)** and central **(c)** impacted sectors.

Table 2.1 - Hydrogeological, meteorological and stratigraphic dataset.

Table 2.2 - Magnitude (m) and rising velocity (m/yr) during GR period (1990-2015).

Table 2.3 - Number and area of buildings and agricultural soils affect by GF.

Table S1 (supplementary material) - Natural and anthropogenic causes of groundwater level rising (GWLr) and some of main case studies reported in literature.

Table S2 (supplementary material) - Natural and anthropogenic causes of groundwater flooding (GF) and some of main case studies reported in literature.

Section 2.2

Figure 2.12 - **a)** Geological map of the Campanian Plain, **b)** Schematic geological cross-sections A-A' and B-B' (Celico et al., 1998 modified) and **c)** Hydrogeological map of the eastern plain of Naples.

Figure 2.13 - Groundwater level maps for the years: **a)** 1989; **b)** 1994; **c)** 2002; **d)** 2013.

Figure 2.14 - LoS velocity maps (mm/yr) of the study area. **a)** ERS-1/2 data in ascending geometry; **b)** ERS-1/2 descending; **c)** ENVISAT ascending; **d)** ENVISAT descending.

Figure 2.15 - Piezometric level variation (m) (**a** and **b**) and groundwater rising velocity (m/yr) (**c** and **d**) in the periods 1989-2002 (**a** and **c**) and 2002-2013 (**b** and **d**).

Figure 2.16 - LoS cumulated deformation maps (mm) and of the study area for the periods: (**a**) 1993-2000; (**b**) 2002-2010.

Figure 2.17 - Comparison between annual precipitation, representative trends of groundwater levels and vertical ground deformations for four sectors of study area (1989-2013).

Table 2.4 - Principal sources of hydrostratigraphic, hydrogeological and meteorological data.

Table 2.5 - DInSAR LoS measurement statistics referred to the whole area.

Section 2.3

Figure 2.18 – Hydrogeological complexes and ubication of groundwater samples.

Figure 2.19 – Piezometric contour maps and box plot.

Figure 2.20 - Isoconcentration contour maps and boxplot of Nitrates (**a**), Fluorides (**b**), Iron (**c**) and Manganese (**d**).

Table 2.6 - Piezometric head variation.

Table 2.7 - Hydrochemical variation.

Section 2.4

Figure 2.21 - **a)** Geological map of the Campanian Plain, **b)** Hydrogeological map of the eastern plain of Naples, and **c)** Hydrogeological complexes outcropping in the study area.

Figure 2.22 - Time series of groundwater levels 1) (meters a. and b.s.l.) and pumping rates 2) (m^3/s) for the Lufrano well-field.

Figure 2.23 - Groundwater depth maps (m b.g.l.) for the period November 2013 (**a**) and March 2015 (**b**) and location of the experimental building (EB).

Figure 2.24 - Time series of the piezometric levels (meters a. and b.s.l.) for Lufrano well-field 1) and the rate of growth of GDP in Campania region 2).

Figure 2.25 - Comparison between time series of piezometric levels (m a.s.l.) and electricity bills (euros) for the experimental building (EB; location in Fig. 2.22).

Figure 2.26 - Source: Gisser and Mercado, 1973.

Figure 2.27 - The dynamic evolution of the water table representing groundwater depletion, groundwater rebound and groundwater flooding.

Figure 2.28 - Autocorrelation functions for electricity expenditure and piezometric level.

Figure 2.29 - Partial Autocorrelation functions for electricity expenditure and piezometric level.

Table 2.8 - Total expenditure for the experimental building EB, current euros.

Table 2.9 - A Comparison of Time Series Models.

2.1

Groundwater rebound and flooding in the Naples' periurban area (Italy)

Allocca V.¹, Coda S.¹, Calcaterra D.¹, De Vita P.¹

¹ Department of Earth Science, Environment and Resources, University of Naples Federico II, Naples, Italy

*Corresponding author: vincenzo.allocca@unina.it

Abstract

Groundwater bodies in the urbanized and densely populated aquifers or coastal floodplains may be subjected to groundwater rebound (GR), often causing serious risks of groundwater flooding (GF) to underground structures and infrastructures.

In this paper we present the results of a study carried out in the Naples' periurban area (Italy) to: investigate the dynamics and features of GR and GF phenomena; map flooded sites during 2013-2015 period; provide an interpretative analysis of the factors that control the GF of private buildings and agricultural lands.

At the municipality scale, since 1990 and until 2015, a remarkable and widespread GR was observed, with magnitude up to +16,54 m, triggering an unexpected GF of basements of buildings and agricultural soils. Field surveys proved that there is a time delay of the GF, ranging from 17 to 20 years, compared to the start of GR. Moreover, inhomogeneous distribution of flooding episodes is controlled by anthropogenic and natural factors. The obtained results are fundamental to design mitigation measures to groundwater flooding hazard, and offer new perspectives to make Naples' periurban area more robust, smart and resilient against this new hydrogeological risk, undervalued by Italian legislation and local authorities.

Key words: groundwater rebound, groundwater flooding, aquifer mismanagement, land use change, urban hydrogeology.

Allocca, V., Coda, S., Calcaterra, D., De Vita, P., 20XX. Groundwater rebound and flooding in the Naples' periurban area (Italy). Journal of Flood Risk Management, submitted in February 2020, re-submitted in May 2021 after the 2nd round of revision.

1. Introduction

Urban transformations, climate changes, land use and groundwater use changes have caused groundwater levels rising (GWLr) phenomena worldwide. Indeed, GWLr has been observed in many areas of the world (Wilkinson, 1994; Howard & Israfilov, 2002; Schirmer et al., 2013) and it is considered a current and global issue and an urgent scientific task of the Urban Hydrogeology.

As it will be detailed in the next Section, GWLr may have natural or anthropogenic origin, cause severe socio-economic, environmental and health impacts and have different triggering mechanisms (Kreibich & Thieken, 2008) that operate at different spatial and time scales, from basin, large cities to individual sites and occasional, seasonal to decadal periods.

Among the main anthropogenic causes of the GWLr there is the reduction in abstraction rates of groundwater following a period of high groundwater pumping or overexploitation which kept groundwater levels artificially low. This triggering mechanism of the GWLr is named groundwater rebound (GR) (Crosta & De Caro, 2018). It is typical of urban centres and rural areas developing on unconfined aquifers, and is also observed in abandoned deep mine zones, where decline in anthropogenic activities and then the arrest or uncontrolled reduction of pumping groundwater allowed previous depressed groundwater levels to recover. GR can cause various negative effects such as the ground uplift and deformation of aquifer systems (Chen et al., 2007; Yang et al., 2019), and groundwater flooding (GF) namely *“the emergence of groundwater at the ground surface away from perennial river channels or the rising of groundwater into the man-made ground, including basements of buildings and other subsurface infrastructure”* (Macdonald et al., 2008; 2012). GF phenomenon may have natural and anthropogenic origin, and its impacts can be severe on the environment, cultural heritage, utility activities and human health, and can cause significant socio economic damages and costs (Azuma et al., 2014).

Among the major urban areas of the world affected by GR and GF phenomena there is the Naples metropolitan area. In this mixed-land use area, since the early 90s a widespread GR phenomenon is in progress caused by a drastic reduction and interruption of groundwater pumping from public and private wells. Some previous studies based on literature data have analysed GR phenomenon at the large scale (Allocca & Celico, 2008). Others recent studies analysed others GR-induced phenomena at local

scale, such as ground uplift by an integrated use of hydrogeological and DInSAR monitoring data (Coda et al., 2019a, b), and as variation of groundwater contamination level (Coda et al., 2019d). However, within Naples' periurban area, it is still missing a monitoring-based systematic analysis of the GR and GF phenomena; similarly, a mapping of flooded sites of structures and agricultural soils is still absent. This research aims to fill these gaps and advance the understanding of GR and GF phenomena occurring within Naples' periurban area at the municipality scale. From a methodological point of view, our paper contributes to providing an integrated vision of origin, spatio-temporal evolution and characteristic of GR and GF processes, in a "cause-effect" perspective, based on long-time hydrogeological analysis and flood and hydrogeological monitoring, as well as on numerous field geological data.

Therefore, in this paper a deep investigation of both GR and GF processes at an experimental site of the Naples metropolitan area is carried out, exploiting a unique and long-lasting hydrogeological dataset, as well as new hydrogeological monitoring and field surveys performed in the 2013-2015 period. The study is focused on three main goals: (i) to develop a high-resolution 2D hydro-stratigraphic and hydrogeological conceptual model of the pyroclastic-alluvial aquifer system, based on stratigraphic logs of 149 boreholes and 127 wells; (ii) to characterize, at the municipality scale, GR and GF phenomena, to improve knowledge about their spatio-temporal dynamics; (iii) to map flooded sites during investigated period, by a citizen participatory approach, and analyse natural and anthropogenic factors that locally control GF of private buildings and agricultural lands.

The paper is structured as follows. Section 2 provides an overview of the literature as to the various types of GWLr and GF phenomena. Section 3 describes the geological, hydrographic and hydrogeological characteristics of the study area, as well as land use and groundwater environment changes. Section 4 shows the data and the methodological approach used for the analysis of GR and GF phenomena, whereas Section 5 exposes the results obtained. Finally, in the Sections 6 and 7, result discussion and concluding remarks are presented).

2. GWLr and GF: an overview

As already pointed out, GR is only one of the possible typologies of GWLr. Albeit not always GR (and GWLr) engenders GF, recent literature has pointed out that among the many possible triggering mechanisms of GF, the one activated by GR is increasingly observed, as we document below.

To begin with, GWLr may have natural or anthropogenic origins (for the resume of case studies and references see Table S1 in supplementary materials), and the main natural causes listed in literature are:

- increase of seawater level induced by climate change and glacial isostatic adjustment;
- natural consolidation of compressible sediment layers or bradysismic/volcano-tectonic land subsidence in coastal area, with consequent local sea-level increase;
- seasonal variations of the rainwater infiltration and groundwater recharge by channel network, during and after heavy flash flood phenomena.

Conversely, the main anthropogenic causes of GWLr so far investigated in literature are:

- artificially increased groundwater recharge within the urban aquifers due to infiltration of imported water for domestic, irrigation and industrial consumption;
- increased recharge to seepage from septic tanks systems or leakages from sewage systems, as well as increased recharge from leaking water mains and over-irrigation of parks and gardens, irrigation canal leakage, irrigation return;
- underground constructions (e.g. tunnels, deep foundations, underground parks, subway stations, basements of buildings) in saturated zones of urban aquifers;
- anthropogenic land subsidence in coastal and estuarine area and consequent local sea-level rise;
- reduction of abstraction of groundwater (i.e. GR).

In accordance with Macdonald et al. (2008), Hughes et al. (2011) and Naughton et al. (2017), is possible to identify different scenarios of GF triggered by different mechanisms, that can be classified as having natural and anthropogenic origin (Table S2 in supplementary materials). In the first group it is possible to list:

- flooding in alluvial lowland related to the water table rising above the land surface in response to extreme high intensity and/or prolonged extreme rainfall in unconfined and consolidated aquifers;
- flooding in small alluvial flatlands related to the rapid response of groundwater levels to precipitation and limited storage capacity in shallow and unconsolidated sedimentary aquifers with a good hydraulic connection with river networks;
- flooding from groundwater in alluvial deposits by-passing or circumventing river channel flood defence structures;
- flooding in lowland karst systems induced by ephemeral karst lakes (turloughs), or groundwater-induced flood occurs when intense groundwater discharge via springs and highly permeable shallow horizons discharges to the surface water, causing overbank flooding;
- flooding in coastal lowland areas, driven by sea-level rise under climate changes or during and following severe storms.

As to the GF triggered by anthropogenic causes, the list mainly includes:

- flooding of underground structures creating barriers to groundwater flow;
- flooding of basements of buildings, and subsurface structures and infrastructures induced by GR in urban centres and abandoned mine zones.

The above provided conceptualization of the existing scientific literature clearly points out that GWLr and GF are multi-driven phenomena, widespread at global scale.

The analysis of the main natural and anthropogenic causes of GWLr and GF, in different latitudinal and hydro-environmental, contexts has contributed to implement the methodological approach of this research. Indeed, the present study is concerned with the last category in the lists of anthropogenic GWLr and GF phenomena just described, as observed within the large territory of the Naples' periurban area.

3. Description of the study area

3.1 Geology and geomorphology

The study area, extended over about 14 km², corresponds to the municipalities of Casalnuovo di Napoli and Volla, located within the Naples metropolitan area (Italy).

From a geological point of view, the study area is located in the central-southern sector of the Campanian Plain (Fig. 2.1a), a large alluvial plain formed in the Pliocene-Pleistocene by the filling of a regional semi-graben structural depression, which was originated along the western side of the southern Apennines, during the opening of the Tyrrhenian Sea. Starting from 300 k-yrs (Rolandi et al., 2003), an intense volcanic activity occurred across the Campanian Plain with the formation of the Phlegraean Fields and Somma-Vesuvius volcanic districts. In the last 25 k-yrs, in addition to the deposition of volcanoclastic products, further sedimentation and erosional processes led to the filling of the structural depression by 1000-3000 m of alluvial, marine and fluvio-palustrine sediments.

According to the updated geological data (ISPRA, 2019), four geological complexes have been identified in the study area (Fig. 2.1d): Holocene pyroclastic-fluvial sediments (PF); ash-fall pyroclastic deposits (P), dated 39.3-39.8 k-yrs; Holocene pyroclastic, alluvial-marine and palustrine sediments (PAP) as well as late Holocene volcanic and alluvial deposits (VA). Furthermore, the northern and central-northern sectors are characterized by a tuff horizon, corresponding to the Campanian Ignimbrite (CI), in a zeolitized yellow facies, dated 39.28±0.11 k-yrs (De Vivo et al., 2001). This tuff horizon does not crop out in the study area, being only recognizable in boreholes, with a thickness variable up to 40 m. Specifically, in the central-southern and southern sectors of the study area (Fig. 2.1d), CI is absent due to erosion of paleo-Sebeto river and locally substituted by silt and clay deposits, as well as by lenses of peat and volcanic rocks (Bellucci et al., 1990).

From a morpho-structural point of view (Figs. 1a and 1c), the study area is subdivided between two catchment basin, Regi Lagni to the north, and the Sebeto River to the south, latter known as Volla river. The northern sector, crossed by Santo Spirito stream (Fig. 1c) is part of the lowland floodplain of Regi Lagni, named the Acerra structural depression (Fig. 1a). The southern sector, crossed by Cozzone and Volla rivers and Reale Lufrano channel, is lowland floodplain of subsiding tectonic depression, the Sebeto Valley (Fig. 1a) set on Quaternary-active faults such as the buried deep Magnaghi-Sebeto fault. In

these sectors, the landscape morphology is quite flat, with very gentle slopes, dipping up to 1%, and altitude varying from 25 to 12 m a.s.l., respectively. The two catchment basins are locally separated by a watershed divide, formed by the pyroclastic deposits of the Avellino plinian eruption (3780 yr B.P.) of Somma-Vesuvius volcano (Rolandi et al., 1998), which crosses the central sector of the study area (Fig. 1c), where the ground surface reaches altitudes up to 45 m a.s.l., and slopes up to 4%.

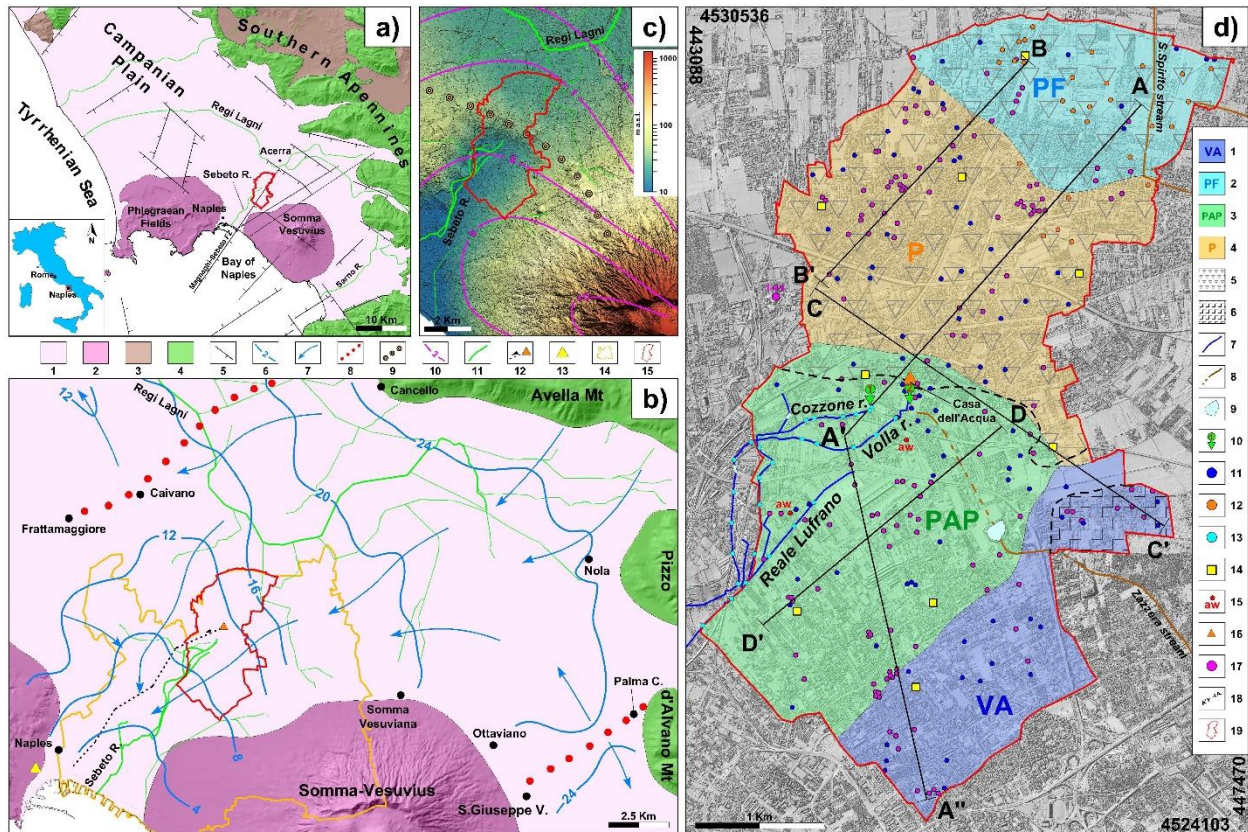


Figure 2.1 - a) Geological map of the Campanian Plain; b) Hydrogeological map of the eastern plain of Naples; c) Geomorphological setting of study area, and d) Hydrogeological setting of the study area. Legend of 1a), 1b) and 1c): 1) Quaternary epiclastic deposits; 2) Quaternary volcanic deposits; 3) Miocene deposits; 4) Mesozoic Apennine platform carbonates; 5) Normal fault; 6) Groundwater contour line (m a.s.l.; Esposito, 1998, simplified); 7) Groundwater flow direction; 8) Groundwater divide; 9) Watershed boundary; 10) Isopach (thickness meters) of the ash-fall deposits of Avellino eruption (Rolandi et al., 1998); 11) Hydrographic network system; 12) Bolla aqueduct; 13) San Marcellino Meteorological Observatory rain gauge (SMMO); 14) Naples and Volla swamps' reclamation Consortium boundary; 15) Study area. Legend of 1d): 1) VA complex; 2) PF complex; 3) PAP complex; 4) P complex; 5) Sector with buried Campanian Ignimbrite (CI); 6) Sector with buried lava rocks; 7) Drainage network system; 8) Urban drainage system (culverts); 9) Tank septic system; 10) Cozzone (1) and Bolla (2) springs; 11) Deep well; 12) Shallow well; 13) River head monitoring point; 14) Monitoring station; 15) Artesian wells; 16) "Casa dell'Acqua" plant; 17) Borehole; 18) Cross-section lines; 19) Study area.

3.2 Hydrography and hydrogeology

With the exception of the central sector, the large part of the study area is generally characterized by a shallow water table and a drainage channel pattern which are typical of floodplain environments (Figs. 2.1b and 2.1d). Historically, the main watercourse was the Sebeto river. Subsequently, in Bourbon epoch (1600-1700) the hydrographic system of the Regi Lagni was artificially created: an ancient work of hydraulic reclamation, consisting of a network of channels dug to drain the ground and surface-waters of marshy Acerra tectonic depression.

The central-southern sector of the study area shows typical morphological features of a swamp land, with a natural and artificial drainage micro-network and some natural emersion of groundwater circulation, represented by the Bolla and Cozzone springs (Fig. 2.1d), which were active until the beginning of the 20th century (Fiorelli, 1926). The Bolla spring, located close to the “Casa dell’Acqua”, was tapped since the 4th century to feed the ancient homonymous aqueduct system serving the city of Naples (Figs. 2.1c and 2.1d). Due to its swampy features, the central-southern sector of the study area was interested by different hydraulic reclamation since 13rd century and a complex natural and artificial drainage network was established to control surficial and groundwater drainage toward the Sebeto river. Other drainage works were carried out later on, since 1917, with the institution of the Naples and Volla swamps’ reclamation Consortium, which is still active today (Fig. 2.1b). However, during the last century the most significant reclaiming interventions were realized by farmers of the floodplain, who manually excavated micro-channels to irrigate agricultural fields and to canalise groundwater and surface-water (Caputo et al., 2000).

This drainage system, which was constantly maintained and managed, consisted of (Fig. 2.2e) longitudinal and transverse open ditches and furrows, that, by crossing and bordering the agricultural fields, created a micro-network interconnected with the main rivers (Fig. 2.2e). Furthermore, some farmers have always used an agronomic technique called “baulatura” (Bazzoffi and Nieddu, 2011), characterized by a convex profile of ground surface, with slight slopes to facilitate water drainage laterally. Starting from the second half of the 20th century, the change of land use (Figs. 2.2a and 2.2b) due to the quick and unplanned urbanization, industrialization and infrastructuring have deeply changed the original aspect of rural territory of floodplain, modifying and cancelling the ancient artificial drainage micro-network system. Today, Volla and Cozzone rivers, Reale

Lufrano channel and Santo Spirito stream represent the local drainage system of groundwater and surface water (Figs. 2.1d and 2.2f), and their hydraulic maintenance is entrusted to the Naples and Volla swamps' reclamation Consortium (Fig. 2.1b).

From a hydrogeological point of view, the study area is a sector of the pyroclastic-alluvial plain of Naples (Fig. 2.1b), where the groundwater circulation at basin scale can be considered unitary and interconnected with the Avella-Pizzo d'Alvano karst and Somma-Vesuvius volcanic aquifers (De Vita et al., 2018). At the local scale, the aquifer is characterized by a porous multi-layered system, recharged by direct effective infiltration (which was estimated equal to about 300 mm/year by; Allocca et al., 2014) and by groundwater flow coming from the upstream plain sector of the study area. Groundwater flow system is locally direct toward the Sebeto river and its tributaries (Fig. 2.1b).

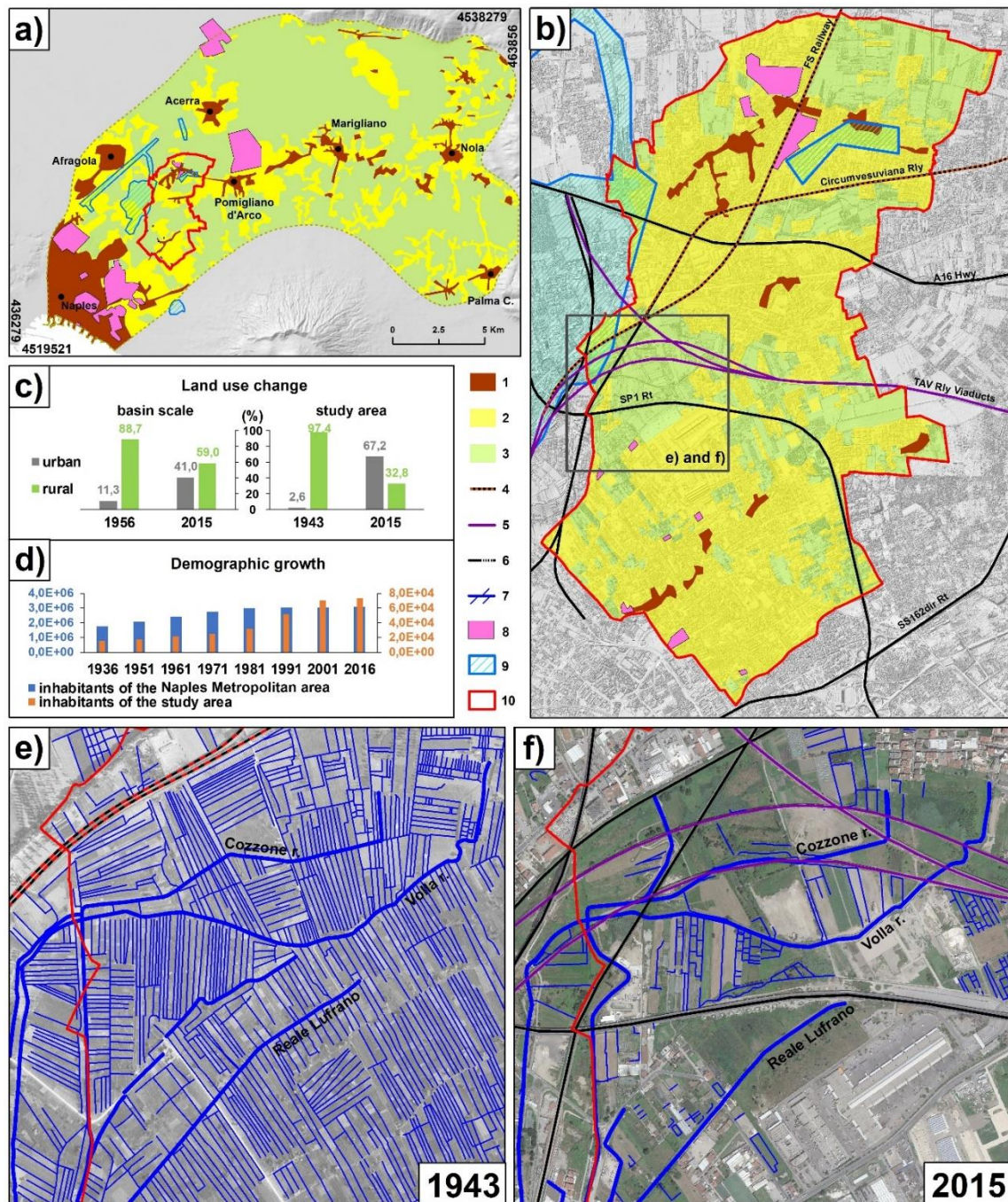


Figure 2.2 - a), b) and c) Land use change at basin and locale scale; d) Demographic growth for Naples Metropolitan area and study area; e) and f) Macro and micro-network drainage system reconstructed for the 1943 (at 1:25000 scale) and 2015 years. 1) Urbanized area in the 1943-1956 period; 2) Urbanized area in 2015; 3) Agricultural area in 2015; 4) Railway infrastructure constructed in the 1890-1910 period (Circumvesuviana Rly and FS Railway); 5) Railway infrastructures constructed in the 1999-2007 period (TAV Rly Viaducts); 6) Road infrastructures constructed in the 1955-1985 period (SP1 Rt, A16 Hwy, SS162dir Rt); 7) Micro-network drainage system; 8) Dismissed industrial site in the 1995-2010 period; 9) Lufrano well field; 10) Study area.

3.3 Groundwater use and land use changes

The study area is one of the most densely populated urban areas of Italy, with nearly 75,000 inhabitants and a population density of about 5,240 inhabitants/km² among highest in Europe. Until the '30s of the last century, floodplain groundwater was mainly used by inhabitants of rural villages for agriculture and local drinking needs, using shallow wells and manual methods for lifting groundwater, like the water-wheel or ancient Arabic system named "noria", moved by power-animals. Since the post-World War II, floodplain groundwater has been intensively exploited for drinking water, agriculture and industry needs through modern pumping systems based on submerged pumps. The most important water-tapping public project was the Lufrano well field realized during 1930-1946, with about 156 wells distributed on an area of several km² (Figs. 2.2a and 2.2b), to meet water demand of the city of Naples. In the '70s and '90s of the last century, the Ponticelli and Acerra well fields were realized respectively (Fig. 2.2b), to provide drinking water to the hinterland of Naples. During this stage, a great number of unauthorized private wells for agricultural and industrial uses were realized with spatial density of 90-100 wells/km².

In the 1970-1989 period, an intensive use of groundwater resources by public and private wells occurred, causing a strong water balance disequilibrium and a groundwater over-exploitation at the basin scale. Consequently, this disequilibrium determined a decline of piezometric levels and a deterioration of groundwater quality by the increase of nitrate, iron, manganese and fluoride concentrations, exceeding the acceptable drinking water standards (Celico et al., 1997). Due to such a groundwater quality deterioration, Lufrano, Acerra and Ponticelli well fields (Fig. 2.2a) were partially or totally abandoned and groundwater withdrawals were drastically reduced (Fig. 2.7). Since 1990s, private withdrawals for rural and industrial use have been drastically reduced, due to process of deindustrialization and land use change (Fig. 2.2b). The land use changed strongly due to the continue and exponential population growth (Fig. 2.2d), as well as the urban and economic development of Naples metropolitan area (Salvati, 2014; Mazzeo, 2009). At the basin scale, from 1956 to 2015 the urbanized zones increased from 11% to 41% of the total territory, while agricultural lands decreased from 88.7% to 59%. At the municipality scale, from 1943 to 2015 the urbanized zones increased from 2.6% to 67.2%, while rural areas declined from 97.4% to 32.8% (Figs. 2.2a and 2.2c). Furthermore, in the 1995-2010 period many industrial sites were dismissed and in the 1999-2007 period three great railway

viaducts of high-speed rail were constructed, with foundations characterized by deep piles with 1.20 m diameter and length up to about 41 m below the ground surface (Fig. 2.2b).

4. Data and methodologies

4.1 Hydro-stratigraphic data

Using a LiDAR dataset (<http://sit.cittametropolitana.na.it/lidar.html>), a Digital Elevation Model (DEM) of the study area, with 1×1 m cells, was implemented in a GIS environment and used for field surveys. A high-resolution 2D hydro-stratigraphic model of the pyroclastic-alluvial aquifer system was reconstructed based upon a considerable geological and hydrogeological database consisting of: i) deep stratigraphic data of wells available in literature (Coda et al., 2019a; Torrente et al., 2010), ii) new geological maps and cartographic data at 1:50.000 scale of Geological CARTography project (ISPRA, 2019), iii) stratigraphic data of wells and boreholes available in the Geoportal of Italian Geological Survey (<http://portalesgi.isprambiente.it/en>), iv) borehole records archive of Casalnuovo di Napoli and Volla municipalities.

The geological and hydrogeological database is characterized by stratigraphic-lithologic logs of about 149 boreholes and 127 wells (Fig. 2.1c), with an average density around 11.0 per km², and depths variable between 10 and 450 m below the ground level (Table 2.1). All wells and boreholes data collected were organized in a georeferenced database, to manage stratigraphic features and to recognize the different stratigraphic units, marker horizons and lithofacies. For each borehole and well, a vertical log of hydraulic conductivity was obtained, assigning an average value for each lithofacies according to the Freeze and Cherry (1979), based on grain size and rocks types. This approach allowed to recognize the hydrogeological role of each lithofacies and geological formation, as aquifer, aquitard or aquiclude.

Other information on geological and hydrogeological dataset used are summarized in Table 2.1.

Table 2.1 - Hydrogeological, meteorological and stratigraphic dataset. U.D. unavailable data; A, Agricultural; I, Industrial; D, Drinking.

Hydrogeological and meteorological data						
Monitoring period	Type	Total number	Density (No/Km²)	Use	Depth range (m)	Source
August, 1924	Well	85	6.07	A and D	4-12	Fiorelli (1926)
February-September, 1978	Well	U.D.	U.D.	A, I, D and D	U.D.	Celico (1983)
March, 1989	Well	28	1.95	A, I, D and D	10-60	Celico & De Paola (1992)
January, 1993	Well	24	1.67	A, I and D	10-70	Esposito (1998)
February, 1994	Well	24	1.67	A, I and D	10-70	Celico et al. (1995)
February, 2002	Well	30	2.09	A, I and D	10-70	Basin Authority of the North-Western Campania region (2004)
November, 2013	Well	127	9.07	A, I and D	10-60	Field campaign
November, 2013	River head	28	1.95	\	\	Field campaign
March, 2015	Well	127	9.07	A, I and D	10-60	Field campaign
March, 2015 - ongoing	Piezometer	9	0.64	\	10-30	Field campaign
March, 2015	River head	28	1.95	\	\	Field campaign
1924-2015 (annual rainfall) 2013-2015 (monthly rainfall)	Meteorological station	1	\	\	\	San Marcellino Meteorological Observatory (SMMO)
Stratigraphic data						
Monitoring period	Type	Total number	Density (No/Km²)	Use	Depth range (m)	Source
1980-2015	Borehole	148	10.34	Urban planning	10-60	Casalnuovo di Napoli and Volla municipalities database
\	Borehole	1	0.07	Scientific issues	430	Torrente et al. (2010)

4.2 Hydrogeological data and drainage network density

From November 2013 to March 2015, a six-month frequency hydrogeological monitoring of groundwater levels was carried out on 136 wells and piezometer and 28 river heads (Fig. 2.1d), using a water level meter. Furthermore, since March 2015 a high frequency data acquisition system by 9 monitoring stations with pressure sensors and data loggers was installed and used to carry out slug tests. To characterize GR phenomenon, a temporal comparison between historical groundwater levels, new piezometric measurements, annual and monthly meteorological data, and groundwater pumping data was performed. To such a purpose, multi-temporal maps of groundwater flow and maps of piezometric head variations were reconstructed by interpolation of piezometric levels (Table 2.1) using the Triangulated Irregular Network (TIN) method. Piezometric data of the whole dataset were plotted in temporal box-plot diagrams. Depth of water table maps were carried out for each period by subtracting the groundwater elevation raster from DEM. Finally, to analyze the modifications of the local micro-network drainage system during the last century, and its possible influence on GF phenomenon, a temporal comparison between historical image of the 1943 of the Italian Military Geographic Institute (Fig. 2.2e) and high resolution aerial photograph derived by 2015 satellite image (Fig. 2.2f) was carried out, and for two periods the network drainage density was estimated.

All the cartographic products were elaborated in GIS environment using ESRI's ArcMAP software 10.1 version.

4.3 Flood monitoring

From November 2013 to March 2015, a six-month frequency monitoring and mapping of impacted agricultural soils and private building was carried out, using a citizen science approach. To map, detect the starting date and temporal recurrence of impact of GF on private buildings and agricultural soils, local population received a flooding online questionnaire sent by municipal administration. Subsequently, for each flooded building registered through the online questionnaire, coordinates, altitude, age and type of building, depth and type of foundation, and depth of flooded underground facilities was acquired, by cadastral municipality database and face-to-face interview with owners (Fig. 2.3). In addition, temporal variations of water levels in the flooded structures, conditions of alteration and degradation and visual damage, as well as cracking pattern of structures

were detected. For flooded agricultural lands, coordinates, altitude and amplitudes about land parcel, as well as water levels above surface of flooded soils were measured. Moreover, type of active or passive protective measures aimed to flooding mitigation were detected. Finally, field data allowed to achieve multi-temporal maps of GF of private buildings and agricultural soils, producing the first municipal groundwater flooding GIS data-base.

ID: B12 / A7		IMPACT FIELD SCHEDE		Date: 3/3/15	
B12	Building	A7	Rural soil		
WGS84 - UTM 33N		WGS84 - UTM 33N			
X: <u>444619.00</u> Y: <u>4527603.00</u>		X: <u>444680.00</u> Y: <u>4527550.00</u>			
GW depth (m b.g.l.): <u>2.70</u>		GW depth (m b.g.l.): <u>-0.10</u>			
GW elev. (m a.s.l.): <u>15.50</u>		GW elev. (m a.s.l.): <u>14.90</u>			
Year of impact occurrence: <u>2007</u>		Year of impact occurrence: <u>2008</u>			
Type of building: <u>townhouse</u>		Land use: <u>farmland</u>		Flooding mitigation intervents:	
Type of foundation: <u>mat</u>		Elevation (m a.s.l.): <u>14.80</u>		<input type="checkbox"/> Raising of ground level	
Year of construction: <u>1990</u>		Impacted surface (m2): <u>1700</u>		<input type="checkbox"/> Excavation of drainage channels	
Depth of impacted structure (m b.g.l.): <u>3.00</u>		Max water height a.g.l. (m): <u>+0.20</u>		<input type="checkbox"/> Single or multiple pumping well point	
Impacted surface (m2): <u>150</u>		Photo:		<input type="checkbox"/> Other: _____	
Max water height above floor (m): <u>0.80</u>					
Structural damage:		<input type="checkbox"/> Raising of basement floor <input type="checkbox"/> Basement waterproofing <input type="checkbox"/> Single or multiple pumping well point <input type="checkbox"/> Other: _____			
<input checked="" type="checkbox"/> Yes:		<input type="checkbox"/> Garage <input checked="" type="checkbox"/> Cellar <input type="checkbox"/> Elevator shaft <input type="checkbox"/> Only foundation			
<input checked="" type="checkbox"/> Efflorescence		Flooding mitigation intervents: <input type="checkbox"/> Raising of basement floor <input type="checkbox"/> Basement waterproofing <input type="checkbox"/> Single or multiple pumping well point <input type="checkbox"/> Other: _____			
<input checked="" type="checkbox"/> Cracking		Type of impacted structure: <input type="checkbox"/> Garage <input checked="" type="checkbox"/> Cellar <input type="checkbox"/> Elevator shaft <input type="checkbox"/> Only foundation			
Photo:		Type of building: <u>townhouse</u> Type of foundation: <u>mat</u> Year of construction: <u>1990</u> Depth of impacted structure (m b.g.l.): <u>3.00</u> Impacted surface (m2): <u>150</u> Max water height above floor (m): <u>0.80</u>			
		* m a.s.l. (meters above sea level); m b.g.l. (meters below ground level); m a.g.l. (meters above ground level).			

Figure 2.3 - Field schede for flooded buildings and agricultural soils.

5. Results

5.1 2D hydro-stratigraphic model and groundwater flow pattern

The 2D hydro-stratigraphic model allowed, for the first time, to represent the geometry and architecture of the aquifer system down to about -400 m b.s.l., defining the top and bottom of two different aquifers. Figures 2.4 and 2.5 show a heterogeneous aquifer system, characterized by a multi-layered discontinuous aquifer, which laterally evolves in a single aquifer. Starting from the northern sector (Figs. 2.4, 2.5a and 2.5b), an unconfined shallow aquifer, in the PF complex, and a deep semi-confined aquifer, in pyroclastic-alluvial deposits underlying CI horizon, occur. Both the aquifers have an average thickness of about 10 m and one 100 m, respectively, and they show small differences in terms of potential heads, although there are local variations of groundwater flow directions (Figs. 2.4 and 2.5). The central sector is characterized by a single deep semiconfined aquifer in pyroclastic-alluvial deposits underlying the CI horizon. In the southern sector, where CI is absent, a single phreatic shallow aquifer is observed, locally characterized by artesian groundwater flow condition due to shallows aquicludes (lens of silts, clays and peaty levels) within the PAP complex (Fig. 2.4).

Figures 2.5a and 2.5b compare groundwater flow patterns of the deep and shallow aquifer system for November 2013 and March 2015, respectively. While Figures 2.5d and 2.5e show groundwater flow scheme of the shallow unconfined aquifer for northern sector. For the deep semi-confined aquifer, in the northern and central sectors (Figs. 2.5a and 2.5b) groundwater flow is about NE-SW, thus being consistent with groundwater scheme at basin scale. In the southern sector, the groundwater flow direction is mainly E-W, converging towards Cozzone and Volla rivers and Reale Lufrano channel, which locally are physically continuous with groundwater flow and behaving as gaining streams.

For the shallow unconfined aquifer of northern sector (Figs. 2.5d and 2.5e), groundwater circulation is oriented towards N and S, bypassing thus the IC top, and Santo Spirito stream feeds only partially the underlying shallow aquifer, as the concrete stream bed is positioned at a level higher than the water-table. For the shallow aquifer, the hydraulic gradient varies between 5.9×10^{-4} and 2.0×10^{-2} , whereas for the deeper water table it varies between 8.7×10^{-4} and 4.3×10^{-2} .

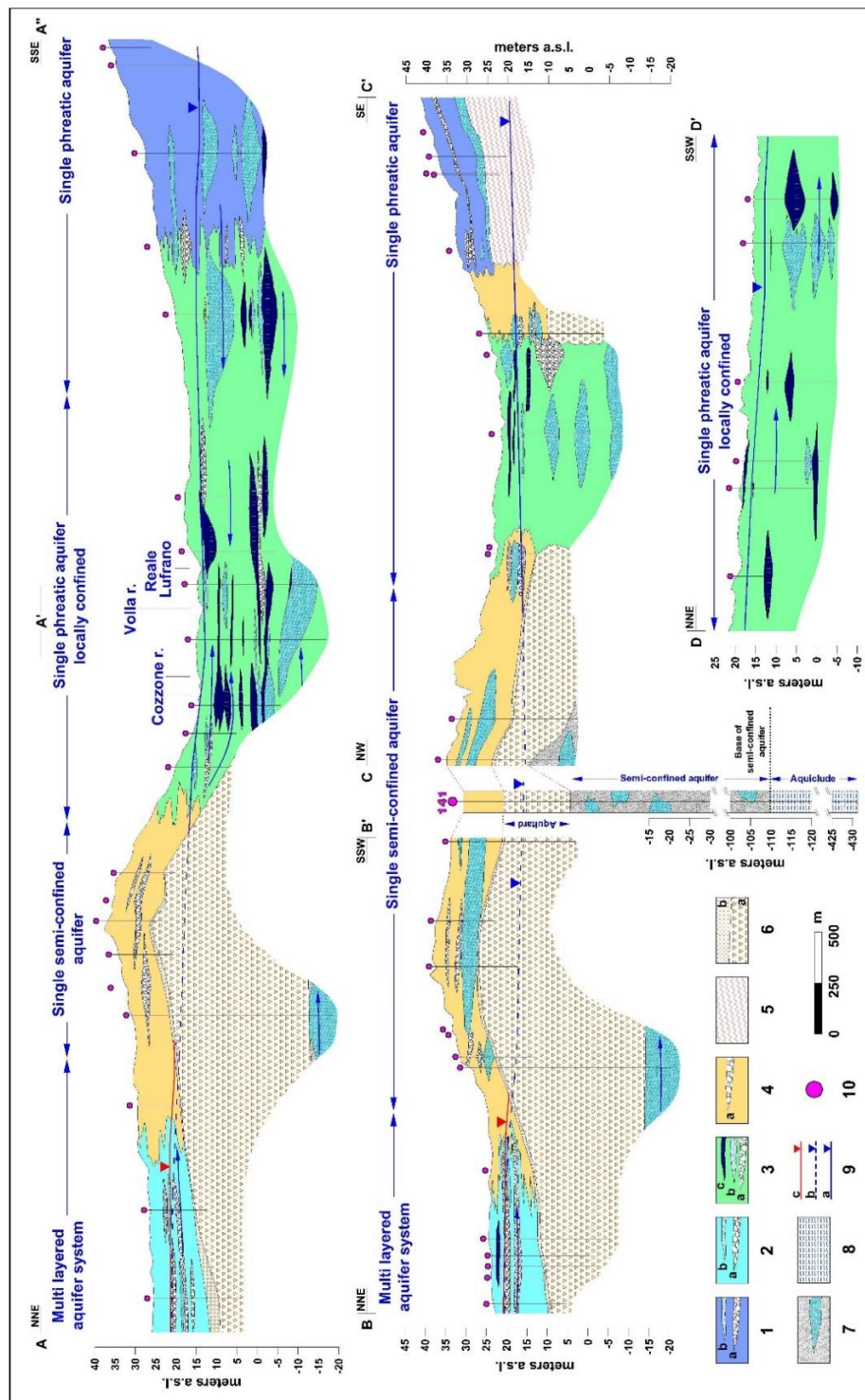


Figure 2.4 - 2D hydro-stratigraphic model. 1) VA complex (sandy silts) with interbedded: a) pumiceous lapilli horizons; b) sandy horizons; 2) PF complex (sands, silts and sandy silts) with interbedded: a) pumiceous lapilli horizons; b) sands e pumiceous lapilli horizons; 3) PAP complex (sandy silts, silts and clays) with interbedded: a) pumiceous lapilli horizons; b) sands, paleosols, and peat levels, c) marshy clay-sands and clay-silts; 4) P complex (silty sands) with interbedded: a) pumiceous-scoriaceus lapilli horizons; 5) Somma-Vesuvius lavas; 6) Lithoid (a) and incoherent (b) CI; 7) Deep semi-confined pyroclastic-alluvial aquifer (silty sands and sands); 8) Basal aquiclude (marine clays) 9) Phreatic (a) and semi-confined (b) piezometric level of the deep aquifer, and phreatic level of shallow aquifer (c); 10) Borehole.

For the 2013-2015 period, temporal variations of groundwater levels for both aquifers are shown in Figure 2.5c and 2.5f. Both water table levels display a generalized rise, with a magnitude variable at the municipality scale. For the deeper aquifer (Fig. 2.5c), the highest magnitude amounts to 2.44 m, and was recorded in the northern-western sector of the study area, whereas low values, smaller than 0.10 m, were observed in the south-western sector, near the Cozzone and Volla rivers and Reale Lufrano channel, having the latter a fixed piezometric heads. For the shallow unconfined aquifer (Fig. 2.5f), the highest magnitude amounting to 1.54 m was recorded in the northern-eastern sector of the study area.

Finally, in Figure 2.5g monthly rainfall trend is shown. Downward trend in the time series suggests that the rise of piezometric levels measured between 2013 and 2015 is not related to a change in the groundwater recharge rate.

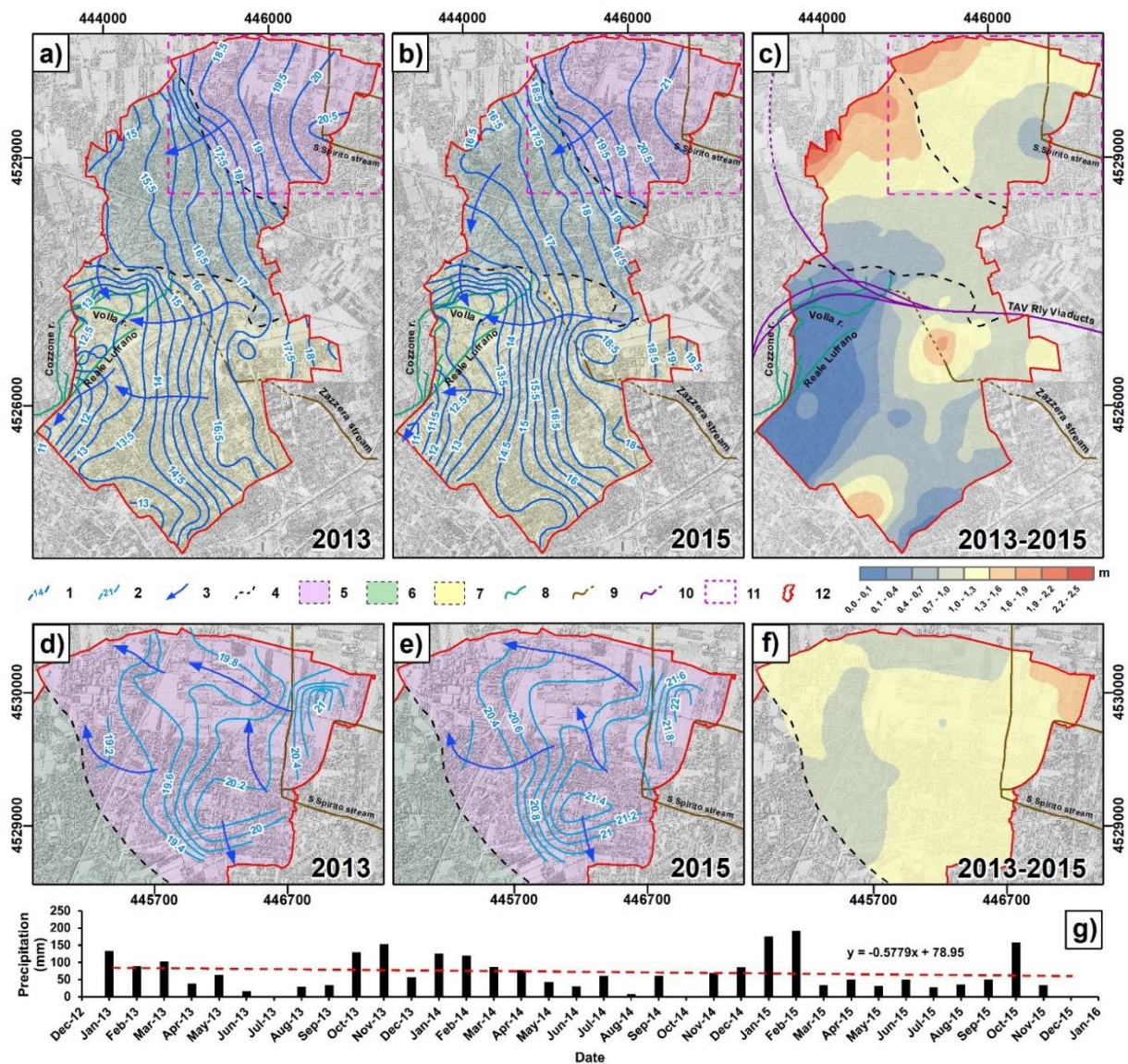


Figure 2.5 - Groundwater flow pattern of the deep and shallow aquifer, for the period (a and d) November 2013, (b and e) March 2015, and piezometric head variations between these measurement periods (c and f). (g) SMMO' monthly rainfall. 1) Piezometric contour line of the deep aquifer (m a.s.l.); 2) Piezometric contour line of the shallow aquifer (m a.s.l.); 3) Groundwater flow direction; 4) Aquifer type boundary; 5) Sector with shallow and deep aquifer; 6) Sector with deep semi-confined aquifer; 7) Sector with phreatic aquifer, locally confined; 8) Surface and groundwater drainage network; 9) Urban drainage system (culverts); 10) Railway infrastructures constructed in the 1999-2007 period; 11) Box of Figs. 2.5d, 2.5e and 2.5f; 12) Study area.

5.2 GR characterization

Figures 2.6a and 2.6b shown groundwater elevation (m a.s.l.) and groundwater depth (m b.g.s.) for eight hydrodynamic scenarios, respectively, each representative of the hydrogeological history of the aquifer system from 1924 to 2015. Here, the attention is focused on three scenarios, because they are particularly significant in explaining the

groundwater level evolution and indicative of two subsequent hydrogeological phases (1924-1989 and 1989-2015), which were characterized by declining and rising groundwater levels, respectively.

The first one is the 1924 scenario, indicative of a hydrogeological equilibrium for the aquifer system. Groundwater was used for local agriculture and drinking needs for villages habitants, by shallow wells and manual abstraction methods. Water table levels vary from 22.45 to 9.68 m a.s.l., equal to 34.01 and 0-0.50 m b.g.s.. The second one is the 1989 scenario, representative of a groundwater overexploitation period. Intense groundwater pumping (about 4.2 m³/s for drinking use, see Fig. 2.7b) by numerous public and private deep wells caused a considerable water budget deficit (Allocca & Celico, 2008) and piezometric levels depletion up to -2.06 m b.s.l., equal to 42.47 m b.g.s.. The third one is the 2015 scenario, representative of present-day hydrogeological conditions, in which aquifer system has almost recovered 1924 hydrogeological equilibrium due to strong reduction of groundwater pumping. Piezometric level increased up to 21.58 and 10.53 m a.s.l., equal to 36.49 and 0-0.50 m b.g.s..

In Figure 2.6c, the three scenarios are highlighted as piezometric profiles along a NE-SW oriented section to show the vertical lowering and raising of the water table in the study area.).

In the box plot of Figure 2.7a, the temporal trends of piezometric levels are reported. Each trend shows that the GR phenomenon has started in 1990 and is widespread in the whole study area, with a magnitude up to maximum of 16.54 m. In agreement with Coda et al. (2019a), the 1990-2015 period was characterized by two subperiods, each one with different magnitude and rising velocity of the GR (Table 2.2). The 1990-2002 subperiod is characterized by a mean magnitude of about 4.10 m (up to a maximum of 14.43 m) and a mean velocity of 0.32 m/yr (up to a maximum value of 1.11 m/yr). In the 2002-2015 subperiod, a reduction of the magnitude is observed, with mean values of about 3.49 m (up to a maximum of 6.51 m), and a mean velocity of about 0.27 m/yr (up to a maximum of 0.50 m/yr). The remarkable variability of the GR is strongly dependant on the distance from the abandoned Lufrano well field (Figs. 2.2b and 2.6), considered as the hypocentre of the piezometric deformation induced by Lufrano pumping, and observed at the local and basin scale. Therefore, the highest magnitude of piezometric rise is observed (Table 2.2) in the central-western sector of study area, in correspondence of the eastern boundary of Lufrano well field, as this sector is closer to the area of the well field.

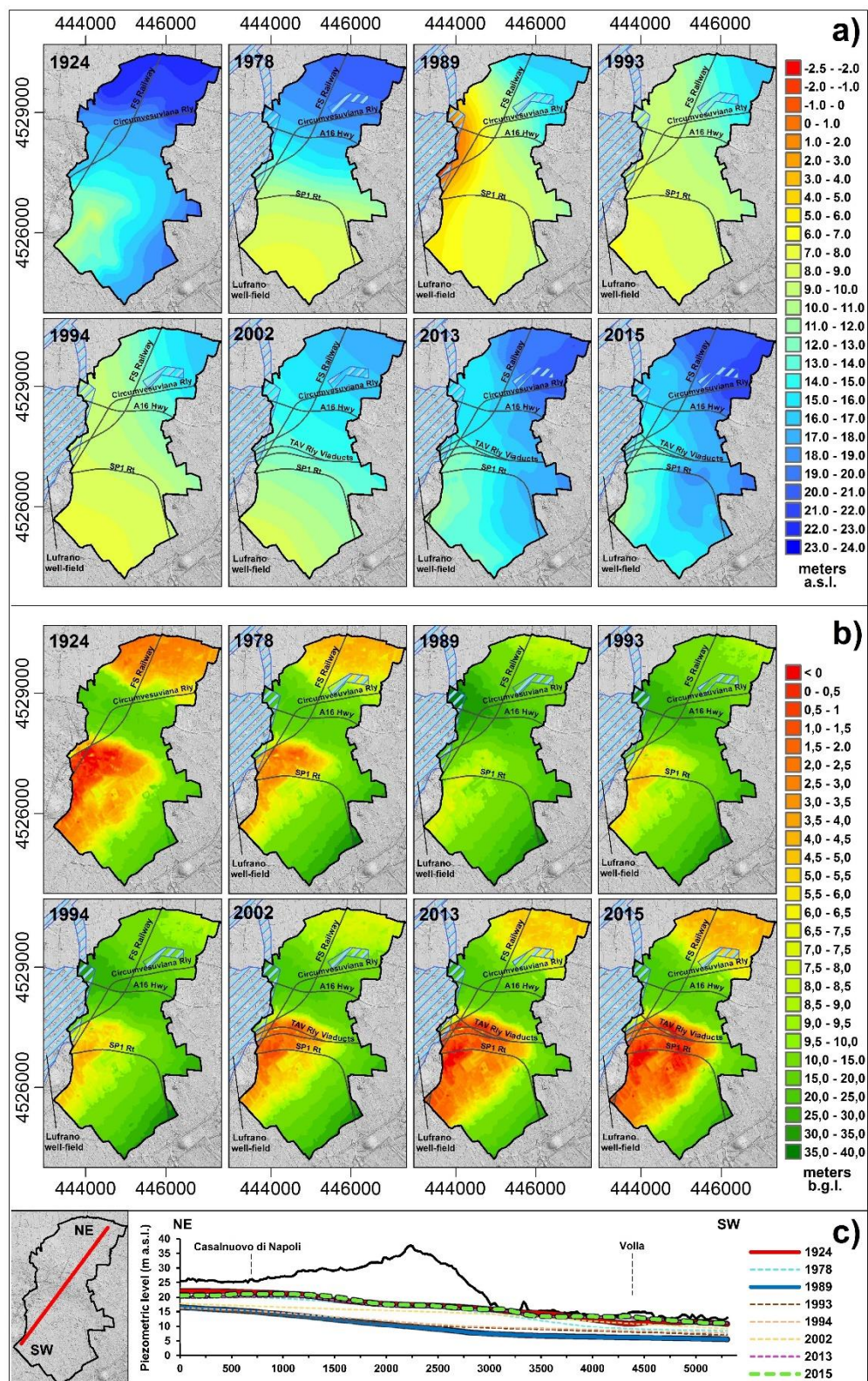


Figure 2.6 - Hydrodynamic scenarios in the period 1924-2015, in terms of (a) piezometric heads (m a.s.l.), (b) depth of water table (m b.g.l.) and (c) piezometric profiles (m a.s.l.).

Moreover, the comparison between the time series of groundwater levels, withdrawals (Fig. 2.7b) and annual rainfall (Fig. 2.7c) confirms that climate-induced changes have not played a significant role on GR at the decadal scale, in agreement with the downward sloping trend in the mean annual precipitation index observed at the regional scale (De Vita et al., 2012). Finally, data suggest that a not significant role on GR was played by deep foundations of railway viaducts constructed in the 1999-2007 period, since the rising groundwater levels were recorded both upstream and downstream of these civil engineering works (Figs. 2.2b, 2.5c and 2.6b).

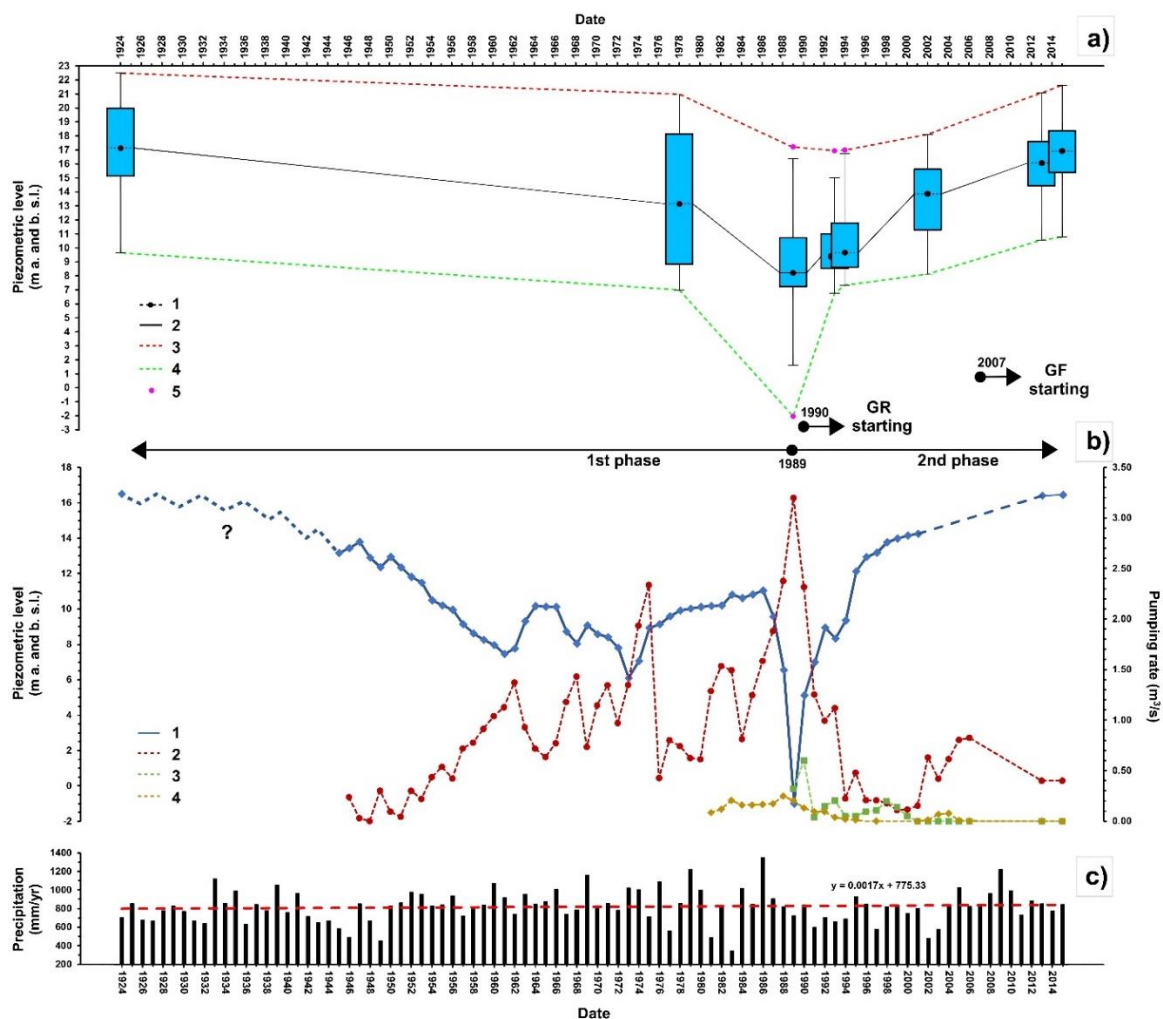


Figure 2.7 - a) Box plots of piezometric levels (m a. and b. s.l.) in the study area; **b)** Piezometric levels (m a. and b. s.l.) and withdrawals (m³/s) in Lufrano, Acerra and Ponticelli well fields; **c)** SMMO' annual rainfall. Legend **a)**: 1) Median piezometric head; 2) Median trend; 3) Maximum trend; 4) Minimum trend; 5) Outliers; Legend **c)**: time series of: 1) piezometric levels Lufrano well-field; 2) Lufrano well-field withdrawal; 3) Acerra well-field withdrawal; 4) Ponticelli well-field withdrawal.

Table 2.2 - Magnitude (m) and rising velocity (m/yr) during GR period (1990-2015).

Period and Sub-period of the GR	Magnitude (m)			Rising velocity (m/yr)		
	Minimum	Mean	Maximum	Minimum	Mean	Maximum
Period 1990-2015	3.50	7.88	16.54	0.13	0.30	0.64
Sub-period 1990-2002	0.47	4.10	14.43	0.04	0.32	1.11
Sub-period 2002-2015	0.29	3.49	6.51	0.02	0.27	0.50

5.3 GF features

Flooding online questionnaire data, field surveys and mapping display that GF phenomena affect private buildings and agricultural lands. By contrast, there are no public structures, infrastructures and cultural resources impacted by GF, as occurs in other sectors of the Naples metropolitan area (Stellato et al., 2020).

In the study area, the first GF episodes of private buildings and agricultural lands respectively, in 2007 and 2010 was registered, with a time delay variable from 17 to 20 years in comparison to the beginning of the GR, started in 1990. In a “cause-effect” perspective, the GF episodes observed are the consequence of piezometric levels rise induced by stop of groundwater pumping for public and private use. However, unlike the GR process, widely distributed at the municipality scale (Figs. 2.5 and 2.6), the GF phenomenon shows a sectorialized pattern, with a distribution spatially and temporally inhomogeneous, as a typical leopard spots-shape (Figs. 2.8 and 2.10). Indeed, the private buildings and agricultural soils affected by flooding are only located in the northern and southern sectors of the study area. In particular, in the northern sector only few private buildings (Figs. 2.8b and 2.8c) are impacted by shallow unconfined water table, with flooding episodes of garages, cellars and lift shafts. Conversely, no flooded agricultural lands were detected in this sector. Moreover, collected field data by citizen’s participatory survey shows that these private buildings were constructed in the 1990-2000 period, when groundwater levels of aquifer system, affected by groundwater pumping for drinking, industrial and agricultural use (Figs. 2.2b and 2.6), were locally characterized by depth variable between about 9 and 6 meters from ground surface (Fig. 2.6b).

Similarly, in the southern sector, only few private buildings (Figs. 2.8d and 2.8e) reveal flooded underground structures (garages and cellars) and flooded ground-floors of private buildings. These underground structures were constructed in the 1985-1995 period, when stressed piezometric levels by pumping for drinking, industrial and agricultural use, were locally characterized by depth about 6 meters below ground surface (Fig. 2.6b). In addition, in this sector, unlike the northern one, some agricultural lands are affected by flooding episodes, with local outcropping of the shallow water table (Figs. 2.8d and 2.8e) near drainage channels of Cozzone, Volla and Lufrano rivers

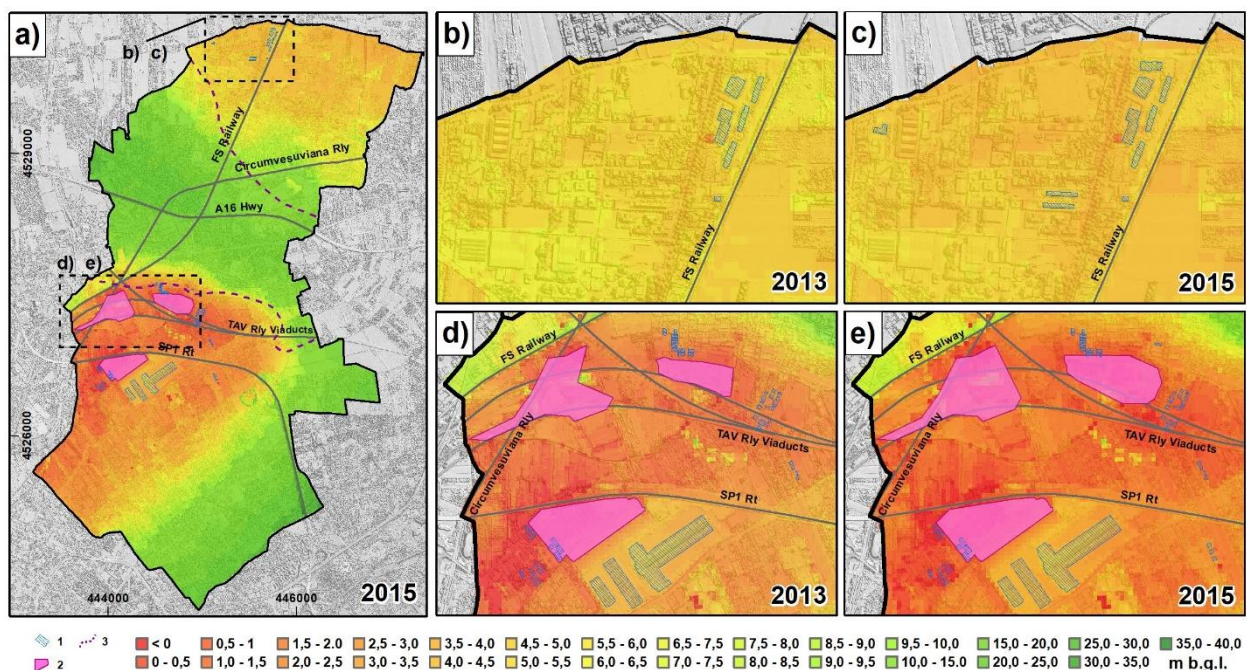


Figure 2.8 - Maps of the groundwater depth (m b.g.l.) in the deep (a, d and e) and in the shallow aquifer (b and c), and spatio-temporal distribution of GF episodes in the period November 2013-March 2015. 1) Flooded buildings; 2) Flooded agricultural soils; 3) Boundary of aquifers reported in Fig. 2.5.

In Table 2.3 the temporal variability of GF phenomenon observed at the municipality scale is shown. In 2013, 44 private buildings have been flooded (with a total buildings surface equal to 61898 m²), among which 6 are located in the northern sector, and 38 in the southern sector (Figs. 2.8b and 2.8d). In 2015, flooded buildings increased to 52 (with a total area of flooded buildings of about 66000 m²), among which 10 are located in the northern sector and 42 in the southern sector (Figs. 2.8c and 2.8e). From 2013 to 2015, the number of private buildings and surface of agricultural soils flooded has increased of about 15 and 20%, respectively (Table 2.3).

Table 2.3 - Number and area of buildings and agricultural soils affect by GF.

Period	Private buildings		Agricultural soils
	No.	Area (m ²)	Area (ha)
November 2013	44	61898.16	20.60
March 2015	52	65916.85	25.36
Δ (2015-2013)	8 (+15.38%)	4018.68 (+6.10 %)	4.76 (+19.77%)

The inhomogeneous spatial distribution of GF episodes observed during the monitoring period is linked to the local hydrostratigraphic and geomorphological characteristics of aquifer system. In the northern sector, shallow aquifer hosted within in PF complex is very flat (Fig. 2.1d) and it's characterized by unconfined groundwater flow, with a water table oscillating between 3,5 and 5,7 m below surface. Consequently, the private buildings with underground structures (garages, cellars and lift shafts), located at a depth greater than 3.5 m from surface, are constantly flooded, with greater impact in the winter period, during intense and prolonged rains that recharge the shallow pyroclastic-alluvial aquifer.

In the central sector, where outcrop the P complex (Fig. 2.1d), the aquifer is characterized by a single deep semiconfined aquifer in pyroclastic-alluvial deposits underlying the CI horizon (Figs. 2.4 and 2.5). Despite the presence of numerous private and public buildings with underground structures (garage, cellars, and ancient underground cavities dug into the tuff horizon) located at greater depths up to 15-20 m from ground surface, in this sector there aren't groundwater flooding phenomena due to the presence of a semiconfined groundwater flow condition (Figs. 2.4 and 2.5).

In the southern sector, the complex floodplain aquifer hosted within the PAP complex (Fig. 2.1d) is phreatic, with a shallow water table oscillates between 0,0 and 1,5 m below soil surface. Consequently, the private buildings with underground structures (garages, cellars and lift shafts), located at depth greater than 1.5 m from ground surface, are constantly flooded, especially during winter recharge phase of shallow floodplain aquifer when groundwater table increase. The unconfined groundwater table morphology is

controlled by floodplain hydrographic network, driving groundwater flow toward Cozzone, Volla and Reale Lufrano rivers (Figs. 2.5a and 2.5b). At the local scale, artesian flow conditions are caused by the presence of discontinuous lenses of low permeability of silts, clays and peaty horizons within the PAP complex.

Moreover, the map of spatial distribution of GF episodes, observed during the monitoring period, shows that, with respect to the local groundwater flow (Figs. 2.5a, 2.5b, and 2.5c), the impacted private buildings and agricultural lands are located upstream and downstream of civil engineering structures (Figs. 2.8 and 2.10). Consequently, the “barrier effect” of the impervious deep foundation on the groundwater flow, that in some cases may occur (Attard et al., 2016), is absent or negligible in the study area at the municipality scale. Therefore, field evidences show that a not significant role, in terms of triggering causes of GR and GF dynamics, was played by deep foundations of the three great railway viaducts of high-speed rail constructed in the 1999-2007 period (Figs. 2.6 and 2.8). The time variability of GF, i.e. the increase in the number of buildings and the extension of the flooded ground surface between 2013 and 2015 period, is attributable to the fact that groundwater levels rising was in progress during the monitoring period (Figs. 2.5c, 2.5f and 2.7b).

As shown in Figure 2.9, GF phenomena is causing tangible and intangible damages: i) on private buildings and its facilities (garages, cellars and lift shafts) due to the structural deformations (vertical and horizontal cracks), groundwater infiltration and deterioration of foundations and pillars (photo a, b, c, d, e, f, g and h); ii) on rural environment, because of the scarce healthiness of the flooded territory and total loss of agricultural soils (photo i, j, k, l, m and n). Moreover, among possible socio-economic impacts of the above described damages, it is possible to envisage loss in the local estate market, due to drop of buildings and rural soils prices, but also consequences for the health of flooded populations, due to poor conditions in terms of environmental hygiene in water-damaged buildings

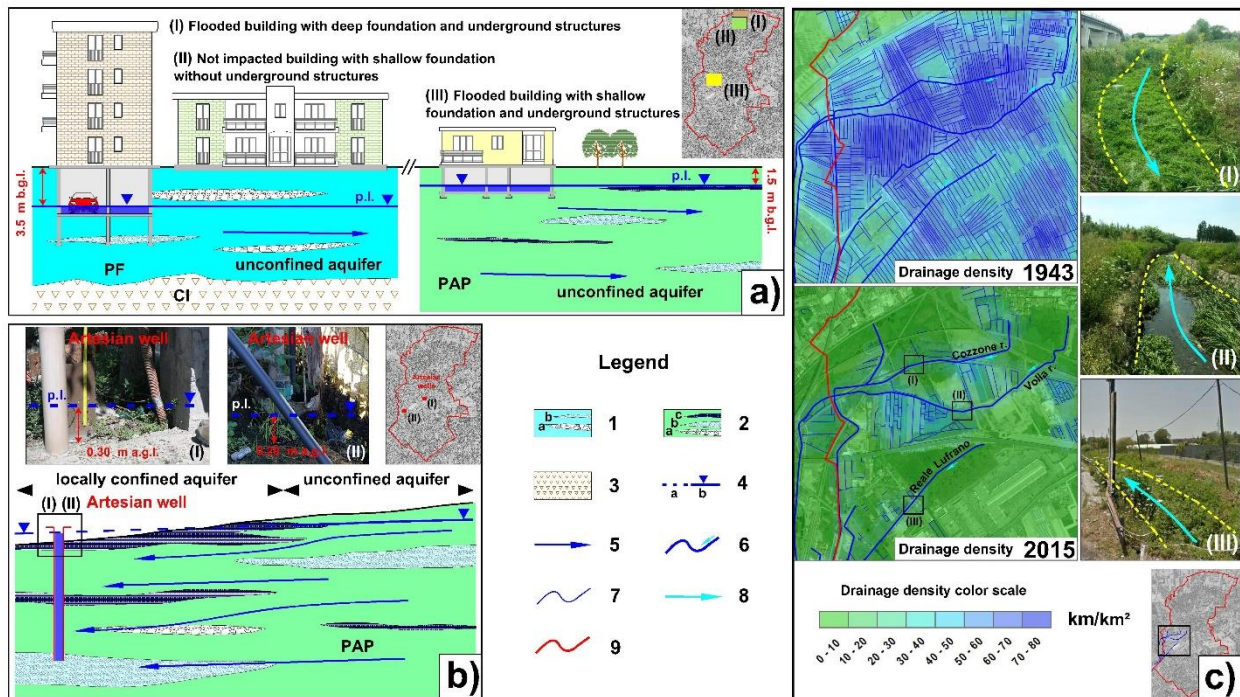


Figure 2.9 - Anthropogenic and natural factors controlling GF. a) Impacted buildings with depth of the flooded underground structures; **b)** Local condition of artesian aquifer; **c)** Drainage density modification of network system from 1943 to 2015 (Figs. 2.2e and 2.2f) and current maintenance state with occlusion of channels. 1) PF complex; 2) PAP complex, 3) CI tuff horizon; 4) Confined (a) and unconfined (b) piezometric levels (red number in the box a): maximum piezometric level p.l. (m b.g.l.); 5) Groundwater flow direction; 6) Surface and groundwater drainage macro-network system; 7) Agrarian drainage micro-network system; 8) Surface water flow direction; 9) Study area.

6. Discussion

The floodplain aquifer of the study area, although relatively small in terms of extension, shows significant heterogeneity in the geometry of the aquifer and groundwater flow.

By comparing the map of groundwater level rise with the one of groundwater flooding, it is recognizable an apparent mismatch between the location of flooded sites and rate of rising groundwater levels (Figs. 2.10a, 2.10b and 2.10c).

For the northern sector, the flooded private buildings are located away from Santo Spirito stream (Fig. 2.10b), in an area where the unconfined shallow aquifer is characterized by a medium rate of rising piezometric levels, ranging from 0,7 to 1,3 m, and a flat surface morphology, with slopes less than 1%. In the same sector, the deep semiconfined aquifer (Fig. 2.10a) does not impact private buildings, although it's characterized by of groundwater rise up to 2,5 m.

For the southern sector, the flooded private buildings and agricultural soils are located near Cozzone, Volla and Reale Lufrano drainage channels, where the unconfined shallow

aquifer is characterized by a low rate of rising groundwater levels, ranging from 0,1 to 0,4 m (Fig. 2.10c), and land morphology is flat, with slopes less than 1%.

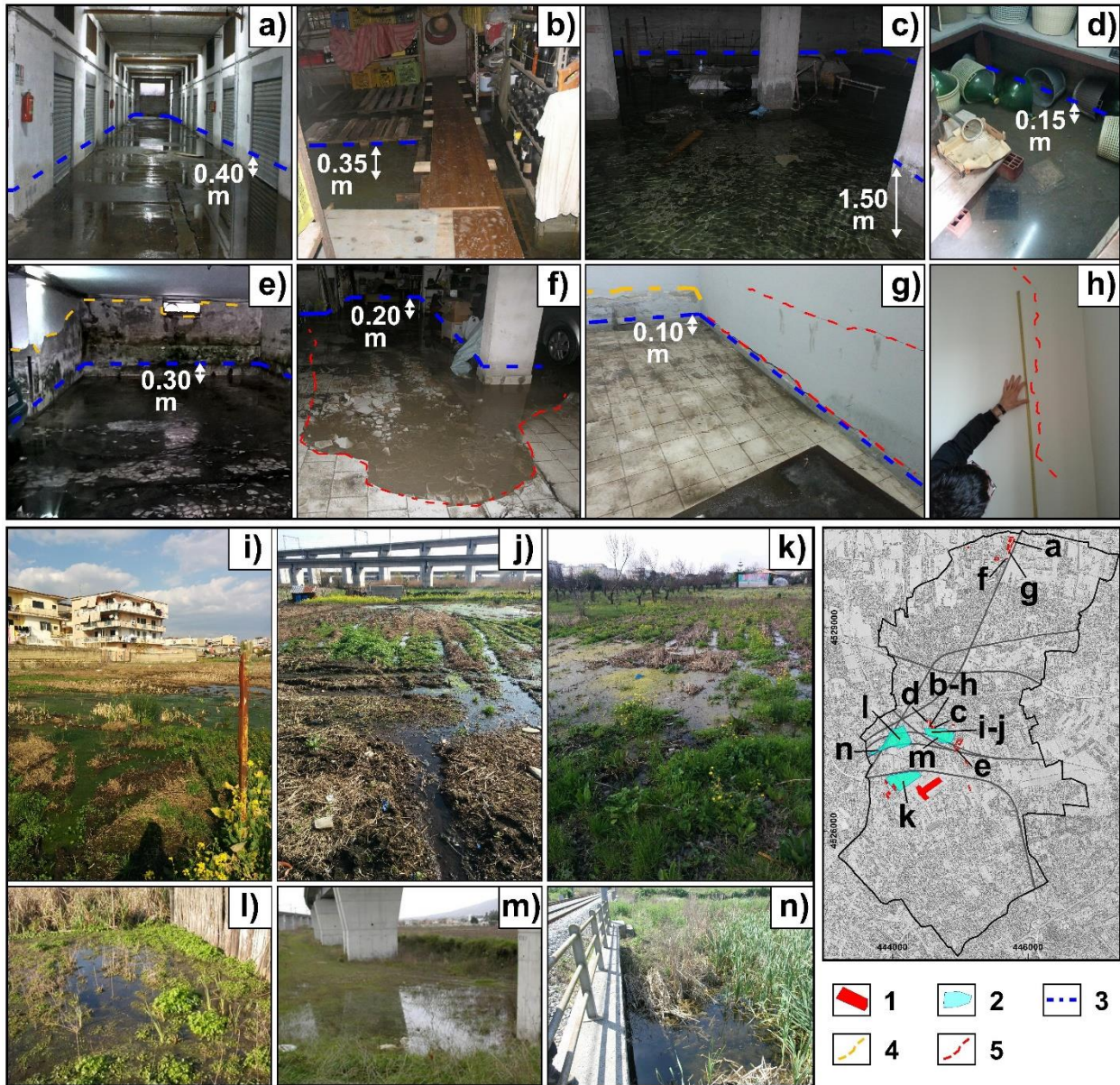


Figure 2.10 - Damages on buildings and agricultural soils. 1) Flooded buildings; 2) Flooded agricultural soils; 3) Maximum height reached by piezometric level; 4) Height reached by efflorescence and deterioration of pillars and walls; 5) Vertical and horizontal cracks.

The heterogeneities in the geometry and structure of flood plain aquifer, hydro-geomorphological and anthropogenic factors acting at the local scale may explain inhomogeneous distribution of the GF episodes, with this typical leopard spots-shape, that certainly is not random. Based on field evidence, a hydrogeologically-based interpretation of the GF phenomenon has been proposed, highlighting the natural and

anthropogenic factors that locally control the GF spatial distribution of private buildings and agricultural soils. Among the anthropogenic factors facilitating GF it is possible to quote: i) an erroneous design of private buildings, built in the period 1985-2000, performed with non-waterproofed underground structures deeper than current groundwater levels (see Fig. 2.11a); ii) the total disappearance of the ancient agricultural drainage micro-network system due to urbanization, infrastructuring and abandonment of agricultural lands, as it is well recognizable from the strong downsizing of the local drainage density from 45.1 to 8.7 km/km² (Fig. 2.11c) and drainage capacity of the local phreatic aquifer-river system; iii) the loss of hydraulic efficiency of the main drainage system of Cozzone, Volla e Reale Lufrano river, due to the poor maintenance state of channels and total occlusion by spontaneous vegetation (Fig. 2.11c) that locally causes a water flow blockage effect.

As to the natural factors, lithology and structure of the aquifer have a key control on GF, shaping the spatial distribution of GF according to the presence of a shallow phreatic water table and thickness of unsaturated zone.

In the northern sector of the study area, the interaction between the anthropogenic facilitating factors and thickness of unsaturated zone lower than 4 meters has been observed to be associated with GF of private buildings.

In the southern sector, where GF has involved buildings and agricultural soils, a thickness of unsaturated zone lower 1,5 meter has been observed to be associated to GF of private buildings (Fig. 2.11a). Differently, the presence of low permeability shallow lenses (silts and/or peat lenses), that locally cause permanent artesian conditions of groundwater (up to +0.20÷0.40 m a.g.s.), is a mitigating factor for GF of soils, as observed in some not flooded soils (Fig. 2.11b) characterized by the presence of artesian wells; similar evidences has been observed in other alluvial aquifers including lowland and upland floodplains (Dochartaigh et al., 2019; Cloutier et al., 2014).

The findings here discussed innovate the existing literature by providing new evidences for the study area, based on an intensive effort in data monitoring, that has never been undertaken in previous literature. This allows a better understanding of the triggering mechanisms and anthropogenic/natural factors that locally control groundwater flooding of private building and agricultural lands in Naples' periurban area. Moreover, the hydrogeological monitoring has allowed to define two safe piezometric thresholds for both sector impacted. These piezometric thresholds, equal to about 3,5 m and 1.5 m b.g.s., for northern and southern sector respectively (Fig. 2.11a), correspond to maximum

thickness of the unsaturated medium to be considered in future designs of underground structures, in order to prevent interactions with groundwater and floodings for non-waterproofed buildings.

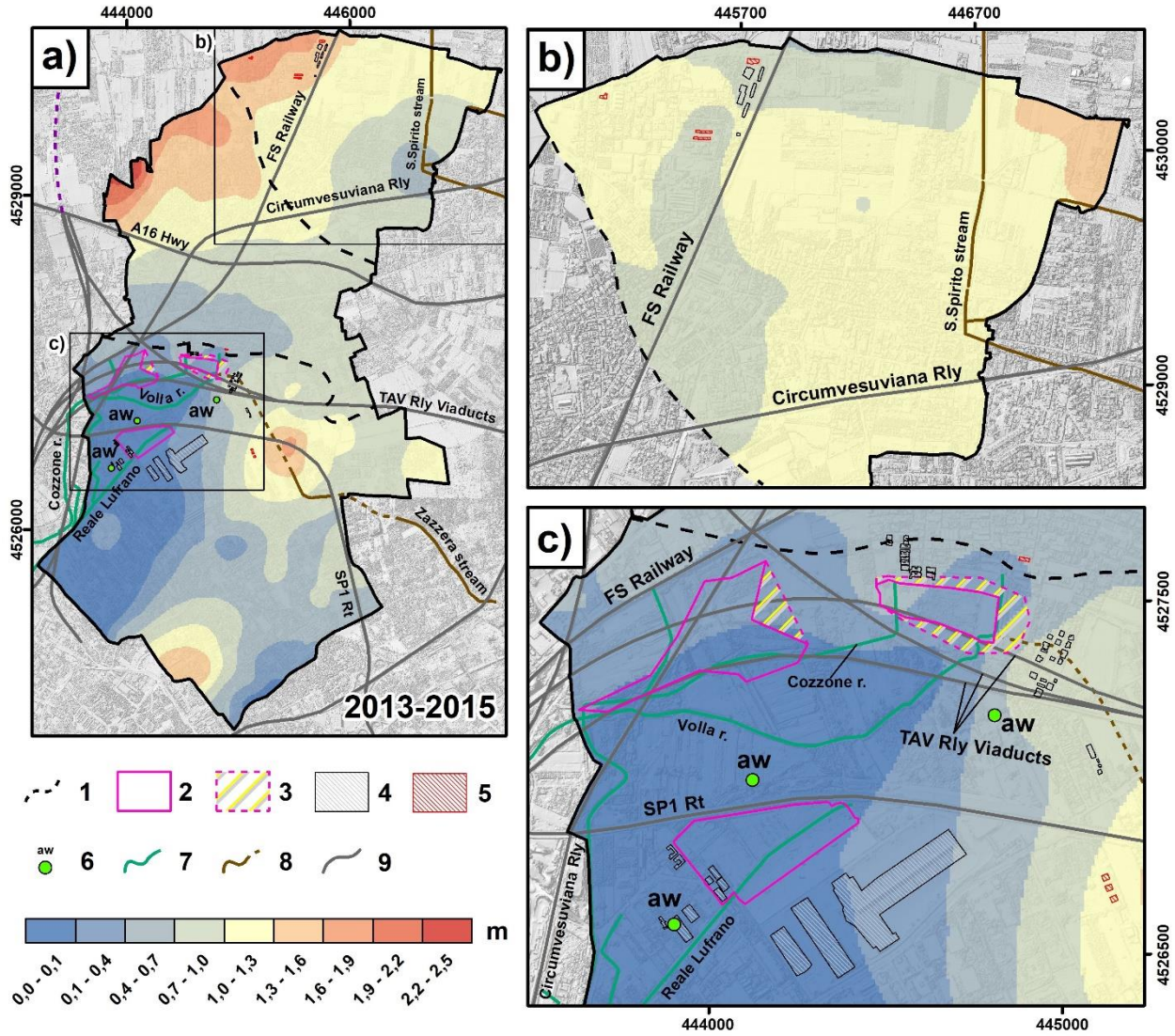


Figure 2.11 - Piezometric head variations in the period November 2013 March 2015 for the deep semi-confined aquifer (a and c) and the shallow one (b), and spatio-temporal distribution of GF in the northern (b) and central (c) impacted sectors. 1) Aquifer type boundary; 2) 2013' flooded agricultural soli; 3) 2015' increment of flooded agricultural soil; 4) 2013' flooded building; 5) 2015' increment of flooded building; 6) artesian well; 7) surface and groundwater drainage network; 8) urban drainage system (culverts); 9) linear infrastructure.

7. Conclusions

In an experimental site of the Naples' periurban area, the cause, spatio-temporal evolution and structures of GR phenomenon were analyzed and characterized by hydrogeological monitoring of 136 wells and piezometers in the 2013-2015 period, as well as analysis of hydro-stratigraphic and historical hydrogeological data starting from 1924. Moreover, by a citizen participatory monitoring approach and detailed field surveys on private buildings and agricultural soils, the GF phenomenon induced by GR was characterized and mapped, for the 2013-2015 period, creating the first flooding inventory map at the municipal scale.

By the field investigations and monitoring, the following findings and major conclusions were obtained:

- Starting from second half of the 20th century and until 1989, an extraordinary modification of groundwater flow pattern was observed, due to mismanagement and overexploitation of the pyroclastic-alluvial aquifer system, causing groundwater levels depletion, up to -2.06 m b.s.l.;
- Conversely, from 1990 to 2015 a remarkable and widespread GR phenomenon was registered, with values up to $+16.54$ m, triggering an unexpected groundwater flooding of agricultural soils and private buildings constructed in the 1985-2000 period;
- First GF episodes started in 2007 and 2010 for private buildings and agricultural soils, respectively, indicating a considerable time delay variable from 17 to 20 years, in comparison to the beginning of GR process;
- Despite GR measured from 1990 to 2015 encompasses the entire study area, with different magnitudes and velocity, the GF phenomenon occurs only in the northern and southern sectors, showing a typical leopard spots-shape and an inhomogeneous distribution as it is locally controlled by anthropogenic and natural factors;
- For both sectors impacted, a safeguard piezometric threshold have been identified to consider in future for new underground structures designs, in order to avoid direct interactions with water table or flooding of non-waterproofed structures;
- At the municipality scale, a not significant role on GR and GF phenomena was played by annual and monthly precipitation variations and deep foundations of railway infrastructures constructed in the 1999-2007 period in the study area.

These findings were not reported and discussed by previous studies because of the absence of monitoring data, and allow a better understanding of mechanisms and anthropogenic/natural factors that locally control groundwater flooding phenomena.

The methodological approaches used to characterize GR and GF phenomena in the Naples' periurban area can be applicable and exportable to other urban and rural environments in southern Italy, as well as to other Italian floodplains and cities, that are currently experiencing similar urban groundwater problems. The obtained results are important to identify structural and non-structural measures aimed at increasing urban resilience and enhancing safety of local communities, and to develop groundwater flooding susceptibility maps, as new tools for the prevention of the risk and correct urbanization planning in the Naples metropolitan area.

Supplementary Material

Table S1 – Natural (a) and anthropogenic (b) causes of groundwater level rising (GWLr) and some of main case studies reported in literature.

a)	GWLr causes		
	Triggering mechanisms	Case studies	References
Natural	Increase of seawater level induced by climate change and glacial isostatic adjustment.	Lagos city (Nigeria); Osaka (Japan); coastal zones of Bangladesh; Ganges-Brahmaputra-Meghna Delta (India); Oahu (Hawaii); Chesapeake Bay region (Maryland and Virginia, USA).	Vink et al. (2007); Yasuhara et al. (2007); Oyedele et al. (2009); Shamsudduha et al. (2009); Stocchi & Spada (2009); Singh et al. (2010); Eggleston & Pope (2013); Habel et al. (2017).
	Natural consolidation of compressible sediment layers or bradysismic/volcano-tectonic land subsidence in coastal area, with consequent local sea-level increase.	Upper Adriatic shoreline and archaeological site of Cumae (Italy).	Gambolati et al. (1998); Todesco et al. (2014); Stellato et al. (2020).
	Seasonal variations of the rainwater infiltration and groundwater recharge by channel network, during and after heavy flash flood phenomena.	Dresden (Germany); Brno (Czech Republic); Sacramento (California, USA); Fairbanks (Alaska, USA); Wisconsin (USA); Alberta (Canada); Rome (Italy); England and Wales (UK).	Nelson (1978); Cobby et al. (2009); Kreibich & Thieken (2009); Hughes et al. (2011); Gotkowitz et al. (2014); Abboud et al. (2018); Julínek et al. (2020); Mancini et al. (2020).

b)	GWLr causes		
	Triggering mechanisms	Case studies	References
Anthropogenic	Artificially increased groundwater recharge within the urban aquifers due to infiltration of imported water for domestic, irrigation and industrial consumption.	Las Vegas (Nevada, USA); San José (California, USA); Riyadh (Saudi Arabia); Kuwait City (Kuwait); Aswan City (Egypt).	Rushton & Al-Othman (1994); Al-Rashed & Sherif (2001); Dean & Sholley (2006); Selim et al. (2014).
	Increased recharge to seepage from septic tanks systems or leakages from sewage systems, as well as increased recharge from leaking water mains and over-irrigation of parks and gardens, irrigation canal leakage, irrigation return.	Jeddah (Saudi Arabia); Yuma (Arizona, USA); Greely and Fort Collins (Colorado, USA); Doha (Qatar), Cairo (Egypt), Saudi Arabia; Tabrik (Iran); Azerbaijan.	Nelson (1978); George (1992); Abu-Rizaiza (1999); Al-Sefry & Şen (2006); Alekperov et al. (2006).
	Underground constructions (e.g. tunnels, deep foundations, underground parks, subway stations, basements of buildings) in saturated zones of urban aquifers.	Barcelona city (Spain).	Pujades et al. (2012); Font-Capo et al. (2015); Attard et al. (2016).
	Anthropogenic land subsidence in coastal and estuarine area and consequent local sea-level rise.	Chesapeake Bay region (Maryland and Virginia, USA).	Eggleston & Pope (2013).
	Reduction of abstraction of groundwater (i.e. GR).	London, Birmingham, Nottingham, Liverpool (UK); Barcelona (Spain); New York city, Buffalo city (New York, USA); Louisville (Kentucky, USA); San Bernardino (California, USA); Buenos Aires (Argentina); Milan metropolitan area and Naples city (Italy); Tokyo Bay area (Japan); north-eastern Ukraine.	Soren (1976); Nelson (1978); Henton (1981); Whitesides et al. (1983); Wilkinson (1985; 1994); Blower (1987); Brassington & Rushton (1987); Hernández & González (1997); Adams & Younger (2001); Jakovljevic et al. (2002); Vázquez-Suñé et al. (2005); Dean & Sholley (2006); Allocca & Celico (2008); Celico et al. (2001); Corniello et al. (2003); Hayashi et al. (2009); Kusaka et al. (2016); Gattinoni & Scesi (2017); La Licata et al. (2018).

Table S2 – Natural and anthropogenic causes of groundwater flooding (GF) and some of main case studies reported in literature.

		GF causes		
		Triggering mechanism	Case studies	References
Natural	Flooding in alluvial lowland related to the water table rising above the land surface in response to extreme high intensity and/or prolonged extreme rainfall in unconfined and consolidated aquifers.	UK's major floodplains.	Macdonald et al. (2012); Hughes et al. (2011).	
	Flooding in small alluvial flatlands related to the rapid response of groundwater levels to precipitation and limited storage capacity in shallow and unconsolidated sedimentary aquifers with a good hydraulic connection with river networks.	Oxford floodplain (UK).	Macdonald et al. (2008).	
	Flooding from groundwater in alluvial deposits by-passing or circumventing river channel flood defence structures.	Kisalföld (Hungary).	Vekerdy & Meijerink (1998).	
	Flooding in lowland karst systems induced by ephemeral karst lakes (turloughs), or groundwater-induced flood occurs when intense groundwater discharge via springs and highly permeable shallow horizons discharges to the surface water, causing overbank flooding.	Ireland karst plains.	Naughton et al. (2012; 2017).	
	Flooding in coastal lowland areas, driven by sea-level rise under climate changes or during and following severe storms.	Coastal areas of California (USA).	Hoover et al. (2017).	
Anthropogenic	Flooding of underground structures creating barriers to groundwater flow.	Barcelona city (Spain).	Font-Capo et al. (2015).	
	Flooding, induced by GR, of basements of buildings, and subsurface structures and infrastructures, in urban centres and abandoned mine zones.	England (UK); Barcelona (Spain); New York city, Buffalo city (New York, USA); Louisville (Kentucky, USA); San Bernardino (California, USA); Buenos Aires (Argentina); Italy; Tokyo Bay area (Japan); north-eastern Ukraine.	Soren (1976); Nelson (1978); Henton (1981); Whitesides et al. (1983); Wilkinson (1985; 1994); Blower (1987); Brassington & Rushton (1987); Hernández & González (1997); Adams & Younger (2001); Jakovljevic et al. (2002); Vázquez-Suñé et al. (2005); Dean & Sholley (2006); Allocca & Celico (2008); Hayashi et al. (2009); Kusaka et al. (2016); Gattinoni & Scesi (2017); La Licata et al. (2018).	

2.2

Coupled ground uplift and groundwater rebound in the Metropolitan City of Naples (southern Italy)

Coda S.¹, Tessitore S.¹, Di Martire D.¹, Calcaterra D.¹, De Vita P.¹, Allocca V.^{1*}

¹ Department of Earth Science, Environment and Resources, University of Naples Federico II, Naples, Italy

*Corresponding author: vincenzo.allocca@unina.it

Abstract

Subsidence and ground uplift are phenomena that may have natural or anthropogenic origin and cause strong socioeconomic and environmental impacts, especially in urban areas. In this paper, the coupling between ground uplift and groundwater rebound in a complex multi-layered aquifer system in the metropolitan city of Naples (southern Italy) has been investigated. By an integrated use of hydrogeological and DInSAR monitoring data covering the periods 1989–2013 and 1993–2010, respectively, the spatio-temporal evolution of natural ground deformation following the strong reduction and interruption of groundwater pumping has been analysed. Hydrogeological monitoring data have shown large-scale groundwater rebound, with the highest amplitude of approximately 16 m and a groundwater rising velocity up to approximately 1.0 m/yr. DInSAR data show a general ground uplift with a magnitude of approximately 40 mm on average, except for the southern sector of the study area where some local natural and human-induced subsidence has been identified. A comparison between trends of groundwater level and ground displacement indicates that the ground uplift is linked to a poro-elastic rebound mechanism in the porous aquifer system, which is triggered by the increase of pore pressure, while the rate of ground displacement is controlled by the hydrostratigraphic characteristics of the multi-layered aquifer system. The results improve the knowledge of man-induced deformation in complex urban aquifers affected by groundwater rebound and highlight that the implementation of an appropriate hydro-mechanical deformation model is a necessary step to correctly model and manage a new geohazard in a highly urbanized environment.

Key words: groundwater rebound, aquifer deformation, ground uplift, subsidence hydrogeology, DInSAR, Naples, Italy.

Coda, S., Tessitore, S., Di Martire, D., Calcaterra, D., De Vita, P., Allocca, V., 2019. Coupled ground uplift and groundwater rebound in the metropolitan city of Naples (southern Italy). Journal of Hydrology 569, 470–482.

1. Introduction

Ground deformation is a global phenomenon, acting on different space and time scales and with natural or anthropogenic genesis (Szostak-Chrzanowski & Chrzanowski, 2014; Galloway et al., 2016), the measurement and study of which have been strongly fostered in recent decades by satellite interferometric techniques. Among the wide range of land deformation types, vertical displacement of the ground, related to human-induced variations of groundwater levels, can be considered as a major threat to urbanized areas and an additional effect of inefficient aquifer management (Le Mouélic et al., 2002; Teatini et al., 2005; Gambolati et al., 2005; Ishitsuka et al., 2014). Such phenomena, usually involving wide areas, can lead to heavy socioeconomic and environmental impacts, especially if affecting urbanized and coastal areas where structures and infrastructure can be damaged even more by flood and seawater intrusion (Abidin et al., 2001; Teatini et al., 2005; Phienweij et al., 2006; Aldiss et al., 2014; Kusaka et al., 2015; Zhang et al., 2015). In these cases, stopping groundwater overexploitation can result in groundwater rebound, which, depending on the type of aquifer and water table depth, can trigger ground uplift (Colombo et al., 2017). In such a case (Madrid aquifer, Ezquerro et al., 2014; Santa Clara Valley, Chaussard et al., 2017), characterized by multiphase materials, the coupling between pore fluid and the soil skeleton can be considered elastic, thus respecting the basic model first proposed by Biot (1941). Consequences on built-up areas can be unpredictably severe if the cause-effect mechanisms have not been previously analysed by means of hydrogeological (Giudici et al., 2000; Teatini et al., 2011; Zhang et al., 2015; Gattinoni & Scesi, 2017) and geotechnical models (Tomàs et al., 2011; Tessitore et al., 2015; Chaussard et al., 2017; Pujades et al., 2017). Therefore, especially in shallow porous aquifers, integrated and effective monitoring of groundwater level and ground deformation is essential to manage inherent hazards and risks. Several studies have dealt with the importance of integrated monitoring to correctly analyse the effects of groundwater level variations on ground vertical movements (e.g., King et al., 2007; Jacob et al., 2010; Amoruso et al., 2014), which also hinged on satellite-based (InSAR) deformation measurements (Galloway & Hoffmann, 2007; Herrera et al., 2009; Cigna et al., 2012; Modoni et al., 2013; Tessitore et al., 2016; Béjar et al., 2016; Boni et al., 2016; Notti et al., 2016; Fiaschi et al., 2017; Mateos et al., 2017). In this framework, satellite technologies give breakthrough advantages, as compared to in situ measurements,

allowing scientists to accomplish regional-scale mapping and monitoring of ground deformation with lower costs (Tomás et al., 2014). In addition, satellite technologies turn out to be very useful in knowing the spatial extent and the temporal development of the phenomenon.

In the present work, ground uplift and groundwater rebound, due to strong reduction of groundwater exploitation of a multi-layered porous shallow aquifer system, have been identified, for the first time, as affecting two municipalities of the metropolitan city of Naples (Italy). The study has been based on a coupled analysis of multi-temporal hydrogeological and Differential Interferometry Synthetic Aperture Radar (DInSAR) data, covering the periods of 1989-2013 and 1993-2010, respectively.

Hydrogeological characteristic and groundwater level evolution in this area have been widely studied during the last couple decades (Allocca & Celico, 2008; 2010; Allocca et al., 2016). The principal outcome of these studies has been the recognition of a gradual recovery of piezometric levels since 1990, which was caused by a drastic reduction of groundwater exploitation (ended in 1989) of the pyroclastic-alluvial aquifer (Allocca & Celico, 2008). Since 2007, the aftermath of this groundwater rebound has caused serious problems with groundwater flooding of agricultural soils and underground structures/infrastructures (Allocca et al., 2016), such as basements, underground parks, and subway tunnels, which were built while considering the preceding phase of low groundwater level.

The hydrogeological dataset available for the 1989-2013 period has been used to obtain high-resolution, multi-temporal mapping of the groundwater levels and circulation patterns, as well as time-lapse piezometric-head increase and rising-velocity maps. DInSAR data, covering the monitoring periods of 1993-2000 and 2002-2010, were processed through a PS-InSAR technique (Ferretti et al., 2000) in the framework of the Italian First Not-ordinary Plan of Environmental Remote Sensing project (Costabile, 2010). Such data have been used to obtain cumulative ground deformation maps for the aforementioned periods that can be compared with groundwater level variations. In this paper, a hydrogeologically based interpretation of the ground deformation measurements will be presented, demonstrating that: i) the ground uplift is consistently correlated to the spatial and temporal evolution of groundwater rebound; and ii) local patterns of vertical ground movement, diverging from the general uplift trend, are controlled by other anthropogenic and natural processes.

The paper is structured as follows. Section 2 provides additional information on the geological setting of the study area, previously described in Chapter 2.1. Section 3 shows the monitoring time-series used for the analysis and the methods applied, whereas the Section 4 exposes the results obtained. Finally, in Sections 5 and 6 the discussion and conclusions are presented, respectively.

2. Further geological information about the study area

From a geological point of view (Fig. 2.12a), the study area is located in the south-central sector of the Campanian Plain, a large alluvial plain formed in the Pliocene-Pleistocene by the filling of a regional semi-graben structural depression, which originated along the western side of the southern Apennines during the opening of the Tyrrhenian Sea (Patacca et al., 1990). In detail, the study area is delimited to the west by the Phlegraean Fields volcanic system, to the east by the carbonate massif of Avella-Pizzo d'Alvano and to the south by Somma-Vesuvius volcano (Fig. 2.12a). The deep structural setting is characterized by a subsiding tectonic depression, the Sebeto Valley, set on Quaternary-active faults (Bellucci, 1994; 1998; Cinque et al., 2011; Lanari et al., 2002), such as the deeply buried Magnaghi-Sebeto fault zone (Magnaghi-Sebeto FZ) and the deeply buried faults on the northern edge of Somma-Vesuvius volcano (Figs. 2.12a and 2.12b). Locally, these fault systems, trending NE-SW and NW-SE, engender one of the most seismically active fault zones in the Neapolitan area. Moreover, they give rise to an extensional tectonic stress field and gravitational sliding around the base of the Somma-Vesuvius edifice (Figs. 2.12a and 2.12b), as evidence of ground deformation processes from seismological, mesostructural, interferometric, petrochemical and micropalaeontological data show (Bianco et al., 1998; Bruno et al., 1998; Cinque et al., 2000; Lanari et al., 2002; Bruno et al., 2003; Marturano et al., 2013).

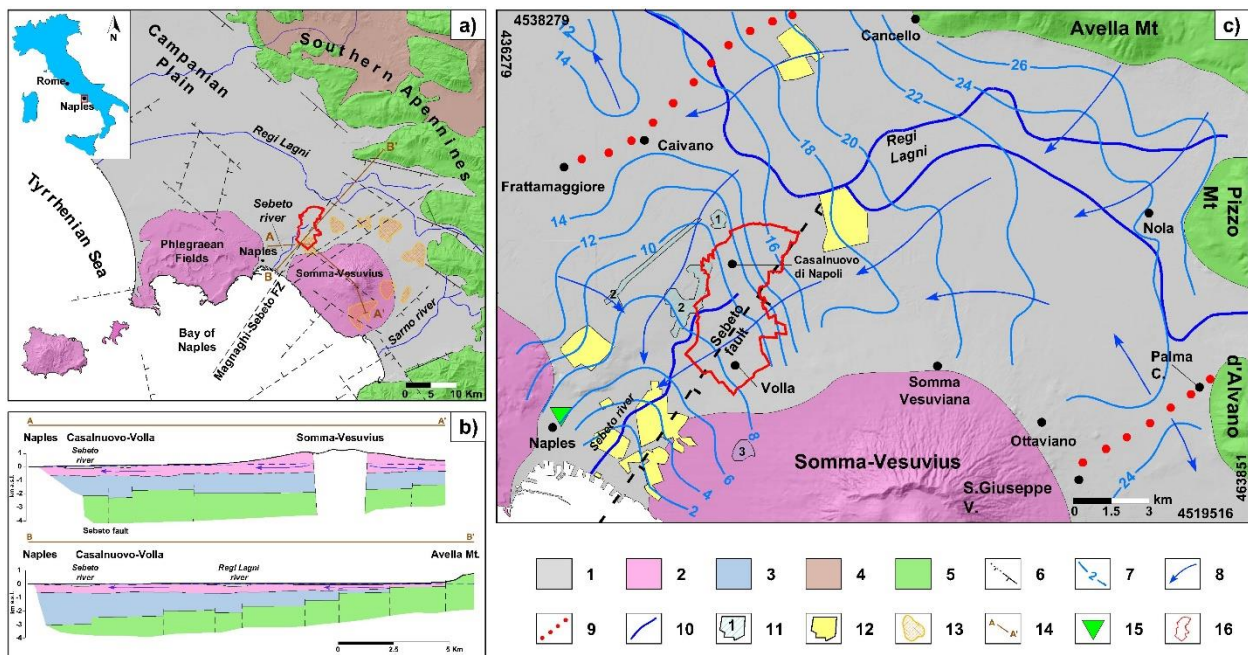


Figure 2.12 - a) Geological map of the Campanian Plain, b) Schematic geological cross-sections A-A' and B-B' (Celico et al., 1998 modified) and c) Hydrogeological map of the eastern plain of Naples. 1) Quaternary epiclastic deposits; 2) Quaternary volcanic deposits; 3) Quaternary-Miocene deposits; 4) Miocene deposits; 5) Mesozoic Apennine platform carbonates; 6) normal fault (modified after Orsi et al, 1996 and Bruno et al., 1998); 7) groundwater contour line (m a.s.l.; Esposito, 1998); 8) groundwater flow direction; 9) groundwater divide; 10) hydrographic network; 11) drinking-water well field of Acerra (1), Lufrano (2) and Ponticelli (3); 12) industrial well field; 13) ring-style subsidence area (Lanari et al., 2002); 14) cross-section lines A-A' and B-B'; 15) Rain gauge station of the San Marcellino Meteorological Observatory; 16) study area.

3. Data and methodologies

3.1 Hydrogeological data

Stratigraphic data from 148 boreholes (Fig. 2.1d) with depths variable between 10 and 60 m (Table 2.4) were collected and filed into a Geographical Information System platform. To reconstruct a 2D hydrostratigraphic model of the aquifer system (Fig. 2.4), hydraulic conductivity was estimated for each stratigraphic interval of all boreholes with Freeze & Cherry (1979) empirical relationships, which are based on grain size for porous aquifers and lithology for rock aquifers (Allocca et al., 2018). Moreover, the role of the aquifer or aquitard/aquiclude was assigned to each sediment lithofacies and geological formation. Piezometric measurements have been carried out in wells and boreholes during a long-term monitoring period from 1989 to 2013 (Table 2.4). In particular, piezometric data from 1989 to 2003 were collected during field surveys carried out by private companies, public agencies and researchers and then published in scientific or technical papers (Celico & de

Paola, 1992; Esposito, 1998; Autorità di Bacino Regionale Nord Occidentale della Campania, 2004). The most recent hydrogeological data, from 2013, came from a field measurement campaign carried out on approximately 130 wells (Fig. 2.13d) by a research project developed under an agreement signed by the Casalnuovo di Napoli and Volla municipalities (Allocca et al., 2016). Furthermore, annual rainfall data recorded by the rain gauge station at the San Marcellino Meteorological Observatory were collected from 1946 to 2013 (Table 2.4).

The hydrostratigraphic and hydrogeological database has been managed in a QGIS environment, allowing the reconstruction of multi-temporal maps of groundwater level, groundwater level change, mean velocity of groundwater level rise and groundwater circulation models by the kriging geostatistical method (Oliver & Webster, 1990). The following outcomes have been created: i) four water-table contour maps (Fig. 2.13), ii) two maps of the spatio-temporal variation of the piezometric head (Figs. 2.15a and 2.15b), and iii) two maps of the mean velocity of groundwater level rise (Figs. 2.15c and 2.15d). The piezometric head variation maps (Δh , m) were reconstructed by overlapping piezometric data for the years 1989, 2002 and 2013. Starting from these datasets, the two maps of spatio-temporal variation of the piezometric head have been calculated by a respective comparison of 2002 with 1989 and 2013 with 2002 data. Then, maps of groundwater rise velocity (m/yr) were generated by dividing the piezometric head variation observed in each of the two time-spans by the time lapse of each period.

Figure 2.13 shows groundwater level evolution in the study area for the period of 1989-2013. In 1989, (Fig. 2.13a), due to strong groundwater withdrawal of up to 5-6 m³/s (Allocca & Celico, 2008), the water-table suffered a strong piezometric lowering, reaching values as low as -2.0 m below sea level, and a deviation of the groundwater flow directions oriented towards the Lufrano well-field (Fig. 2.12c). Since 1990, as consequence of a drastic reduction in groundwater pumping, a gradual rise of the piezometric level began (Allocca & Celico, 2008; Allocca et al., 2016), which is clearly recognizable on the groundwater level maps of 1994 and 2002 (Figs. 2.13b and 2.13c). The rising groundwater level continued until 2013. The map from that year (Fig. 2.13d) is well comparable with those related to the beginning of the last century (Allocca & Celico, 2008; Allocca et al., 2016) when no groundwater pumping was being carried out, showing an almost complete recovery of groundwater levels. Moreover, the piezometric contour pattern shows that groundwater circulation converges towards the drainage axis represented by the Sebeto River and its tributaries (Cozzone and Volla rivers, see Fig. 2.1c).

Table 2.4 - Principal sources of hydrostratigraphic, hydrogeological and meteorological data. n.d.: not detected.

Type	Total number	Density (No/km ²)	Monitoring period	Use	Depth range (m)	Screen typology	Source
Wells	28	1.95	March, 1989	Drinking and Agricultural	40-60	Open at bottom	Celico & de Paola (1992)
Wells	24	1.67	February, 1994	Industrial and Agricultural	40-70	Open at bottom	Esposito (1998)
Wells	30	2.09	February, 2002	Industrial and Agricultural	40-70	n.d.	Autorità di Bacino Nord Occidentale della Campania (2004)
Wells	108	7.55	December, 2013	Domestic and Agricultural	30-60	Open at bottom	Allocca et al. (2016)
Boreholes	148	10.48	\	\	10-60	Open at bottom	Bellucci (1994); Allocca et al. (2016)
Meteorological station	1	\	1946-2013	\	\	\	San Marcellino Meteorological Observatory

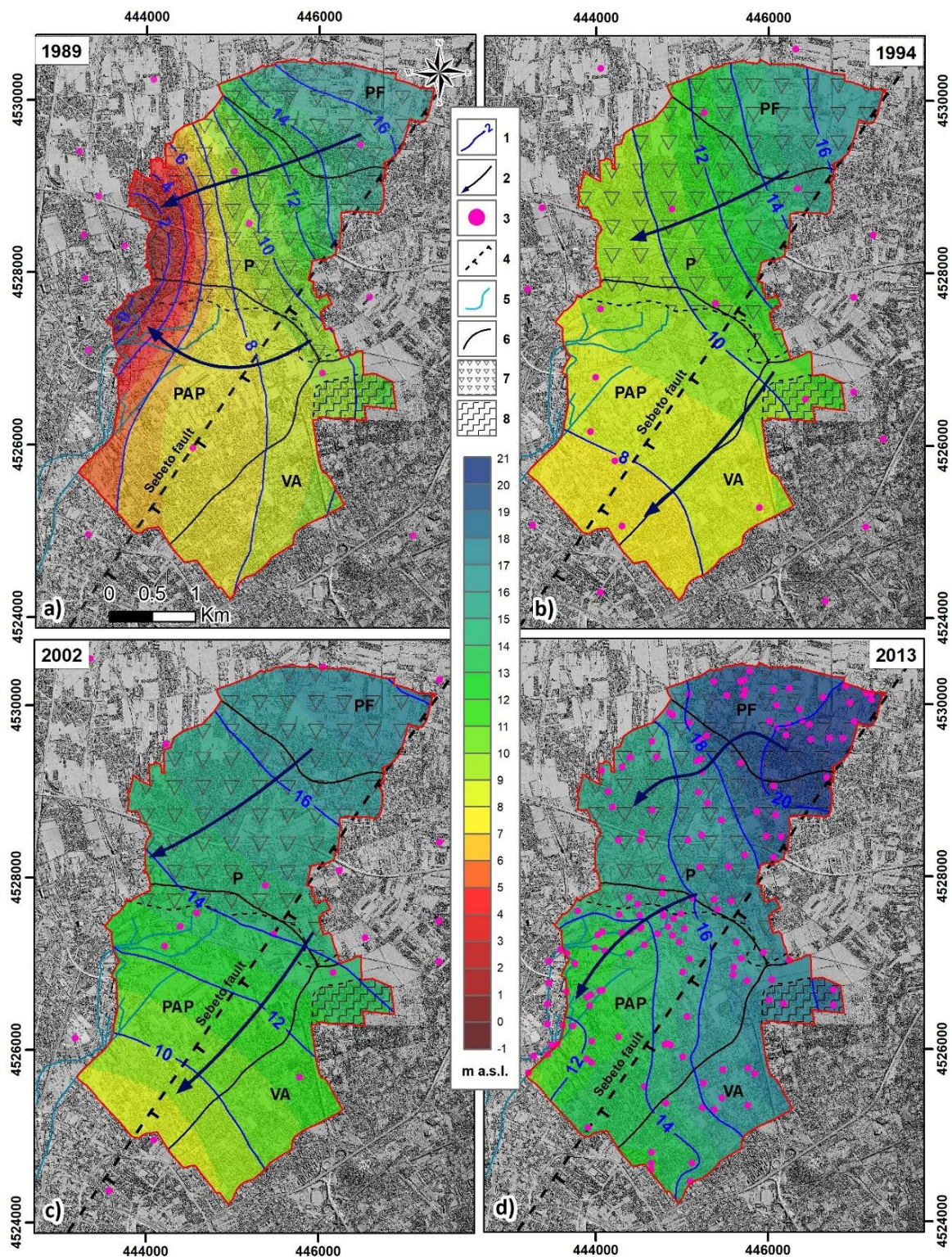


Figure 2.13 - Groundwater level maps for the years: a) 1989; b) 1994; c) 2002; d) 2013. 1) groundwater contour line (m a.s.l.); 2) groundwater flow direction; 3) monitoring network; 4) buried deep Sebeto fault; 5) groundwater drainage network; 6) hydrogeological complex boundary; 7) sector with buried CI; 8) sector with buried lava rocks.

3.2 DInSAR data

DInSAR data consist of ground deformation measurements for each satellite acquisition date projected along the Line of Sight (LoS) direction, which allows displacement maps, profiles and time series (TS) to be produced.

In the present work, SAR data gathered and processed by the Italian First Not-ordinary Plan of Environmental Remote Sensing project have been used under a specific agreement with the Italian Ministry of Environment (MATTEM). Specifically, 139 images taken by the ERS-1/2 (67 and 72 images in ascending and descending geometry, respectively) and 92 by the ENVISAT satellite (52 and 40 images in ascending and descending geometry, respectively), covering the monitoring periods of 1992-2000 and 2002-2010 (Table 2.5), were processed through the PS-InSAR technique (Ferretti et al., 2000). A cumulative LoS-projected displacement varying between -100 mm and $+50$ mm (1993-2000) and between -120 mm and $+40$ mm (2002-2010) was measured (Table 2.5).

DInSAR mean velocity maps are shown in Figure 2.14, where for the 1993-2000 period, a general uplift (approximately 1.6 ± 1.1 mm/yr on average) in the northern sector of the area and an extended subsidence in the southern one (approximately 3 ± 12 mm/yr on average) were observed. Then, for the second observation period (2002-2010), a drop in the displacement rates for both sectors was observed. Specifically, the maximum uplift rate (projected along the LoS) of approximately 1 cm/year, detected in the first monitoring window by ERS satellite, decreased by approximately 50% in the second time-span as is also confirmed by the ENVISAT measurements. A small area affected by a localized subsidence with a maximum mean rate of -12.4 mm/year was also recognized in the 2002-2010 period (Figs. 2.14c and 2.14d).

Table 2.5 - DInSAR LoS measurement statistics referred to the whole area.

	ERS asc	ERS desc	ENVI asc	ENVI desc	
	Jan 1993- Dec 2000	Nov 1992- Dec 2000	Nov 2002- Aug 2010	June 2003- June 2010	
Max velocity	6.4	8.7	3.6	5.4	mm/yr
Mean velocity	0.5 ± 1.8	1.0 ± 1.7	-0.6 ± 1.2	-0.1 ± 1.3	mm/yr
Min velocity	-11.4	-10.8	-12.7	-12.4	mm/yr
Max deformation	37.6	49.6	33.6	41.9	mm
Mean deformation	-1.5 ± 16.5	-7.7 ± 18.2	-5.8 ± 11.7	-1.1 ± 11.8	mm
Min deformation	-95.6	-104.2	-123.3	-99.3	mm

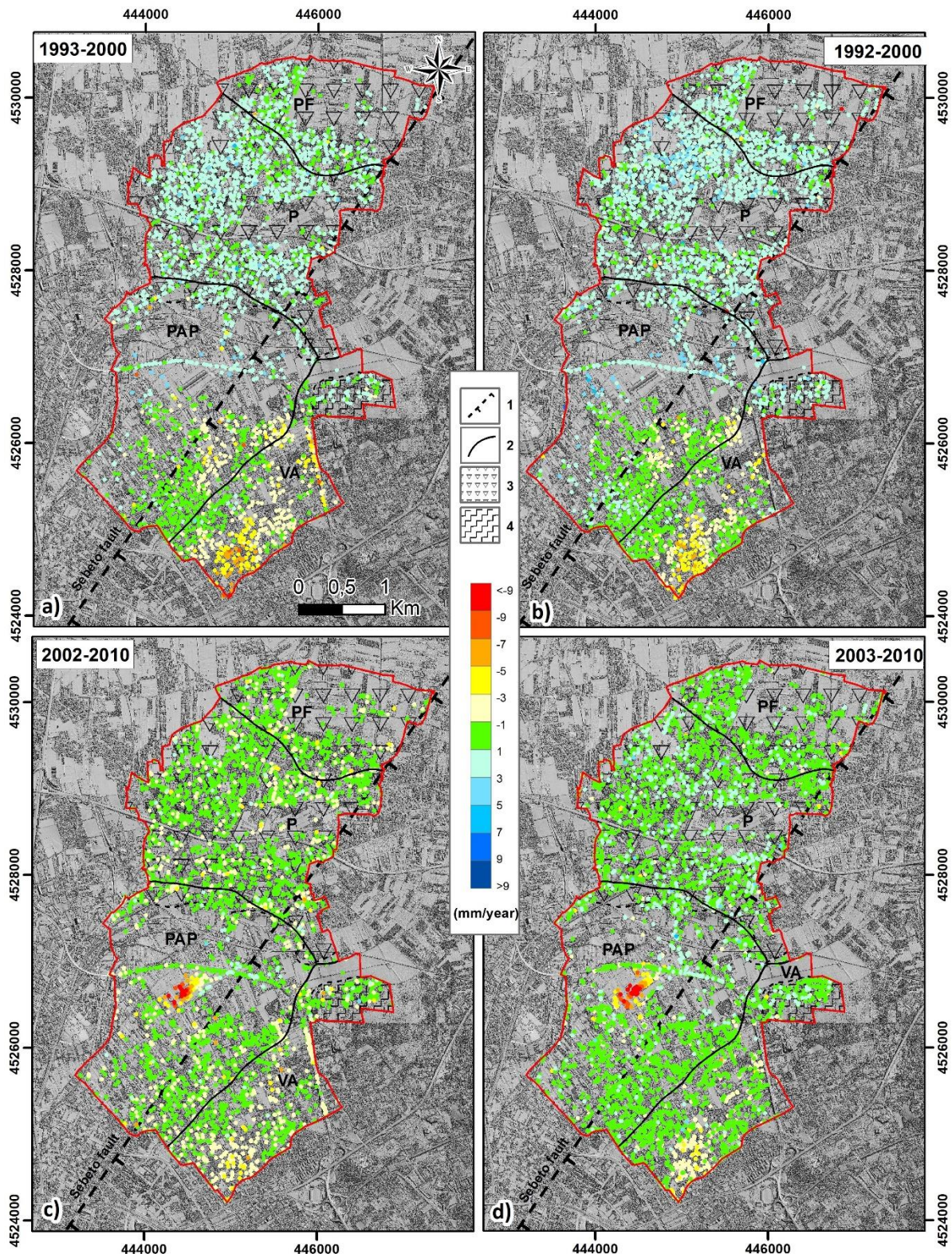


Figure 2.14 - LoS velocity maps (mm/yr) of the study area. **a)** ERS-1/2 data in ascending geometry; **b)** ERS-1/2 descending; **c)** ENVISAT ascending; **d)** ENVISAT descending. 1) Buried deep Sebeto fault; 2) hydrogeological complex boundary; 3) sector with buried CI; 4) sector with buried lava rocks.

4. Results

4.1 Groundwater rebound assessment

Post-pumping groundwater level increments (Δh) (Figs. 2.15a and 2.15b) and groundwater rise velocity maps (v) (Figs. 2.15c and 2.15d) have been reconstructed. The results show that groundwater rebound, following the interruption of pumping, was widespread throughout the study area in the period from 1989 to 2013. In particular, for the 1989-2002 period (Phase 1 in Fig. 2.15a), the water table showed a general rise, although spatially variable, ranging from a minimum of 0.5 m to a maximum of 14.0 m. The groundwater rebound with the highest magnitude (approximately 14 m) was recorded in the west-central zone of the study area (western side of P and PAP sectors, in Fig. 2.15a), closer to the Lufrano well field (Fig. 2.12c) where pumping ceased in 1989 (Fig. 2.7). Inversely, the minimum piezometric head increments (approximately 1 m) were observed in the southern sector where groundwater levels are constrained by the hydraulic potential boundary of the Sebeto River and its tributaries as well as by the greater distance from the Lufrano well field.

Water table increment values for the 2002-2013 period (Phase 2 in Fig. 2.15b) highlight a reduction in the groundwater rise, with values ranging from a low of 0.0-1.0 m to a peak of 6.0 m. The highest values were recorded in the south-eastern side, in an area distant from the Lufrano well field, whereas the minimum piezometric head increments were observed in the west-central zone (western side of P and PAP sectors, in Fig. 2.15a), which is close to the Lufrano well field.

Furthermore, groundwater rise velocity maps (Figs. 2.15c and 2.15d) reveal that rates as high as 1.0 m/yr were observed in the 1989-2002 period (Phase 1). The highest velocities (even higher than 2.2 m/yr), occurring between 1989 and 1994 (data not shown), were observed in the west-central portion of the study area (Fig. 2.15a), close to the deactivated Lufrano well field.

In the period spanning from 2002 to 2003 (Phase 2), groundwater rise velocity decreased, with maximum rates of approximately 0.6 m localized in the north-eastern sector of the study area.

Comparing the mean groundwater rise velocities of the two phases, a general deceleration of approximately 30% was registered. These results allow us to conclude that the rising groundwater levels, recorded from 1989 to 2013, can be considered to be

groundwater rebound caused by the drastic reduction of groundwater pumping in the surroundings of the study area (Fig. 2.12c). Furthermore, the spatio-temporal variability of the groundwater rebound was recognized to be strongly dependant on the distance from the abandoned Lufrano well field. In addition, given the absence at a local scale of significant changes in annual rainfall regime (Fig. 2.7), it is possible to consider (Allocca et al., 2017) the “precipitation variable” as insignificant when explaining the groundwater rise observed, which is consistent with the downward sloping trend of the mean annual precipitation index observed at a regional scale (De Vita et al., 2012).

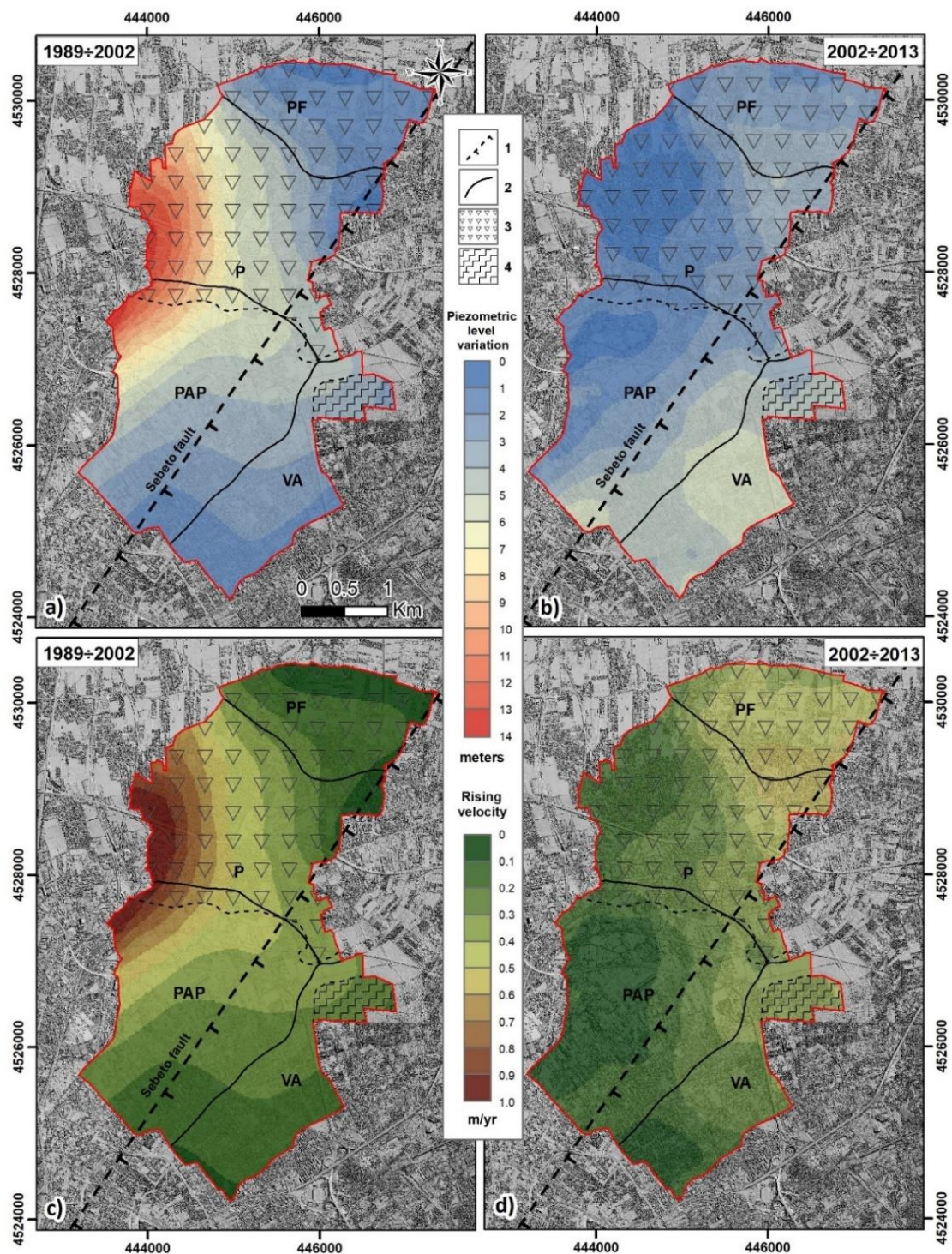


Figure 2.15 - Piezometric level variation (m) (a and b) and groundwater rising velocity (m/yr) (c and d) in the periods 1989-2002 (a and c) and 2002-2013 (b and d). 1) buried deep Sebeto fault; 2) hydrogeological complex boundary; 3) sector with buried CI; 4) sector with buried lava rocks.

4.2 Satellite-based deformation maps

The cumulative LoS displacement maps (Displ) of the study area for the periods of 1993-2000 and 2002-2010 have been reconstructed (Figs. 2.16a and 2.16b). All the DInSAR measurements in ascending geometry have been interpolated through the Inverse Distance Weighted (IDW) technique to obtain spatially continuous maps that have been very useful for analysing the spatial variability of the phenomenon and profiles of deformation along assigned alignments.

The interpolated maps obtained from the ERS and ENVISAT data (in the ascending acquisition mode) for the whole study area have a mean cumulative LoS deformation of -0.9 ± 13.4 mm and of -6.2 ± 9.2 mm, respectively.

As it is possible to observe in Figure 2.16a, a widespread ground uplift can be observed in the northern and north-central portions of the study area, reaching the highest magnitude in its upper left corner (approximately 30 mm along the LoS; see also Table 2.5). Such observation matches well with the post-pumping hydrogeological changes observed (Figs. 2.15a and 2.15b). Furthermore, due to the slowing of the groundwater level rise in the period 2002-2010, the whole ground uplift seems to have been reduced in intensity in the same period (<15 mm/yr).

Several subsidence phenomena were recognized (Fig. 2.16) that affect the southern sector of the study area where composite interactions with other natural and anthropogenic factors occur.

The first phenomenon, identified in the southern margin of the study area from both the ERS and ENVISAT satellites, has a maximum cumulative LoS deformation, respectively, of -90 mm and -40 mm (ERS and ENVISAT ascending). Accordingly, such subsidence seems to have registered as a decrease of approximately 50% across the two time-spans, as also observed by Bonano et al. (2012). This local land subsidence is due to natural processes, attributable to volcano-tectonic dynamics recognized as occurring around the Somma-Vesuvius volcano (Lanari et al., 2002).

A more recent subsidence area has been identified for the 2003-2010 period from the ENVISAT satellite (Fig. 2.16b) and has turned out to be related to construction in the 2006-2008 period of the CAAN (Agri-Food Centre of Naples), a large structure extending over approximately 362.000 m² (Fig. 2.16b) used as a wholesale market and considered to be one of the largest in Italy.

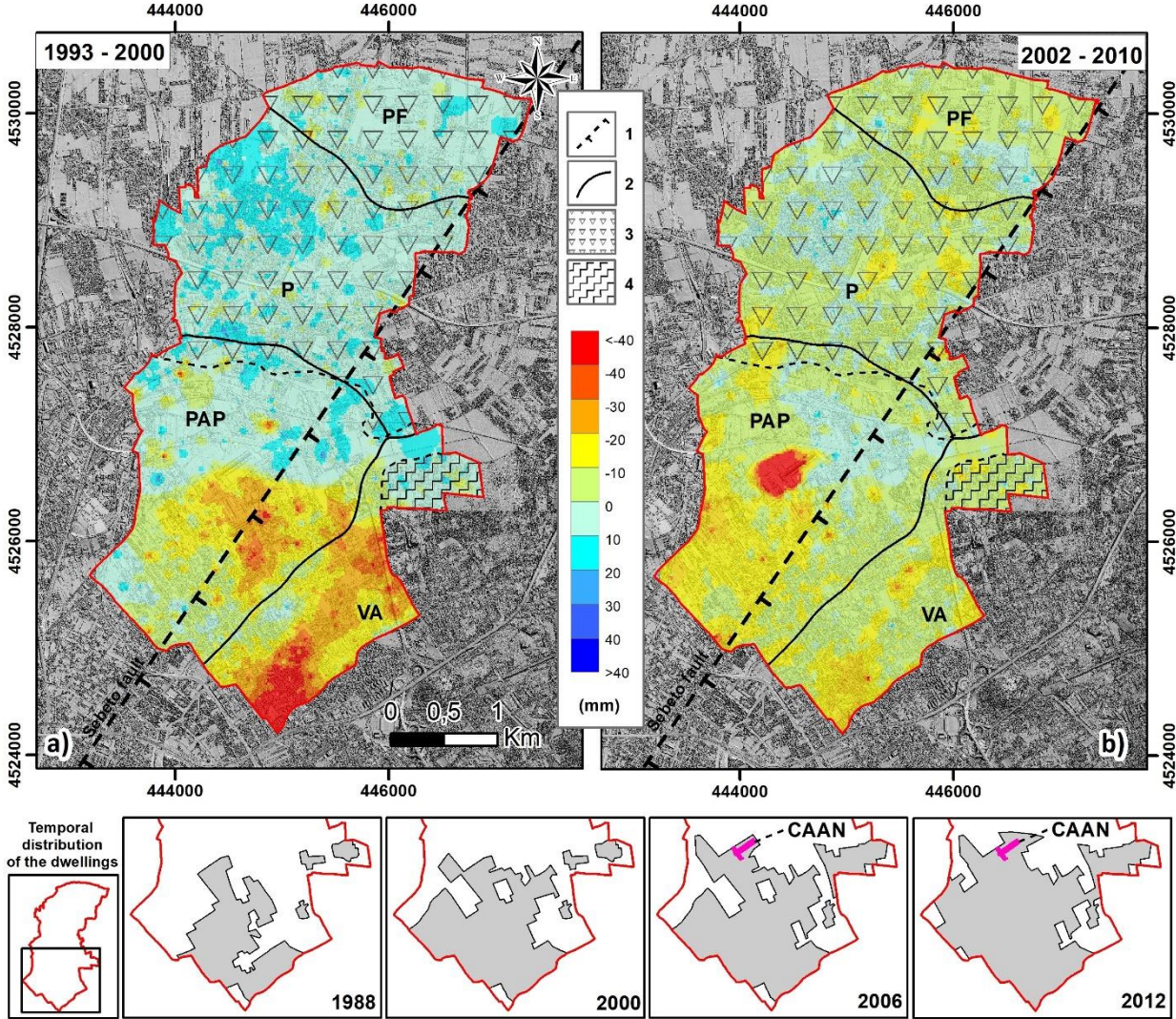


Figure 2.16 - LoS cumulated deformation maps (mm) and of the study area for the periods: (a) 1993-2000; (b) 2002-2010. Bottom graphs: a focus on the temporal distribution of the dwellings between 1988 and 2012 for the southern sector of the study area. 1) Buried deep Sebeto fault; 2) hydrogeological complex boundary; 3) sector with buried CI; 4) sector with buried lava rocks.

5. Discussion

By comparing the trends of groundwater level rise, ground deformation and annual precipitation (Fig. 2.17) during the post-pumping period (1989-2013), several interesting correlations have been observed. Thus, a hydrogeologically based interpretation of the deformation mechanisms has been proposed, highlighting the hydrostratigraphic factors that control rates of ground displacement.

For the northern sector of the study area (PF graph, in Fig. 2.17), a positive global trend for both groundwater level rise and ground uplift is recognizable, with a piezometric variation of up to approximately 7 m observed from 1989 to 2013 (Figs. 2.15a and 2.15b) and a deformation of up to +20 mm (Figs. 2.16a and 2.16b) recorded in the period from 1993 to 2010. The link between the observed phenomena can be ascribed, reasonably, to the elastic rebound of the aquifer under the unloading of effective stress caused by the increase of pore pressure, which is related to the recovery of groundwater levels in the unconfined shallow aquifer (graph PF, Fig. 2.17; Fig. 2.1d). This interpretation is known as pore-elastic rebound of an aquifer (Biot, 1941; Waltham, 2002; Ishitsuka et al., 2017) and originated from the relaxation of elastically compressed aquifers when pore-water pressure is recovered. It is also consistent with experimental results of water injection programmes carried out at the subsided site of the Wilmington oilfield in California (Allen & Mayuga, 1969; Teatini et al. 2011), although other authors (Vilardo et al., 2009) interpreted this phenomenon as an increase in pore-water pressure in agricultural soils induced by flood episodes from artificial channels and tributaries of Regi Lagni river, in the Somma-Vesuvius northern sector (Figs. 2.12a and 2.12c).

Furthermore, in the north-central sector (P graph, Fig. 2.17), similar positive trends for both phenomena can be recognized. However, although in this sector there has been a piezometric level rise of approximately 14.5 m from approximately 1.0 to 15.0 m a.s.l. (Figs. 2.13, 2.15a and 2.15b), the ground uplift measured is about +40 mm (Fig. 2.16). In this case, the smallest ground uplift rate observed in the north-central sector can be related to the involvement of groundwater rebound, mainly in the deep semi-confined tufaceous aquitard (Figs. 2.4 and 2.17), which it is characterized by a lower elastic deformability than incoherent pyroclastic-alluvial deposits. Such observation confirms that ground uplift is not just related to rising groundwater levels, but also dependent on other hydrogeological and geotechnical factors (i.e., aquifer type, permeability heterogeneities, elastic properties).

In the southcentral sector (graph PAP, in Fig. 2.17), the piezometric level rise was approximately 5.0 m, recovering the pyroclastic-alluvial-palustrine aquifer (Figs. 2.4 and 2.16), while heterogeneous ground deformation behaviour was observed by: a) ground uplift of about +25 mm in the northern margin related to piezometric level rise; and b) land subsidence of about –80 mm on average along the southern sector due to volcano-tectonic dynamics of Somma-Vesuvius or settlement and consolidation caused by new local buildings (Figs. 2.16 and 2.17). The ground uplift resulting from pore-water pressure increase and pore-elastic rebound would have probably affected a more extensive area if there was no interaction with other contrasting phenomena. In fact, beyond the human-induced ground subsidence resulting from an intense urbanization in the 1990s (Fig. 2.16a) and the construction of the CAAN (Fig. 2.16b) during the 2006-2008 period, another natural process affects the southern margin of the PAP sector. In fact, according to Lanari et al. (2002) this local ground subsidence is characterized by a peculiar annular shape (Terada, 1929) occurring around the northern foot of Somma-Vesuvius (Fig. 2.12a). This peculiar style of ground deformation is caused by gravitational loading of the volcanic edifice coupled with extensional tectonic stress along Quaternary-active faults, such as the Sebeto deep fault (Fig. 2.12), which showed evidence of activity in the late Pleistocene-Holocene (Cinque et al., 2000). This phenomenon is analysed in the VA graph (Fig. 2.17) where despite the positive trend of groundwater levels equal to approximately 6.0 m, a continuous subsidence of up to –85 mm was registered.

Finally, Figure 2.17 clearly shows that the significant upward trend in the piezometric level and vertical ground deformation observed in the 1989-2002 period was not triggered by a change in the local precipitation's regime since this does not display any substantial change during the same interval of time.

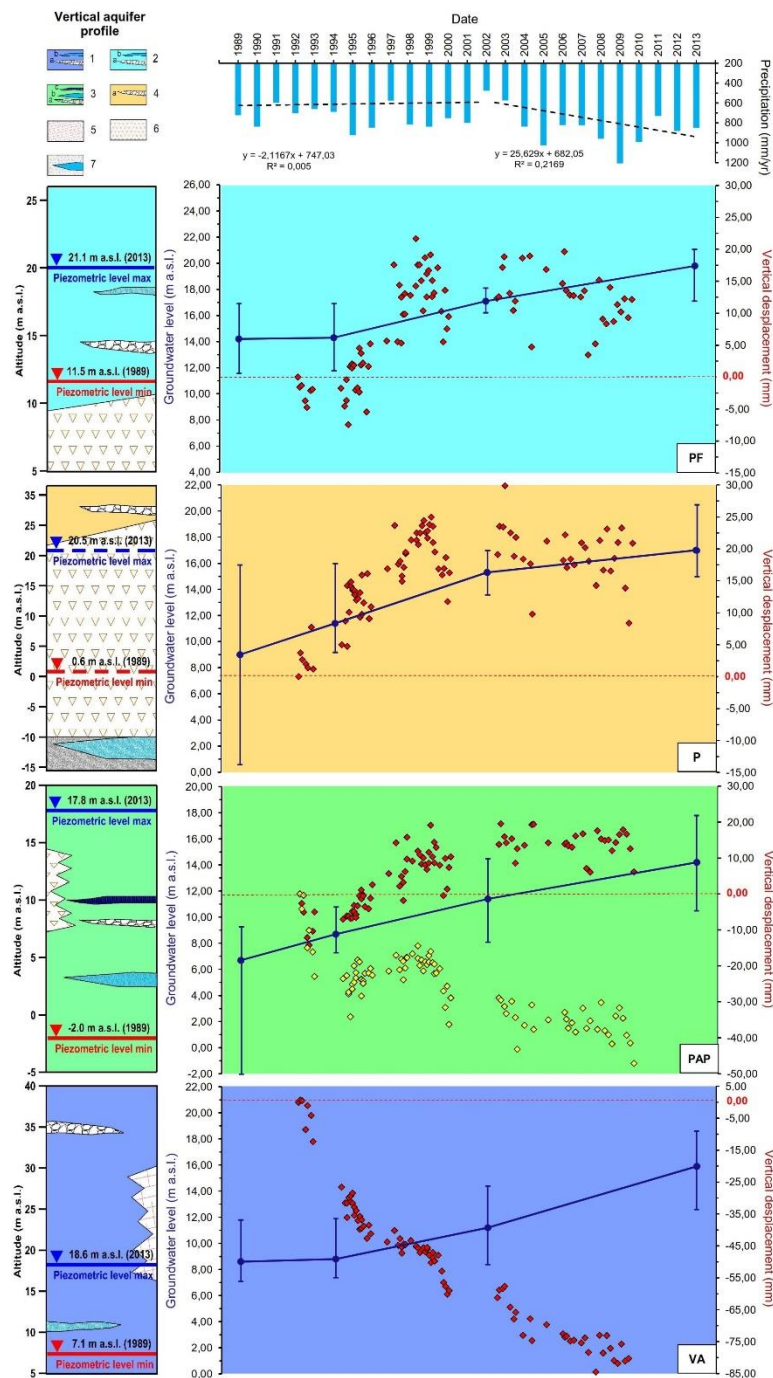


Figure 2.17 - Comparison between annual precipitation, representative trends of groundwater levels and vertical ground deformations for four sectors of study area (1989-2013). In the graphs, blue lines indicate the average piezometric levels, for the whole sector, while the whiskers the minimum and the maximum ones. 1) VA complex (sandy silts) with interbedded: a) pumiceous lapilli horizons; b) sandy horizons; 2) PF complex (sands, silts and sandy silts) with interbedded: a) pumiceous lapilli horizons; b) sands and pumiceous lapilli horizons; 3) PAP complex (sandy silts, silts and clays) with interbedded: a) pumiceous lapilli horizons; b) sands, paleosols, and peat levels, c) marshy clayey-sands and clayey-silts; 4) P complex (silty sands) with interbedded: a) pumiceous-scoriaceus lapilli horizons; 5) Somma-Vesuvius lavas; 6) lithoid (a) and incoherent (b) CI tuff; 7) deep semi-confined pyroclastic-alluvial aquifer (silty sands and sands).

6. Conclusions

Integrated use of hydrogeological and DInSAR data has allowed the investigation of coupling between groundwater rebound and ground deformation in the multi-layered pyroclastic-alluvial aquifer of the Casalnuovo di Napoli and Volla municipalities (metropolitan city of Naples, Italy). By means of approximately 20 years of hydrogeological and DInSAR monitoring data covering the period of 1993-2010, the spatio-temporal evolution of ground deformation has been analysed for the period following the strong reduction of groundwater pumping.

Hydrogeological monitoring data show that groundwater level rise occurred extensively throughout the study area in the 1989-2013 period (Figs. 2.15a and 2.15b) with a maximum amplitude of 16 m observed in the west-central sector, where the highest velocities of groundwater rise have been recorded with a magnitude of up to approximately 1.0 m/yr (Figs. 2.15c and 2.15d).

DInSAR data show general ground uplift during the time span of 1993-2010 (Figs. 2.16a and 2.16b). Such a phenomenon has turned out to have a magnitude of approximately 40 mm on average, except for the southern sector of the study area where some local natural and human-induced subsidence (with a maximum magnitude of 130 mm) have been identified.

Comparisons between trends of groundwater level and ground displacement (Fig. 2.17) indicate that the ground uplift is linked to a probable poro-elastic rebound mechanism in the aquifer system. Such a phenomenon was caused by piezometric level rise following groundwater pumping interruption, related effective stress unloading and deformation recovery.

The obtained results advance the knowledge of the complex and often unforeseen interactions between human actions and geohazards, allowing for more effective urban planning. In particular, the study area is a relevant example of urban planning that was carried out by taking into account a non-natural groundwater level condition, kept low for decades by strong groundwater exploitation. A consequence of this difficult-to-predict scenario is groundwater flooding hazards among other geohazards affecting the study area, such as those due to coastal, fluvial, volcanic and earthquake phenomena. Another related hazard to be studied are the effects of the interaction between groundwater and foundations on the stability of buildings, which were designed for low groundwater table conditions. In conclusion, the results of this study open new

perspectives in the management of such a type of geohazard, which would need the implementation of an appropriate coupled hydro-mechanical model for correct risk management.

2.3

Variation of groundwater contamination related to groundwater rebound in the eastern plain of Naples

Coda S.^{1*}, De Tommaso G.², Iuliano M.², Jantáková N.³, Villani R.¹, Allocca V.¹

¹ Department of Earth Science, Environment and Resources, University of Naples Federico II, Naples, Italy

² Department of Chemical Sciences, University of Naples Federico II, Naples, Italy

³ Department of Hydrogeology, Faculty of Natural Sciences, Comenius University in Bratislava, Bratislava, Slovakia

*Corresponding author: silvio.coda@unina.it

Extended Abstract

Groundwater has always played a strategic role in the development of human activities. Therefore, its appropriate management represents a crucial node in order to avoid aquifer overexploitation, which can lead to deterioration of groundwater qualitative and quantitative status.

In 1980s, the pyroclastic alluvial aquifer of the eastern plain of Naples has been an example of mismanagement. At the end of the 80s, the withdrawals for drinking, industrial and agricultural purposes reached a maximum value of about 6 m³/s, exceeding the mean annual water budget of the aquifer of approximately 2,65 m³/s (Allocca & Celico, 2008). This overexploitation has caused the progressive decline of piezometric levels reaching, locally, lowering up to 15 m and extraction of highly mineralized waters coming from deeper parts of the aquifer characterized by slow circulation and redox conditions, with consequent increase in Fe, Mn and fluoride concentrations of natural origin. In addition, high NO₃ values were found in water, coming from the use of nitrogen fertilizers in agricultural activity as well as from urban and industrial waste (Celico et al., 1997). High contamination values of groundwater caused the drastic reduction of drinking water abstractions and groundwater pumping for industrial and rural use, the latter favoured also by deindustrialization processes and

land use change, from rural to semiurban, of the study area. Consequently, since 1990 the groundwater rebound phenomenon has occurred (Allocca & Celico, 2008), which has had strong socio-economic and environmental impacts. In the last decades, the piezometric level rising has caused groundwater flooding in subway tunnels, buildings, agricultural land and archaeological sites, as well as ground uplift with consequent damage to structures and infrastructures (Coda et al., 2019a).

The present study aims to investigate, for the 1992-2017 period, a third effect of groundwater rebound in addition to flooding and uplift, that is the variation of contamination from Fe, Mn, NO₃ and fluoride in an experimental area of 14 km² in the eastern plain of Naples.

The study was carried out by: i) sampling of water on 15 wells and chemical analyses to determine the concentrations of Fe, Mn, NO₃ and fluorides, in November 2017; ii) comparison between piezometric levels in the period 1989-2017 and the areal distribution of the aforementioned contaminants in the period 1992-2017, to identify the variations in relation to the increase in piezometric levels.

The preliminary results show a strong contamination of groundwater, both natural and anthropogenic, with values of Fe, Mn, fluorides and NO₃ exceeding the thresholds imposed by Italian legislation for human consumption. Nevertheless, the comparison with historical hydrogeochemical data shows a slight improvement in natural contamination (Fe, Mn and fluorides), as proof of the reactivation of a faster circulation in the aquifer deriving from the increase in saturated thickness. The reduction of the vadose zone has favoured the achievement of groundwater contaminants coming from the surface, in fact the concentrations of nitrates, coming mainly from the agricultural activity in the study area, have strongly increased.

In conclusion, from these results emerge the need to implement an appropriate hydrogeological and hydrochemical monitoring of the aquifer, to preserve and improve the quality of this strategic water resource.

Key words: groundwater rebound, aquifer deformation, ground uplift, subsidence hydrogeology, DInSAR, Naples, Italy.

Coda, S., De Tommaso, G., Iuliano, M., Jantáková, N., Villani, R., 2019. Variation of groundwater contamination related to groundwater rebound in the eastern plain of Naples. Proceedings of the XI Convegno Nazionale Dei Giovani Ricercatori in Geologia Applicata. 19-21 September 2019, Matera (Italy).

1. Data and methodologies

To analyze the piezometric and hydrochemical variations in the period 1993-2017, the only historical series available in the scientific literature (relative to the years 1993 and 2003) and the data coming from a hydrogeological campaign carried out in 2017 were used.

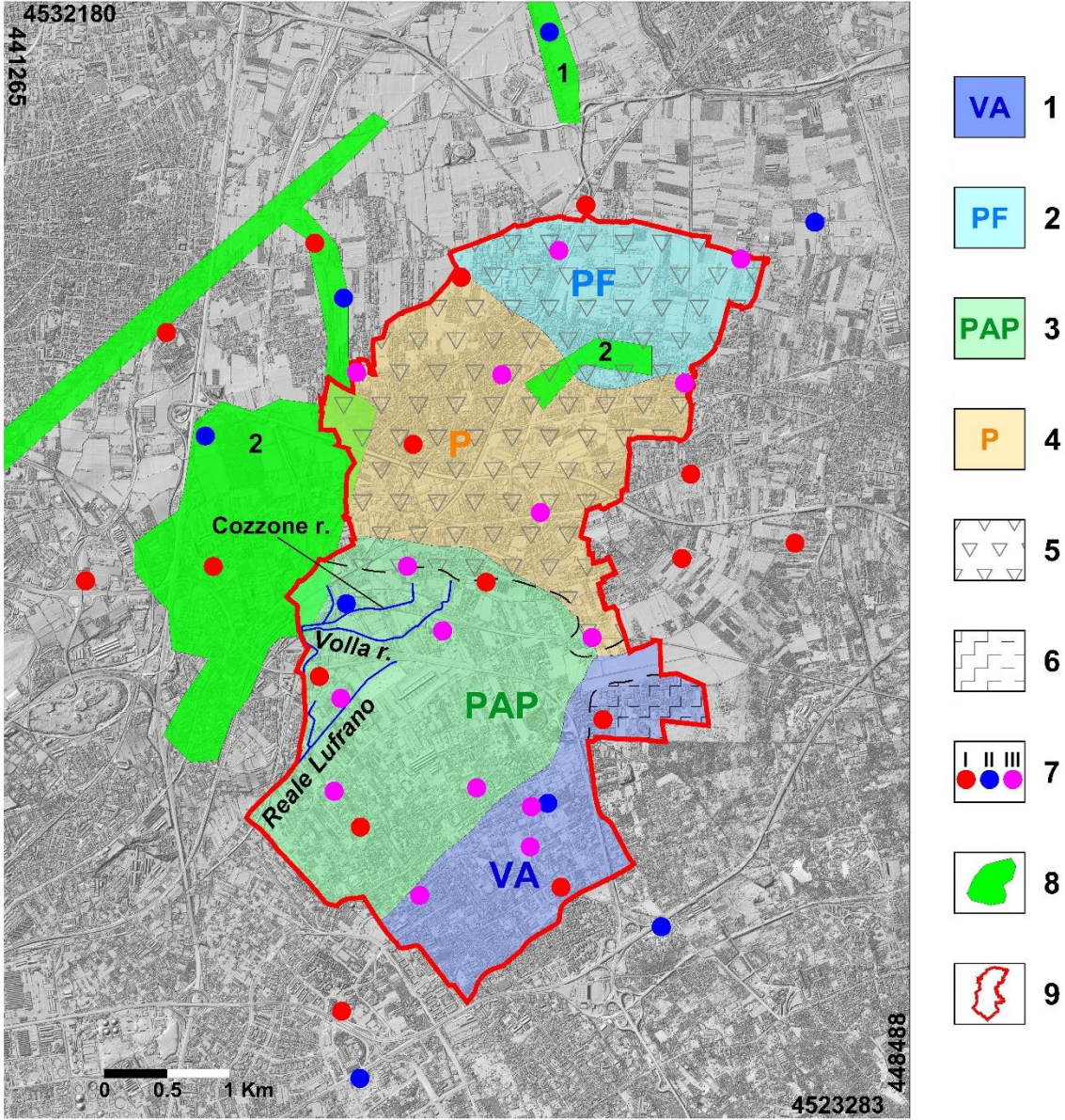


Figure 2.18 – Hydrogeological complexes and ubication of groundwater samples. 1) VA complex; 2) PF complex; 3) PAP complex; 4) P complex; 5) Sector with buried Campanian Ignimbrite (CI); 6) Sector with buried lava rocks; 7) 1993 (I), 2003 (II) and 2017(III) sampling networks; 8) Acerra (1) and Lufrano (2) well-fields; 9) study area.

1.1 Piezometric data

- 1993's piezometric contour map: Celico et al, 1997; Esposito 1998;
- 2003's piezometric contour map: AdB, 2004;
- 2017's piezometric head of 101 wells included in a monitoring network (Coda et al, 2019a).

2017's data have been interpolated through Kriging geostatistical method to elaborate a piezometric contour map.

1.2 Hydrochemical data

- 1993's isoconcentration contour map of nitrates, fluorides, Fe and Mn: Celico et al 1997;
- 2003's hydrochemical analysis of 8 groundwater samples (Fig. 2.18 - AdB, 2004);
- 2017's hydrochemical analysis of 15 groundwater samples taken from monitoring network wells (Fig. 2.18).

2003' and 2017' data have been interpolated through Natural Neighbor method to obtain isoconcentration contour maps of nitrate, fluoride, Fe and Mn.

2. Results

2.1 Piezometric levels variation

Results show a progressive increase of piezometric head for the whole period considered (Fig. 2.19). The entity of the groundwater levels increase is summarized in Table 2.6. The maximum median value of piezometric head is 16,4 m a.s.l., reached in 2017, increasing of about 4,4 m from 1993 to 2003 and 2,8 m from 2003 to 2017. The rising rate decrease from 0,44 m/yr (in the first period) to 0,20 m/yr (in the second period). This deceleration of groundwater rebound phenomenon is in according to previous studies conducted in the same area (Coda et al., 2019a).

Table 2.6 - Piezometric head variation.

Year	Piezometric head (m a.s.l.)		
	min	max	median
1993	6,7	16,9	9,4
2003	8,1	18,1	13,8
2017	10,4	21,5	16,4

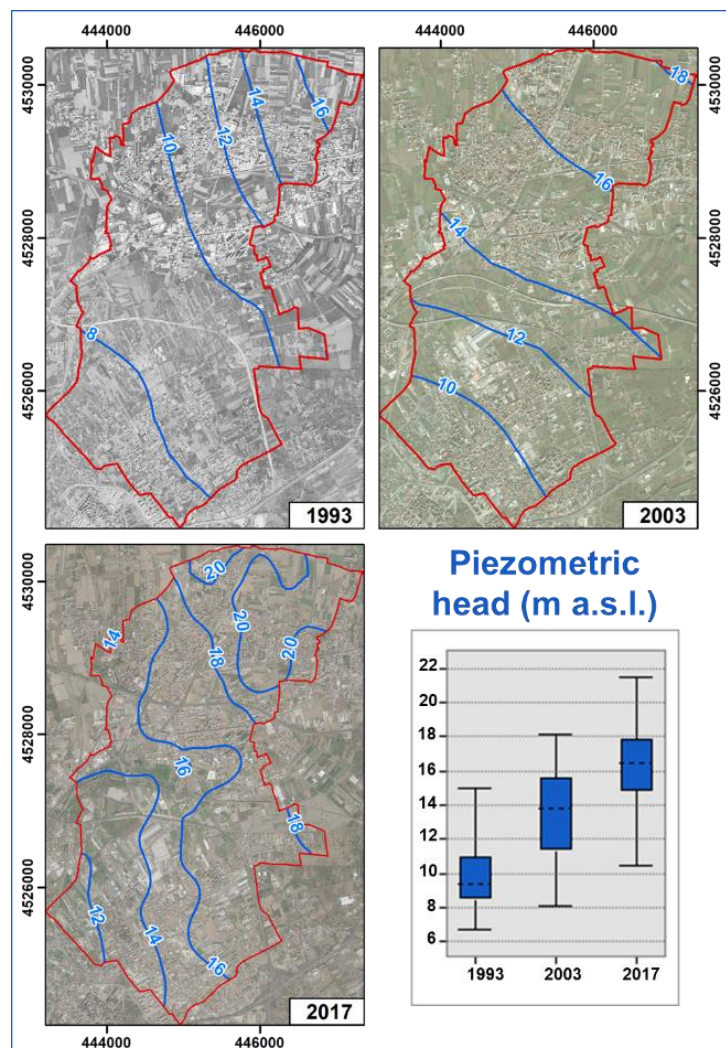


Figure 2.19 – Piezometric contour maps and box plot.

2.2 Variation of contamination

In the period 1993-2017, the hydrochemical characteristics of groundwater have undergone two different trends of variation in the compounds considered. For the nitrates (Tab. 2.7 and Fig. 2.20a), it was recorded a median increment of about 25% (~20 mg/l). Instead fluorides, Fe and Mn occurred an inverse trend (Tab. 2.7 and Figs 2.20b, 2.20c and 2.20d) with a median value of decrement of about 33% (1 mg/l), 67% (0,04 mg/l) and 50% (0,01 mg/l) respectively. The results of the raster analysis are summarized in Table 2.7.

Table 2.7 - Hydrochemical variation.

Year	Nitrate (mg/l)			Fluoride (mg/l)		
	min	max	median	min	max	median
1993	33,7	134,5	88,1	1,9	3,3	3,0
2003	31,2	152,0	114,8	2,0	3,5	3,0
2017	16,5	156,5	109,8	0,9	3,7	2,0
Year	Fe (mg/l)			Mn (mg/l)		
	min	max	median	min	max	median
1993	0	0,28	0,06	0	0,10	0,02
2003	0,03	0,18	0,09	0	0,04	0,01
2017	0	0,05	0,02	0	0,05	0,01

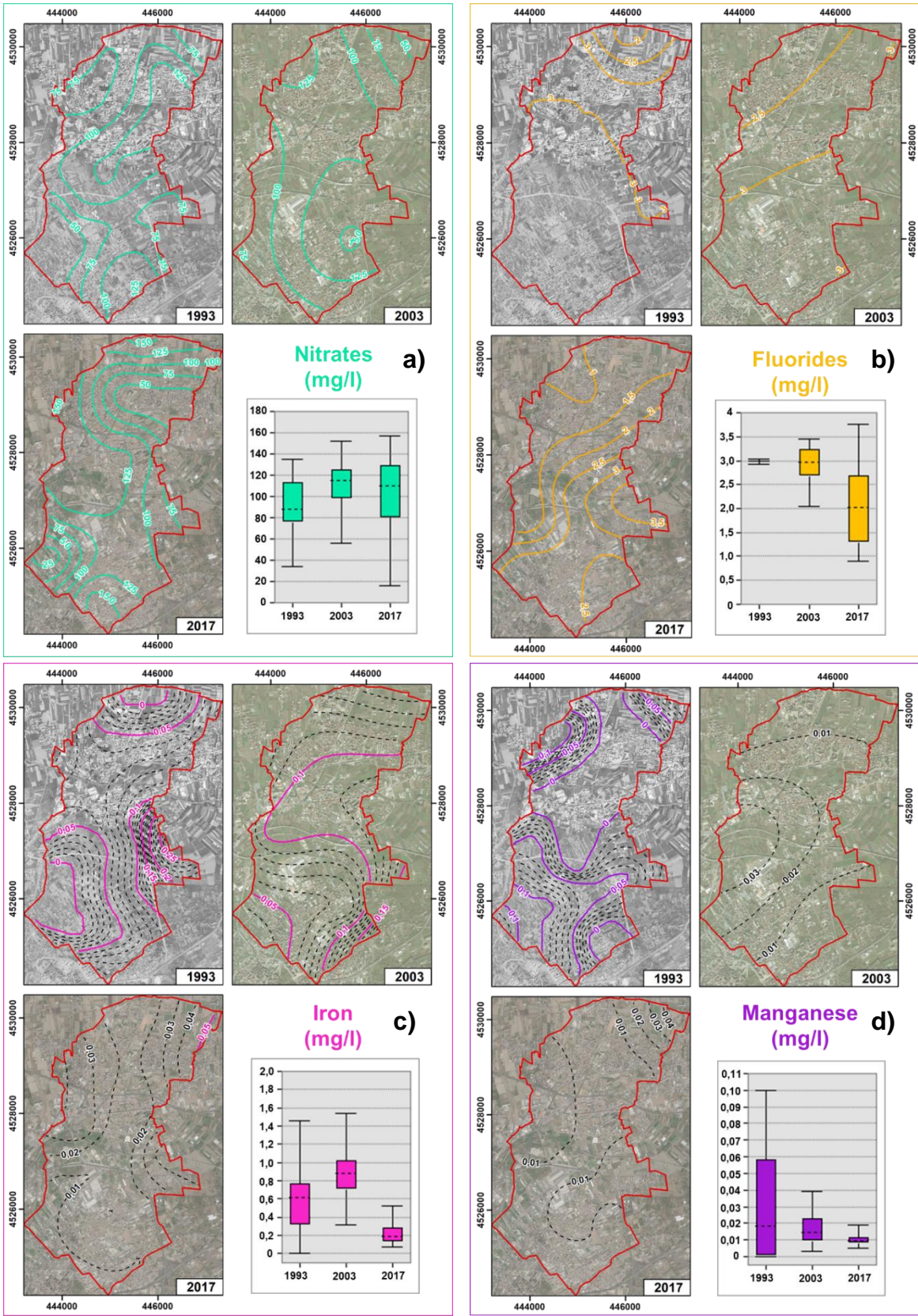


Figure 2.20 - Isoconcentration contour maps and boxplot of Nitrates (a), Fluorides (b), Iron (c) and Manganese (d).

3. Discussion and conclusions

From the comparison between the variation of piezometric levels and the concentrations of the chemical compounds, a relation emerged. Piezometric and nitrates variations had a positive trend. The nitrates produced by the human activity coming from the surface and the reduction of the water table depth increased the concentration of this pollutant which reach groundwater (reducing the time travel).

A negative trend is observed in the natural contamination. The 80' high concentration of fluorides, Fe and Mn, caused by the mobilization of highly mineralized water and an anoxic environment, have suffered an average sharp reduction. This can be attributed to the lack of mobilization of deep fluids due to interruption of pumping. In addition, the increase of the aquifer thickness and the reactivation of faster horizontal flows have led to a greater oxygenation of groundwater and dilution of these natural pollutants.

The results, despite the heterogeneity of the dataset used, allowed to detect a direct relation in the piezometric and nitrates trends, and an inverse one between piezometric and flourides, Fe and Mn trends. These evidences show another effect of the groundwater rebound phenomena in the study area, in addition to flooding and ground uplift.

2.4

Integrating hydrogeological and economic analyses of groundwater flooding in an urban aquifer: the plain of Naples (Italy) as a case study

Allocca V.^{1*}, Castellucci L.², Coda S.¹, Caromaldi M.³, De Vita P.¹, Marzano E.⁴

¹ Department of Earth Science, Environment and Resources, University of Naples Federico II, Naples, Italy

² University of Rome Tor Vergata and Niccolò Cusano, Rome, Italy

³ University of Rome Niccolò Cusano, Rome, Italy

⁴ Department of Economic and Legal Studies, University of Naples Parthenope and CESifo, Naples, Italy

*Corresponding author: vincenzo.allocca@unina.it

Abstract

The economics of groundwater resources management has been concerned mostly with the issue of overexploitation of water resources. However, in recent decades many urban and rural areas have experienced the negative effects of a rise in the groundwater level all over the world and in Europe. Making use of geological and hydrological features information, we propose the coastal alluvial plain of Naples as a case study to investigate and model the phenomenon of groundwater flooding in alluvial/flood plains in an economic setting. We also provide an estimate of the economic impact of groundwater flooding on property values by using the defensive expenditure method. Our results show that for the management of groundwater to be efficient is fundamental to know and to take into account the natural dynamic of the groundwater reserve involved, either in the direction of quantity depletion (the *overexploitation regime*) and in that of groundwater rebound (the *rebound regime*). Since the level of each groundwater reserve moves according to its long run natural laws, the short-sight decisions taken with respect to land uses imply increasing economic costs in the medium and long terms.

Key words: groundwater management, groundwater rebound/flooding, land use, defensive expenditure, Naples, Italy.

Allocca, V., Castellucci, L., Coda, S., Caromaldi, M., De Vita, P., Marzano E., 20XX. Integrating hydrogeological and economic analyses of groundwater flooding in an urban aquifer: the plain of Naples (Italy) as a case study. Journal of Cleaner Production, submitted in April 2021

1. Introduction

The economics of groundwater resources management has been concerned mostly with the issue of overexploitation of water resources. However, in recent decades many urban and rural areas have experienced the negative effects of a rise in the groundwater level. All over the world and in Europe phenomena of groundwater flooding (GF) have increased (Wilkinson, 1985; Vasquez-Sune et al., 1997; Robinson et al., 2001; Beretta et al., 2004; Pinault et al., 2005; Kreibich et al., 2009; Macdonald et al., 2012; Lamé, 2013). The GF phenomenon can be associated with various causes. First, it can emerge as a response of large aquifers in floodplains to prolonged extreme rainfall. Second, it may be produced by a substantial reduction in water abstraction due to anthropogenic events such as a deindustrialization process which entails an unforeseen reduction in the withdrawals. Third, the deterioration of water quality due to the reaching of a low water table following persistent overdraft, may make the public authority to stop pumping the wells. The latter two causes are at the origin of the phenomenon usually referred to as groundwater rebound (GR) which is the object of our analysis. According to the scientific literature, an important cause in the rising of groundwater level in urban areas is actually a strong reduction in the anthropogenic withdrawals for either reasons above. This is the case with the municipality of Casalnuovo di Napoli, located in the eastern plain of Naples, which is our study area (Allocca and Celico, 2008; Colombo et al., 2018). To the best of our knowledge, a fully comprehensive analysis of the phenomenon and of its socio-economic consequences is still lacking. Only in recent years the European legislator has become acquainted with the need of regulating flooding phenomena (Directive 2007/60/EC) but still it does not explicitly consider the rise of groundwater level as a cause of flooding. On the other hand, there is scant evidence about the economic impact of GF, since most of the existing research has been so far focused on valuing the economic damages of flooding caused by extreme precipitations and/or river inundations (Merz et al., 2010; Kunreuther, et al., 2020; Dobrovicová et al., 2013). Little attention has been given to both the theoretical approach to address the GR issue and the actual events of inundations caused by an aquifer regaining its natural level. Moreover, when addressing the economic problems of optimal groundwater management, the perspective is in general that of avoiding the “depletion” of the reserve as it is in fact an important and often crucial source of water provision to satisfy urban and rural demand for water

(Vaux, 2011; Jakeman et al., 2016). In other words, to avoid depletion appears to be the target and the possibility of GR is overlooked. In our view this lack of attention may be explained in two ways. The concern for the serious problem of facing water scarcity may easily imply to forget even the possibility of facing an opposite event while the need to address such a problem through an interdisciplinary approach is historically undermined and not met. In fact, a hydrogeological analysis can provide a realistic picture about the changing level of an aquifer in response to the combination of natural and man-made causes. Any aquifer's water level responds to its long-term natural laws and to the anthropogenic activities. Once this interaction is taken into account, GR phenomena can be predicted and their economic costs estimated. The purpose of this article is threefold. First, we choose the coastal alluvial plain of Naples as a case study for identifying the basic features necessary to investigate and model the phenomenon of GF in alluvial/flood plains. Second, we attempt to develop a methodology for addressing our research question on the basis of a truly interdisciplinary approach. Third, we provide a conservative estimate of the impact of groundwater flooding on property values. To this scope, we use the defensive expenditure method (Bartik, 1988; Abdalla et al., 1992; Champ et al., 2017) to empirically estimate the elasticity of monetary damages of rising water table.

The article is structured as follows. Section 2 describes the data and methods, including an historical reconstruction of the dynamics of groundwater levels influenced by socioeconomic drivers in the study area. In section 3 we propose a theoretical model of the GR/ GF phenomena, provide an econometric estimate of the economic costs for the study area and give our results. Discussion and concluding remarks are reported in Section 4.

2. Data description and methods

2.1 Study area

The study area is located in the central sector of eastern plain of Naples and corresponds to the municipality of Casalnuovo di Napoli (Fig. 2.21). In this municipality, located in the Metropolitan City of Naples and extended about 7.30 km², live nearly 50.000 inhabitants giving place to a quite high population density of about 6.849 inhabitants/km². The study area is delimited, to the west, by the Phlegraean Fields volcanic system, to the east by the carbonate massif of Avella-Pizzo d'Alvano and to the south by the Somma-Vesuvius volcano (Figs. 2.21a and 2.21b). The territory of Casalnuovo di Napoli municipality is included in two river basins, the Sebeto in the south, and the Regi Lagni in the north (Fig. 2.21b). The territory, whose altitude ranges from 12 to 45 m a.s.l., is characterized by a flat morphology, slightly sloping toward the course of the Sebeto river, which was known since Greek-Roman times. By a geological point of view, the study area is located in the central-southern sector of the Campanian Plain (Fig. 2.21a), a large alluvial plain formed in the Pliocene-Pleistocene by the filling of a regional semi-graben structural depression, which was originated along the western side of the southern Apennines, during the opening of the Tyrrhenian Sea (Patacca et al., 1990). By a hydrogeological point of view, the territory is characterized by a porous multi-layered aquifer system (Allocca and Celico, 2008; Allocca et al., 2016; De Vita et al., 2018; Coda et al., 2019a; 2019b; 2019c). In the northern and central-northern sectors, the aquifer system consists of a shallow unconfined volcanoclastic-alluvial aquifer and by a deep semi-confined pyroclastic-alluvial aquifer underling the CI horizon (Fig. 2.21c). In the central-southern and southern sectors, the aquifer system is characterized by semiconfined and phreatic aquifers, respectively, although at local scale in the southern sector the groundwater flow can be confined by shallow lower-permeability lens of clayey-sands, clayey-silts and peats. The water table deep is about 4 meters in the northern sector and about 0,5 m in the southern one. The groundwater is flowing overall from north-east toward south-west, contributing to Cozzone and Volla river discharge (Fig. 2.21c). The aquifer system is recharged by direct effective infiltration (Allocca and Celico, 2008; Allocca et al., 2014) and by lateral groundwater flow coming from the adjoining aquifer sector, whose groundwater basin is extended up to the carbonate Avella-Pizzo d'Alvano and volcanic Somma-Vesuvius aquifers (Fig. 2.21b).

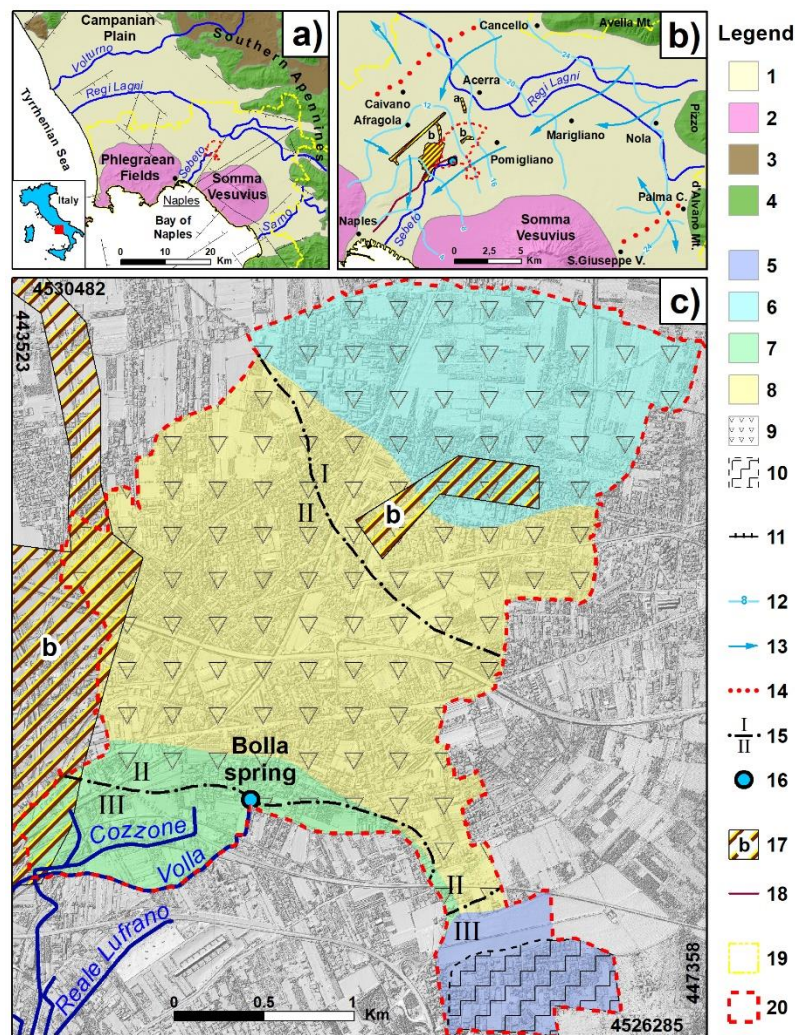


Figure 2.21 - a) Geological map of the Campanian Plain, b) Hydrogeological map of the eastern plain of Naples, and c) Hydrogeological complexes outcropping in the study area. 1) Quaternary epiclastic deposits; 2) Quaternary volcanic deposits; 3) Miocene deposits; 4) Mesozoic Apennine platform carbonates; 5) VA complex (volcanic and alluvial deposits); 6) PF complex (pyroclastic-fluvial deposits); 7) PAP complex (pyroclastic, alluvial, palustrine and marine deposits); 8) P complex (pyroclastic deposits); 9) sector with buried Campanian Ignimbrite (CI) tuff horizon; 10) sector with buried lava rocks 11) normal fault; 12) groundwater contour line (m a.s.l.; Esposito, 1998); 13) groundwater flow direction; 14) groundwater divide; 15) boundary of type of aquifer (I multi layered, II single semi-confined, III single phreatic) 16) Bolla spring; 17) drinking-water well field of Acerra (a) and Lufrano (b); 18) IV century Bolla aqueduct; 19) Metropolitan City of Naples boundary; 20) study area.

According to data provided by Corine Land Cover inventory¹, the land use in the Casalnuovo di Napoli municipality is characterized mostly by urbanized zones which cover about 65% of the territory. The agricultural zone, extending over the rest 35%, is especially found in the southern sector of the municipality and only marginally in the

¹ <https://land.copernicus.eu/pan-european/corine-land-cover>, last accessed November 23rd 2019.

northern sector (respectively green and cyan shaded areas in Figure 2.21c). Historically, the southern sector of the study area was characterized by a typical swampy-flat morphology, and by a complex hydrographic micro network and numerous water springs, such as the Bolla spring (Fig. 2.21c) which was tapped since the IV century by the “Bolla” aqueduct for feeding the city of Naples (Celico et al., 1995) and has been active until the beginning of the twentieth century (Fiorelli, 1926).

2.2 Hydrogeological data

In order to analyze the groundwater dynamics in the study area, we exploit two different time series dataset. The first one, yearly collected, helps to frame the problems connected with GF detected in the study area (Fig. 2.22). This is our original hydrogeological dataset of manually-recorded water level measurements and pumping rates and covering the period 1946-2013 (Allocca and Celico, 2008; Coda et al., 2019a; 2019b). The data refer to the Lufrano well fields (Figs. 2.21b and 2.21c) and thus show the dynamic relationship between groundwater level and withdrawals in the study area, but they are also representative of the groundwater dynamics in the Naples eastern plain (Allocca and Celico, 2008).

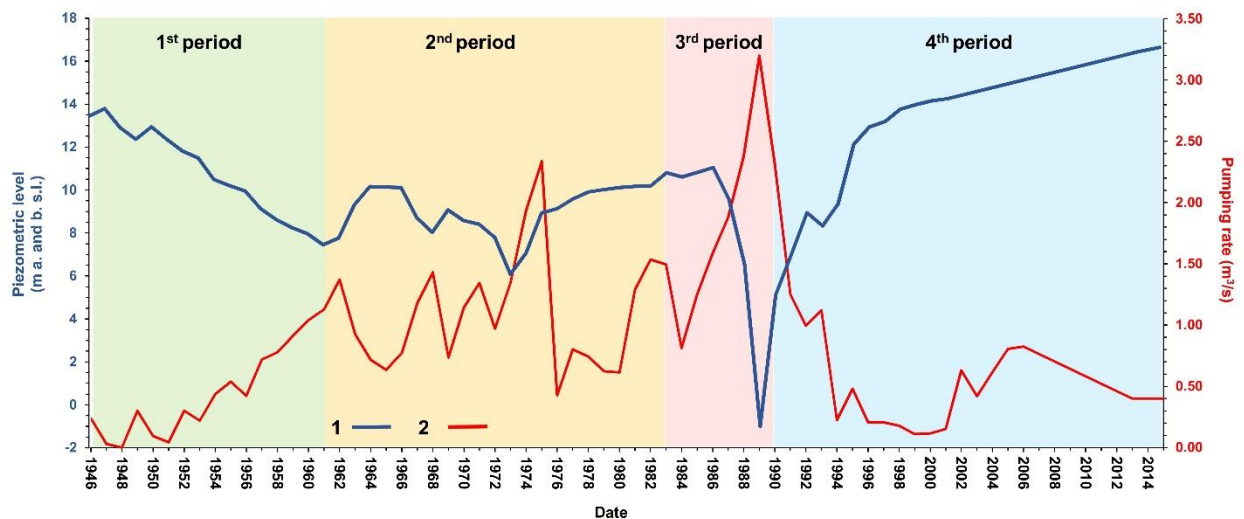


Figure 2.22 - Time series of groundwater levels 1) (meters a. and b.s.l.) and pumping rates 2) (m^3/s) for the Lufrano well-field.

The Lufrano well field was developed soon after WWII to supply drinking water to the Naples city and its hinterland. Therefore, the dynamics depicted in Figure 2.22 were influenced by socio economic drivers originated in the metropolitan area of Naples. In Figure 2.22, the existence of negative co-movement between the two-time series is

evident, and we find that the turning points of the piezometric level and withdrawals are almost perfectly synchronised. As expected, a more intense exploitation of the wells in the Lufrano area is associated to a decline in the recorded level of the groundwater. A first inspection to the data depicts a scenario characterized by four different periods:

1. 1946-1960: in this period piezometric data indicate a falling aquifer level due to the increase in pumping rates;
2. 1961-1983: notwithstanding ample volatility in the withdrawals, this phase was characterized by a stabilization of the piezometric levels around 9,0 m a.s.l. on average; after a peak in 1976, a decline in the pumping rate has brought an increase of the piezometric levels to about 12 m a. s. l.;
3. 1984-1990: in this period overexploitation has occurred due to a sharp increase in withdrawals peaking up to 3 m³/s in 1989. A decline in the annual rainfall regime observed in those years added to the high withdrawals. A severe drought is in fact documented by Allocca and Celico, (2008). As a consequence, a downward jump in the piezometric levels, which brought the level down to -1,5 m below sea level, was registered;
4. 1991 onward: since the early '90s the groundwater table started to rise at an average rate of about 1,0 m per year. Only in the more recent period 2013-2015, the average rising rate of piezometric levels was limited to around 0.16 m per year (Allocca et al., 2016).

The second hydrogeological dataset consists of piezometric measurements systematically recorded during the period 2015-2020, by monitoring and automated equipment, in the Casalnuovo di Napoli municipality (Coda et al., 2019a). This is again our original hydrogeological dataset for the study area, of automatically-recorded water level measurements at daily frequency, by means of monitoring piezometers.

Finally, in order to depict the actual scenario of groundwater levels and flooding in the study area, we refer to two maps of the groundwater level depth provided by Allocca et al. (2016). These maps are the result of an intense program of hydrogeological monitoring of groundwater levels carried out during the period November 2013-March 2015. The monitoring has involved 83 wells, with the support of 3 monitoring stations of groundwater table levels.

The maps in Figure 2.23, compare the sectors affected by GF in November 2013 (map 2.23a) and in March 2015 (map 2.23b), namely the northern sector named S1 and the

southern one named S2 in Figure 2.23. Albeit the impact of flooding is similar in the two sectors, the local characteristics are very different.

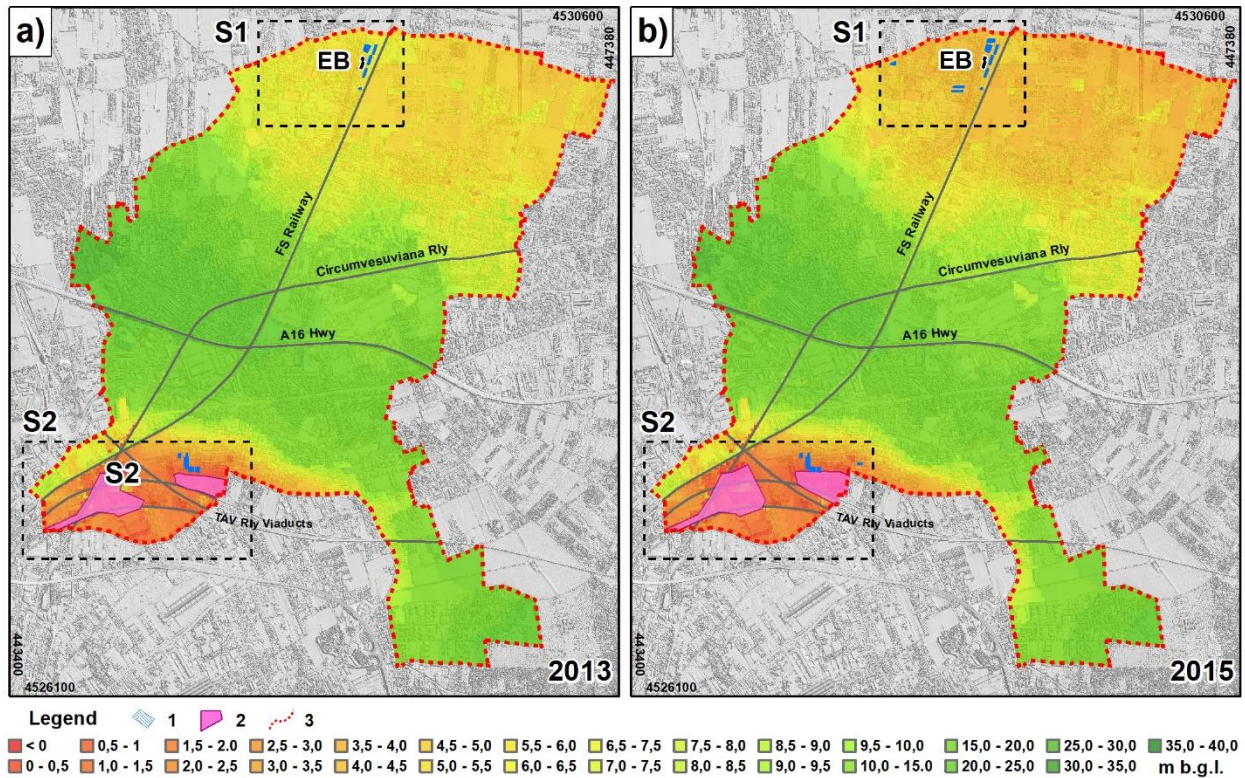


Figure 2.23 - Groundwater depth maps (m b.g.l.) for the period November 2013 (a) and March 2015 (b) and location of the experimental building (EB). 1) Flooded private buildings; 2) Flooded agricultural lands; 3) Study area.

Actually, the piezometric level is about 4 meters below ground surface in S1 while it ranges from 0 to about 1 meter below ground surface in S2, where flooding is affecting also agricultural lands. In the northern sector (S1), the recorded flooding episodes are only related to private properties, amounting to 6 private buildings in 2013. In the southern sector (S2), characterized by a typical swampy-flat morphology, the recorded flooding episodes are affecting either private buildings amounting to 7 ones in 2013 and agricultural land namely 11.99 ha in the same year. The map clearly shows that the impact has widen in 2015, either in rural areas, bringing the flooded area to 15.15 ha (S2) or in private properties, affecting 10 buildings in the northern sector (S1) and 8 buildings in the southern sector (S2). The important message we get from these figures is that the GF phenomenon is not a static one.

2.3 Economic data

Two different time series datasets were used for the sake of our economic analysis. The first dataset, yearly collected, is taken from the National Accounts, and includes, for the period 1952-2008, the time series of the monetary rate of growth of GDP in the Campania region.

Socio-economic drivers, namely urbanisation and economic development, have certainly shaped the pattern in withdrawals and consequently the water table levels as displayed in Figure 2.22 above. It is therefore interesting to compare the time series of the piezometric level with that of the GDP growth rate in the Campania region as we do in Figure 2.24.

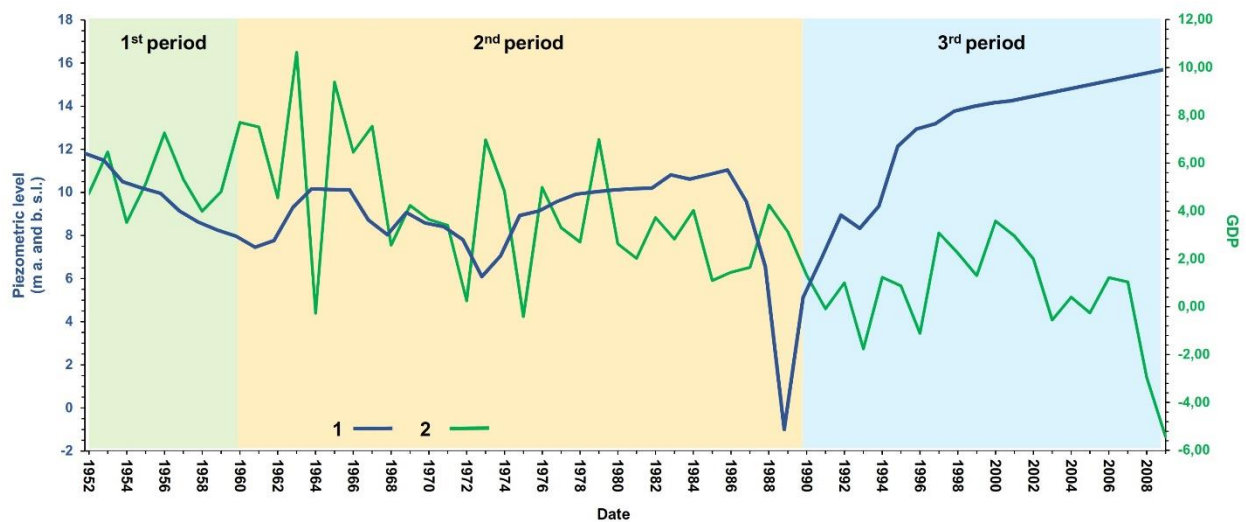


Figure 2.24 - Time series of the piezometric levels (meters a. and b.s.l.) for Lufrano well-field 1) and the rate of growth of GDP in Campania region 2).

We observe that the latter is characterized by three different regimes. During the period 1951-1967 the average growth rate was about 6%, but later it halved in the period 1968-1990, and continued to decline at a pace of 0.5% on average after 1990 and onward. This confirms the idea that the years characterized by a lowering of groundwater table were those showing a rising rate of growth of the Campania economy. The downsizing phase of the economic performance, instead, is coincident with a stabilization of the piezometric levels, whereas the decades starting with the '90s have witnessed a severe slowdown of the economic performance of the Campania region and a coexisting rise in the piezometric level. Of course, these stylized facts, differently from those reported in Figure 2.22, do not imply any kind of causality relationship. Nonetheless, they may signal the

existence of possible interlinkage worth to be further investigated, although this goes beyond the scope of the present analysis.

The second economic dataset, related to the period from January 2015 to July 2018, is a time series of bi-monthly expenditure for electricity consumption in a representative building of the study area, namely the one referred to as “La Palma building”. This experimental building (EB in Figure 2.23) is located in the Northern sector of the Casalnuovo di Napoli municipality (see area S1 in Figure 2.23).

It is a private construction, built in 1995. It is a quite large construction: 6 floors, 40 apartments, and 24 shops at the ground level. Each apartment has its own underground garage and a total of 43 garages are located in the basement of the building. At the construction stage, as shown in Figure 2.22, the piezometric levels recorded in the plain of Naples around the study area, was about 9 m a.s.l., compared to the current piezometric level of about 16 m a.s.l. in the Casalnuovo di Napoli territory. Starting from 2010, flooding episodes were suffered by the underground structure of the building: elevator foundations and garages. As it is shown in Table 2.8, since then the administration of the building has undertaken important interventions to mitigate the impact of underground flooding². All the intervention can be classified as private reactive adaptation or defensive expenditures (Grothmann and Reusswig, 2006; Bartik, 1988; Abdalla, et al., 1992; Champ et al., 2017).

All the expenditures listed in Table 2.8 are classified as “extra ordinary ones” in the bookkeeping of the building administration meaning that they come from unusual causes.

The typologies of expenditures include geological and hydrogeological surveys reports, construction and maintenance/substitution of micro-pumps plant, maintenance of damaged elevators, electricity consumption and expenditure for legal and technical support (solicitors, geologists, engineers). A brief history of the extraordinary expenditures tells us that in 2010 the first intervention concerned a mitigation initiative aimed at restoring the use of the elevators, followed by the appointment of a group of technicians to assess the origin of the flooding. Later, starting from 2011, an increasing number of pumps were installed. The electricity expenditure has grown considerably after the installation of the well point system, as shown in Table 2.8. The expenditure ranges from a minimum of 2,748 euros in 2011 when the pumping system was installed,

² The data are taken from the bookkeeping records provided by the administration of the building.

to a maximum of about 12,000 euros in 2015, when the full set of micro-pumping plants were working.

Table 2.8 - Total expenditure for the experimental building EB, current euros (Source of data: Our elaboration on data provided by the building administration).

Expenditures typology	2010	2011	2012	2013	2014	2015	2016	2017	2018
Construction of micro-pumps plant	0	3143	1212	13095	0	4210	0	0	0
Maintenance / substitution of pumps	0	1000	1000	1000	1000	1000	1000	1000	1000
Maintenance of damaged elevators	3024	0	0	0	0	0	0	0	0
Electricity consumption for the use of pumps	0	2748	3114	2807	11239	11832	9354	7122	9070
Expenditure for legal and technical consulting (geologists, engineers,...)	1094	2385	0	0	0	0	0	0	0
Total expenditure	4118	6528	2212	16902	12239	17042	10354	8122	10070

By matching hydrogeological data with the consumers bills for electricity consumption, we get a bi-monthly dataset of 22 observations, spanning from January 2015 to July 2018. In Figure 2.25, we show the time series of the piezometric level in Casalnuovo di Napoli municipality over the last four years and the electricity expenditures related to the building under investigation. Figure 2.25 clearly shows that there is a time mismatch between the piezometric levels and the electricity bills: the turning points of the electricity expenditure (the red line) are lagging behind those of the piezometric levels (the blue line). We take note of this time mismatch in our estimation.

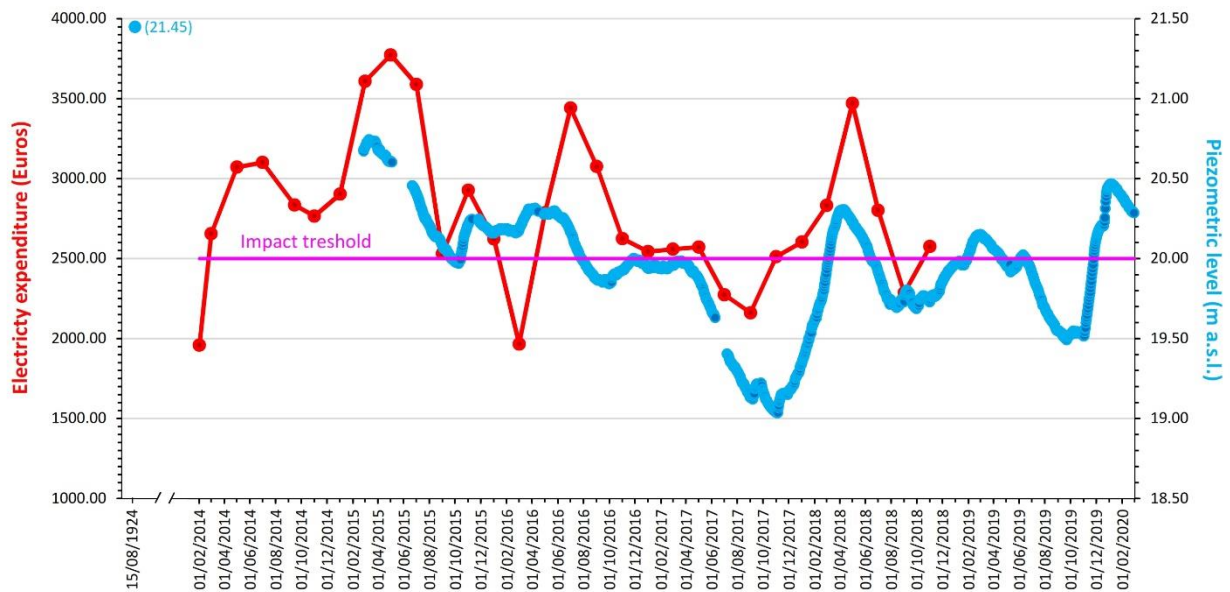


Figure 2.25 - Comparison between time series of piezometric levels (m a.s.l.) and electricity bills (euros) for the experimental building (EB; location in Fig. 2.23).

2.4 Methodology

As we have documented in the data Section, the flooding affecting the territory of the study area is originated by a sudden stop in the withdrawals and therefore the flooding episodes that followed are a good example of a groundwater rebound phenomenon (Allocca et al., 2019). Making use of this hydrogeological setting and resorting to a hydrogeological theoretical model, we are able to arrive at an estimation of the economic costs of the groundwater flooding due to a rebound effect.

2.4.1 A theoretical dynamic analysis of groundwater

The hydrogeological model by Gisser and Mercado (1973) is our starting point as we share their purpose of integrating hydrogeological and economic analyses. We depart from them under several aspects and first of all for the sector considered. A simple scheme of groundwater management in a single-cell aquifer model is provided by these authors who integrate economic and hydrologic analysis in the agriculture sector. We borrow this approach to model, in a single scheme, groundwater overexploitation and groundwater rebound/flooding events with reference to an urban area.

The single-cell aquifer model used by Gisser and Mercado (1973) assumes a uniform headwater throughout the basin allowing to model the water table dynamics as follows:

$$AS \frac{dH}{dt} = R + R_a + (\alpha - 1)W - W_n \quad (1)$$

where AS is the *storativity* of the aquifer given by the product of the area A and the storage coefficient S. R and R_a , are the recharge volumes, respectively, natural and artificial (supposed to be zero), and W and W_n are withdrawals, anthropic and natural ones. The parameter α controls for the share of return flow. Assuming natural discharge, W_n , to be a linear function of the water table level, H :

$$W_n = a + bH \quad (2)$$

one gets the steady state level of the water table H_s by substituting [2] into [1] and solving for the water table.

The solution of the dynamic equation for given level of withdrawals, W , is:

$$H = [R + R_a + (\alpha - 1)W - a]/b + \{[bH_0 - R - R_a + (\alpha - 1)W + a]/b\} \exp\left\{\frac{-b}{AS}t\right\} \quad (3)$$

where the first term in square brackets is the steady state level of the water table, H_s . The larger the anthropic withdrawals W , i.e. the water demand for irrigation in the model, the lower is, *coeteris paribus*, the water table level. In addition, Equation 3 clearly shows that when an excess of pumping occurs at time 0, the water level dynamic is negative and the water table decline will continue unless a reduction in withdrawals will take place or an artificial recharge is implemented. Figure 2.26, reproducing Figure 2.22 of Gisser and Mercado (1973), provides the graphical representation of the model for the case of $H_m > H_s$ (panel a) and for the case of $H_m < H_s$ (panel b) were H_m represents the minimum allowable level of water. Overcoming it implies “unacceptable damage for a long time period” (Gisser and Mercado, 1973). This is represented by the reaching of the point A in Panel a. The model proceeds by modelling the water demand for irrigation as a linear function of water price and were the costs of pumping increase with the lowering of the water table and by integrating these economic aspects with the hydrogeological ones. Under these circumstances as far as withdrawals increase and pumping costs and water price rise, the demand for water decreases thus restoring the hydrological balance.

This mechanism applies to two cases depicted in Figure 2.26 panel a) and b). When the steady state level H_s is above the minimum allowable one H_m as in panel b), no policy is needed to mitigate the falling dynamic in water table level. When instead the critical threshold H_m is reached earlier than the steady state H_s (point A in panel (a)), a policy is

necessary to avoid the unacceptable damage stemming from overcoming H_m . Various policies can be suited to this end such as artificial recharging or demand restrictions. We use this setting for our analysis.

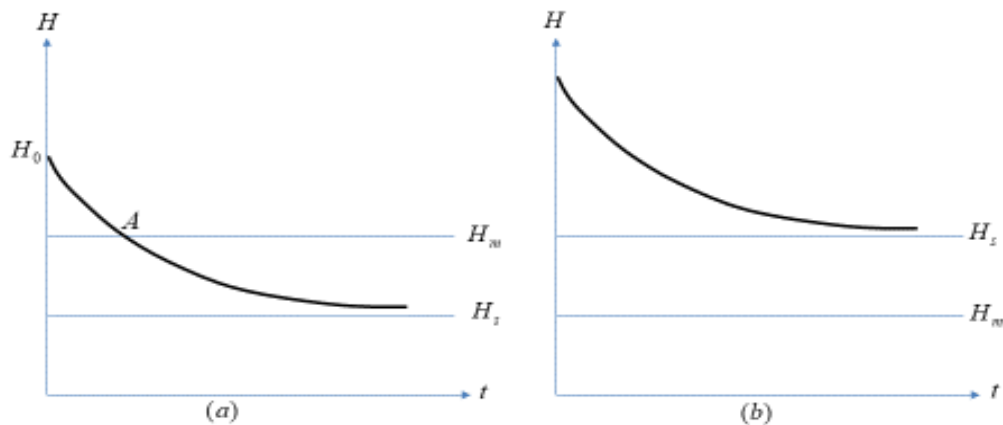


Figure 2.26 - Source: Gisser and Mercado, 1973.

2.4.2 The defensive expenditure analysis

In the theoretical economic literature, groundwater is mainly considered as a depletable resource and frequently a common property one, where entry is restricted by land ownership. For these reasons, the scarcity rent should be paid by current users and included in the efficient pricing of the resource (Koundouri, 2004; Koundouri et al., 2017 for a survey of dynamic models in groundwater management). When the management of groundwater is not inspired by optimal rules, social negative effects follow as in our study area.

From an empirical point of view, we aim to model the economic damages suffered by residents in the study area. Flooding is producing serious damages with remarkable impacts and economic consequences in the vast area of the eastern plain of Naples. The hydrogeological hazard of the flooding is related to underground structures and infrastructures (e.g., building foundations, underground car parks, tunnels and subways), since it produces an increase in the hydrostatic stress exerted on buildings, the corrosion of foundations and a groundwater pollution arising from the saturation of polluted soils (Colombo et al., 2018). In order to assess the economic impact of flooding in our study area, we adopt a defensive expenditure approach. This method, which is less data demanding compared to others, allows us to estimate the impact of the flooding

through the willingness to pay by the residents for protecting themselves against such events. In other words, we take as monetary damage the actual costs bore by residents and arising from groundwater pumping installations necessary to prevent the negative effects. These expenditures represent a lower bound on the costs imposed by environmental deterioration and thus the willingness to pay to prevent it.

By using expenditure and hydrogeological data as described in Section 2, we estimate the following model:

$$\ln E_t = \alpha + \beta \ln P_{t-2} + \varepsilon_t \quad (4)$$

where E_t is electricity expenditure at time t and P_{t-1} is piezometric level at time $t-2$. Electricity bills are bimonthly as customers are charged for consumption in the 2 previous months. For this reason, the explanatory variable, the piezometric level, is two months lagged. All variables are log transformed. Adopting OLS method to estimate eq. (4), may lead to spurious results when selected variables are non-stationary. To overcome this issue, a VAR model of the first-differenced series is estimated.

3. Results

3.1 Water table dynamics when the pumping regime changes

The Gisser and Mercado (1973) model, as reported in Figure 2.26, is our starting point to frame in a single picture groundwater overexploitation and groundwater rebound. Two remarks are necessary to explain how we depart from it besides the sector, already mentioned. First, we extend the model to include groundwater rebound and second, as our study area suggests, we take into account the reasons for a sudden and unforeseen stop in the withdrawals and their consequences.

First, even when the steady state water table level H_s , is higher than the minimum allowable water table level, H_m , it can happen that ever-increasing withdrawals push the trajectory of water exploitation toward the threshold level H_m . This is the case when water abstraction is driven by socio macroeconomic drivers, such as the rate of growth of GDP and the rate of growth of population, leading to a continuous increase in withdrawals to meet a growing water demand for multi purposes. Under these circumstances, what we observe is a repeated shift of the steady state level of the water table as shown in the

graphical analysis reported in Figure 2.27. The shift is triggered by the increase in the water demand, W :

$$H_S = \frac{R + R_a - (\alpha - 1)W - a}{b} \quad \text{for } t < t_b \quad (5)$$

$$H_S = \frac{R - a}{b} \quad \text{for } t > t_b$$

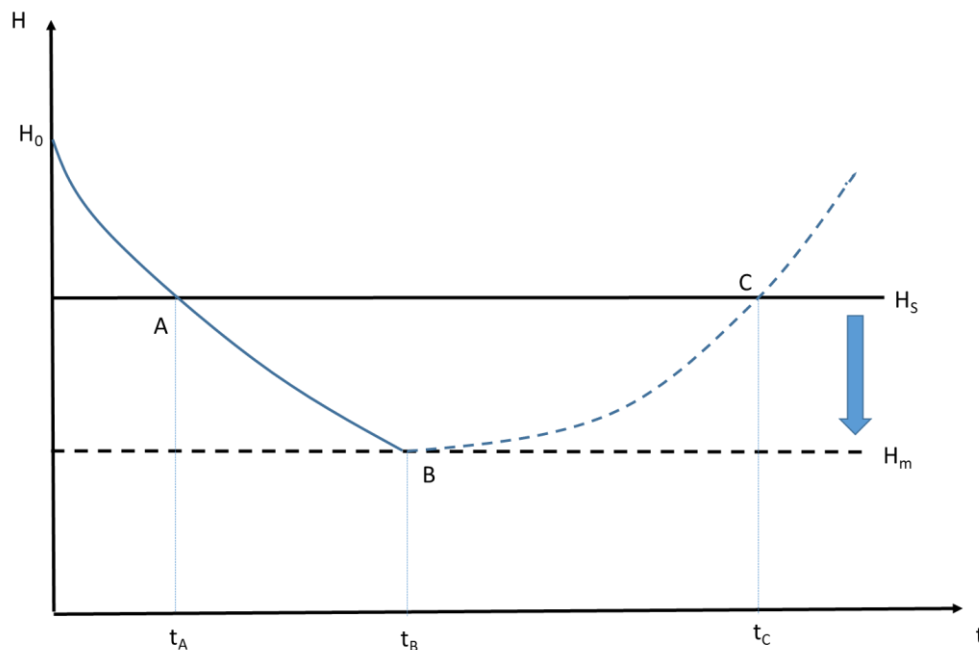


Figure 2.27 - The dynamic evolution of the water table representing groundwater depletion, groundwater rebound and groundwater flooding.

The downward movement of the H_S locus can be also summarized by the trajectory AB in the water table level. The downsizing in the steady state water table finds a lower bound when the minimum allowable water table level, H_m is reached.

Second, when water table reaches the H_m threshold, a change in the regime of water exploitation is likely to occur on the base of the water quality deterioration that follows. The local authority changing strategy is what originates the groundwater rebound: the regime of withdrawals changes so dramatically to bring the water abstraction to a rate, \bar{w} , lower than the recharge, R , and possibly down to zero in extreme cases.

In our modified setting two different regimes are identified. The first one is the pattern starting from point A on the H_S water table level. When pumping exceeds recharge, groundwater stock is depleted down to the level H_m in B and we refer to it as *overexploitation regime*. This is a clear example of short-sighted, inefficient exploitation of the natural resource. But this is not the end of the story because a short-sighted groundwater management may cause further problems in the presence of an abstraction regime change, given by a sudden slowdown in withdrawals. The

sudden interruption in the withdrawals originates a GR, represented, in our scheme, by a jump into the trajectory of the water table, characterized by $W = \bar{w} < R + Ra - Wn$. In this case, according to Equation (5), the water table level starts to rise. The trajectory moving from point B towards C and above is the graphical representation of the *groundwater rebound regime*. In this case, the risk of flooding becomes a serious threat that is more likely to occur when:

- a) the interval of time during which water table level has been low is long lasting ($t_A - t_C$ in Figure 2.27);
- b) land uses have completely ignored the natural regime of water table level, taking for granted that the “true” water table level was the lowest one observed during the overexploitation regime.

This suggests that quantity depletion impact, i.e., the *overexploitation regime*, and quality deterioration effects can interact to shape a likely scenario of GF. Albeit quantity and quality concerns arising from abstraction of groundwater have been addressed in the economic literature, to the best of our knowledge, no analyses are provided for valuing the economic costs produced by a groundwater regaining its natural level (i.e., *groundwater rebound regime*). In the next section we document how the hydrogeological dynamics observed in the study area implies the economic costs suffered by local residents.

3.2 A conservative estimate of the economic costs of groundwater flooding

As shown in Table 2.9, the electricity costs vary according to the number of pumping plants as well as to a function of the hydrogeological conditions triggering the flooding. To investigate this relationship, we estimate the elasticity of electricity expenditure to the piezometric level as described in equation (4). When selected variables are non-stationary, estimating equation (4) with OLS method could return spurious results. Durbin Watson test statistic and Breusch-Godfrey LM test for autocorrelation indicate the potential for the residuals to be non-stationary, as we reject the assumption of no serial correlation. The test results are also confirmed by the autocorrelation and partial autocorrelation plots as shown in Figures 2.28 and 2.29. A linearly declining autocorrelation functions can be noted in the case of piezometric level while less regular pattern is highlighted in the case of electricity expenditures. In each case we have a high value of the first partial autocorrelation function, indicating non-stationarity (Fig. 2.28).

Table 2.9 - A Comparison of Time Series Models (dependent variable electricity expenditures).

Variables	OLS	Detrended Regression	First Differences
Piezometric level (t-2)	4.191*** (1.314)		
Piezometric level (residuals)		4.843** (2.273)	
Piezometric level (differentials)			6.213** (2.776)
Constant	-4.630 (3.937)	0.0108 (0.0306)	0.00230 (0.0339)
Observations	24	24	23
R-squared	0.316	0.171	0.193

Standard errors in parentheses

*** p<0.01, ** p<0.05, * p<0.1

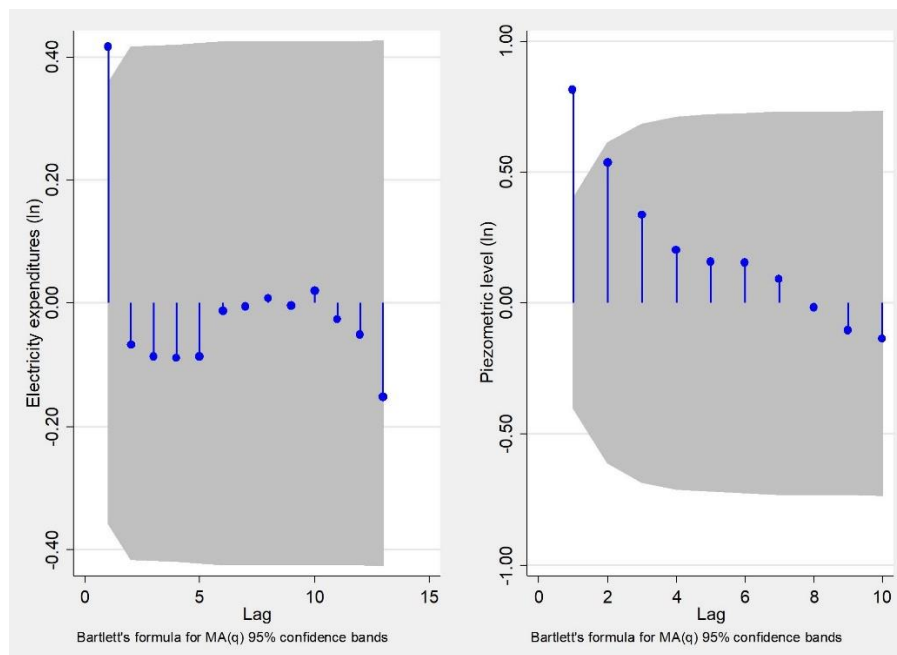


Figure 2.28 - Autocorrelation functions for electricity expenditure and piezometric level.

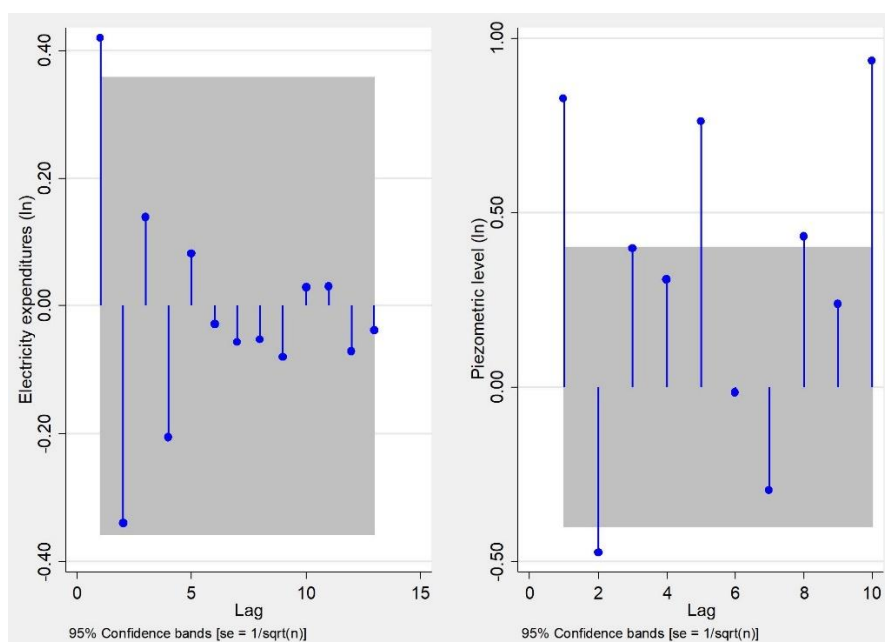


Figure 2.29 - Partial Autocorrelation functions for electricity expenditure and piezometric level.

In order to test for stationarity of the series, we apply Augmented Dickey-Fuller (ADF) (Dickey and Fuller, 1981) test for unit root and we choose the lag lengths that reflect the best fit to the variables by using different selection-order criteria. Akaike's information criterion (AIC), Schwarz's Bayesian information criterion (SBIC), and the Hannan and Quinn information criterion (HQIC) suggest to use two lags for electricity expenditures and three lags for piezometric level. The ADF test with two lags is -2.915 , greater than the critical value -3.592 by significant level of 5%. So the null hypothesis of unit root cannot be rejected for electricity expenditures. We fail to reject the null hypothesis of a unit root, also in the case of piezometric level because the ADF test with three lags is -3.562 , slightly greater than the critical value -3.600 , the significant level of 5%. Since time series variables appear to be non-stationary in variable levels, the first differences of the variables are considered. It is found that the null hypothesis of unit root is rejected at 1% significance level. Hence, the differences become stationary and consequently the related variables are integrated of order one. To deal with this problem, we could detrend the variables and check for the presence of a cointegrating relationship between electricity expenditures and piezometric level. After detrending the variables from a deterministic trend, ADF test is performed to check stationarity. In each case, we fail to reject the null hypothesis of a unit root. Moreover, the two variables may share a common trend. Johansen tests for cointegration reveals that the presence of a cointegrating relationship is rejected. At maximum rank zero, the trace statistic (13.8) does not exceed critical values (15.41). Therefore, it accepts the null hypothesis so that the time series variables electricity expenditures and piezometric level are not cointegrated. Thus, we estimated a VAR model of the first-differenced series. The results are reported in Table 2.9.

The estimated elasticity of electricity expenditure to the piezometric level is quite high in the first differences model, 6.2 meaning that for one point percentage increase in the piezometric level, electricity expenditure will grow by 6.2 per cent. In the reasonable assumption that in the future

the piezometric level will reach its historical level of 21.45 m a.s.l as measured in August 1924 (Fiorelli, 1926) from its average present one of 20.33, we calculate that the electricity expenditure will rise by 34.1 per cent. One can expect an analogous increase in such expenditures also for all the other buildings affected by the inundation whose number has already grown from 13 in 2013 to 18 in 2015³. The lesson one may learn is that with the rise of groundwater level, the defensive expenditure will grow and will continue to grow until a decision is taken by the municipality to permanently counteract the effects of the reduction in the withdrawals due to the deindustrialization of the area and to the changes in agricultural land use.

4. Discussion and conclusions

There are several studies addressing groundwater risk of depletion while very few, if any, addressing the case of water rebound, not to mention the GF. Our research meant to contribute to fill this gap, showing that the study of GR and GF in an economic perspective can add important insights in the analysis of dynamically efficient use of groundwater resources.

The story of the study area we investigate tells that a crucial issue is the degree of awareness of local stakeholders. As we have stated since the beginning of this article, the issue of GF is a quite new one in the hydrogeological literature, it is almost neglected by the environmental legislation and it is completely unknown to the local policy makers. In addition, as our dynamic scheme shows, GR and GF are triggered by a regime change from a phase of overexploitation to a phase of sudden decline in water abstraction. Therefore, the occurrence of GF can be consistent with a hydrological scenario characterized by an history of low risk of GF, as well pointed out by Beltran et al. (2018) through a meta-analysis of the impact of flood risk on property prices in floodplains. These authors find that the risk perception of individuals declines with the time elapsed since the last flood event. A similar result is found by Bin and Landry (2013) for North-Carolina (USA), suggesting that the low frequency of events implies that individuals take their decision in a fashion that could seem irrational depending instead from their experience of a limited number of information. A similar experience is observed in the

³ In addition to the estimation of defensive expenditure, we found that for a representative apartment of this building the market price in two different instants of time, namely 2010 and 2020 shows that the property value has declined sharply from 1800€ per m² in 2010 to 1400 € per m² in April 2020. In a hedonic price setting, this information gives an idea of the market consequences of the environmental deterioration caused by groundwater flooding.

eastern plain of Naples, where the tendency of the groundwater body to recover its long run equilibrium was overlooked by individuals, who usually look only at the most recent history when undertaking their economic activities. The nature of “mean reverting process” that characterizes the groundwater body in the Casalnuovo di Napoli area, jointly with the lack of land use planning and a faded memory of the past hydrogeological history of the territory, has shaped the current scenario of GF. Things may change if the economic damages were valued and known by the stakeholders. For this reason, we attempted to estimate such damages. In fact, we have documented a non-negligible wealth loss associated to GF of a representative private building in the study area, and a quite high elasticity of the cost of defensive/adaptation expenses. The current scenario is signalling that defensive costs are ever increasing with time until a permanent solution is found, with negative consequences on property values. These concerns are reinforced by considering that the top piezometric level historically recorded, has not been recovered yet. Differently from private precautionary-adaptation expenditures to mitigate “standard” flood damages, such as inundation by a river due to exceptional rainfall, here the private mitigation effect is only temporary as the cause of flooding comes from a groundwater rising to its natural level. We expect similar conclusions from addressing the damage costs valuation for the other affected buildings and probably for the other damaged items in the plain of Naples. In fact, documented flooding events have been reported with respect to underground public transportation infrastructures, agricultural zones, business zones such as parking space and commercial activities, and even archaeological sites.

A clear policy recommendation follows as well as a warning. Before taking decisions in terms of land use and land use changes in a mixed environment, mostly urban but not only, a scientific investigation on the natural long-term cycle of the aquifer involved is indeed necessary and functional for an efficient use. For the best possible management of land and water, integration between hydrological and economic aspects is necessary. Finally, it may be worth warning about how difficult and costly are remediation policies when damages have been produced. This is to say that overlooking the possibility of GR, and therefore GF, is extremely dangerous in terms of medium and long run effects and moreover, it can be avoided.

3

Lufrano and Acerra well-fields

Uplift evidences related to the recession of groundwater abstraction in a pyroclastic-alluvial aquifer of southern Italy

Abstract.....	105
1. Introduction.....	107
2. Study area.....	109
3. Data and methodologies	111
3.1 Hydrogeological data.....	112
3.2 DInSAR data.....	113
4. Results.....	115
4.1 Piezometric head variation maps.....	115
4.1 Satellite-based deformation maps.....	116
5. Discussion	118
6. Conclusions.....	122

List of Figures and Tables

Figure 3.1 - **a)** Hydrogeological map of Campanian Plain (De Vita et al., 2018). **b)** Lufrano and Acerra well field area.

Figure 3.2 - 2D hydrostratigraphic model of the aquifer system.

Figure 3.3 - Piezometric level and pumping rates.

Figure 3.4 - Location of boreholes and long-term piezometric monitoring wells (**a**), and groundwater flow scheme for the years: 1989 (**b**), 2002 (**c**), 2006 (**d**).

Figure 3.5 - LoS velocity maps (mm/yr) of the study area by ERS1/2 (**a**) and ENVISAT (**b**) data.

Figure 3.6 - Piezometric level variation (m) in the period 1989-2002 (**a**) and 2002-2006 (**b**).

Figure 3.7 - DInSAR-derived displacement maps: **a)** ERS-1/2, 1992-2000 period; **b)** ENVISAT, 2002-2006 period.

Figure 3.8 - Groundwater levels and ground vertical deformations along the section traces A-A' (**a**) and B-B' (**b**, **c** and **d**).

Figure 3.9 - Scheme of the radius of influence of the wells field during the recovery period.

Figure 3.10 - Piezometric levels and vertical displacement of the wells 22A (**a**), 119 (**b**) and sn2 (**c**).

Table 3.1 - DInSAR LoS measurement statistics referred to the whole area.

Table 3.2 - DInSAR LoS measurements referred to the whole area.

3

Uplift evidences related to the recession of groundwater abstraction in a pyroclastic-alluvial aquifer of southern Italy

Coda S.¹, Confuorto P.¹, De Vita P.¹, Di Martire D.^{1*}, Allocca V.^{1*}

¹ Department of Earth Science, Environment and Resources, University of Naples Federico II, Naples, Italy

*Corresponding authors: diego.dimartire@unina.it; vincenzo.allocca@unina.it

Abstract

Aquifer mismanagement is a common anthropogenic cause of subsidence and uplift phenomena in alluvial plains, representing one of the main natural hazards in urban areas due to related damage to urban structures and infrastructures. In this work, the groundwater rebound phenomenon occurred in the last decades of the 20th century in Lufrano area (Metropolitan area of Naples, Southern Italy) has been studied by integrating geological data, hydrogeological continuous monitoring and spaceborne SAR information derived from ERS-1/2 and ENVISAT satellites. In the period 1989-2006, Lufrano area, which hosts an important well field made up of 180 wells extracting groundwater for drinking use, suffered an initial over-exploitation of the aquifer which was followed by a sudden and severe decrease of the volume abstraction, resulting this last in a rapid ground uplift. The coupled analysis of hydrogeological and DInSAR data have shown a correspondence between piezometric level rise (up to 15 m) and ground uplift (up to 50 mm) trends in the period 1989-2006. In order to examine the spatio-temporal evolution of the phenomena and the cause-effect relationships, showing the link between the two phenomena and their rates, longitudinal cross-sections were carried out and comparisons between piezometric level rise and time-series of displacements were reconstructed. The obtained results represent a first contribution to the definition of ground deformation related to groundwater level rise phenomena, providing a basis for future studies focused on the modelling of the hydro-mechanical properties of the aquifer.

Key words: aquifer mismanagement; groundwater rebound; uplift; DInSAR; Italy.

Coda S., Conforto P., De Vita P., Di Martire D., Allocca V., 2019. Uplift Evidences Related to the Recession of Groundwater Abstraction in a Pyroclastic-Alluvial Aquifer of Southern Italy. Geosciences 9, 215.

1. Introduction

The study of ground vertical deformations is particularly difficult in geologically complex areas, especially where volcano-tectonic processes are predominant, because causes of deformation are not clearly recognizable, being subject to composite temporal variabilities.

In addition to natural processes such as long-term tectonic movement (Perrone et al., 2013; Chen & Liu, 2020), or earthquakes occurrence (Meltzner et al., 2006; Chini et al., 2008), anthropogenic factors can contribute to ground deformation phenomena. In urban and rural areas, a common cause of vertical displacement is related to human-induced changes of water table (Galloway et al., 1999). Several studies have shown the strong correlation between groundwater abstractions and subsidence (Amin & Bankher, 1997; González-Morán et al., 1999; Carminati & Martinelli, 2002). In particular, drastic piezometric lowering causes pore pressure decreases leading to consolidation in cohesive deposits and compaction in incoherent ones (Lofgren & Klausing, 1969).

In many cases, a drastic decrease or cessation of the withdrawal lead to a progressive recovery of piezometric levels (Wilkinson, 1994). According to the geological setting and changes in water table depth, surface ground deformation, both negative and positive (subsidence and uplift, respectively) can be induced. Groundwater level changes can modify the stress state of the aquifer-system materials, triggering different deformation mechanisms, such as the hydrocompaction of sandy deposits, inducing subsidence phenomena (Amin & Bankher, 1997; Terranova et al., 2015), or the volume increase in porous deposits, generated by the elastic recovery during the increase of pore-water pressure, whether a plastic component can couple the predominant elastic behavior (Biot, 1941; Allen & Mayuga, 1969); furthermore, also an increase of the pore water pressure in heavily fractured rock mass, leading to uplift due to expansion of the rock matrix, may be induced (Donnelly, 2009).

Subsidence and uplift triggered by anthropogenic groundwater level fluctuations affect the structures and infrastructures, representing one of the most damaging geohazards in metropolitan areas. Therefore, monitoring and quantitative assessment of surface displacements is of paramount importance for local administrations responsible for land and risk management, being them committed to locate and estimate the source and the amount of deformation and thus providing fundamental information to mitigate the risk. In this sense, a Remote Sensing technique, such as Spaceborne Differential Interferometry SAR (DInSAR) is a worldwide-known tool capable to provide precise information over wide areas, by overlying a stack of SAR images and generating interferograms. Such features are able to provide a deformation measurement over definite targets on the ground. DInSAR techniques have been largely implemented on large metropolitan areas, such as Mexico City (Strozzi & Wegmuller, 1999; Osmanoglu et al., 2011), Murcia (Tomás et al., 2010), Rome (Zeni et al., 2011), London (Bonì et al., 2016; 2018; Milillo et al., 2018).

One of the most common advantages of using SAR-based systems is the opportunity of having a detailed picture of the situation over wide areas and across a long time span: when available, a dataset of more than 26 years (1993-actual), covered by different satellite acquisitions, may be used to analyze a given area, with a detail not-comparable with other techniques. This may allow to correlate short deformation periods to single man-induced events (such as fluid withdrawal or injection).

In this paper, the hydrogeological behavior of Lufrano area (metropolitan city of Naples, southern Italy) has been investigated through an accurate reconstruction of past hydrodynamic scenarios, linked to a deformation trend reconstructed by spaceborne SAR data.

The pyroclastic-alluvial aquifer of this sector of the Campanian Plain has undergone an intense phase of over-exploitation in 1980s. Drinking water abstractions from about 180 wells of Lufrano and Acerra well fields have led to a deficit in the mean annual water budget of the aquifer (Allocca & Celico, 2008), inducing a rapid decline of the groundwater level (up to 16 m) and a deterioration of groundwater quality (Celico et al., 1994). In 1989, this latter issue led to a partial and/or total abandonment of withdrawals followed by a groundwater recovery started in 1990 (Allocca & Celico, 2008; Allocca et al., 2016; Coda et al., 2019a).

To analyze the phenomenology under consideration, piezometric levels from 1989 to 2006 and the cause-effect relationship with deformations, measured by ERS and ENVISAT data (1993-2006) have been analyzed, showing an overlap of the two phenomena in several time intervals. Since 1990, a first period, characterized by a general subsiding trend in the whole Neapolitan plain and an uplift in Lufrano area was recognized. The latter may be induced by the rapid recovery of the piezometric levels, as a consequence of the groundwater exploitation drastic reduction of the pyroclastic-alluvial aquifer (Allocca & Celico, 2008). Following 2000, a mild deceleration of the groundwater rebound and consequently of the uplift is identified. Moreover, a geological interpretation has been given in those areas where the uplift and the piezometric rebound showed different behavior in the time-span considered.

The integration of interferometric data and piezometric levels thus provided a better definition and characterization of the hydrogeological setting and its interference on ground deformation phenomena, assisting the development of well-tailored mitigation measurements.

2. Study area

The study area, extending about 40.6 km², is located NE of the city of Naples (southern Italy) over the central sector, of the structural depression of the Campanian Plain (Fig. 3.1), a large coastal pyroclastic-alluvial plain. Such depression, formed during the Upper Pliocene along tectonic ridges belonging to the regional tectonic extensional phase, was filled during the Quaternary by volcanic deposits from the intense volcanic activity of the Phlegraean Fields and Somma-Vesuvius volcanoes, started 300 k-yrs ago (Rolandi et al., 2003), and by alluvial and marine sediments, in the last 25 k-yrs.

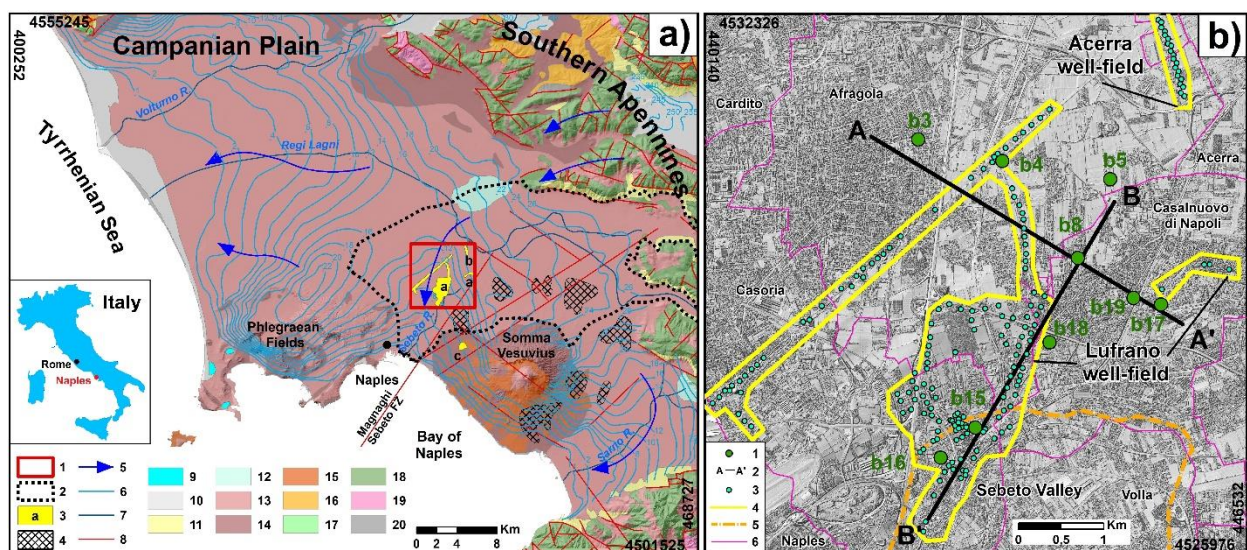


Figure 3.1 - a) Hydrogeological map of Campanian Plain (De Vita et al., 2018). Legend: 1) study area; 2) hydrogeological basin of eastern plain of Naples; 3) drinking-water well fields of Lufrano (a), Acerra (b), Lufrano and Ponticelli (c); 4) ring-style subsidence area (Lanari et al., 2002); 5) groundwater flow direction; 6) piezometric contour line (m a.s.l.); 7) hydrographic network; 8) normal fault; 9) lake; 10) alluvial-coastal complex; 11) epiclastic continental complex; 12) travertines complex; 13) ash-fall pyroclastic complex; 14) ash-flow pyroclastic complex; 15) volcanic rock complex; 16) arenaceous-conglomeratic complex; 17) carbonate complex of the Matese-Mount Maggiore and Mount Alpi Unit; 18) carbonate complex of the Picentino-Taburno Unit; 19) dolomite-marly complex of the Picentino-Taburno Unit; 20) clayey-calcareous complex of the Sicilian Units. **b)** Lufrano and Acerra well field area. Legend: 1) borehole; 2) hydrostratigraphic section trace; 3) drinking-water well; 4) well fields area; 5) Seбето Valley (Volla depression) northern boundary; 6) municipal boundary.

The carbonate bedrock lies beneath a cover of marine, alluvial and pyroclastic deposits, at a maximum depth of 3000 m (Bellucci, 1994). It is dislocated by fault systems, mainly with extensional component (Ortolani & Aprile, 1985; Costanzo & Nunziata, 2014). The buried Magnaghi-Seбето and Somma-Vesuvius faults have created locally an extensional tectonic field, as shown by the evidences in the late Pleistocene-Holocene activity (Cinque et al., 2000; Santangelo et al., 2017) and by a gravitational sliding around the base of the

Somma-Vesuvius edifice (Bianco et al., 1998; Lanari et al., 2002), leading to a subsiding tendency of the plain (Fig. 3.1a).

Figure 3.1a resumes the hydrogeological setting and groundwater flow scheme of Campania plain, elaborated by different authors (Celico et al., 1994; Esposito, 1998; De Vita et al., 2018). The central-eastern sector of Campania plain is occupied by the hydrogeological basin of the eastern plain of Naples. The study area represents a drainage zone for the groundwater of this sector, which is recharged both by the direct contributions of precipitations and by the groundwater seepage from the surrounding carbonate aquifers from NE and E (De Vita et al., 2018).

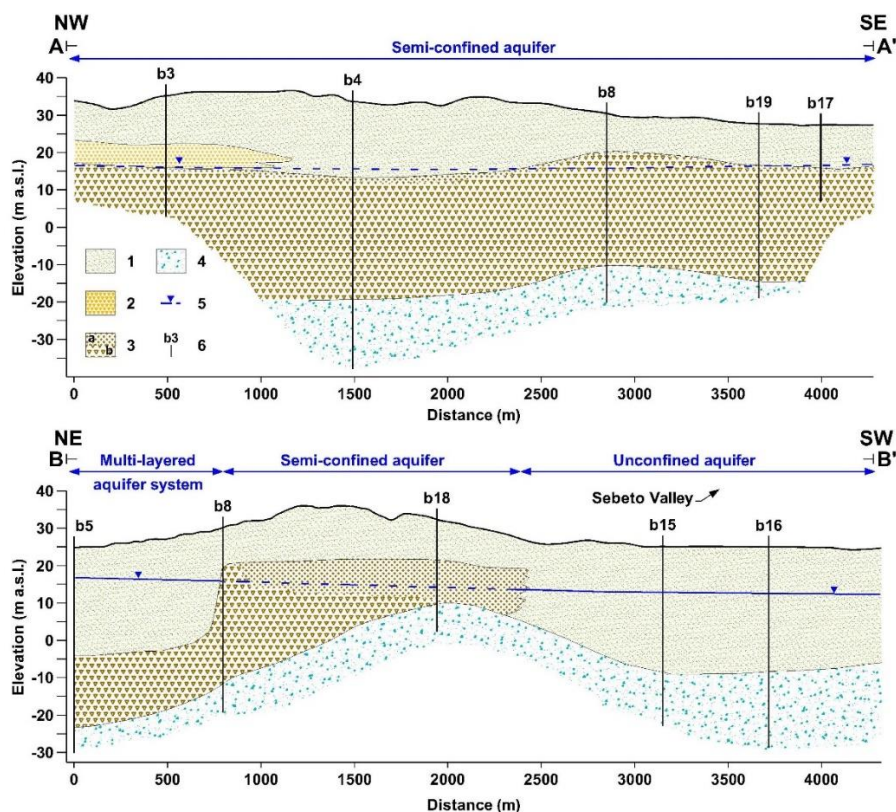


Figure 3.2 - 2D hydrostratigraphic model of the aquifer system. Legend: 1) shallow pyroclastic-alluvial-lacustrine complex; 2) Neapolitan Yellow Tuff (NYT); 3) Campanian Ignimbrite (CI) in incoherent (a) or lithoid (b) facies; 4) deep pyroclastic sandy complex; 5) phreatic (a) and semi-confined (b) piezometric level; 6) borehole. See Figure 3.1b for the location of section traces and boreholes.

The groundwater circulation is conditioned by the stratigraphic heterogeneity of the alluvial plain, which results in a multi-layered aquifer system (hydrostratigraphic sections, A-A' and B-B', in Fig. 3.2). Thus, three main complexes may be recognized: a phreatic shallow aquifer hosted in the pyroclastic-alluvial deposits, a tufaceous aquitard layer, attributable to the Phlegraean eruption of the Campanian Ignimbrite (CI, dated to

39.28 ± 0.11 k-yrs; De Vivo et al., 2001) and a deep semi-confined aquifer, hosted in the coarse pyroclastic deposits pre-CI. In the southern sector, defined Sebeto Valley (Fig. 3.1b) (Bellucci, 1994), the tufaceous horizon is absent and the aquifer is characterized by a unitary phreatic aquifer, consisting of pyroclastic, lacustrine and marine deposits.

After the World War II, the study area of Lufrano has hosted a wells field for abstraction of drinking water from the pyroclastic-alluvial aquifer of the eastern plain of Naples. In 1989 the Acerra well field was constructed to accommodate the growing demand for water. At this time a total number of about 180 wells were in operation (Fig. 3.1b), with pumping rates up to 4,0 m³/s (Fig. 3.3). This generated a deficit in the mean annual water budget of the aquifer of approximately 2,65 m³/s (Allocca & Celico, 2008).

This mismanagement of groundwater resources caused the overexploitation of the pyroclastic-alluvial aquifer, with a rapid decline of the groundwater level, reaching a maximum piezometric decrease value of 16 m in 1989 (Allocca & Celico, 2008). The extraction of highly mineralized waters coming from deeper parts of the aquifer, characterized by slow circulation, has led to an increase in Fe, Mn and fluoride concentrations (elements naturally contained in deposits of volcanic origin) (Celico et al., 1994; Esposito, 1998). The groundwater quality deterioration led to the withdrawals drastic reduction of Lufrano well field. Therefore, starting from 1990, a continuous groundwater rebound has occurred, observed both at the whole hydrogeological basin and at local scales (Allocca & Celico, 2008; Allocca et al., 2016). In different zones of the eastern plain of Naples, environmental effects of groundwater rebound were noticed, as groundwater flooding events affecting basements, railway tunnels, agricultural lands and archaeological sites (Allocca & Celico, 2008; Allocca et al., 2016), and ground deformation related to the increase of water pore pressure (Coda et al., 2019a).

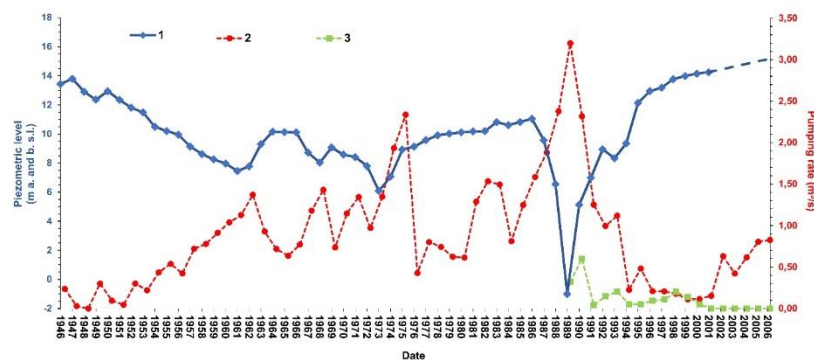


Figure 3.3 - Piezometric level and pumping rates. 1) Lufrano well-field piezometric level; 2) pumping rate of the Lufrano well field, 3) pumping rate of the Acerra well field.

3. Data and methodologies

3.1 Hydrogeological data

Stratigraphical data of 9 boreholes (Figs. 3.1b and 3.4a) were used to reconstruct the aquifer structure of the study area, correlating the lito-stratigraphical information to the corresponding role in the groundwater flow. Therefore, two orthogonal hydrostratigraphic cross-sections were created (A-A' and B-B' in Fig. 3.2) to characterize the 2D structure of the aquifer. The stratigraphical dataset derives from the database of Italian Higher Institute for Environmental Protection and Research (ISPRA, 2019).

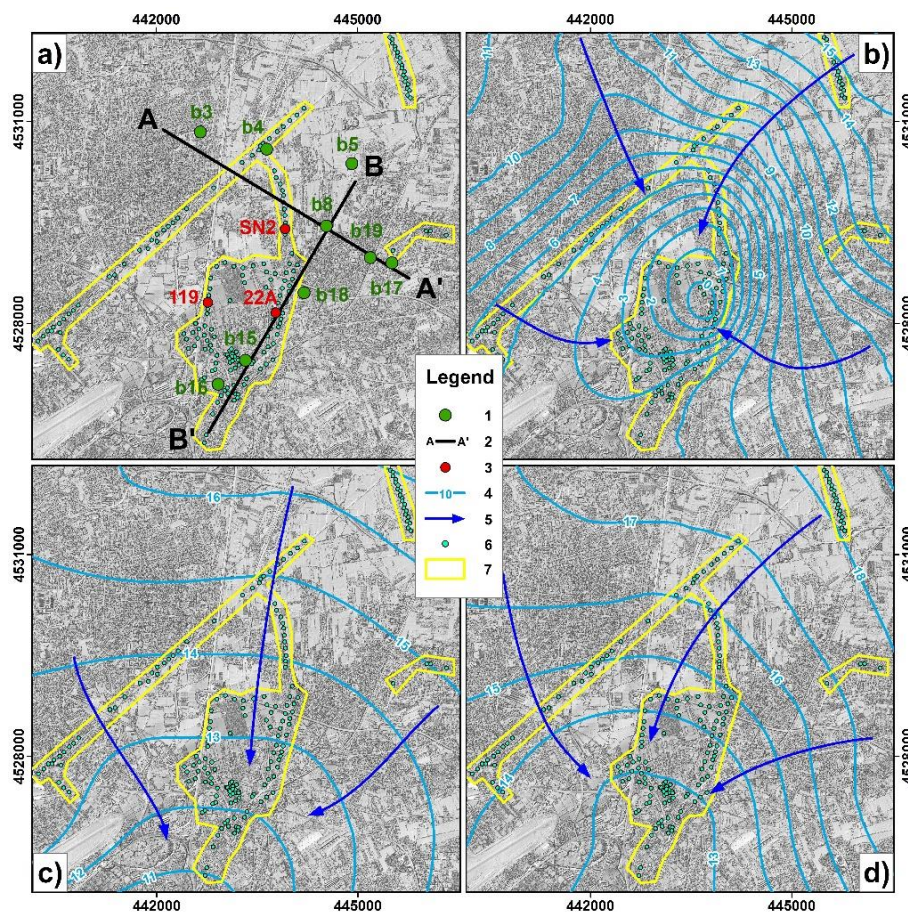


Figure 3.4 - Location of boreholes and long-term piezometric monitoring wells (a), and groundwater flow scheme for the years: 1989 (b), 2002 (c), 2006 (d). Legend: 1) borehole; 2) trace of hydrostratigraphic cross-section; 3) long-term monitoring well; 4) water table contour (m a.s.l.); 5) groundwater flow direction; 6) drinking-water well; 7) wells field area.

To analyze the dynamics of groundwater rebound in the period 1989-2006, the spatio-temporal variations of piezometric head were reconstructed by overlapping piezometric data for 1989, 2002 and 2006. These data were collected during field surveys carried out

by private companies, public agencies and researchers (Celico & De Paola, 1992; Esposito, 1998; AdB, 2004; Dati, 2006). Piezometric contour maps were digitalized in GIS environment, (Figs. 3.4b, 3.4c and 3.4d) to calculate two piezometric head variation maps (Δh , m) for the periods 1989-2002 and 2002-2006. The piezometric contour map of 1989 (Fig. 3.4b) shows the historical minimum groundwater levels, corresponding to the groundwater maximum over-exploitation period. In this case, values below the sea level have been reached in the central sector of the Lufrano well field. In 2002-2006 maps (Figs. 3.4c and 3.4d), an increase in piezometric head is observed as well as the depression cone absence induced by groundwater withdrawal previously detected.

Furthermore, the hydro-stratigraphic conceptual model and additional piezometric data obtained by the long-term monitoring (for the period 1985-1998, deriving by a survey of the A.M.A.N. aqueduct company) of three wells of Lufrano wells field (Fig. 3.4a) were used to observe the possible spatial and temporal correlation between water table rise and ground deformation.

3.2 DInSAR data

SAR dataset belongs to the Italian First Not-Ordinary Plan of Environmental Remote Sensing project (PST-A-1 in Italian) (Costabile, 2010; Di Martire et al., 2017), and it was released for scientific use in the framework of an agreement with the Italian Ministry of Environment. In detail, the PSInSAR (Ferretti et al., 2001) and PSP-DifSAR (Costantini et al., 2008) techniques were implemented to process 139 ERS-1/2 (67 acquired over ascending orbit) and 92 ENVISAT (52 in ascending orbit) images, covering the time-span 1992-2000 and 2002-2010. In this work, only ascending data have been used. All the PSs maps contain information about velocities of displacement, coherence, cumulated displacement and standard deviation. The assumption of the PSInSAR basic technique is the capability of identifying individual radar reflectors, the so-called permanent scatterers, which are targets that remain coherent over long time intervals, thus allowing to measure a displacement time series. A detailed description of the PS technique can be found in Ferretti et al. (2001). The basic assumption, on the other hand, of the PSP technique is that every PS is identified and analyzed only working with pairs of points called arcs; for further details about the algorithm interested readers can refer to Costantini et al. (2008). In this work, PSs have been interpolated by means of Inverse Distance Weighted (IDW) algorithm.

Figure 3.5 shows the PS velocity maps related to the two time-span considered: in Figure 3.5a, ERS data highlights a general uplifting trend for the study area distributed among 7465 PSs, with highest and lowest values of displacement rate of 12.25 and -15.44 mm/yr, respectively. In Figure 3.5b ENVISAT data display a general stable pattern except for subsidence phenomena registered in the SE and SW areas. Here, highest and lowest values of deformation rates are, among the 7816 PSs, of 5.4 and -16.2 mm/yr. Stability ranges of the two PSs velocity maps have been calculated multiplying 1.5 times the standard deviation of stable points, which is, for ERS and ENVISAT data, 0.62 and 0.65, respectively. In Table 3.1 the PSs main figures are resumed.

Table 3.1 - DInSAR LoS measurement statistics referred to the whole area.

Displacement rate	ERS1/2 1993-2000	ENVISAT 2002-2006
Highest value	12.25 mm/yr	5.40 mm/yr
Lowest value	-15.44 mm/yr	-16.20 mm/yr
Mean value	0.87 mm/yr	-0.62 mm/yr
Standard deviation	0.62	0.65
PS density	183.8 PSs/km ²	192.5 PSs/km ²

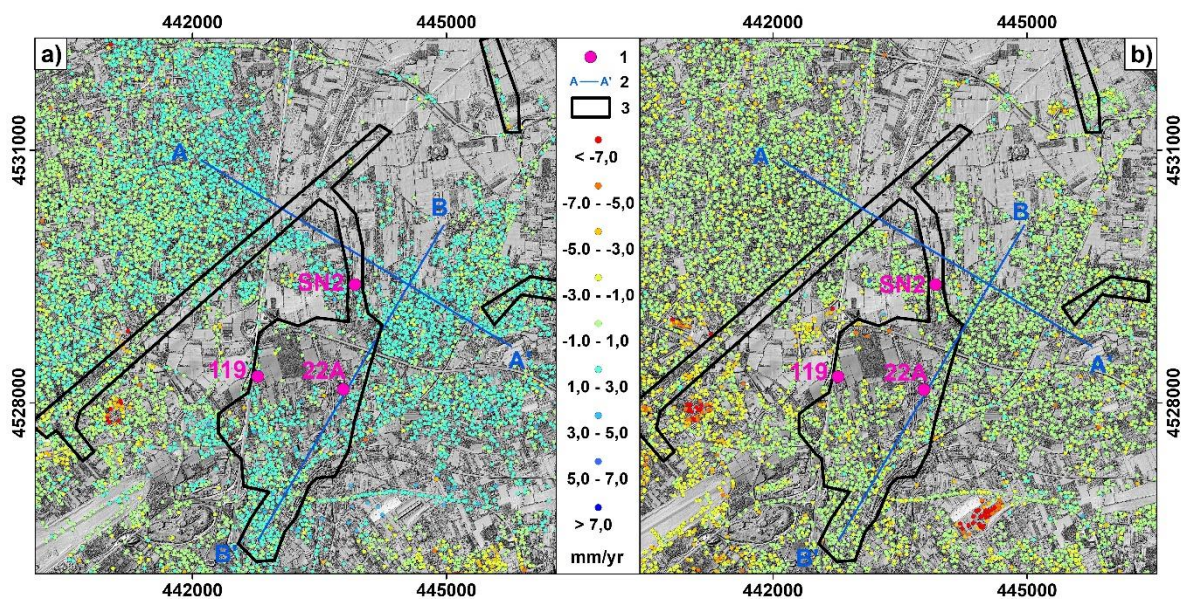


Figure 3.5 - LoS velocity maps (mm/yr) of the study area by ERS1/2 (a) and ENVISAT (b) data. Legend: 1) long-term monitoring well; 2) trace of hydrostratigraphic cross-section; 3) wells field area.

4. Results

4.1 Piezometric head variation maps

The groundwater recovery is clearly recognizable in the piezometric head variation maps (Figs. 3.6a and 3.6b). A significant rise, in the period 1989-2002, with values up to 13 meters in the central sector of the study area may be recognized (Fig. 3.6a). In the same sector, during the following five years (period 2002-2006), the groundwater recovery continued with a slower trend and with values between few centimeters and 3 meters (Fig. 3.6b).

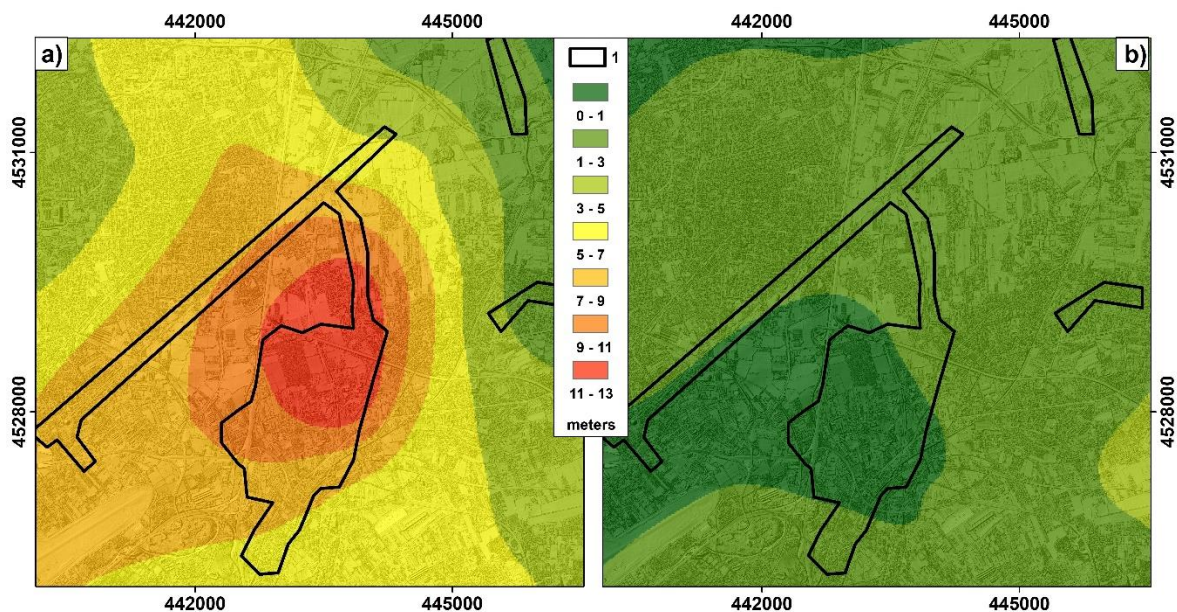


Figure 3.6 - Piezometric level variation (m) in the period 1989-2002 (a) and 2002-2006 (b). Legend: 1) drinking-water well; 2) well fields area. The piezometric variation values were classified using a constant interval of 2 m.

The maximum groundwater recovery, for the whole period considered, is of 15 m, thus reaching values of piezometric head height similar to 1946 (see Fig. 3.3). The calculated piezometric rising values are consistent with previous studies carried out in the surrounding areas (Coda et al., 2019a). Those works also showed that the rise is not induced by an increase in the precipitation regime but rather by the drastic reduction of the groundwater abstraction.

4.1 Satellite-based deformation maps

Two different cumulative displacement maps were elaborated, starting from the ERS-1/2 and ENVISAT data, for the time-spans 1993-2000 and 2002-2006, respectively. The interpolation has been carried out by means of IDW algorithm, obtaining a continuous map of 50 m-cell resolution. Such value has been chosen according to the ERS and ENVISAT resolution (20x4 m) and to the PS density of the area. The interpolation process enables the examination of the whole area of interest, measuring values surrounding the prediction location for any unmeasured location. Hence, the interpolation has permitted to generate spatial profiles of deformation, providing precise information on displacement rates in different areas. The 1993-2000 ERS1/2 data map (Fig. 3.7a) shows a general uplifting deformation pattern in Lufrano area, with maximum values of displacement of 38 mm in the time-span considered (Tab. 3.2). Moreover, more than 20 PSs have displacement value higher than 20 mm and about 270 PSs are characterized by displacement higher than 10 mm. Their distribution is mostly concentrated in the Lufrano area, in the inhabited area adjacent to the wells field. It is worth to point out also a subsiding trend in the area located to SE of Lufrano area, falling within the ring-style subsidence areas (see Fig. 3.1a) (Lanari et al., 2002), with values of displacement ranging from -20 to -60 mm for about 100 PSs. Other subsiding bowls are located in the western sector of the study area, with values of deformation up to -50 mm.

ENVISAT data ranging from 2000 to 2006 (Fig. 3.7b) also shows both uplifting and subsiding trends. However, the distribution of PSs showing uplift is slightly different from the previous dataset: the area of Lufrano, indeed, shows a generally reduced trend of uplift, with many PSs characterized by lower values of deformation, with average values of about 10 mm at the last time period considered (2006). On the other hand, the subsiding trend in the SE area shows a general slowdown, unless some PSs showing values of deformation up to -100 mm all distributed over the Agrifood Centre of Napoli (CAAN) of Volla town. Such deformation can be related to the consolidation of the terrains after the beginning of the building, completed in 2008, extending for more than 350.000 m². The western sector of the study area also confirms a subsiding trend, over the same areas identified in the previous dataset.

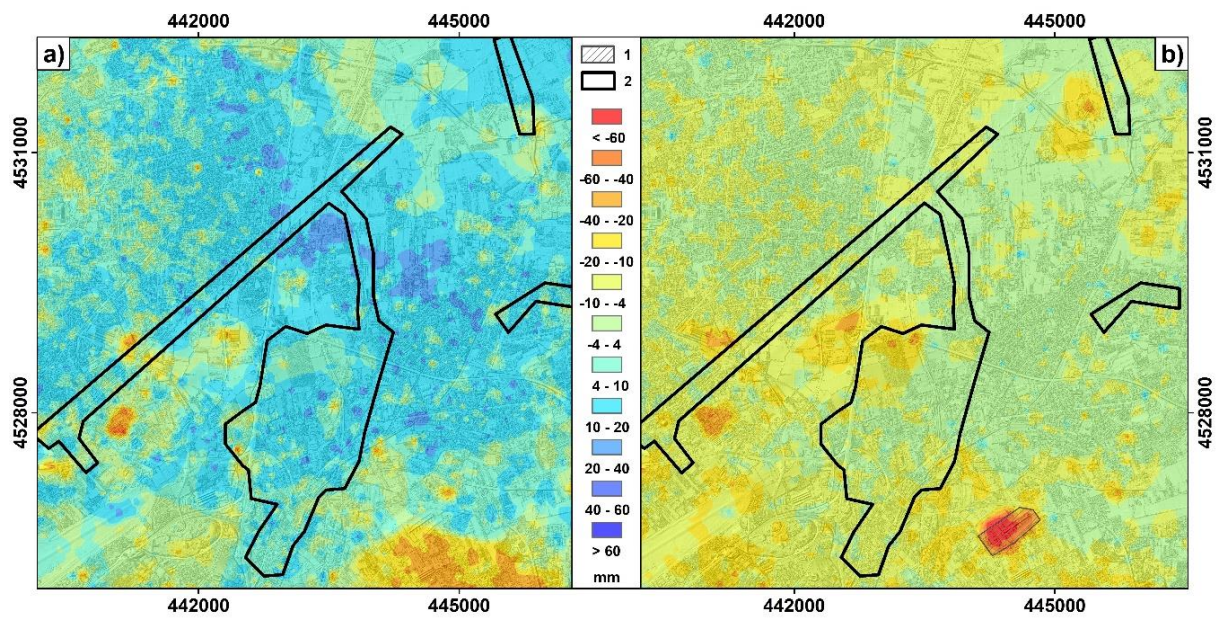


Figure 3.7 - DInSAR-derived displacement maps: a) ERS-1/2, 1992-2000 period; b) ENVISAT, 2002-2006 period. Legend: 1) Agrifood Centre of Naples (CAAN); 2) wells field area.

Table 3.2 - DInSAR LoS measurements referred to the whole area.

Vertical displacement	ERS1/2 1993-2000	ENVISAT 2002-2006
Highest displacement	63.60 mm	19.81 mm
Lowest displacement	-73.58 mm	-95.39 mm
Mean displacement	7.94 mm	-5.11 mm
Standard deviation	2.7	2.6

5. Discussion

In this work, a coupled analysis of hydrogeological and interferometric data was carried out in order to find a cause-effect relationship between the rise of piezometric levels and the ground uplift.

The spatial comparison between the piezometric and ground deformation profiles, calculated along the cross-sections A-A' and B-B' (Fig. 3.8), shows that the deformation behavior depends on the local structure of the aquifer. In detail, along the A-A' cross-section (Fig. 3.8a), in the periods 1989-2002 (referred to piezometric data) and 1993-2000 (referred to interferometric data) an average piezometric rise of about 7.7 meters and an average uplift of 14.4 mm was recorded. In the period 2002-2006, the groundwater rebound was lower (1,6 m) and no appreciable soil deformation was detected, being this trend generally recognizable throughout the whole study area, as shown in Figures 3.6 and 3.7. For the entire cross-section, the piezometric changes concern the deep semi-confined aquifer leading to an increment of the potential head rather than a rise of the water table. The homogeneity of the aquifer system influences the deformation profile pattern, which shows up slightly rough.

Along the B-B' cross-section, for the stretch characterized by a multi-layered aquifer system, the piezometric rise affected the shallow phreatic aquifer (Fig. 3.8b), with values of about 8 m (first period) and 5 m (second period), and a maximum value of average vertical displacement of about 16 mm was recorded. The sector characterized by a strong heterogeneity in the aquifer's structure shows the greater spatial irregularity of the vertical displacement (Fig. 3.8c); the piezometric rise (up to 16 m in the entire period) has involved the deep aquifer, in the first period in phreatic condition and then partially semi-confined with the tufaceous aquitard in incoherent facies. The last sector (Fig. 3.8d) is characterized by an unconfined aquifer, in which a piezometric rise of about 5 m (in the first period) correspond to an average uplift of about 10 mm.

Therefore, the integrated monitoring and analysis of piezometric rise and deformation highlighted the different behavior of different sectors of the plain, being characterized by extremely heterogeneous structures. The shallow phreatic aquifer of the NE multi-layered system showed the highest displacement values (Fig. 3.8b), while the unconfined aquifer of the S sector the lowest values (Fig. 3.8d). The strongly heterogeneous sector in the central sector is characterized by an irregular displacement pattern (Fig. 3.8c).

The radius of influence of the wells field during the recovery period has been also analyzed, by plotting together piezometric head variations and displacement rates (Fig. 3.9). Piezometric head variations have been compared with ERS data, for the first period (see Figs. 3.5a and 3.6a), along four profiles, starting from the maximum piezometric rise area and towards NW, NE, SW and SE directions. Such comparison shows very similar decreasing trend in all four directions, both for displacement and for piezometric change entities. Higher displacement rates can be found in proximity of the area interested by the maximum piezometric recovery, while they decrease moving away from this sector. This further analysis confirms the relationship between recovery of the piezometric level and vertical displacements, showing how the distance from the wells field influences surface deformation.

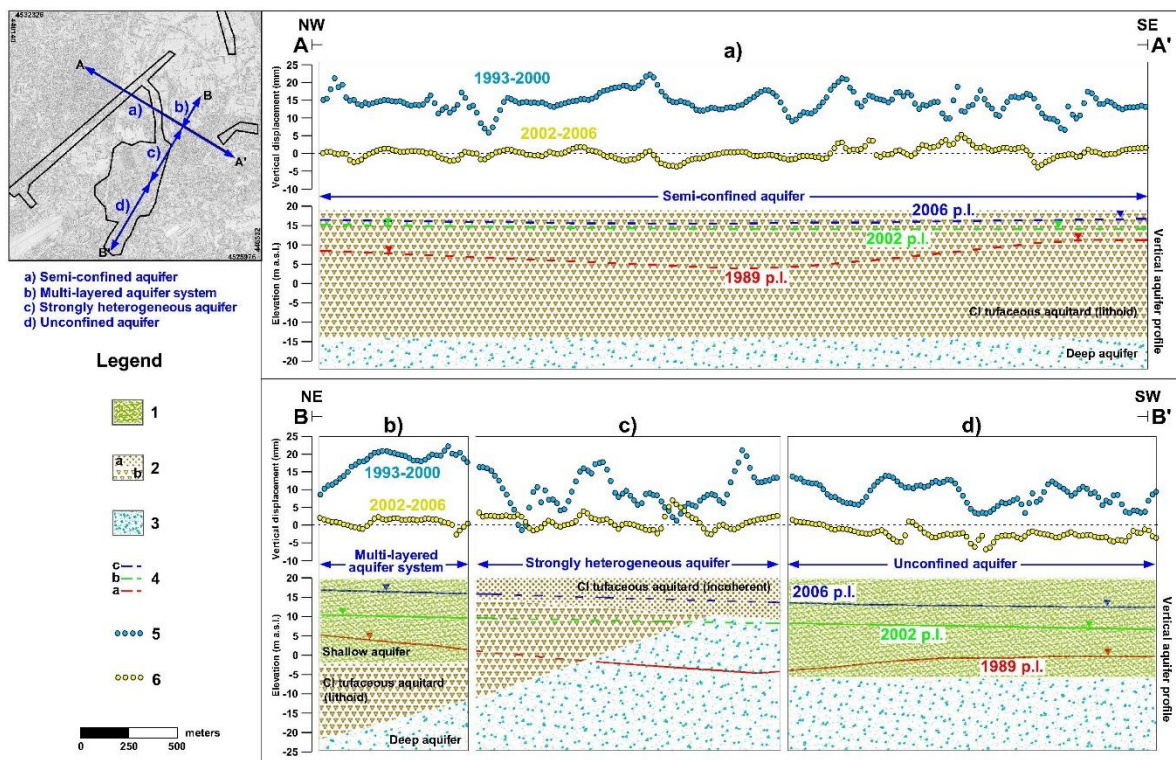


Figure 3.8 - Groundwater levels and ground vertical deformations along the section traces A-A' (a) and B-B' (b, c and d). Legend: 1) shallow pyroclastic-alluvial-lacustrine complex; 2) Campanian Ignimbrite (CI) in incoherent (a) or lithoid (b) facies; 3) the deep pyroclastic sandy complex; 4) piezometric level (m a.s.l.) for the years 1989 (a), 2002 (b) and 2006 (c); 5) vertical displacement (mm) in the period 1993-2000; 6) vertical displacement (mm) in the period 2002-2006.

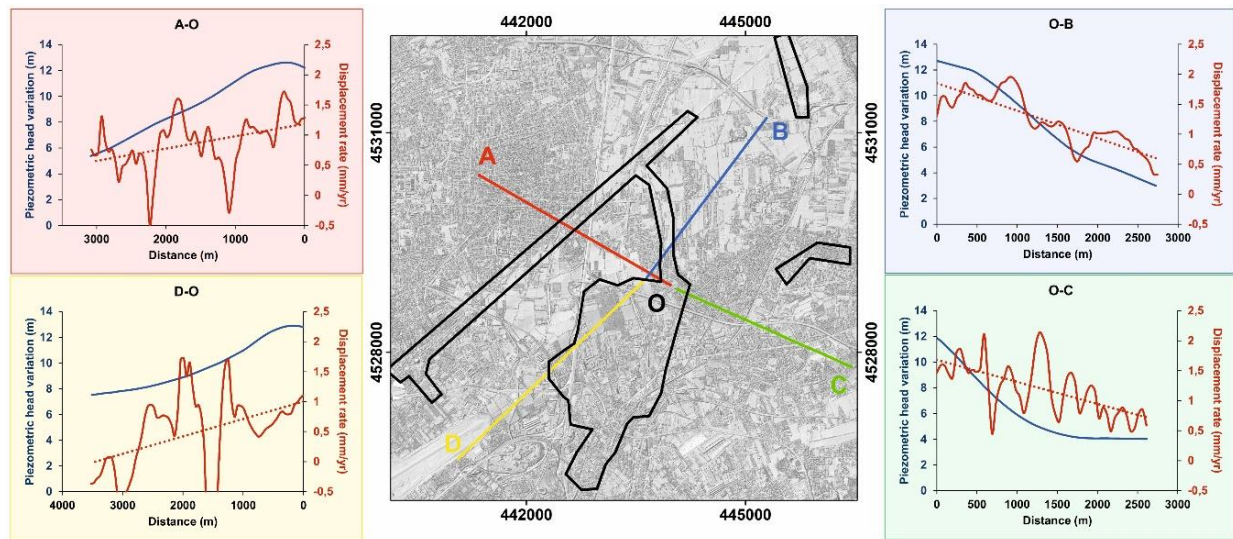


Figure 3.9 - Scheme of the radius of influence of the wells field during the recovery period. In the middle, study area with profile traces. On both sides, ERS (period 1992-2000) displacement rates (see Fig. 3.5a) vs piezometric head variation (period 1989-2002, see Fig. 3.6a) along the section traces.

The correlation between the piezometric level rise and the vertical displacement can be observed not only along spatial profiles, but also over the whole analysis period, by interpreting the time-series related to three wells of Lufrano wells field (Fig. 3.10). Comparing the deformation data to the piezometric data, the strong correlation between the trends can be observed. Two different phases are recognizable (Figs 3.10a and 3.10b): a first one (until 1997) is characterized by a piezometric rising rate of about 1,5 m/yr and 1,3 m/yr, and an average displacement rate of about 2,5 mm/yr and 3,2 mm/yr for the wells 22A and 119 respectively, followed by a second phase characterized by a stable trend both for piezometric and for displacement data. Nevertheless, in the well sn2 (Fig. 3.10c), ground deformations show a non-linear trend, being characterized by average displacement rate of 1,5 mm/yr in the first period and by a stable trend in the second one. Conversely the rate of piezometric rise is constant for both periods (1,2 m/yr).

It must be stated also that, in a general uplifting trend of Lufrano area, also some subsiding areas are recognized in the two investigation periods. On one hand, the subsiding area of the SE sector might be reconducted to the volcano-tectonics dynamics of Somma-Vesuvius complex, as documented by Lanari et al. (2002), which is characterized by a peculiar annular shape, along the northern footslope of the volcano. Such phenomenon is more evident in the 1992-2000 period, being characterized by higher deformation, with respect to the following time-span (2002-2006). Furthermore, the values of ERS displacement rates and cumulative deformation of this work are in

agreement with those calculated by Lanari et al. (2002): the average PS velocity of such sector is -0.4 while the cumulative deformation average is 52 mm, being thus consistent with the ranges of Lanari et al. (2002).

On the other hand, the area where the CAAN was constructed most likely suffered local settlements phenomena and consolidation of the terrains during the building period. This trend can be observed only in the ENVISAT analysis.

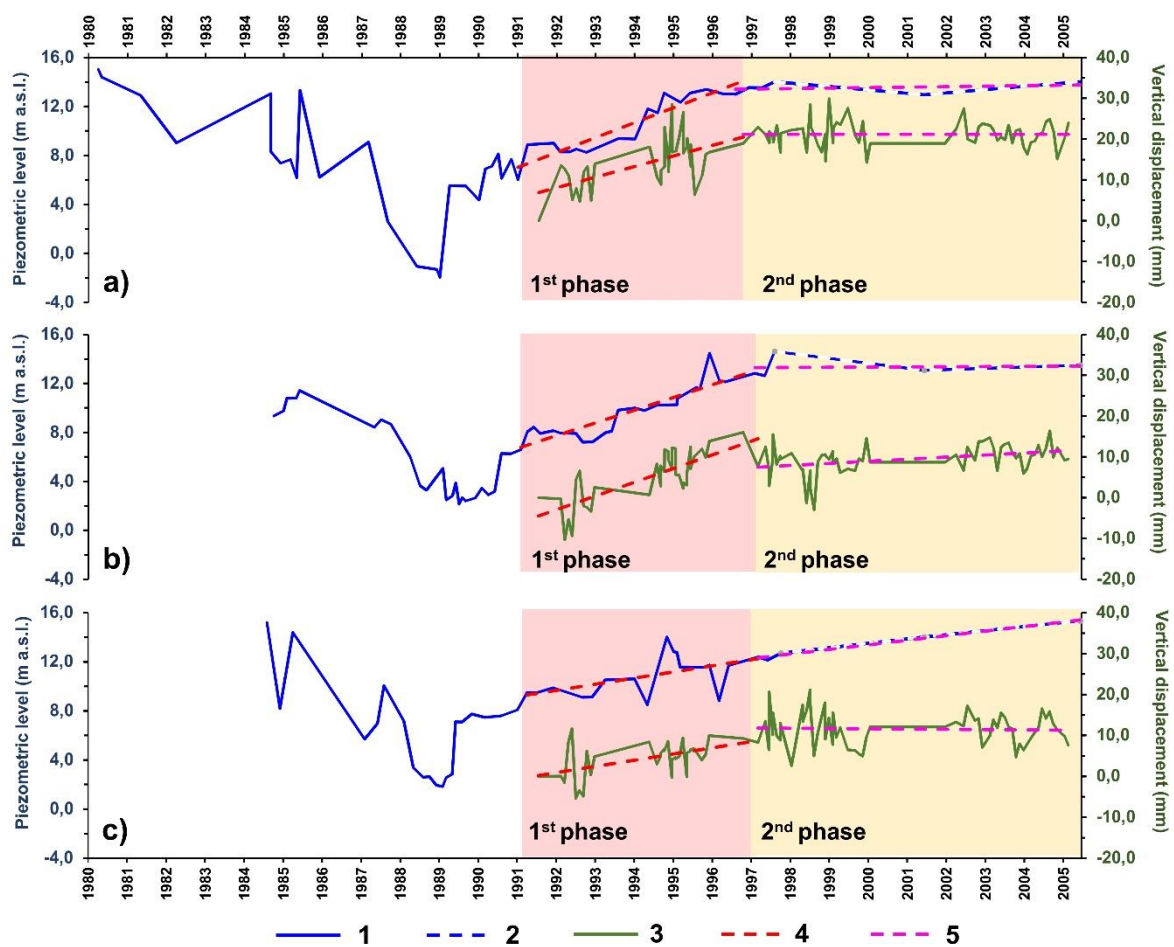


Figure 3.10 - Piezometric levels and vertical displacement of the wells 22A (a), 119 (b) and sn2 (c). Legend: 1) piezometric level (m a.s.l.); 2) piezometric level interpolated (see Figs. 3.3c and 3.3d) (m a.s.l.); 3) vertical displacement (mm); 4) trends in the first phase; 5) trends in the second phase.

6. Conclusions

Aquifer mismanagement has always been a main triggering cause for ground deformation, as testified by numerous authors (Lofgren & Klausning, 1969; Amin & Bankher, 1997; Galloway et al., 1999; González-Morán et al., 1999; Carminati & Martinelli, 2002; Bonì et al., 2018; Coda et al., 2019a), with different mechanisms according to the type of aquifer involved. In this work, a pyroclastic-alluvial aquifer has been investigated, analyzing the cause-effect relationship between groundwater level rise and ground deformation. Lufrano area is characterized by a well field intensely overexploited in the 70-80s. Because of water quality deterioration, a sudden reduction of the groundwater pumped volumes occurred, causing the so-called rebound of the piezometric level. Such event has had consequences on the ground, causing a significant uplift phenomenon, which was detected by the SAR satellites, such as ERS-1/2 and ENVISAT, in the period 1993-2006. The spatio-temporal evolution of ground deformation, covering the period of 1993–2006, was analyzed by means of DInSAR data, linking this phenomenon to the significant reduction of groundwater pumping, started 1989, as observed by hydrogeological data.

Hydrogeological monitoring data show, for 1989–2006 period, that groundwater level rise was widespread throughout the study area, with a maximum amplitude of 14 m in the central sector and a piezometric rising rate up to 1.5 m/yr. During the time span of 1993–2006, DInSAR data show general ground uplift, even though characterized by a non-linear trend with a magnitude up to 50 mm following a piezometric rising rate up to 1.5 m/yr. Moreover, the radial influence of the study area has been analyzed, showing how the deformation is mainly located in the range of Lufrano well field. Temporal comparisons between groundwater levels and ground displacement trends indicate that the land uplift may be due to poro-elastic rebound mechanism (Biot, 1941; Allen & Mayuga, 1969) in the multi-layered aquifer system, triggered by piezometric level rise following the groundwater pumping interruption.

The obtained results increase the knowledge on the effects induced by groundwater rebound affecting the study area, characterized by a high fluvial and groundwater flooding susceptibility. Therefore, to a consistent analysis of complex and interactive phenomena, such as those observed in the study area, where groundwater rebound, ground uplift and groundwater flooding coexist, the implementation of appropriate hydrogeological and hydro-mechanical models and groundwater flooding susceptibility

assessment methods are needed for a correct management of different hydrogeological risks.

4

Cumae archaeological site

Natural and Anthropogenic Groundwater Contamination in a Coastal Volcanic-Sedimentary Aquifer: The Case of the Archaeological Site of Cumae (Phlegraean Fields, Southern Italy)

Abstract.....	127
1. Introduction.....	129
2. Description of the Study Area.....	132
3. Materials and Methods.....	136
3.1 Hydrogeological Survey.....	136
3.2 Hydrochemical Sampling and Analysis.....	137
3.3 Isotopic Monitoring.....	138
4. Results.....	139
4.1 Hydrogeology.....	139
4.2 Hydrochemistry.....	141
4.3 Isotopic Survey.....	148
5. Discussion.....	152
6. Concluding Remarks.....	154
Supplementary Material.....	156

List of Figures

Figure 4.1 - (a) Geological map of Campanian Plain and (b) hydrogeological map of the eastern sector of Phlegraean Fields. (c) Geomorphological setting, hydrographic network and (d) land use of the hydrographic and hydrogeological basin of study area.

Figure 4.2 - (a) Geological map of study area and hydrogeological monitoring network. (b) 2D hydrostratigraphic model of the aquifer system.

Figure 4.3 - Groundwater flow patten in March 2014 ((a) and (b)) and July 2014 ((c) and (d)) for the shallow ((a) and (c)) and deep ((b) and (d)) aquifer.

Figure 4.4 - Spatial distribution of hydrochemical facies of shallow and deep wells, for the period (a) March 2014 and (b) July 2014, and (c) Langelier–Ludwig diagram.

Figure 4.5 - Box plots of climatic, hydrogeological, and hydrogeochemical parameters for the whole monitoring period, with indication of recharge, recession, fertilization and pumping phases; (a) rainfall and air temperature; (b) piezometric levels; (c) groundwater temperature; (d) electric conductivity; (e) concentration of NO_3^- , (f) SO_4^{2-} , (g) B, (h) Cl⁻, (i) ^{222}Rn , (j) F⁻, (k) As and (l) $\delta^{18}\text{O}$ isotopic ratios.

Figure 4.6 - Bubble maps of values of physico-chemical parameters (T (a) and (b) and -EC (c) and (d)), concentrations of major ions and trace elements (NO_3^- (e) and (f), Boron (g) and (h), SO_4^{2-} (i) and (j), Cl⁻ (k) and (l), F⁻ (q) and (r) and Arsenic (o) and (p)) and isotopes (^{222}Rn (m) and (n) and $\delta^{18}\text{O}$ (s) and (t)) in Rc and Rs periods for the shallow and deep wells.

Figure 4.7 - Plots of (a) $r[\text{SO}_4/\text{Cl}]$ vs. $[\text{Cl}]$, (b) $r[\text{Mg}/\text{Cl}]$ vs. $r[\text{Br}/\text{Cl}]$, (c) $r[\text{B}/\text{Cl}]$ vs. $[\text{B}]$ and (d) $r[\text{B}/\text{Cl}]$ vs. $r[\text{Br}/\text{Cl}]$ in shallow and deep wells.

Figure 4.8 - (a) $\delta^{18}\text{O}$ vs. δD diagram in shallow and deep wells during the recharge and the depletion hydrological phases in shallow and deep wells. (b) Monthly variations of d-excess in shallow and deep wells.

Figure 4.9 - (a) $\delta^{18}\text{O}$ vs. $\delta^{15}\text{N}$ of dissolved nitrate in shallow and deep wells. (b) Cross-plot of the $\delta^{15}\text{N}$ composition of dissolved NO_3^- vs. the natural log of N- NO_3^- concentrations (in mg/L) in shallow and deep wells in the recharge and the depletion periods. (c) $\delta^{11}\text{B}$ vs. $r[\text{B}/\text{Cl}]$ in shallow and deep wells plot in the recharge and the depletion periods. (d) $\delta^{11}\text{B}$ vs. $r[\text{Cl}/\text{Mg}]$ in shallow and deep wells in the recharge and the depletion periods.

Figure 4.10 - Hydrogeological–hydrogeochemical isotope conceptual model of study area, in natural conditions (a) and during pumping (b). (c) Trends of parameters showed in Figure 4.5.

Table S3 (supplementary material) - Hydrogeological, hydrochemical and isotopic monitoring data of groundwater in the Cumae archaeological site.

4

Natural and Anthropogenic Groundwater Contamination in a Coastal Volcanic-Sedimentary Aquifer: The Case of the Archaeological Site of *Cumae* (Phlegraean Fields, Southern Italy)

Stellato L.¹, Coda S.², Arienzo M.², De Vita P.², Di Rienzo B.¹, D'Onofrio A.¹, Ferrara L.³, Marzaioli F.¹, Trifuoggi M.³, Allocca V.^{2*}

¹ Centre for Isotopic Research on Cultural and Environmental Heritage (CIRCE), Dipartimento di Matematica e Fisica, Università degli Studi della Campania Luigi Vanvitelli, Caserta, Italy

² Department of Earth Science, Environment and Resources, University of Naples Federico II, Naples, Italy

³ Department of Chemical Sciences, University of Naples Federico II, Naples, Italy

*Corresponding author: vincenzo.allocca@unina.it

Abstract

Archeological sites close to coastal volcanic-sedimentary aquifers are threatened by groundwater contaminated by natural and anthropogenic processes. The paper reports on a hydrogeological, chemical (major, minor and trace elements) and isotopic ($\delta D-H_2O$, $\delta^{18}O-H_2O$, $\delta^{15}N-NO_3$, $\delta^{18}O-NO_3$, $\delta^{11}B$, ^{222}Rn) survey of groundwater at the *Cumae* archaeological site, which is located in the coastal north-western sector of the volcanic district of Phlegraean Fields (southern Italy), where groundwater flooding phenomena occur. Results show the presence of a complex coastal volcanic-sedimentary aquifer system where groundwater quality is influenced mainly by: (i) aquifer lithology and localized ascent of magmatic fluids along buried volcano-tectonic discontinuities, (ii) mixing of groundwater, deep mineralized fluids and seawater during groundwater pumping, and (iii) nitrate contamination >50 mg/L from non-point agricultural sources. Moreover, δD and $\delta^{18}O$ point toward fast recharge from seasonal precipitations, while the isotopic ratios of N and O in nitrate reveal the contribution of mineral and organic fertilizers as well as leakage from septic tanks. Results can assist the local archaeological

authority for the safeguarding and management of the archaeological heritage of the *Cumae* site.

Key words: coastal volcanic-sedimentary aquifer; natural and anthropogenic contamination; ^{222}Rn ; water isotopes; nitrate isotopes; archaeological site; Phlegraean Fields; southern Italy.

Stellato L., Coda S., Arienzo M., De Vita P., Di Rienzo B., D'Onofrio A., Ferrara L., Marzaioli F., Trifuoggi M., Allocca V., 2020. Natural and Anthropogenic Groundwater Contamination in a Coastal Volcanic-Sedimentary Aquifer: The Case of the Archaeological Site of Cumae (Phlegraean Fields, Southern Italy). Water, 12(12), 3463.

1. Introduction

Coastal aquifers are generally used to supply freshwater, especially in arid and semiarid areas (Zepeda Quintana et al. 2018). More than 60% of the global population is concentrated in coastal areas comprising only 10% of the Earth's surface. This percentage is expected to rise to 75% (Unsal et al., 2014; Chatton et al., 2016). Water use for anthropic activities is a key driver in the hydrologic regime of coastal aquifers (Ferguson & Gleeson, 2012) and demand for both human consumption and agricultural/industrial uses (Renau-Pruñonosa et al., 2016) threatens water resources. This is even more dramatic in arid and semiarid areas where periods of higher demand for freshwater coincide with those of greater water scarcity (Unsal et al., 2014). According to the Intergovernmental Panel on Climate Change (IPCC) (IPCC, 2007), the vulnerability of a coastal aquifer is the degree of being influenced or coping with sea-level rise and/or groundwater abstraction. Hence, coastal aquifer water quality can be endangered by high groundwater demand related to population growth and climate changes leading to a change of the dynamic equilibrium between fresh groundwater and seawater intrusion (Russak & Sivan, 2010; Ferguson & Gleeson, 2012; Werner et al., 2013; Colombani et al., 2016).

In coastal aquifers, salinization induced by seawater intrusion and human activities are the most important cause of groundwater degradation (Vengosh, 2003; Custodio, 2010). Therefore, an effective and targeted management is needed in order to preserve water resources in such complex systems (Kim et al., 2003; Custodio, 2010; Carreira et al., 2014). Among anthropic activities, agricultural practices (use of mineral and/or organic fertilizers and groundwater abstraction) are the more frequent causes of groundwater quality deterioration (Kim et al., 2003). In fact, fertilization and irrigation increase nutrient concentration in groundwater above threshold values, especially for dissolved nitrate, released mainly by the use of synthetic and natural fertilizers (91/676/CE EU Directive). Nitrate is especially dangerous for children and old people because it interacts with hemoglobin, hindering oxygen flow to cells (methemoglobinemia) (Pastén-Zapata et al., 2014), and can also form nitrosamine, which is considered to be a carcinogenic compound (Lin, 1990; Tricker & Preussmann, 1991). Septic tanks and sewage systems can also release total inorganic nitrogen to groundwater bodies (Aravena et al., 1993; Zhang et al., 2018). Moreover, nitrogen compounds can also promote, together with phosphorous, eutrophication of freshwater bodies of rivers, lakes and marshy areas of coastal zones (Braun, 2007; Kitsiou & Karydis, 2011; Zhou et al., 2020). In sedimentary-

volcanic aquifers proximal to an active volcanic system, as in the present study, the upwelling highly mineralized fluids can also cause groundwater mineralization and, as a consequence, have an impact on archaeological artifacts and infrastructure (Nord et al., 2005; de Beer & Matthiesen, 2008; Kreyens et al., 2020).

The major concern of local authorities in charge of managing water resources in such complex systems is the identification of the sources of pollution and the comprehension of processes influencing the concentration of contaminants in groundwater, aimed at planning effective countermeasures for groundwater bodies' quality protection and restoration (Werner et al., 2013). However, the identification of pollution sources is not an easy task because of the presence of: (1) more than one source, (2) point and diffuse sources and (3) several biogeochemical processes which can alter contaminant concentration (Kendall, 1998). The management of water resources in a coastal area requires an accurate characterization of aquifers' recharge, groundwater pathways and identification of groundwater contamination sources which can be effectively carried out by an integrated hydrogeological, hydrostratigraphical, hydrochemical and isotopic assessment (Custodio, 1987; Petelet-Giraud et al., 2016; Zhao et al., 2017; Abu Al Naeem et al., 2019). In many cases, the use of stable isotopes of elements allows the identification of sources characterized by different isotopic compositions (Vengosh et al., 1999; Pastén-Zapata et al., 2014; Stellato et al., 2010; De Giorgio et al., 2018; Martinelli et al., 2018; Ducci et al., 2019). In particular, the measurement of natural and anthropogenic isotopic tracers can provide information about groundwater recharge and mixing (δD and $\delta^{18}O$) (Wood & Sanford, 1995; Gonfanti et al., 1998; Thyne et al., 1999; Coplen et al., 2000), help identify groundwater hydro-facies and seawater intrusion (major ions and trace elements) (Richter & Kreitler, 1993; Herczeg & Edmunds, 2000; Genereux et al., 2002; Petelet-Giraud et al., 2016), can give information about the upwelling of mineralized fluids as well as aquifers' homogeneity (^{222}Rn , $\delta^{11}B$) (Stellato et al., 2008; 2013; Wu et al., 2016; Liu et al., 2019) and identify nitrate pollution sources ($\delta^{15}N$ and $\delta^{18}O$ of nitrates, $\delta^{11}B$) (Vengosh et al., 1994; Kendall, 1998; Widory et al., 2004; Xue et al., 2009; Ducci et al., 2019). In recent years, archaeological research carried out in coastal plains of southern Italy (Allocca & Celico, 2008; Allocca et al., 2016; Coda et al., 2019c) and archaeological sites of the Mediterranean region (Abdallah & Abd El-Tawab, 2013) has seen a setback including reburial of some artefacts, due to rising groundwater and consequent flooding, as observed in the *Cumae* archaeological site (in the province of Naples) which is among the most important and visited in southern Italy. It is located within the Phlegraean Fields

Regional Park, which hosts a large supervolcano situated to the west of Naples (Caputo et al., 2010) and in 2006 has been included in the World Heritage sites of UNESCO. The *Cumae* archaeological site hosts the partially buried ruins of the Greek to medieval city of *Cumae*. The site includes different artefacts, cultural remains and ancient monuments, dating back to the Greek, Roman and Byzantine epochs (Capano et al., 2015). In particular, the Monumental Roman Necropolis, a small sub-flat coastal plain area, has been studied since 1809 and archaeological research still continues.

Given the relevance of this archaeological site, the conservation and protection of ancient ruins is a principal task. The deterioration of in situ archaeological deposits (Holden et al., 2006) can be accelerated by environmental and hydrogeological changes. Moreover, the conservation and management of archaeological resources, especially in rural areas, is threatened by the use of fertilizers and pesticides, irrigations, tillage and drainage. In particular, the lithology of the buried artifacts can be damaged by corroding compounds bearing groundwater (Van der Noort, 1996; Van der Noort et al., 2001).

Considering the interference between groundwater and archaeological structures, a multidisciplinary approach based on a hydrogeological, hydrogeochemical and isotopic monitoring has been adopted in order to characterize the natural and anthropogenic processes affecting groundwater quality in the *Cumae* coastal aquifer. The measurements concerned water levels, temperature, pH, electric conductivity, major and minor ion concentrations, trace elements and isotopes ($\delta\text{D-H}_2\text{O}$, $\delta^{18}\text{O-H}_2\text{O}$, $\delta^{15}\text{N-NO}_3$, $\delta^{18}\text{O-NO}_3$, $\delta^{11}\text{B}$, ^{222}Rn). The analysis of the temporal and spatial distributions of each parameter and the identification of natural and anthropic sources of groundwater contamination are central to assessing the potential threat to these ancient ruins.

2. Description of the Study Area

The *Cumae* archaeological site extends over about 3.0 km² and is located in the north-western coastal sector of the active volcanic district of the Phlegraean Fields bordering the Tyrrhenian coast of southern Italy (Figs. 4.1a and 4.1b). It is part of the Phlegraean wetlands area and of Mount Cumae's coastal Forest, both belonging to the Phlegraean Fields Regional Park. It includes the ancient city of *Kyme*, the first Greek colony in Italy founded in the 730 B.C. and inhabited until 1207 A.C. (Caputo et al., 2010).

During the Holocene, primary and secondary volcanism of the Phlegraean Fields controlled the geological and geomorphological evolution of this coastal sector (Fig. 4.1b). Caldera forming eruptions produced typical circular landforms and buried normal fault zones. In addition, eustatic sea-level fluctuations modified the coastline leading to lacustrine and palustrine environments in the coastal plain (Sacchi et al., 2014).

From a geological point of view, the *Cumae* archaeological site is located directly adjacent to the western edge of the Campanian Ignimbrite (CI) caldera, dated 39 ka BP (De Vivo et al., 2001) (Figs. 4.1a and 4.1b). Several buried normal faults, fractures and deep crater rims characterize this sector of the Phlegraean Fields. The study site is characterized by a complex coastal volcanoclastic-sedimentary sequence, formed by sandy silts, silts, clays and peats of marine, alluvial and lagoon-palustrine environments, laterally passing into aeolic sands next to the shoreline (Bravi et al., 1996; ISPRA, 2015). This sedimentary coastal complex has unconsolidated ash-fall pyroclastic deposits formed by fine ashes and pumices and consolidated yellow tuffs. The transition from a volcanic to coastal environment produced a strong lithostratigraphic heterogeneity (Figs. 4.1b, 4.2a and 4.2b).

The local geomorphology is typical of a coastal plain, with altitudes between 0 and 16 m a.s.l. (Fig. 4.1c). From the sea toward the inland area, the site is characterized by a dune system and a wetland in the retro-dunal zone (Fig. 4.1c). The Cuma Mount, a 85 m a.s.l. high remnant of a pre-CI volcanic building older than 39 ka (ISPRA, 2015), rises from the flat morphology of the coastal plain (Figs. 4.1b and 4.1c).

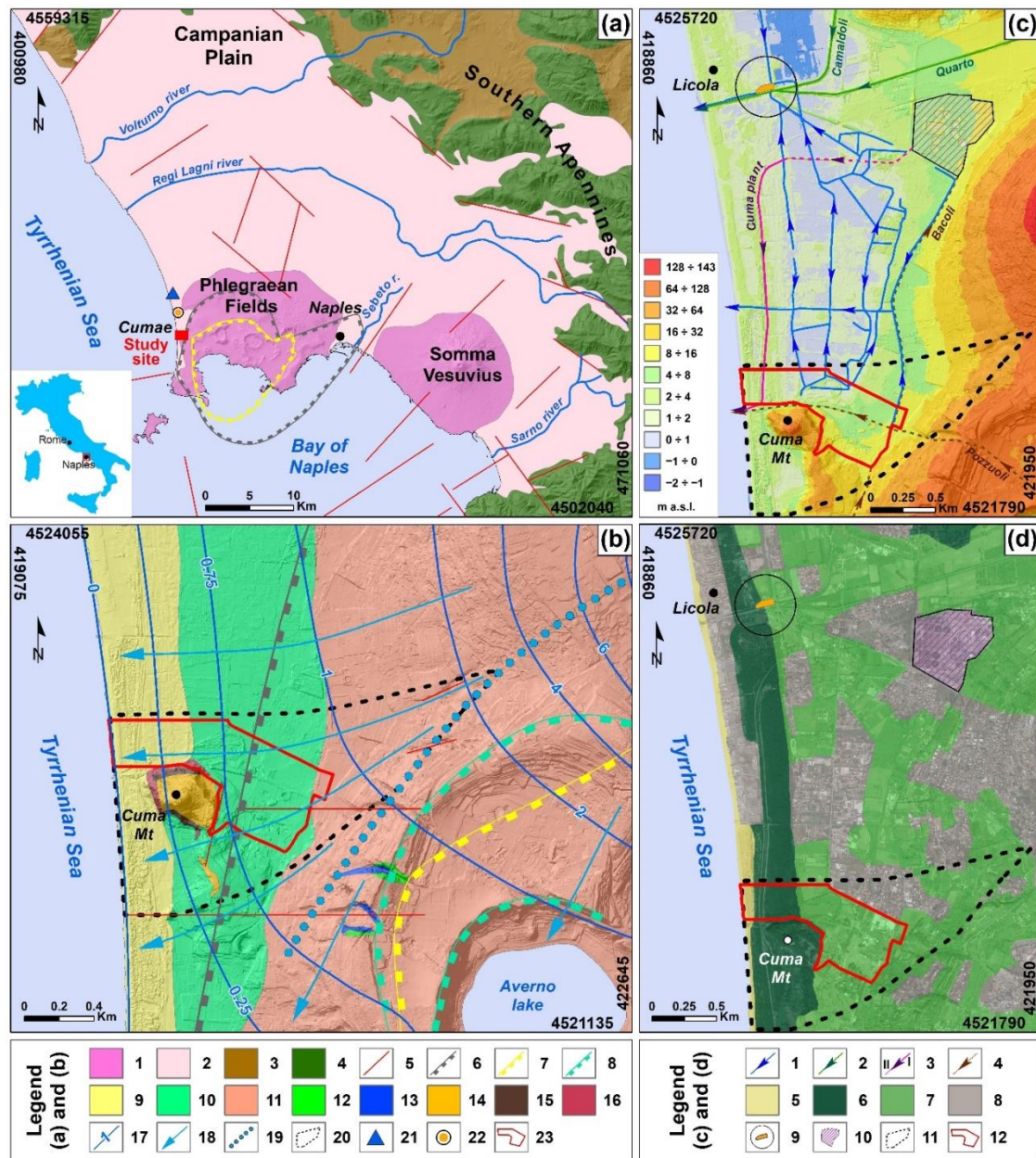


Figure 4.1 - (a) Geological map of Campanian Plain and (b) hydrogeological map of the eastern sector of Phlegraean Fields (after ISPRA, 2015 modified). Legend: (1) Quaternary epiclastic deposits; (2) Quaternary volcanic deposits; (3) Miocene deposits; (4) Mesozoic Apennine platform carbonates; (5) buried fault; (6) Campanian Ignimbrite (CI) caldera boundary; (7) Neapolitan Yellow Tuff (NYT) caldera boundary; (8) buried caldera boundary; (9) Eolic deposits; (10) Pyroclastic-fluvio-palustrine deposits; (11) Pyroclastic deposits; (12) Baia's tuffs; (13) Gauro's eruption deposits; (14) Neapolitan Yellow Tuff; (15) Museum Breccia; (16) Cuma Mt lavas; (17) groundwater contour line (m a.s.l.); (18) groundwater flow direction; (19) groundwater divide; (20) hydrogeological basin of study area; (21) Licola pluviometric station; (22) Licola draining station; (23) study area. (c) Geomorphological setting, hydrographic network and (d) land use of the hydrographic and hydrogeological basin of study area. (1) Reclamation draining channel; (2) surface water channel; (3) open-air (i) and underground (ii) Cuma wastewater treatment plant discharge channel; (4) underground wastewater channel; (5) beach; (6) Mediterranean bush and pinewood; (7) agricultural land; (8) urban area; (9) Licola drainage station; (10) Cuma wastewater treatment plant; (11) hydrogeological basin of study area; (12) study area.

From the hydrogeological point of view, the groundwater flow system is unitary (Fig. 4.1b) at the basin scale (Celico et al., 1992; De Vita et al., 2018), although it is locally influenced by hydraulic heterogeneity of volcano-sedimentary succession, groundwater pumping and reclamation drainage channel system. The hydrogeological basin which includes the study site (Fig. 4.1b) extends for about 1.7 km² with a groundwater flow oriented toward the coastline in the west (Fig. 4.1b). It is characterized by a grade of vulnerability to pollution from medium to high (Tufano et al., 2020). At the small scale, the study site hosts a porous multilayered aquifer system (Figs. 4.2a and 4.2b) formed by a shallow phreatic aquifer in the pyroclastic and pyroclastic-alluvial-lacustrine sediments (pyroclastic (P) and pyroclastic-alluvial-lacustrine (PAP) complexes) and a semiconfined deep aquifer in the older pyroclastic deposits (DPs complex), separated by a deka-m thick lithic tuffaceous aquitard (YT). In the coastal zone, this YT aquitard is absent resulting in one single unconfined shallow aquifer (Fig. 4.3a), hosted in the dune complex (Allocca et al., 2018).

The surface hydrography is controlled by a reclamation drainage system of micro-channels, which locally crosses the whole retro-dunal zone of the coastal plain and whose altitude is very close to the sea level or just below it (Fig. 4.1c). It was built during the last two centuries, draining surface and groundwater either to the sea directly or through the Licola mechanical pumping station. In addition, open-air and underground channels carry wastewater to the Cuma wastewater treatment plant and to the sea (Figs. 4.1c and 4.2a).

Land use consists prevalently of agricultural lands, corresponding to about 70% of the study area (Fig. 4.1d), in which intensive cultivation is practiced by applying pesticides and chemical and organic fertilizers. About 30% is covered by Mediterranean bush and pinewood ending with a narrow stretch of beach. Moreover, within the hydrogeological basin, sparsely urban areas are present, which are partially covered by a sewage network and, where it is locally absent, septic tanks are used. The climate is of Mediterranean type, characterized by hot dry summers and moderately cool and rainy winters. The range of mean annual air temperatures is approximately 13–15 °C and the average annual rainfall is about 700 mm/year (Allocca et al., 2014).

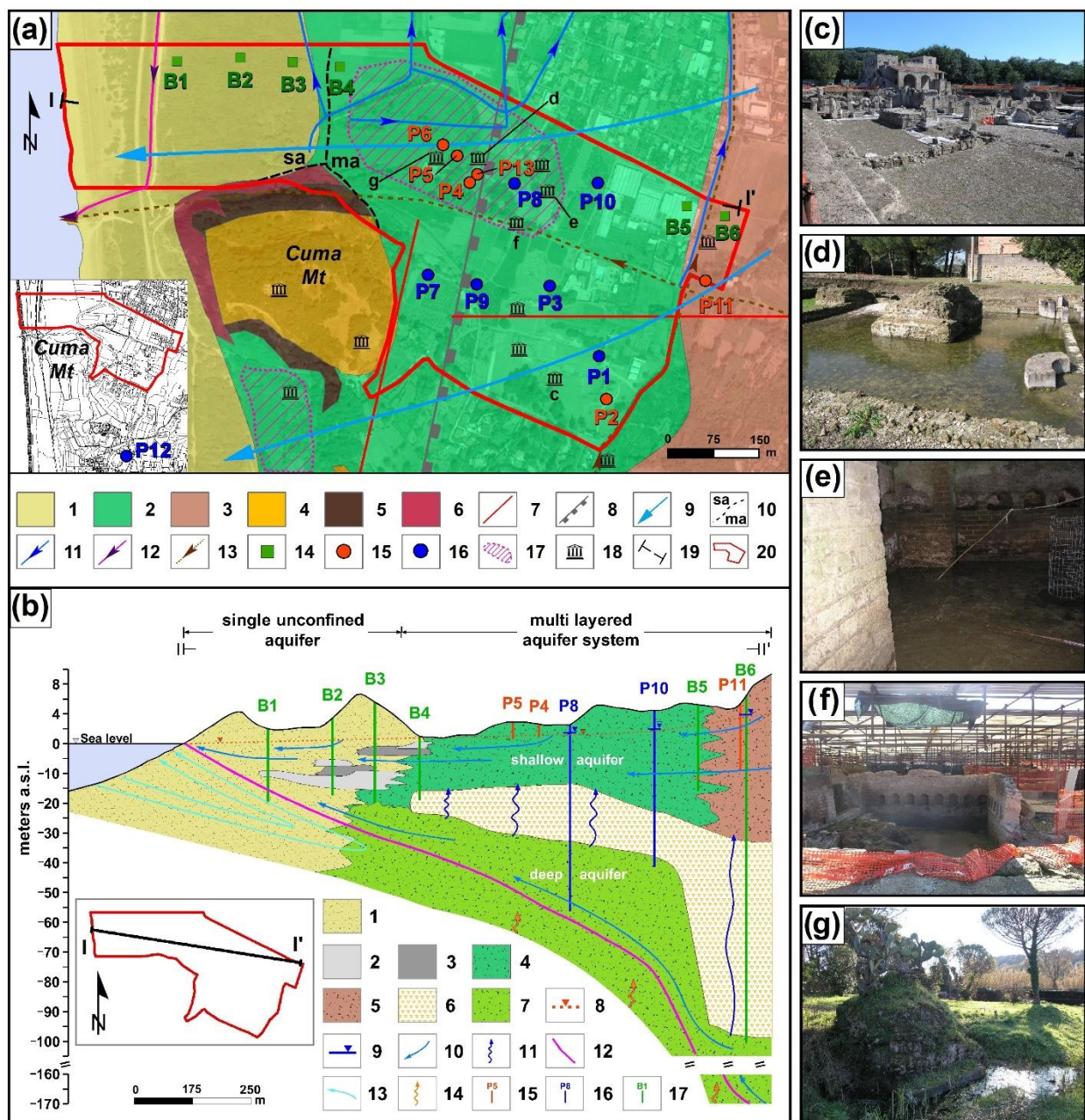


Figure 4.2 - (a) Geological map of study area and hydrogeological monitoring network. Legend: (1) Eolian deposits; (2) Pyroclastic-fluvio-palustrine deposits; (3) Pyroclastic deposits; (4) NYT; (5) Museum Breccia formation; (6) Cuma Mt lavas; (7) buried fault; (8) CI caldera boundary; (9) groundwater flow direction; (10) single unconfined aquifer (sa) and multilayered aquifer system (ma) sectors; (11) groundwater draining channel; (12) Cuma plant discharge channel; (13) underground wastewater channel; (14) borehole; (15) shallow well; (16) deep well; (17) groundwater flooding (GF) area; (18) archaeological site of Necropolis (GF impacted in (d)–(g)); (19) trace of hydrostratigraphic section; (20) study area. **(b)** 2D hydrostratigraphic model of the aquifer system. (1) Dune complex; (2) silts; (3) clays and peaty deposits; (4) pyroclastic-alluvial-lacustrine (PAP) complex; (5) pyroclastic (P) complex; (6) tuffaceous aquitard (YT) aquitard; (7) pyroclastic deposits (DPs) complex; (8) piezometric level of shallow unconfined aquifer; (9) piezometric level of deep semiconfined aquifer; (10) groundwater flow direction; (11) vertical groundwater flow direction; (12) Fw-Sw interface; (13) saline groundwater flow; (14) high mineralized fluids rising; (15) shallow well; (16) deep well; (17) borehole.

Finally, in the last two decades, the study area has been recognized as affected by hydro-environmental criticalities which endanger the state of conservation of artefacts, cultural remains and ancient monuments of the *Cumae* archaeological site (Figs. 4.2a, 4.2d–g). Indeed, as observed in other sectors of the Metropolitan City of Naples (Allocca et al., 2016; Coda et al., 2019a; 2019b; 2019c), the rising of groundwater level and related Groundwater Flooding (GF) phenomena have been registered, causing damage to structural and decorative features of buried archaeological artefacts. Both hydrological processes are mainly attributed to the rising of sea levels from the Roman period to the present in the central area of Mediterranean basin (Lambeck et al., 2004) and to local volcano-tectonic land subsidence (Todesco et al., 2014). Consequently, since the early 2000s numerous GF episodes, with groundwater levels up to +1.20 m at the base of some archaeological remains, have been observed in the retro-dunal zone, at the Monumental Roman Necropolis of the *Cumae* archaeological site (Figs. 4.2a, 4.2e–g), despite the local presence of a man-made micro-channel reclamation drainage system (Fig. 4.2a).

3. Materials and Methods

Eleven field campaigns were carried out from December 2013 to February 2015. Water table level was monitored and groundwater samples were collected in thirteen domestic and agricultural wells: 6 shallows wells (P2, P4, P5, P6, P11, P13, up to 15 m depth, Fig. 4.2a) and 7 deep wells (P1, P3, P7, P8, P9, P10, P12 up to 80 m depth, Fig. 4.2a) on a monthly frequency. The wells P1, P3, P7, P8, P10 and P12 were equipped with submersible pumps used for purging and sampling while the wells P2, P4, P5, P6, P9, P11, and P13 were sampled by bailer, after rinsing it three times with sample water.

Physico-chemical parameters (i.e., temperature, pH, electrical conductivity, alkalinity) were measured by field analysis. Hydrochemistry (i.e., major ions and trace elements), isotopic ratios (i.e., $\delta^{18}\text{O}$ and δD in water, $\delta^{15}\text{N}\text{--NO}_3$ and $\delta^{18}\text{O}\text{--NO}_3$, $\delta^{11}\text{B}$) and ^{222}Rn specific activity was determined in groundwater samples in the laboratory. Results of hydrogeological, hydrochemical, and isotopic monitoring are listed in Table S3 in the supplementary materials.

3.1 Hydrogeological Survey

In order to analyze groundwater flow and the spatio-temporal variation of the piezometric levels, a groundwater monitoring network was reconstructed inside the

Cumae archaeological park (Fig. 4.2a). The piezometric levels were monitored monthly from December 2013 to February 2015 in 6 shallow wells (P2, P4, P5, P6, P11, P13, up to 15 m depth) and in 7 deep-wells (P1, P3, P7, P8, P9, P10, P12 up to 80 m depth). Monitoring was performed by a water level meter (BFK-100 model, PASI, Italy). The ground elevation of the wells was measured by the DGPS technique (K9 Series RTK, KOLIDA Instrument, China) and verified through the reconstruction of a Digital Elevation Model (DEM) derived from a LiDAR survey (Città Metropolitana di Napoli, 2020) with $1 \times 1 \text{ m}^2$ cells, implemented in a GIS environment. Multitemporal maps of groundwater table elevations were constructed for both the shallow and the deep aquifers, through the Triangulated Irregular Network (TIN) interpolation method applied to the piezometric levels in March and July 2014, representative of recharge (Rc) and recession (Rs) periods, respectively. Daily pluviometric time series were recorded by Regional Civil Protection at the Licola (Naples, Italy) gauge station (Fig. 4.1a).

3.2 Hydrochemical Sampling and Analysis

Physico-chemical parameters as pH, electrical conductivity (Electrical conductivity (EC), $\mu\text{S}/\text{cm}$) and temperature (T, $^{\circ}\text{C}$) were measured in situ by a multiparametric probe (Mod. Sea Bird Electronics 911 Plus CTD; Sea-Bird Electronics). Alkalinity was determined in the laboratory by a titrimetric method.

In order to determine major anions and cations (i.e., HCO_3^- , SO_4^{2-} , Cl^- , Br^- , F^- , Ca^{2+} , Mg^{2+} , Na^+ , K^+) and trace elements (i.e., As, B, etc.), water samples were collected in 1 L high-density polyethylene (HDPE) bottles avoiding air bubbles and stored at $+4 \text{ }^{\circ}\text{C}$. The samples for trace elements determinations were filtered ($0.45 \mu\text{m}$) and acidified in the field. Anions and cations were determined by ion chromatography (IC Metrohm 850 Professional). Cations were separated by a Metrosep C4 250/4.0 column using 3.0 mM HNO_3 as eluent and a flow rate of 0.9 mL/min, whereas anions were separated by a Metrosep A supp7 250/40 column using 3.6 mM Na_2CO_3 as eluent at a flow rate of 0.7 mL/min. The accuracy of the analyses was checked by the ionic balance; analyses with an ionic balance within $\pm 5\%$ range were considered acceptable. For trace element determinations, the filtered samples were acidified with a 3% *v/v* HNO_3 solution and analyzed by inductively coupled plasma with mass spectrometry (ICP-MS, Aurora M90, Bruker Daltonics, Billerica, MA, USA). Hydrochemical analyses were conducted at the Chemical Science Department, University of Naples Federico II.

3.3 Isotopic Monitoring

Water samples for ^{222}Rn determinations were sampled by means of a 10 mL plastic syringe, avoiding contact with air according to the sampling procedure suggested by the U.S. Environmental Protection Agency (US EPA, 1978) and modified by Belloni et al. (1995) to perform liquid scintillation counting (LSC) measurements and were analyzed at least 3 h after the collection to allow equilibrium to be reached between ^{222}Rn and its daughters; counting time was 15 min; blank samples and a certified ^{226}Ra reference sample were counted together with the water samples at every counting session at the Center for Isotopic Research on Cultural and Environmental heritage (CIRCE) of the Department of Mathematics and Physics, University of Campania "Luigi Vanvitelli" (San Nicola la Strada, Italy). The lower detectable level was 0.5 Bq/L. Three replicates were sampled at each site.

Water samples for $\delta^{18}\text{O}$ and δD analyses were collected in 50 mL narrow neck HDPE bottles, leaving no headspace to avoid contact with air and horizontally stored at 4 °C (Clark and Fritz, 1997). $\delta^{18}\text{O}$ and δD isotopic ratios of 0.45 μm filtered samples, reported as permil (‰) relative to Vienna Standard Mean Ocean Water, were analyzed by a TC/EA-ConfloIII-IRMS system (DeltaV, Thermo Fisher) at CIRCE. The precision of the measurements was 0.1‰ and 1‰ for $\delta^{18}\text{O}$ and δD , respectively.

$\delta^{15}\text{N}$ and $\delta^{18}\text{O}$ of dissolved nitrate, reported as permil (‰) vs. AIR and VSMOW, respectively, were measured in groundwater samples by means of the silver nitrate method (Silva et al., 2000) and analyzed by a TC/EA-ConfloIII-IRMS system (Delta V, Thermo Fisher, Waltham, MA, USA) CIRCE. The precision of the whole procedure involving the preparation protocol of aqueous samples, reference materials and the IRMS analysis of solid AgNO_3 salt was 0.7‰ and 1.2‰ for $\delta^{15}\text{N}$ and $\delta^{18}\text{O}$, respectively.

Water samples for $\delta^{11}\text{B}$ determination were collected in two shallow wells (P5 and P11) and in five deep wells (P1, P3, P7, P8, P10) in April (recharge phase) and July (recession phase) 2014 in 1000 mL narrow neck HDPE bottles, leaving no headspace to avoid contact with air and stored at room temperature. The chemical procedure for boron isotope measurement was based on the GAMA method (Eppich et al., 2011): all samples were filtered on nylon membrane filters (0.45 μm) to remove particles and loaded on a boron-specific ion exchange resin, Amberlite IRA743 (Ying-Kai et al., 2003; Baek et al., 2007). In each procedural batch, about 20 boron samples, blanks (1 machine plus 1 procedural), 1 boric acid reference material (NIST SRM951: 1 processed and 1 unprocessed), and 1

internal boric acid standard as a Quality Check (QC) were prepared loading about 50 µg of dissolved boron onto the resin. Boron isotopic measurements were performed by a Thermo Fisher Scientific Neptune Plus (High Resolution Multicollector) ICP-MS at the CIRCE (Centre for Isotopic Research on Cultural and Environmental heritage) laboratory, Dept. of Mathematics and Physics, University of Campania “Luigi Vanvitelli” (Caserta, Italy). The analysis procedure involved data calibration through procedural reference materials (SRM951) and internal standards measurements applying Quality Assurance (QA) rules. The instrumental precision was about 0.15‰ for signals >1 V.

²²²Rn specific activity in groundwater was measured to infer information about aquifer heterogeneity and deep fluid rise to the surface. The stable isotopes of the water molecule, ¹⁸O and ²H, were used to study groundwater origin, recharge and mixing processes since they are incorporated within the water molecule and are hydrologically conservative. Nitrogen and Oxygen isotopic ratios of dissolved nitrate and isotopic ratios of Boron stable isotopes were studied to identify possible groundwater contamination sources and their attenuation processes as well as groundwater origin.

4. Results

Maps of groundwater flow and spatial distributions of the physico-chemical parameters were carried out, for March 2014 and July 2014, considering representative of recharge (Rc) and recession (Rs) hydrological periods, respectively. The temporal variation of each analyzed parameter was reported in box plot diagrams of the shallow and deep wells for each campaign. In addition, cross-plots of molar ratios and isotopes allowed us to identify clusters in samples and sources of groundwater contamination and salinization.

Results were interpreted to implement a conceptual hydrogeological–hydrogeochemical model of the study area, highlighting the natural and anthropogenic processes influencing the hydrochemical characteristics of the volcano-sedimentary aquifer.

4.1 Hydrogeology

Figure 4.3 shows the piezometric maps of the shallow and the deep aquifers in the Rc and Rs periods.

The shallow phreatic aquifer flows in the pyroclastic (P), pyroclastic-alluvial-lacustrine (PAP), and Dune complexes (Fig. 4.2b) with a generalized W-E orientation. In the central sector, a groundwater divide splits the flow in a northern and a southern circulation in

correspondence with the volcanic relief of Cuma Mt. Piezometric heads in shallow piezometers varied between 0 and 3.68 m a.s.l with a mean gradient of about 3.0×10^{-3} in March 2014 (Fig. 4.3a), and between 0 and 3.58 m a.s.l. with a mean gradient of about 2.9×10^{-3} in July 2014 (Fig. 4.3c). The difference between the level maximum during the recharge period (March) and level minimum during the dry season (July) is 0.1 m. Piezometric contour maps show a similar pattern in both considered periods. Nevertheless, minor local differences are observed in the retro-dunal zone. During recharge, highest water table elevation is reached, and the reclamation micro-channel system partially drains groundwater (Fig 4.3a). This evidence is not registered during the Rs period (Fig. 4.3c), in which the piezometric levels are below the channel base not influencing groundwater flow. No influence on the Pozzuoli and Bacoli underground wastewater channels that pass through the study area (Figs. 4.1c and 4.2a) on the piezometric contours (Figs. 4.1a and 4.1c) was observed.

The deep aquifer flows into the DP complex under semiconfined condition, and then joins the shallow aquifer in the coastal Dune complex, where lithic tuffaceous aquitard (YT) is absent. In March 2014 (Fig. 4.3b), groundwater flow was oriented W-E with a split due to the Mt. Cuma solid rock basement, similarly to what happens for the shallow aquifer. Piezometric levels ranged between 0 and 3.82 m a.s.l. with a gradient of 2.8×10^{-3} . In the vegetation period, the deep aquifer was affected by abstraction for irrigation and a significant depression of hydraulic heads—down to -2.3 m a.s.l. in early October 2014 in well P3 (Table S3) and to -0.76 m a.s.l. in July 2014 in well P1 (Table S3 and Fig. 4.3d).

Median values of piezometric levels (PLs) measured in shallow wells were quite constant for the whole monitoring period with a maximum variation of 0.34 m (1.16 m in April and 0.82 m in July 2014) (Table S3). Median values of PLs measured in deep wells are generally higher than those in shallow wells throughout the monitoring year, indicating an upward flow which is inverted only during the Rs, when pumping induces a sharp decrease in PLs (e.g., P1 and P3).

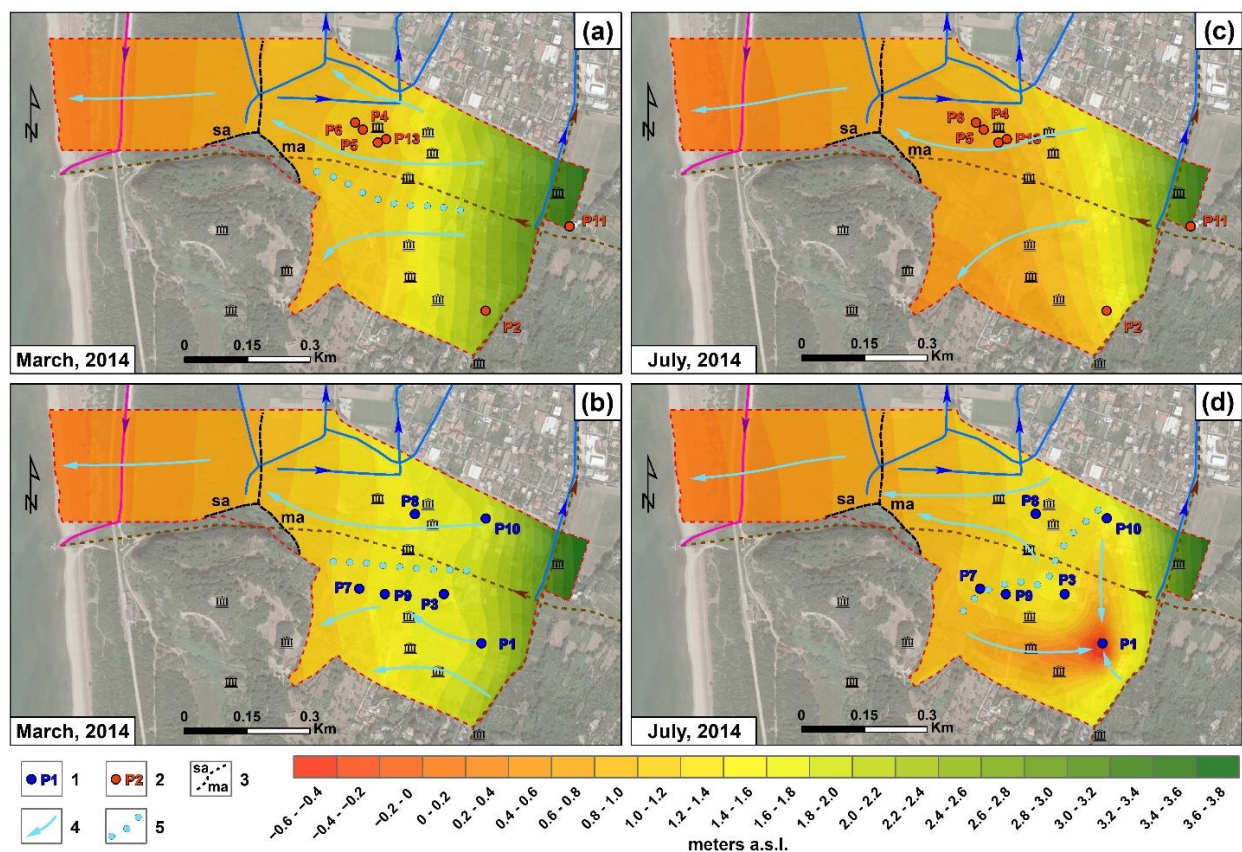


Figure 4.3 - Groundwater flow pattern in March 2014 ((a) and (b)) and July 2014 ((c) and (d)) for the shallow ((a) and (c)) and deep ((b) and (d)) aquifer. Legend: (1) Deep well; (2) shallow well; (3) hydrogeological limit between the single phreatic (sa) and the multilayered (ma) aquifer; (4) groundwater flow direction; (5) groundwater divide.

The comparison between the piezometric levels observed in the two seasons shows that the deep aquifer has higher hydraulic head in the Rc period, causing an upwards oriented vertical flow recharging the shallow aquifer. This relation is locally reversed in the Rs period, when pumping draws the deep aquifer down.

4.2 Hydrochemistry

Physical and chemical parameters determined for groundwater samples taken from the Hydrochemical facies of samples were identified by a Langelier–Ludwig diagram (Langelier & Ludwig, 1942) and mapped for Rc and Rs periods (Fig. 4.4).

Physico-chemical parameter values (electrical conductivity, EC, and temperature, T) and concentration of major ions and trace elements ($[SO_4^{2-}]$, $[Cl^-]$, $[F^-]$, $[NO_3^-]$, [As] and [B]) were plotted in box-plot diagrams considering separately all shallow and deep wells for each campaign, in order to analyze their temporal variation. The same parameters and analytes were mapped through bubbles sized proportionally to their value or

concentration for the month of March and July 2014, in order to analyze their spatial distribution and to highlight local anomalies. In addition, cross-plots of molar ratios, in detail $r[\text{SO}_4/\text{Cl}]$ vs. $[\text{Cl}]$, $r[\text{Mg}/\text{Cl}]$ vs. $r[\text{Br}/\text{Cl}]$, $r[\text{B}/\text{Cl}]$ vs. $[\text{B}]$ and $r[\text{B}/\text{Cl}]$ vs. $r[\text{Br}/\text{Cl}]$, were represented to identify sample clusters and to compare their trend with the sources values (i.e., agricultural drainage, sewage, hydrothermal waters, etc.) (Vengosh, 2003). monitoring network (Fig. 4.2) are listed in Table S3.

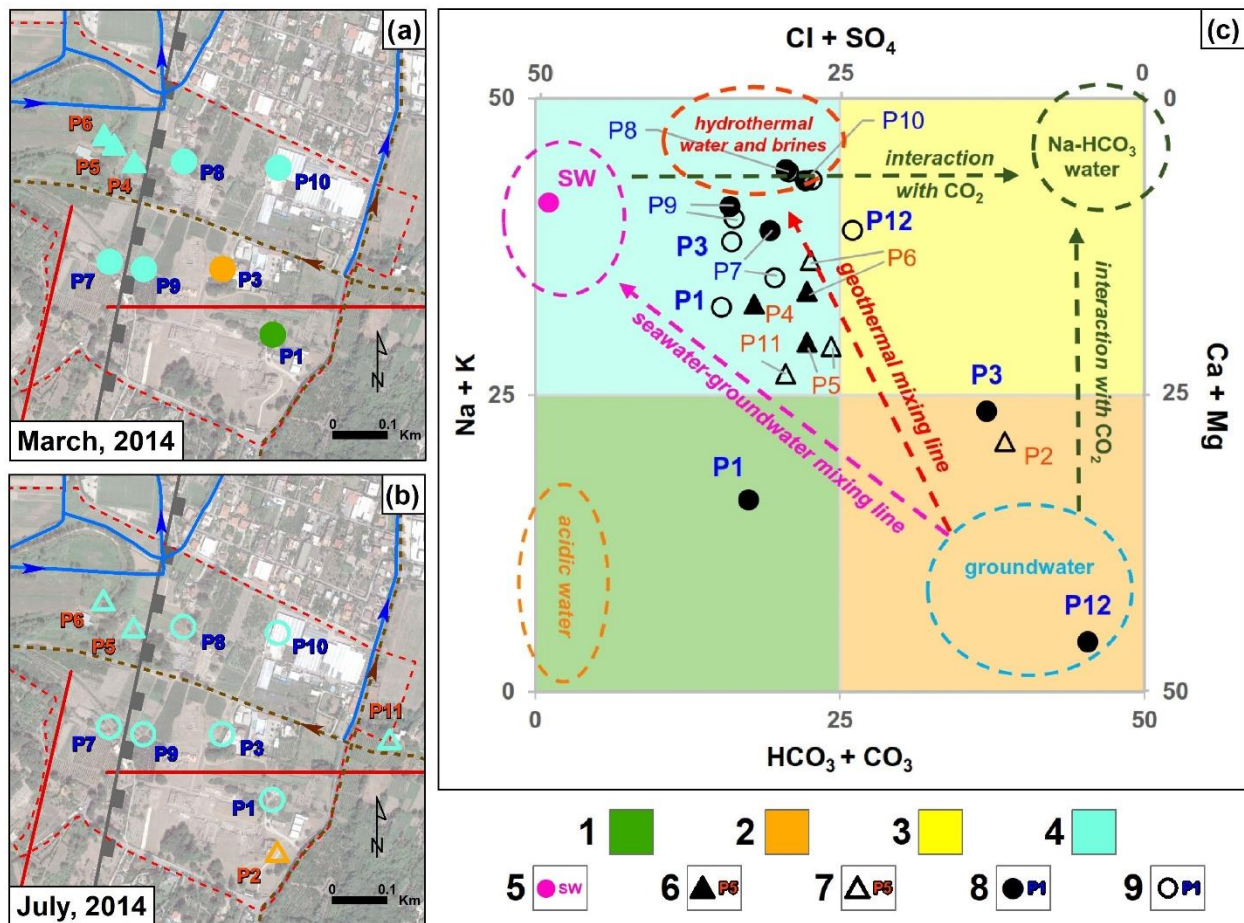


Figure 4.4 - Spatial distribution of hydrochemical facies of shallow and deep wells, for the period (a) March 2014 and (b) July 2014, and (c) Langelier–Ludwig diagram. Legend: (1) CaMg-ClSO₄ type; (2) CaMg-HCO₃ type; (3) NaK-HCO₃ type; (4) NaK-ClSO₄ type; (5) sea water; (6) shallow wells in March 2014; (7) shallow wells in July 2014; (8) deep wells in March 2014; (9) deep wells in July 2014.

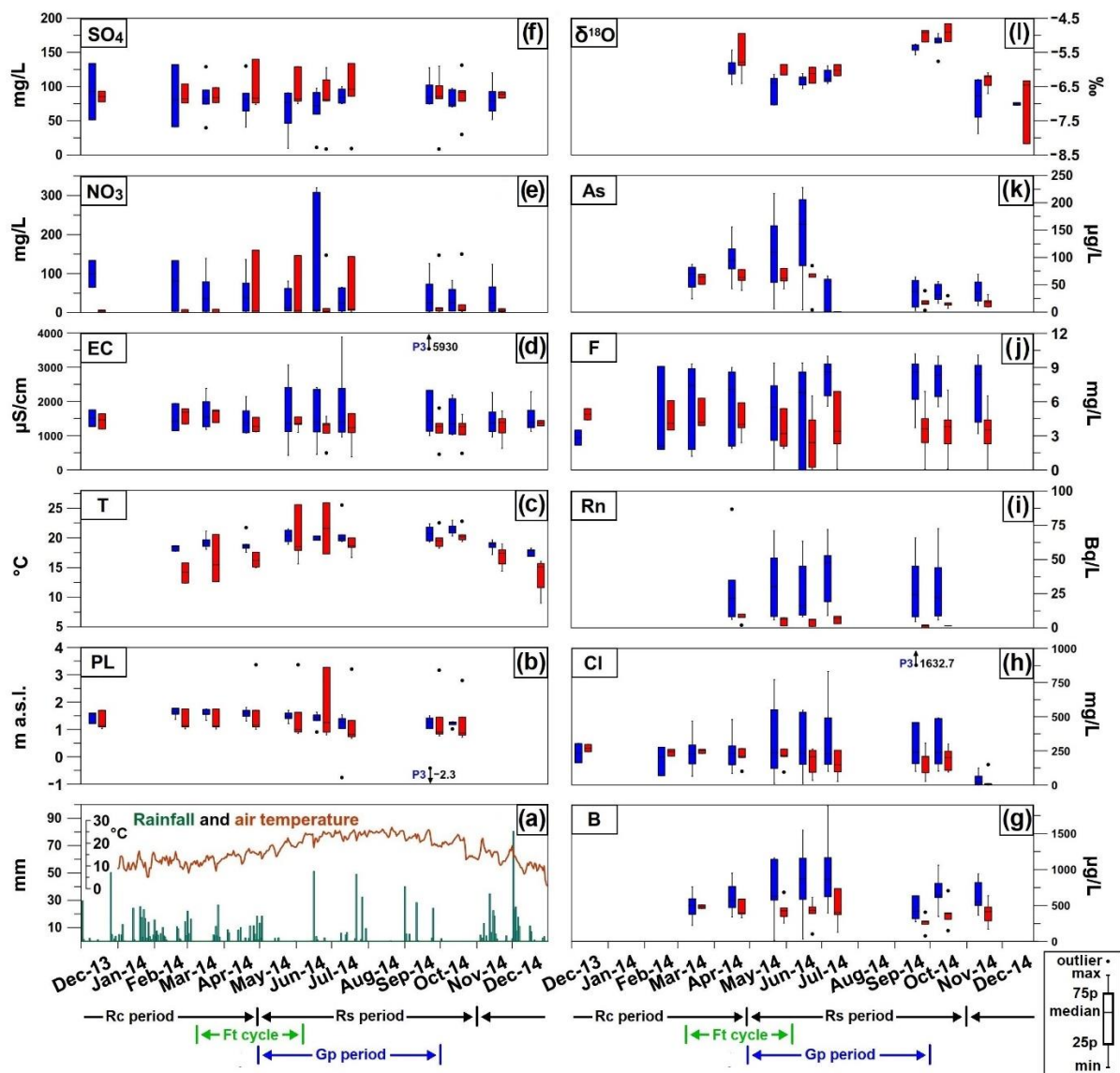


Figure 4.5 - Box plots of climatic, hydrogeological, and hydrogeochemical parameters for the whole monitoring period, with indication of recharge (Rc), recession (Rs), fertilization (Ft) and pumping (Gp) phases; (a) rainfall and air temperature; (b) piezometric levels; (c) groundwater temperature; (d) electric conductivity; (e) concentration of NO_3^- ; (f) SO_4^{2-} ; (g) B, (h) Cl^- , (i) ^{222}Rn , (j) F^- , (k) As and (l) $\delta^{18}\text{O}$ isotopic ratios. Box plots represent the distributions measured in shallow (red) and deep (blue) piezometers.

Groundwater of shallow and deep aquifers prevalently belong to the NaK-ClSO₄ type both in the Rc and Rs periods, as shown in the Langelier–Ludwig diagram (Fig. 4.4). Exceptions are represented by P1 and P3 agricultural deep wells, which belong to CaMg-ClSO₄ and CaMg-HCO₃ types in the Rc period, respectively. Because they are affected by pumping, their hydrochemical facies (temporarily) change toward the NaK-ClSO₄ type, along the geothermal and seawater–groundwater mixing lines, indicating advection from the freshwater seawater interface.

The spatial and the temporal distribution of selected physical and chemical parameters are reported in Figures 4.5 and 4.6. In Figure 4.5, box plots of climatic, hydrogeological and hydrogeochemical parameters for the whole monitoring period, with indication of the recharge (Rc), depletion (Rs), fertilization (Ft) and pumping (Gp) phases. The parameters are rainfall in mm and air temperature, groundwater level, groundwater temperature, EC, $[\text{NO}_3^-]$, $[\text{SO}_4^{2-}]$, $[\text{Cl}^-]$, ^{222}Rn specific activity, $[\text{F}^-]$, $[\text{As}]$, $\delta^{18}\text{O}$. In Figure 4.6 the spatial distribution of the selected parameters is represented for Rc and the Rs in shallow and deep wells by means of bubbles with the radius proportional to parameter values.

Groundwater temperature presents slight differences between the shallow and the deep aquifers. The groundwater temperature trend (Figs. 4.5a and 4.5c) mirrors that of the air temperature, even if the shallow wells show a wider range of variation (between 9.0 °C in December 2014 and 25.9 °C in June 2014) with respect to the deep ones (between 14.2 °C in December 2014 and 25.5 °C in July 2014). This indicates that groundwater temperature of the shallow phreatic aquifer is more influenced by air temperature than the deep semiconfined aquifer. The spatial distribution of groundwater temperature confirms the minor differences between the two aquifers in the Rc and Rs periods (Figs. 4.6a and 4.6b).

Electrical conductivity (EC) remains almost constant during the whole monitoring period (Fig. 4.5d). Minimum values are slightly higher for the deep aquifer (423 $\mu\text{S}/\text{cm}$ compared to 375 $\mu\text{S}/\text{cm}$ of shallow aquifer), and maximum values show strong differences locally (Figs 4.6c and 4.6d). In fact, P1 and P3 wells register maximum values during the Rs period (EC up to 5930 $\mu\text{S}/\text{cm}$ reached in P3 in early October 2014; showed in Fig. 4.5d), in which they are affected by pumping and characterized by the lowest piezometric levels, highlighting a significant increase compared to the Rc period (Figs. 4.6c and 4.6d), as already showed in paragraph 4.1 for P1 and P3.

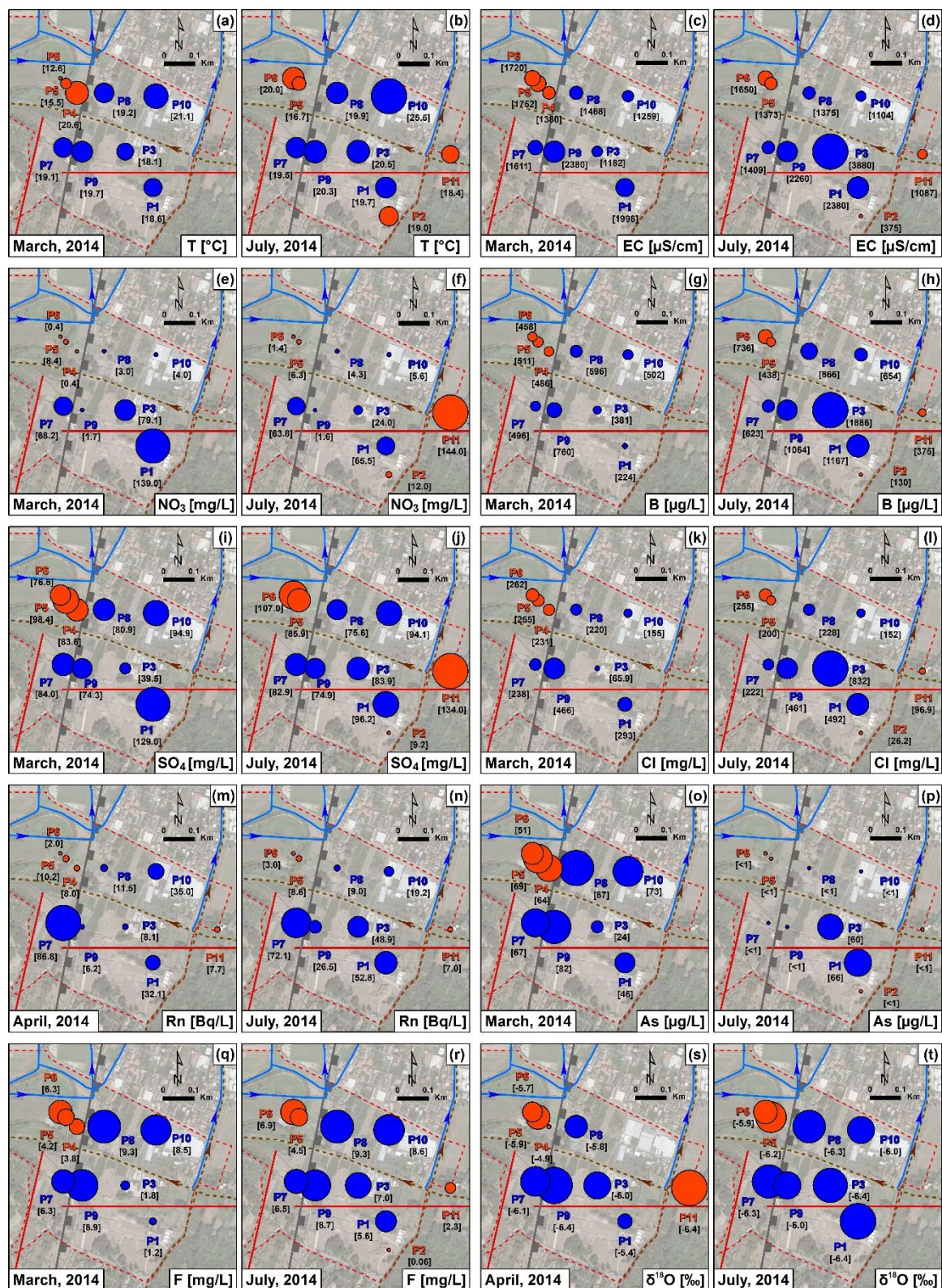


Figure 4.6 - Bubble maps of values of physico-chemical parameters (T (a) and (b) and -EC (c) and (d)), concentrations of major ions and trace elements (NO_3^- (e) and (f), Boron (g) and (h), SO_4^{2-} (i) and (j), Cl^- (k) and (l), F^- (q) and (r) and Arsenic (o) and (p) and isotopes (^{222}Rn (m) and (n) and $\delta^{18}\text{O}$ (s) and (t) in Rc and Rs periods for the shallow (in red) and deep (in blue) wells. Radius of bubbles is proportional to the value of each parameter.

The concentrations of major ions and trace elements, indicators of contamination sources and interactions between groundwater and deep fluids, show higher average concentrations in deep wells, consistently. This can be observed in the concentrations of Cl^- (Figs. 4.5h, 4.6k and 4.6l), F^- (Figs. 4.5j, 4.6q and 4.6r), Boron (Figs. 4.5g, 4.6g and 4.6h), Arsenic (Figs. 4.5k, 4.6o and 4.6p) and ^{222}Rn (Figs. 4.5i, 4.6m and 4.6n). As previously shown for the EC, P1 and P3 deep wells present consistent differences also in the concentration of the above solutes. In detail, they have lower concentrations than the other deep wells in the Rc period. In the Rs period, P1 and P3 are affected by pumping and fluorides increase up to 5.6 and 7.0 mg/L, respectively, approaching the mean of the other deep wells (8.3 mg/L); Boron (1167 and 1888 $\mu\text{g/L}$), Cl^- (492 and 832 mg/L) and Arsenic (66 and 60 $\mu\text{g/L}$) reach the highest concentrations. (Table S3).

During the whole monitoring, nitrate concentrations present high values in the deep wells (Figs. 4.5e, 4.6e and 4.6f), with a median value of 82.4 mg/L compared to only 6.3 mg/L in shallow wells. Nevertheless, maximum values are registered in P11, an agricultural shallow well (Fig. 4.6f), which reaches a concentration above 140 mg/L in the Rs period. A similar behavior was observed regarding sulphate (Figs. 4.6i and 4.6j), where the highest concentration was measured in the P11 agricultural well (≥ 130 mg/L in Rs period). High sulphate concentrations were almost homogeneously distributed both in shallow and deep wells (Fig. 4.5f).

In synthesis, major ions and trace elements highlight significant differences between shallow and deep wells showing recurring site-specific behaviors. Among shallow wells, two main areas can be identified along groundwater flow from upstream wells (P11 and P2, Figs. 4.3 and 4.7) characterized by lower chloride and boron concentrations and higher sulphate concentrations at a sub-zero sea level, i.e., a temporarily submerged area, where the drainage system catches groundwater diffuse outflow (wells P4, P5, P6 and P13; Figs. 4.7a and 4.7c), which is characterized by higher concentrations of solutes, likely influenced by the mixing with mineralized groundwater upwelling (Fig. 4.7a). P11 shows $[\text{SO}_4^{2-}] > 1$ meq/L (equivalent about 50 mg/L), likely due to fertilizer leaching, as $[\text{NO}_3^-]$ also suggests (annual average: 2.4 ± 0.1 meq/L, equivalent to about 150 mg/L) (Table S3 and Figs. 4.6e and 4.6f). The deep wells show very variable solute concentrations and, in particular, upstream wells (P10 and P12, Figs. 4.3 and 4.7) are characterized by lower values of chloride and boron (Figs. 4.7a and 4.7c) while higher values are found in the P1, P7, P8 and P9 wells and in P3 in the abstraction phase which promotes the rise of mineralized groundwater.

In Figure 4.7b, the molar ratio of [Mg/Cl] is reported vs. $r[\text{Br/Cl}]$ to show the origin of shallow and deep groundwater. The molar ratios show a narrow range of variation for shallow groundwater while deep groundwater is characterized by a greater dispersion of the $r[\text{Mg/Cl}]$ values. They are far below the ratio of seawater, making a mixing with hydrothermal waters and a small or null interaction with seawater likely (Cox et al., 1979). Similar trends are highlighted in Figure 4.7c where $r[\text{B/Cl}]$ vs. [B] is plotted with [As] as an additional independent variable, as a tracer of groundwater affected by hydrothermal fluids in the volcanic region (Aiuppa et al., 2006). In general, all the wells (except P1 and P3) are characterized by a linear relation between $r[\text{B/Cl}]$ and [B], covering a wide range of mineralization conditions showed by the different slopes (i.e., $r[\text{B/Cl}]/[\text{B}]$). In particular, the shallow wells group into two main areas: an upstream (wells P2 and P11) and a central area corresponding to the retrodunal depression where flooding is observed (Fig. 4.2a; wells P4, P5, P6 and P13)—both characterized by $[\text{As}] < 100 \mu\text{g/L}$. On the contrary, deep wells (P1, P8, P9 and P10) are characterized by higher [As] in the recharge period and a variable mineralization, which is higher in the drawdown period (Table S3). It is worth noting the behavior of well P3, which has low [As] both in the recharge and the recession periods, while $r[\text{B/Cl}]$ significantly decreases in the recession periods indicating a mixing with more mineralized water. Well P12, upstream of the study area, is characterized by lower [As] and [B], similar to the shallow P11 well. The hypothesis of a hydrothermal origin of the groundwater in the study area is further confirmed by the relation between $r[\text{Br/Cl}]$ and $r[\text{B/Cl}]$ reported in Figure 4.7d, where both shallow and deep groundwater fall into the box of the hydrothermal waters, characterized by $r[\text{Br/Cl}]$ ranging from 6×10^{-4} and 2×10^{-3} and $r[\text{B/Cl}]$ ranging from 2.5×10^{-3} and 1×10^{-1} (Vengosh, 2003). Again, wells P1 and P3 in the recession period during pumping showing a trend toward lower $r[\text{B/Cl}]$ values, suggesting mixing with more mineralized groundwater.

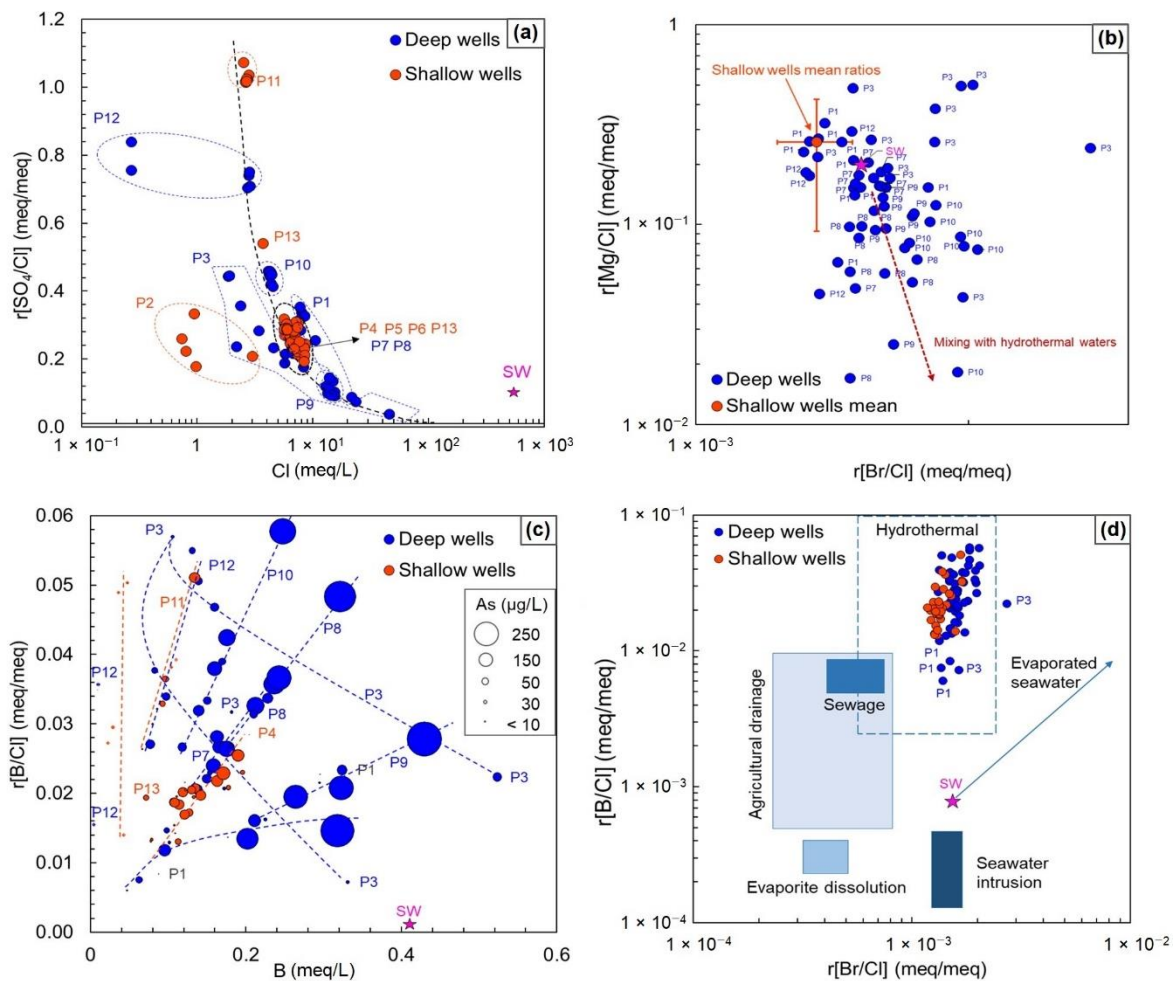


Figure 4.7 - Plots of (a) $r[SO_4/Cl]$ vs. $[Cl]$, (b) $r[Mg/Cl]$ vs. $r[Br/Cl]$, (c) $r[B/Cl]$ vs. $[B]$ and (d) $r[B/Cl]$ vs. $r[Br/Cl]$ in shallow (red circles) and deep (blue circles) wells; the pink star represents seawater (SW). In (c), the area of the circles is proportional to $[As]$ and the dashed lines represent trends of the values measured in each well. In (d), the boxes represent the sources values (i.e., agricultural drainage, sewage, hydrothermal waters, etc.) (after Vengosh, 2003).

4.3 Isotopic Survey

Hydrological isotope data presented in this work refer to the shallow and deep aquifers explored during the 2014 monthly field campaigns. In Figure 4.8a, the dual isotope diagram $\delta^{18}O$ vs. δD reports groundwater measured in shallow and deep wells during the recharge and the dry periods. A Local Meteoric Water Line (MWL; Mt. Vesuvius; Madonia et al., 2014) has been also reported as a reference for the study area samples and the Global MWL (Rozanski et al., 1993) and the East Mediterranean MWL (Gat & Carmi, 1970) as a comparison. Usually, groundwater has a constant isotopic signature throughout a hydrological year, reflecting the mean isotopic composition of local precipitation. Nevertheless, in the study area there is a significant difference between the Rc and the Rs periods, the former presenting more depleted isotopic ratios (Figs. 4.5l, 4.6s

and 4.6t) in both deep and shallow wells. This significant difference indicates the presence of short travel time of groundwater from the area of recharge. In general, isotopic values of shallow and deep wells are quite homogeneous in each hydrological period showing no appreciable differences, likely due to a common origin of the recharge water. Nevertheless, during the depletion period, and in particular in the two campaigns of October 2014 (Table S3 and Fig. 4.8a), both shallow and deep wells show an enrichment trend. The observed horizontal shift from the Mt. Vesuvius MWL toward more enriched $\delta^{18}\text{O}$ values is likely due to recharge by evaporated water or to a more evident mixing with hydrothermal waters due to the dry period (D'Amore et al., 1987; Cartwright et al., 2000; Pauwels et al., 2007; Caliro et al., 2011; Karolytè et al., 2017).

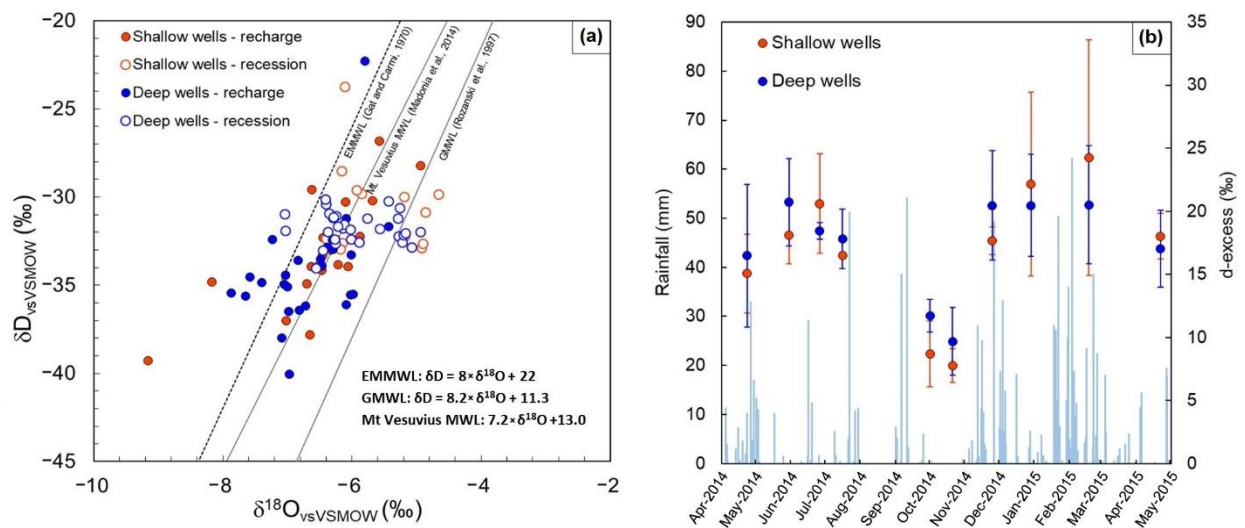


Figure 4.8 - (a) $\delta^{18}\text{O}$ vs. δD diagram in shallow and deep wells during the recharge (closed circles) and the depletion (open circles) hydrological phases in shallow (red circles) and deep (blue circles) wells. (b) Monthly variations of d-excess in shallow (red circles) and deep (blue circles) wells; the circles represent the mean values with 1 sigma standard deviation. In the plot, the daily rainfall amounts (light blue bars) are reported.

In Figure 4.8b, the variation of d-excess measured in shallow and deep wells is reported. The deuterium excess ($\text{d-excess} = \delta\text{D} - 8 \times \delta^{18}\text{O}$; Dansgaard, 1964) is a proxy to infer information about the physical conditions at the time of water vapor formation which influences the isotopic signature of the precipitation (Merlivat & Jouzel, 1979; Froehlich et al., 2002; Pfahl & Sodermann, 2014). In the study area, there are no significant differences between shallow and deep wells in all sampling campaigns, indicating a common recharge for the two aquifers. Nevertheless, a seasonal variation of the d-excess can be observed during the recharge and the depletion phases. In particular, in October 2014 (Rs) the lower d-excess values may indicate a recharge likely from less fractionated

rainwater from air masses formed in conditions of high relative humidity (RH) typical of the Mediterranean basin during summer months when evaporation is at its maximum. Moreover, during the recharge period, the d-excess is higher, indicating a recharge occurring from rains originating from the western Mediterranean basin, as can be also observed from the vicinity of the shallow and deep wells' isotopic signatures regarding the Mt. Vesuvius MWL (Fig. 4.8a).

The recharge altitude of shallow and deep groundwater can be roughly estimated applying the empirical equation for the $\delta^{18}\text{O}$ altitude gradient ($\delta^{18}\text{O} = -5.74 - 0.0026z + 1.144 \times 10^{-6}z^2$) found by Madonia et al. (2014) for Mount Vesuvius, which is close to the study area (Fig. 4.1a). The mean recharge altitude of groundwater in the *Cumae* archeological site has been estimated to be about 200 m a.s.l. considering an average annual $\delta^{18}\text{O}$ value ($n = 93$) of $-6.22 \pm 0.8\text{‰}$, which confirms the local recharge of the aquifer inferred by the seasonal isotopic variations observed.

In order to study the impact of agriculture, which is the prevalent anthropic activity in the study area (see Fig. 4.1d), the distribution of nitrate was measured in deep and shallow wells and is reported in the box plot of Figure 4.5e. Generally, groundwater in the study area has a nitrate concentration lower than 20 mg/L, regardless of whether sampled in deep or shallow wells. The exceptions are represented by P1, P3, and P7 among the deep wells and P11 among the shallow wells, which have a concentration of nitrates above 50 mg/L (see Table S3 and Fig. 4.9a). In the study area, $\delta^{15}\text{N-NO}_3$ composition ranged from 0.6‰ to 23.4‰, while $\delta^{18}\text{O-NO}_3$ composition ranged from -2.6‰ to 26.8‰. In Figure 4.9a, the $\delta^{18}\text{O-NO}_3$ vs. $\delta^{15}\text{N-NO}_3$ diagram (after Kendall, 1998) indicates that the major sources of nitrate are synthetic fertilizers and only to a minor extent manure and septic waste in both shallow and deep wells. In the diagram, a denitrification trend can be clearly seen for the depressed area of the plain, where groundwater flow slows down and the substrate is rich in organic matter typical for retro-dunal environments (Fig. 4.3). The denitrification process affecting groundwater sampled in wells P5, P8 and P10 strongly attenuates nitrate concentration enriching the heavy isotope. This is further confirmed if the regression of $\delta^{15}\text{N-NO}_3$ vs. $\ln[\text{NO}_3]$ is a straight line and the slope quantifies the enrichment factor (ϵ) (Mariotti et al., 1988; Kendall, 1998). In particular, in Figure 4.9b the $\delta^{15}\text{N-NO}_3$ vs. $\ln[\text{NO}_3]$ regression analysis of shallow and deep wells indicates that during both the Rc and the Rs periods groundwater flows toward the denitrification area (Fukada et al., 2003). The denitrification process is more

evident during the Rs phase when the enrichment factor ϵ ranges from -6.5‰ to -4.6‰ with a regression coefficient $R^2 > 0.8$.

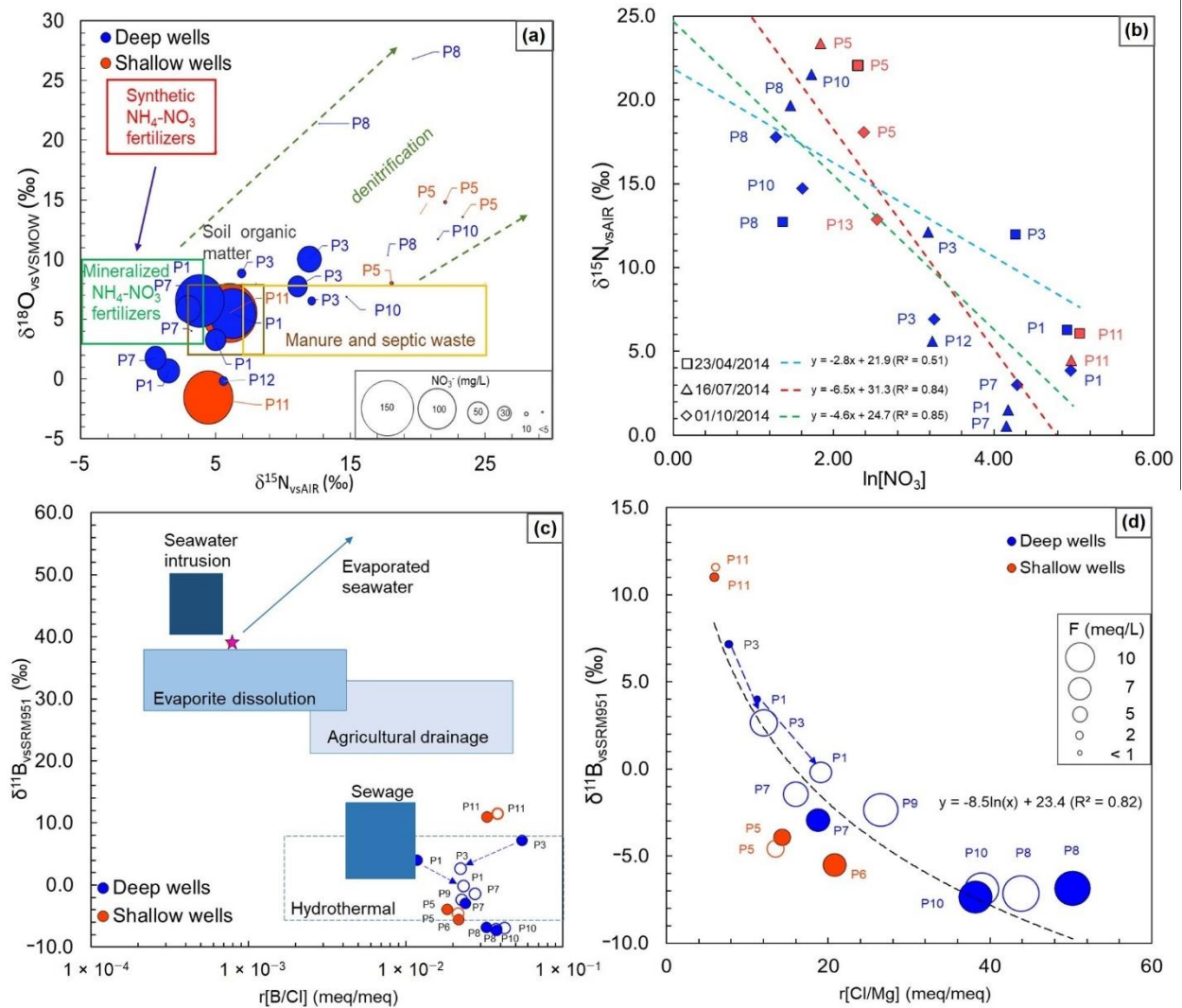


Figure 4.9 - (a) $\delta^{18}\text{O}$ vs. $\delta^{15}\text{N}$ of dissolved nitrate in shallow (red bubbles) and deep (blue bubbles) wells. The area of the bubbles is proportional to $[\text{NO}_3^-]$. The boxes represent the nitrate sources isotopic fingerprint (after Kendall, 1998). (b) Cross-plot of the $\delta^{15}\text{N}$ composition of dissolved NO_3^- vs. the natural log of N-NO_3^- concentrations (in mg/L) in shallow (red) and deep (blue) wells in the recharge (23 April 2014) and the depletion (16 July 2014, 01 October 2014) periods. (c) $\delta^{11}\text{B}$ vs. $r[\text{B/Cl}]$ (after Vengosh, 2003) in shallow (red) and deep (blue) wells plot in the recharge (April 2014, closed circles) and the depletion (July 2014, open circles) periods. The boxes represent the typical sources values; the pink star is seawater (SW). (d) $\delta^{11}\text{B}$ vs. $r[\text{Cl/Mg}]$ in shallow (red) and deep (blue) wells in the recharge (April 2014, closed bubbles) and the depletion (July 2014, open bubbles) periods. The area of the bubbles is proportional to $[\text{F}^-]$.

In Figure 4.9c, the $\delta^{11}\text{B}$ compositions measured in groundwater sampled in shallow and deep wells are plotted vs. the B/Cl molar ratios (after Vengosh, 2003) during the Rc and the Rs periods. The plot shows that groundwater in the study area is mostly mixed with hydrothermal waters influenced by the rise of magmatic fluids. The P11 well, localized

upstream of the study area, is characterized by more enriched $\delta^{11}\text{B}$ values, which could indicate a diffuse fertilizer leaching to groundwater throughout the hydrological year due to agricultural drainage. It is worth noting the behavior of the P1 and P3 wells which during the wet period are characterized by more enriched $\delta^{11}\text{B}$ values with respect to the dry period when pumping is enhanced (P1: from 4.00‰ to -0.19‰ and P3: from 7.15‰ to 2.66‰, respectively) showing a mixing with the hydrothermal component more than seawater ($\delta^{11}\text{B}_{\text{SW}} = 39\text{‰}$). Hence, the salinization of the deep aquifer observed in the dry season (EC from 1.7 mS/cm to 2.4 mS/cm in P1 and from 1.0 mS/cm to 3.9 mS/cm in P3, see Table S3) is likely due to a mixing with deep waters which have been in contact with hydrothermal fluids. The latter hypothesis is further sustained by the plot in Figure 4.9d where $\delta^{11}\text{B}$ is plotted vs. $r[\text{Cl}/\text{Mg}]$, evidencing a mixing between two end-members: groundwater sampled in P11 and in P8/P10. P11 is located upstream of the study site where the aquifer is unconfined and not yet stratified (Figs. 4.2a and 4.2b). In the plot, shallow and deep wells are plotted between the end-members and are characterized by almost constant values of the considered parameters in the dry and the wet seasons, with the exception of P1 and P3. In addition, the plot reports the $[\text{F}^-]$ concentration measured in each well to support the hypothesis of the hydrothermal origin of the waters. In general, an increase in the $[\text{F}^-]$ values is observed from P11 and P8/P10 and P1 and P3 are characterized by a shift toward the more depleted $\delta^{11}\text{B}$ values, and increased $r[\text{Cl}/\text{Mg}]$ and $[\text{F}^-]$ from the Rc to the Rs phase.

5. Discussion

A conceptual model of natural and anthropogenic groundwater contamination processes observed in the archaeological site of Cumae is summarized in Figure 4.10. In Figure 4.10, the hydrogeological–hydrochemical isotope features in relation to local land use, coastal volcanic-sedimentary environment, and hydrogeological characteristics of the aquifer system are represented.

The eastern sector is characterized by a single unconfined aquifer and a regional W-E oriented groundwater flow orthogonal to the shoreline (Fig. 4.10a), within fractured volcanic relief. Toward the coastal plain, at the site scale, a porous two-layered aquifer system has been found (Figs. 4.2a, 4.2b and 4.10a), formed by a shallow phreatic aquifer and a semiconfined deep aquifer, locally separated by a lithic tuffaceous aquitard (YT).

In the coastal zone, the groundwater circulation becomes unitary again within the shallow unconfined aquifer, with the YT aquitard missing.

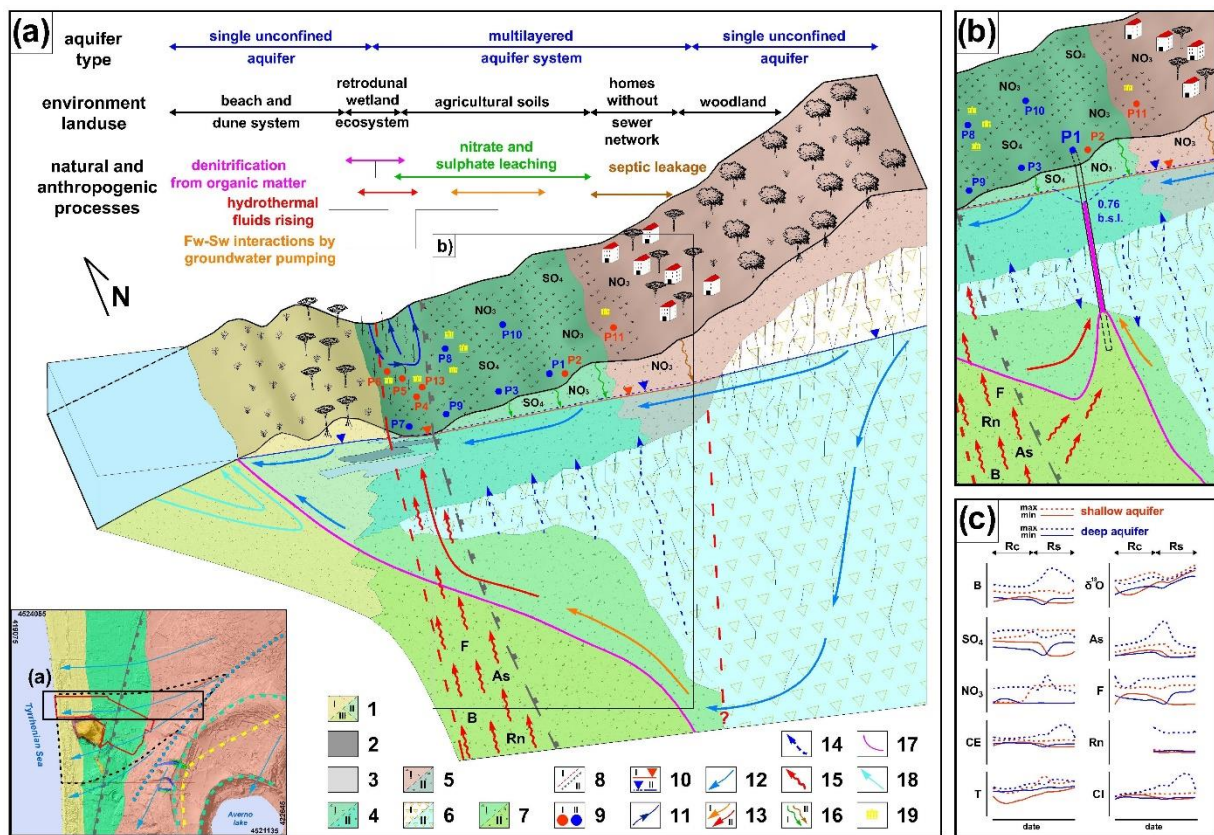


Figure 4.10 - Hydrogeological–hydrogeochemical isotope conceptual model of study area, in natural conditions (a) and during pumping (b). (c) Trends of parameters showed in Figure 4.5, reporting maximum and minimum values of shallow (in red) and deep (in blue) wells with reference to the Rc and Rs periods. The blue and red arrows depict the groundwater flow paths within the aquifer system. The blue arrows indicate shallow groundwater and the red arrows indicate deeper and mineralized groundwater, which interact with the hydrothermal fluids upwelling along deep fractured zone of the CI caldera boundary. Legend: (1) unsaturated (i), freshwater saturated (ii) and saltwater saturated (iii) dune complex; (2) clays and peaty deposits; (3) silts; (4) unsaturated (i) and freshwater saturated (ii) PAP complex; (5) unsaturated (i) and freshwater saturated (ii) P complex; (6) unsaturated (i) and freshwater saturated (ii) YT aquitard; (7) freshwater saturated (i) and saltwater saturated (ii) DP complex; (8) buried normal fault (i) and CI caldera boundary (ii); (9) shallow (i) and deep (ii) wells; (10) piezometric level of phreatic shallow aquifer (i) and deep semiconfined aquifer (ii); (11) groundwater draining channel; (12) groundwater flow direction; (13) mineralized (i) and highly mineralized (ii) groundwater flow direction; (14) vertical groundwater flow direction; (15) high mineralized fluids rising; (16) sulfates and nitrates infiltration from agricultural lands (i) and urban areas (ii); (17) Fw-Sw interface; (18) saline groundwater flow; (19) archaeological site of Monumental Roman Necropolis.

Piezometric monitoring indicated that during the Rc period groundwater flow in the semiconfined aquifer is directed upwards, recharging the shallow aquifer. This hydrogeological evidence has been confirmed by hydrochemical and isotopic data which highlighted a common origin for the shallow and deep groundwater. In particular,

groundwater flowing in the two-layered aquifer is recharged locally (mean recharging altitude: 200 m.a.s.l.) and has a short residence time as indicated by water stable isotopes. Nevertheless, the semiconfined deeper aquifer, if compared with the shallow aquifer (Fig. 4.10c), is characterized throughout the hydrological year by more mineralized groundwater with significantly higher EC and temperature as well as elevated concentrations of chloride, fluoride, boron, arsenic, and ^{222}Rn (Fig. 4.10c), especially in the wells in the central sector of the coastal plain (see P7, P8, P9 and P10 in Fig. 4.10a).

At the local scale, the mineralization observed in shallow and deep wells is strongly influenced by natural processes due to the rise along buried normal faults and deep fractured zones of the western edge of CI caldera boundaries of mineralized magmatic fluids (Fig. 4.10a). Moreover, in some shallow and deep wells (P5, P8, P10 in Fig. 4.10a) located in the drained retro-dunal area of the coastal plain, where groundwater flow slows down and the aquifer lithology is rich in organic matter, a denitrification trend has been highlighted by means of $\delta^{18}\text{O}-\text{NO}_3$ and $\delta^{15}\text{N}-\text{NO}_3$.

The anthropic groundwater contamination is mostly due to non-point agricultural sources and leaking from local septic tanks. High concentrations of nitrate and sulphate have been found in the upstream and recharge areas (well P11) and in a few deep wells (wells P1, P3 and P7). The major source of nitrate is synthetic fertilizers and to lesser extent manure and septic waste in both shallow and deep wells. Finally, in the drawdown period (Fig. 4.10b), when pumping of groundwater used for irrigation lowers hydraulic head in the deep aquifer in correspondence to P1 and P3 agricultural wells, local vertical groundwater flow is reversed and the shallow groundwater leaks. The hydrochemical and isotopic data reveal that groundwater in the two deep wells is highly mineralized, reaching the highest values of EC, chloride, fluoride, boron, arsenic, and ^{222}Rn (Fig. 4.10c), indicating a mixing with more mineralized groundwater of hydrothermal origin and to a minor extent to the mixing with seawater, clearly evidenced by the isotopic ratios of boron.

6. Concluding Remarks

The main purpose of the present study was to investigate, by means of a multidisciplinary approach, a whole hydrologic year to comprehensively assess for the first time the main natural and anthropogenic processes influencing, at the site scale, groundwater quality in the *Cumae* archaeological site with a catchment approach.

Hydrogeological monitoring confirms the presence of a complex coastal volcanic-sedimentary system, whereas all the hydrochemical and isotopic observations show that the groundwater quality is affected mainly by: (i) aquifer lithology and localized rise of mineralized magmatic fluids along buried normal faults of the CI caldera boundary, (ii) interaction and mixing between shallow groundwater, deeper mineralized groundwater and saltwater intrusion during groundwater pumping, and (iii) contamination from non-point agricultural sources.

δD and $\delta^{18}O$ data show a fast recharge from seasonal precipitations originating from evaporated and re-evaporated air masses.

Chemical data evidence nitrate pollution ($>50 \text{ mg L}^{-1}$) occurring mainly in the deep semiconfined aquifer. Isotopic ratios of N and O in dissolved nitrates evidence the contribution of different possible sources: natural, mineral fertilizers and, to a minor extent, manure and possible leaks from septic tanks or sewage systems.

Moreover, in the low lying and drained retro-dunal area of the coastal plain, denitrification processes are highlighted both in the shallow and the deep aquifers.

In conclusion, this study can be considered a valuable contribution to the comprehension of the natural and anthropogenic dynamics of groundwater contamination in the complex coastal volcanic-sedimentary system which hosts one of the most visited archaeological sites in southern Italy. The results obtained are a useful tool to assist and help the local archaeological authority in addressing the problems deriving from groundwater flooding and in decision-making aimed to safeguard and manage the archaeological heritage of the *Cumae* site.

Supplementary Material

Table S3

5

Groundwater Flooding Susceptibility

A novel methodology for Groundwater Flooding Susceptibility assessment through Machine Learning techniques in a mixed-land use aquifer

Abstract.....	163
1. Introduction.....	165
2. Description of the study area	168
2.1 Geological and hydrogeological setting.....	168
2.2 Groundwater rebound and flooding	170
3. Materials and methods.....	173
3.1 Groundwater flooding inventory map and sample size problem.....	174
3.2 Groundwater flooding predisposing factors and variables' selection.....	175
3.3 Models' calibration and evaluation.....	178
3.3.1 Generalized Boosting Model	179
3.3.2 Artificial Neural Network.....	181
3.3.3 Maximum Entropy	182
3.4 Ensemble methods and variables' importance	182
4. Results.....	184
4.1 Optimal sample size	184
4.2 Multi-collinearity analysis of PFs.....	185

4.3	GFS modeling.....	185
4.3.1	Models validation.....	185
4.3.2	Stand-alone and Ensemble models' GFS maps.....	186
4.4	GFS final map.....	188
4.4.1	PFs analysis	190
5.	Discussion.....	191
6.	Conclusions	193
	Supplementary Material.....	195

List of Figures and Tables

Figure 5.1 - Hydrogeological map of eastern plain of Naples and GF inventory.

Figure 5.2 - Hydrogeological and hydrostratigraphic dataset (**a**). **b**) 2D hydro-stratigraphic model of study area. Some flooded buildings (**c** and **d**) and agricultural soils (**e** and **f**) in the study area.

Figure 5.3 - **a**) Box plots of piezometric levels (m a. and b. s.l.) in the study area; **b**) Piezometric levels (m a. and b. s.l.) and withdrawals (m^3/s) in Lufrano, Acerra and Ponticelli well fields; **c**) San Marcellino Meteorological Observatory annual rainfall.

Figure 5.4 - Flowchart of developed methodology applied for GFS mapping.

Figure 5.5 - Groundwater flooding occurrences (**a**) and Predisposing factors maps: **b**) Aquifer type (A_{type}); **c**) Piezometric Level depth (PL_{depth}); **d**) Unsaturated zone thickness ($U_{\text{thickness}}$); **e**) Equivalent hydraulic conductivity of unsaturated zone ($K_{\text{equivalent}}$); **f**) Drainage density (D_{density}); **g**) Land use (L_{use}).

Figure 5.6 - Optimal sample size identification comparing AUC and TSS parameters for the stand-alone models.

Figure 5.7 - Stand-alone (**a-c**) and Ensemble models (**d-g**) maps.

Figure 5.8 - Percentage of area attributed to each GFS class for the stand-alone (**a**) and ensemble models (**b**) after Natural Breaks classification.

Figure 5.9 - Final Groundwater Flooding Susceptibility map (**a**) and focus on flooded buildings and agricultural soils in the impacted sectors of study area (**b** and **c**).

Figure 5.10 - Comparison between percentage of area and percentage of occurrence points falling in each GFS class.

Table 5.1 - Multicollinearity analysis indices for all the predisposing factors used in the work.

Table 5.2 - AUC and TSS average scores of the stand-alone and the ensemble models.

Table 5.3 - Variables importance and their variability in high and very high classes.

Table S4 (supplementary material) - Hydrogeological, hydrological, stratigraphic dataset and GF inventory for the study area.

5

A novel methodology for Groundwater Flooding Susceptibility assessment through Machine Learning techniques in a mixed-land use aquifer

Allocca V.^{1*}, Di Napoli M.², Coda S.^{1*}, Carotenuto F.¹, Calcaterra D.¹, Di Martire D.¹, De Vita P.¹

¹ Department of Earth Science, Environment and Resources, University of Naples Federico II.

² Department of Earth, Environment and Life Sciences, University of Genoa

*Corresponding authors: vincenzo.allocca@unina.it; silvio.coda@unina.it

Abstract

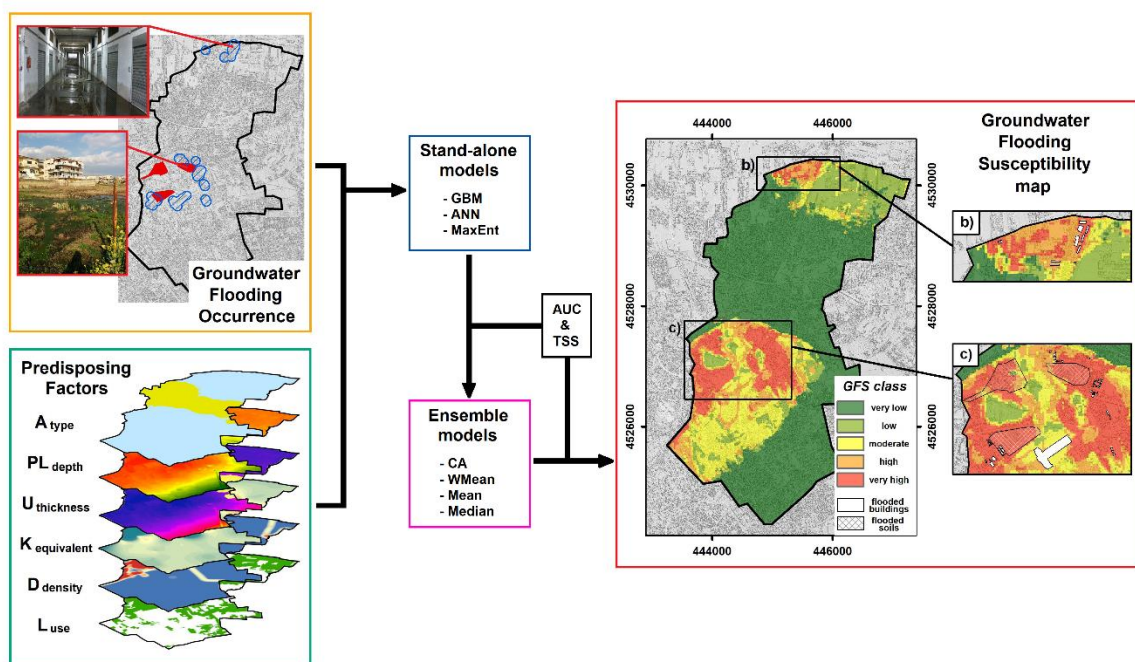
Many areas around the world are affected by Groundwater Level rising (GWLr). One of the most severe consequence of this phenomenon is Groundwater Flooding (GF), with serious impacts for human and natural environment. In Europe, GF has recently received specific attention with Directive 2007/60/EC, which requires Member States to map GF hazard and propose measures for risk mitigation.

In this paper a methodology has been developed for Groundwater Flooding Susceptibility (GFS) assessment, using for the first time Spatial Distribution Models. These Machine Learning techniques connect occurrence data to predisposing factors (PFs) to estimate their distributions. The implemented methodology employs aquifer type, depth of piezometric level, thickness and hydraulic conductivity of unsaturated zone, drainage density and land use as PFs, and a GF observations inventory as occurrences. The algorithms adopted to perform the analysis are Generalized Boosting Model, Artificial Neural Network and Maximum Entropy. Ensemble Models are carried out to reduce the uncertainty associated with each algorithm and increase its reliability. GFS is mapped by choosing the ensemble model with the best predictivity performance and dividing occurrence probability values into five classes, from very low to very high susceptibility, using Natural Breaks classification.

The methodology has been tested and statistically validated in an area of 14,3 km² located in the Metropolitan City of Naples (Italy), affected by GWLr since 1990 and GF in

buildings and agricultural soils since 2007. The results of modelling show that about 93% of the inventoried points fall in the high and very high GFS classes, and piezometric level depth, thickness of unsaturated zone and drainage density are the most influencing PFs, in accordance with field observations and the triggering mechanism of GF. The outcomes provide a first step in the assessment of GF hazard and a decision support tool to local authorities for GF risk management.

Key words: Groundwater Level rising, Groundwater Flooding Susceptibility, Machine Learning algorithms, Ensemble methods, mixed-land use aquifer, Metropolitan City of Naples.



Allocca V., Di Napoli M., Coda S., Carotenuto F., Calcaterra D., Di Martire D., De Vita P., 20XX. A novel methodology for Groundwater Flooding Susceptibility assessment through Machine Learning techniques in a mixed-land use aquifer. Science of The Total Environment, submitted in February 2021; re-submitted in April 2021 after the 1st round of revision.

1. Introduction

Many areas around the world are affected by Ground Water Levels rising (GWLr) phenomena (Whitesides et al., 1984; Schirmer et al., 2013). Despite the different features of the affected territories, urban and rural, coastal and inland, archaeological sites and abandoned mines, a common factor is the management of groundwater resources. Actually, 60% of about 90 GWLr case studies recorded in the literature (Allocca et al., 2021), is associated to Groundwater Rebound (GR) originated by the interruption of groundwater pumping, often following a period of aquifer overexploitation. GR often causes Groundwater Flooding (GF) phenomena, namely “the emergence of groundwater at the ground surface away from perennial river channels or the rising of groundwater into the man-made ground, including basements and other subsurface infrastructure” (Macdonald et al., 2012; 2008). Impacts of GF can be severe on the rural and urban environments, but also on cultural heritage, utility activities and human health, and can cause significant socio-economic damage and costs (Allocca et al., 2018; Abu-Rizaiza, 1999; Aicha et al., 2020; Stellato et al., 2020). In England and Wales the economic loss due to GF is on average £530 million per year, approximately 30% of national annual economic loss due to flooding phenomena (ESI, 2016). In urban areas, flooding damage from groundwater often affected underground structures and infrastructures without necessarily the water table emerging to the ground surface. Unlike coastal, fluvial and pluvial flooding events, GF episodes show relatively long duration, typically lasting for months or years/decades and causing damage 2.5 times greater than those produced by the other flooding types (ESI, 2016). During the last decades, GF was wide-spread across the United States (Gotkowitz et al., 2014), northern and central Europe (Korkmaz et al., 2009; Kreibich and Thieken, 2009; Wett et al., 2002), United Kingdom and Ireland (Hughes et al., 2011; Jerome Morrissey et al., 2020; MacDonald et al., 2014), and in some Italian cities (Beretta et al., 2004; Allocca et al., 2016; Coda et al., 2019a; Gattinoni and Scesi, 2017; La Licata et al., 2018; Mancini et al., 2020; De Caro et al., 2020), in different geological and land use settings, and with various triggering mechanisms and processes.

Macdonald et al. (2008) identifies three possible scenarios of GF triggered by the following mechanisms: i) flooding related to the water table rising above the land surface in response to prolonged extreme rainfalls in unconfined and fractured aquifers; ii) flooding related to the rapid response of groundwater levels to precipitation and limited storage capacity in shallow and porous sedimentary aquifers with a good hydraulic

connection with river networks; iii) flooding induced by GR, i.e. a strong reduction in groundwater abstraction from large aquifers underlying urban centres due to a decrease of industrial activities.

In the current framework of global climate changes, GF is a geohazard to be evaluated in order to set urban areas more resilient and safer, although the associated risk remains disregarded from the general public and still little known in the scientific community (Kreibich et al., 2009). In Europe, flooding from groundwater has recently received attention because of Directive 2007/60/EC, the so-called EU Floods Directive. The EU Floods Directive, transposed into the Italian law Legislative Decree 49/2010, compels Member States to produce groundwater flooding hazard maps and risk mitigation measures, to reduce disasters and harmful effects to the environment and human health (Cobby et al., 2009). However, in the scientific literature there are still few methodological studies focused on this issue and they are mostly concerned with GF induced by extreme rainfall in shallow unconfined aquifer and river-aquifer interactions. These contributions are based on the identification of GF prone areas or, alternatively, on GF risk assessment using as tools GIS, “rule-based” and analytical approaches (Chebanov and Zadniprovska, 2011; Macdonald et al., 2012; McKenzie et al., 2010; Naughton et al., 2017; Plane et al., 2019). More sophisticated methods use frequency analysis (Fürst et al., 2015), hydrological and hydrogeological modelling (Colombo et al., 2018; García-Gil et al., 2015; Habel et al., 2017; Jerome Morrissey et al., 2020; Korkmaz et al., 2009; Mancini et al., 2020; Pinault et al., 2005; Sommer et al., 2009; Upton and Jackson, 2011; Yu et al., 2019) to estimate groundwater level response to rainfall, river-aquifer transfer, sea-level increase and other controlling factors. All authors agree on the difficulty to detect appropriate GF-controlling parameters and probability of occurrence in certain time period for GF risk assessment, and most of the authors adopt a stochastic approach to model them.

The methodology proposed contributes to the scientific debate by developing a new approach to the assessment of Groundwater Flooding Susceptibility (GFS) expressed as spatial distribution of GF probability, given a set of hydrological, hydrostratigraphic and geo-environmental local conditions (predisposing factors; PFs). In the field of susceptibility analysis, it is extremely important to recognize the areas most at risk, and this is recently accomplished with the use of Spatial Distribution Models (SDMs). In different research fields, such as landslide susceptibility mapping (Di Napoli et al., 2020a, 2020b; Lombardo et al., 2016), flooding susceptibility assessment (Arora et al., 2021; Dodangeh et al., 2020), groundwater potential mapping (Rahmati et al., 2016),

groundwater contamination mapping (Barzegar et al., 2018; Pollicino et al., 2021; Sajedi-Hosseini et al., 2018) and ecology (Carotenuto et al., 2020; Fourcade et al., 2014), these methods have already been widely used. SDMs are statistical techniques that connect distribution data (occurrence/presence at known locations) with information on the environmental and/or spatial characteristics at those locations through the application of several Machine Learning Algorithms (MLAs) (Raes and Aguirre Gutierrez, 2018). SDMs can be used to understand and/or to forecast phenomenon distributed over the study area (Elith and Leathwick, 2009). However, uncertainty produced by predisposing factors and typical pros and cons of each SDM algorithm are some of the concerns of these techniques. As the outcomes of the susceptibility assessment, models should yield well-founded scientific information that can help the identification of priority areas and to predict areas with different degrees of susceptibility. Ensemble methods (EM) have been proposed to combine the advantages of each model and to mitigate the effects of their drawbacks (Thuiller et al., 2009). Therefore, the aim of the present study is to evaluate and produce GFS map in the Metropolitan City of Naples (Italy) by using EM. To the authors' knowledge, this is also the first attempt reported in the literature for GFS assessment and mapping through MLAs, considering Generalized Boosting Model (GBM), Artificial Neural Network (ANN) and Maximum Entropy (MaxEnt). A periurban area of about 14 km² has been selected to test the methodological procedure. Since 1990, the test area that has a mixed land-use aquifer is affected by GR due to the groundwater pumping reduction by public and private wells (Allocca et al., 2016; Coda et al., 2019b, 2019c), while since 2007 GF episodes for private buildings and agricultural soils have been registered, for a total of about 55 buildings and 0.25 km².

The remaining parts of the paper are structured as follows. Section 2 describes the hydrogeological conceptual model of the study area, as well as GR and GF phenomena features. Section 3 illustrates data, methodological procedure and MLAs used for the GFS assessment, whereas Sections 4 and 5 expose and discuss the results obtained and the comparison between different models. Finally, Section 6 presents the concluding remarks.

2. Description of the study area

2.1 Geological and hydrogeological setting

The study area, extended over about 14 km², is located within the Metropolitan City of Naples (Italy), between 4530536 m latitude and 447470 m longitude (WGS84-UTM33N) (Fig. 5.1). It corresponds to Casalnuovo di Napoli and Volla municipalities and these sectors are among the most densely populated urban areas of Italy and Europe, with nearly 75,000 inhabitants and a population density of about 5,240 inhabitants/km².

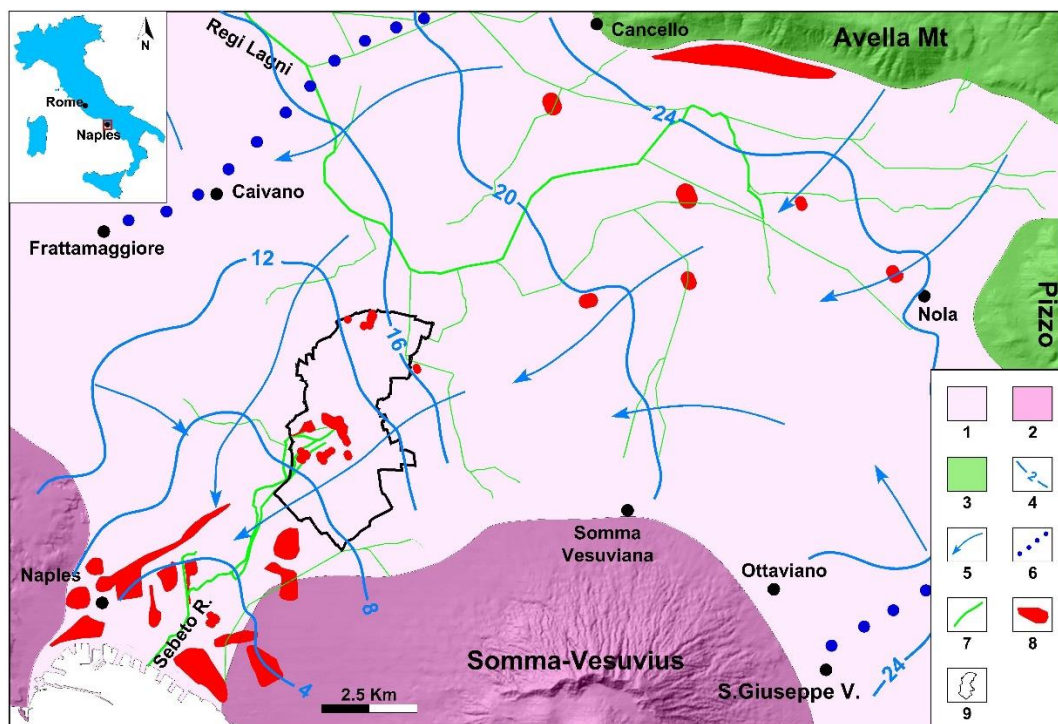


Figure 5.1 - Hydrogeological map of eastern plain of Naples and GF inventory. 1) Quaternary epiclastic deposits; 2) Quaternary volcanic deposits; 3) Mesozoic Apennine platform carbonates; 4) groundwater contour line (m a.s.l.; De Vita et al., 2018, simplified); 5) groundwater flow direction; 6) groundwater divide; 7) hydrographic network system; 8) GF impacted area; 9) study area.

From a geological point of view, the study area is located in the central-southern sector of the Campanian Plain (Fig. 5.1), a large alluvial plain formed in the Pliocene-Pleistocene by the filling of a regional semi-graben structural depression (Patacca et al., 1990). Starting from 300 k-yrs the deposition of volcanoclastic products by intense volcanic activity together with sedimentation and erosional processes led to the filling of the structural depression by 1000-3000 m of pyroclastic, alluvial, marine and fluvial-palustrine sediments.

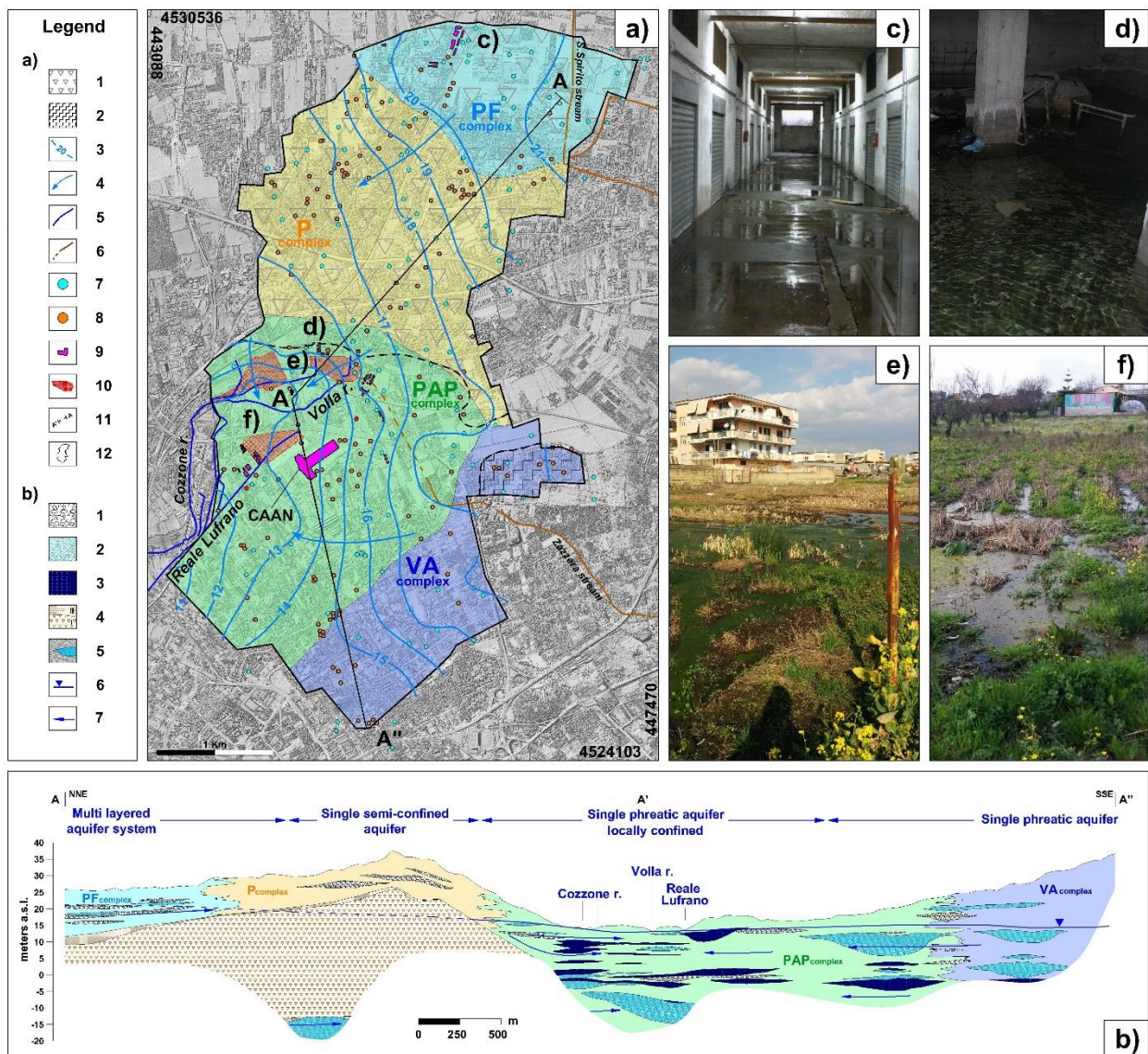


Figure 5.1 - Hydrogeological and hydrostratigraphic dataset (a). **b)** 2D hydro-stratigraphic model of study area. Some flooded buildings (c and d) and agricultural soils (e and f) in the study area (locations are in Fig. 2a). Legend of a): 1) Sector with buried Campanian Ignimbrite (CI); 2) Sector with buried lava rocks; 3) Piezometric contour line (m a.s.l.) in March 2015; 4) groundwater flow direction; 5) Drainage network system; 6) Urban drainage system (culverts); 7) well; 8) borehole; 9) private and public (Agri-Food Centre of Naples – CAAN) flooded building; 10) flooded agricultural soil; 11) cross-section trace; 12) study area. Legend of b): 1) pumiceous lapilli horizons; 2) sandy horizons; 3) marshy clay-sands and clay-silts; 4) Lithoid (I) and incoherent (II) CI; 5) Deep semi-confined pyroclastic-alluvial aquifer (silty sands and sands); 6) piezometric level; 7) groundwater flow direction.

Four geological complexes outcrop in the study area (Fig. 5.2a): Holocene pyroclastic-fluvial sediments (PF); ash-fall pyroclastic deposits (P), dated 39.3-39.8 k-yrs; Holocene pyroclastic, alluvial-marine and palustrine sediments (PAP), as well as late Holocene volcanic and alluvial deposits (VA). Borehole data revealed that the northern and central-northern sectors are characterized by a buried tuff horizon, corresponding to the

Campanian Ignimbrite (CI), in a zeolitized yellow facies, dating back to 39.28 ± 0.11 k-yrs (De Vivo et al., 2001).

The study area is the lowland sector of the Sebeto Valley, a subsiding tectonic depression characterized by a typical floodplain environment. The landscape morphology is quite flat, with very gentle slopes, dipping up to 4% and its altitude varies from 10 to 45 m a.s.l.. The Volla and Cozzone rivers, Reale Lufrano channel and Santo Spirito stream represent the current surface and groundwater drainage systems (Fig. 5.2a).

Concerning the hydrogeological setting, the study area hosts a mixed land-use aquifer (urbanized and rural area account for 67.2% and 32.8%, respectively) characterized by a heterogeneous and discontinuous multi-layered aquifer system recharged by direct effective infiltration (equal to about 300 mm/year; Allocca et al., 2014) and by lateral groundwater flow coming from the upstream aquifer sectors. Starting from the northern sector (Figs. 5.2a and 5.2b), an unconfined shallow aquifer and a deep semi-confined pyroclastic aquifer underlying CI horizon occur. The central sector is characterized by a single deep semiconfined aquifer formed by pyroclastic-alluvial deposits underlying the CI horizon. In the southern sector, where CI is absent, a single phreatic aquifer is observed, which is locally characterized by a semiconfined flow due to shallow and spatially discontinuous aquicludes (lenses of silts, clays and peat levels) within the PAP complex. Groundwater flow is approximately NE-SW oriented (Fig. 5.2a), being consistent with the general groundwater scheme at the basin scale (Fig. 5.1). In the southern sector of study area, the groundwater flow direction is mainly E-W oriented, converging towards Cozzone and Volla rivers and Reale Lufrano channel, which locally are physically continuous with the aquifer and behaving as gaining streams (Fig. 5.2a).

2.2 Groundwater rebound and flooding

During the period 1945-1989, a progressively increasing use of groundwater resources by public and private wells occurred, causing a strong groundwater over-exploitation (Allocca and Celico, 2008) and decline of piezometric levels. Since 1989, public and private withdrawals for drinking water, rural and industrial use have been drastically reduced or suspended, due to groundwater quality deterioration, deindustrialization process and land-use change (Allocca et al., 2021; Coda et al., 2019b). Consequently, from 1990 onward a remarkable and widespread GR has been registered, with values up to about +17 m (Fig. 5.3a; Allocca et al., 2021). Moreover, the comparison between the time series of groundwater levels, withdrawals and annual rainfall (Fig. 5.3) confirms that climate-induced changes have not played a significant role on GR at the decadal scale (Allocca et al., 2017), in agreement with the downward sloping trend in the mean annual

precipitation index observed at the regional scale (De Vita et al., 2012). Currently, GR is still active and the recovery does not take place entirely compared to the levels of 1920s, nevertheless, a slowdown of rate of rise has been recognized despite low withdrawals (Figs. 5.3a and 5.3b). In addition, a decrease of piezometric levels occurred in 2017, preceded by low annual rainfall in the period 2016-2017 (Figs 5.3a and 5.3c), showing a greater influence of precipitation on piezometric variation than the period 1990-2015.

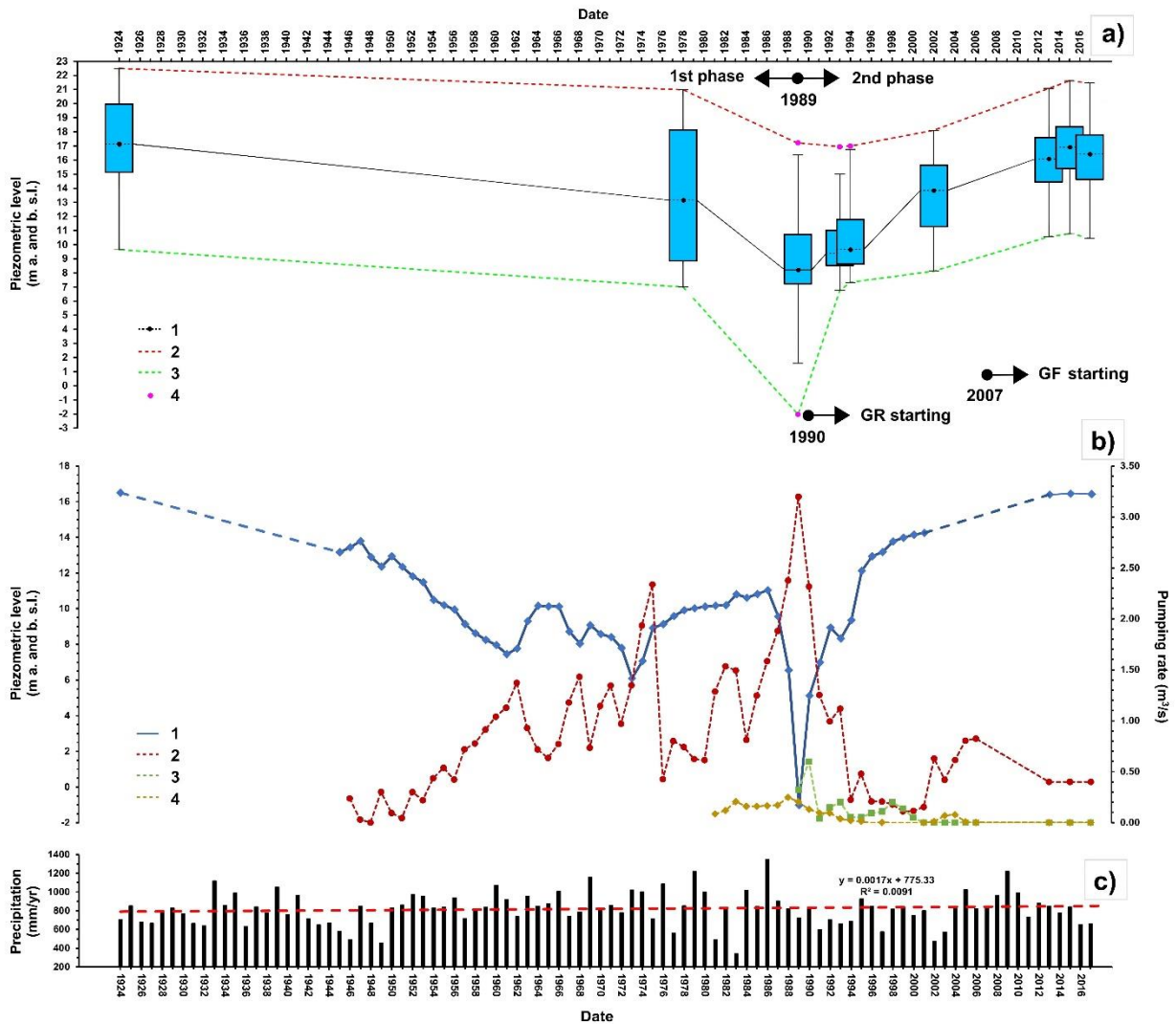


Figure 5.3 - a) Box plots of piezometric levels (m a. and b. s.l.) in the study area; **b)** Piezometric levels (m a. and b. s.l.) and withdrawals (m³/s) in Lufrano, Acerra and Ponticelli well fields; **c)** San Marcellino Meteorological Observatory annual rainfall. Legend **a)**: 1) Median piezometric head; 2) Median trend; 3) Maximum trend; 4) Minimum trend; 5) Outliers; Legend **c)**: time series of: 1) piezometric levels Lufrano well-field; 2) Lufrano well-field withdrawal; 3) Acerra well-field withdrawal; 4) Ponticelli well-field withdrawal. Source of data are listed in Table S4 in supplementary material.

In the last two decades, GR triggered a series of induced phenomena (Coda et al., 2019a; 2019b; 2019c) at basin and local scale. In particular, an unexpected and geographically-discontinuous GF occurred (Fig. 5.1), impacting agricultural soils, private buildings and underground infrastructures. In the study area, the first GF episodes started in 2007 and 2010 for private buildings and agricultural soils respectively, indicating a considerable time delay varying from 17 to 20 years, in comparison to the beginning of GR (Fig. 5.3a). After mapping and monitoring GF in the period 2013-2020 through field survey and submitting a questionnaire to the local population (see Section 3.1), the most severe flooding episode of the last years occurred in the period 2012-2015 with great impact during the winter season (Allocca et al., 2021; Coda et al., 2019a). Flooded rural areas and underground structures (parking spaces, basements, foundations and cellars) have been recognized, up to 55 affected infrastructures concentrating in the northern and southern sectors of the study area (Figs. 5.2a, 5.2c, 5.2d, 5.2e and 5.2f). In particular, in the northern sector only few buildings, constructed in the period 1990-2000, are impacted by flooding in basements, cellars and lift shafts. Whereas, in the southern sector only some buildings, constructed in 1985-1995 period, reveal flooded ground-floors and underground structures. In this sector, unlike the northern one, also some agricultural lands are affected by flooding with outcropping of shallow water table. The GF triggering mechanism and the spatio-temporal variability of the impacted private buildings and agricultural soils are due to some anthropogenic and natural factors (Allocca et al., 2016; 2021), i.e.: i) erroneous design of some buildings, with foundations and structures deeper than current groundwater levels; ii) disappearance of the ancient agricultural drainage micro-network system due to urbanization, infrastructuring and abandonment of agricultural activities, which converged in the principal drainage system (Volla and Cozzone rivers and Reale Lufrano channel); iii) poor maintenance state and partial occlusion of principal drainage channels causing a reduction of their hydraulic efficiency; iv) presence, in some not flooded agricultural soils, of low permeability shallow lenses, that locally cause conditions of artesian groundwater levels (up to +0.20 and +0.30 m a.g.l.).

3. Materials and methods

The procedure employed in this research is the ensemble of MLAs, which included different steps. The methodology flowchart used in this paper is shown in Figure 5.4. It includes (i) creation of a GF inventory map, (ii) definition of appropriate flooding predisposing variables, (iii) modelling GFS map using GBM, ANN and MaxEnt, (iv) performing an accuracy assessment of the models, and (v) flood susceptibility map implementation using an EM approach.

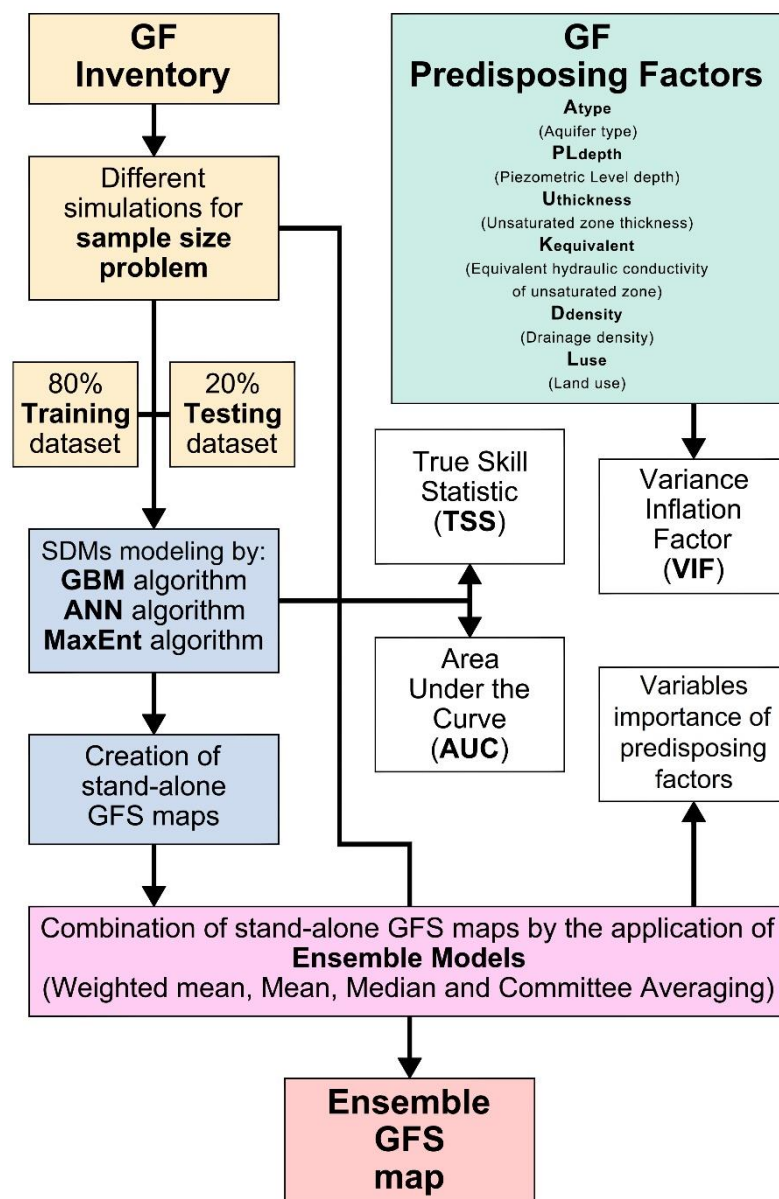


Figure 5.4 - Flowchart of developed methodology applied for GFS mapping.

3.1 Groundwater flooding inventory map and sample size problem

Groundwater flooding inventory is a basic pre-requisite to define the relationship between flood occurrence and its predisposing factors (Rahmati et al., 2016). The reconstruction and analysis of historical and recent GF events are crucial to inform future expectation, considering that areas close to occurrence sites have a greater GF probability. An accurate flood susceptibility analysis requires a precise and reliable flood inventory map, with georeferenced observations (i.e., point locations). In this study, sites, in which flooding phenomena occurred, have been observed in the northern and southern sectors of the study area. In 2013, a questionnaire has been submitted to local population in which it was asked to report the presence of GF impact in the property (Allocca et al., 2021). After that, from November 2013 to January 2020 a six-month frequency monitoring and mapping of GF impacts have been carried out, detecting several characteristics of impacts and their extents variation. A detailed form has been produced for each building and agricultural soil, reporting coordinates, altitude and amplitudes about land parcel, as well as water levels above flooded soils and man-made surface, and any presence of protective measures aimed at mitigating GF (e.g. well-points, waterproofing or lifting of ground/floor). All field data have been used to achieve multi-temporal maps of GF impacts, producing an updated municipal GIS database. This dataset integrated with historical information of flooding available in literature (Allocca and Celico, 2008), facilitates the first GF inventory for the Neapolitan area at basin scale (Fig. 1). The GF inventory map of the study area is shown in Figure 2a, with a total number of 55 buildings and 3 flooded areas, covering a total surface of about 0.25 km². For modeling, GF occurrences map has been implemented creating a 100-m buffer around each impacted building (Fig. 5a). In this way, enlargement of the impacted building areas allowed to avoid the underestimation of impacts recognized by field survey only, including some buildings, in which detection was not possible, that presented similar piezometric and structural characteristics to the ones impacted.

In order to realize trustworthy models of GFS' distribution probability, SDMs need enough information on both the presence (i.e. locations where the event being studied is observed) and the absence (i.e. where the event is not observed) data. Many SDM algorithms require both presence and absence data, whereas other ones rely on presence records only. In some cases, like this research, the geological event has to be recorded as discrete polygons (areal data) over the study area. Unfortunately, this is not the kind of

data SDMs can handle, since they require any single event to fall into just one gridded map's cell into which any of the predisposing factor is provided. Therefore, it is necessary to turn these polygon data into points, each one falling into a single distinct map's cell and virtually representing an unbiased sample of the event occurring simultaneously on a vast area. There are many strategies to create point data and the less biased one is to randomly sample locations inside the polygons. This procedure involves the accurate choice of point locations' number to be sampled, i.e. the sample size. It is widely recognized that, in susceptibility modeling, the prediction accuracy outcomes are heavily connected to the quality of the data used, conditioning factors and inventory (van Westen et al., 2008). In addition, both raster resolution and the number of presence and/or absence records in the training and the testing datasets play a meaningful part (Arnone et al., 2016; Shirzadi et al., 2019). Many studies tested the effects of using different sample sizes on models' performance (e.g., Arnone et al., 2016; Cama et al., 2017; Guisan et al., 2007; Jiménez-Valverde et al., 2009; Shirzadi et al., 2019; Stockwell and Peterson, 2002; Thibaud et al., 2014; Wisz et al., 2008). Although performance generally gains by increasing information, cases of a plateau in model performance, or even decrease, are not rare in the scientific literature (Elith and Graham, 2009; Townsend Peterson and Cohoon, 1999). In this research twelve different sample sizes were tested with 10, 25, 50, 75, 100, 250, 500, 1000, 2500, 5000, 7500 and 10000 points, respectively, randomly sampled inside the polygonal areas (concerning agricultural soils and private buildings). The contribution of all the tested sample sizes on the models' predictive performance was lastly measured by means of accuracy indices, like the Area Under the Curve (AUC; Hanley and McNeil, 1982) and the True Skill Statistics (TSS; Allouche et al., 2006) (AUC and TSS detailed information have been included in the Section 3.3). In the end, the smallest sample size that generated the models with the highest predictive performance, were then used for all the following analyses and modelling procedures. As for the absence data, which simply represent the territories where the event did not occur, we simulated 10000 random locations, considered as pseudo-absences for all the SDM algorithms except MaxEnt (for which they are considered as background points, see details in section 3.3.3).

3.2 Groundwater flooding predisposing factors and variables' selection

Predisposing factors (PFs) are pre-requisites for GFS mapping. Given the extreme complexity of this phenomenon, nowadays there is not a universal guideline to choose

the most suitable PFs (Cobby et al., 2009), as well as for other types of flooding (Dodangeh et al., 2020; Hosseini et al., 2020). Hence, the factors have been selected according to (i) literature reviews reported in Section 1, (ii) hydrogeological conceptual model of the study area reported in Section 2.1 and (iii) triggering mechanism of observed GF (Section 2.2; Allocca et al., 2016; 2021). Therefore, six geo-environmental predisposing variables have been selected and applied in this methodological procedure (Figs. 5.4 and 5.5), including saturated Aquifer type (A_{type}), Piezometric Level depth (PL_{depth}), Unsaturated zone thickness ($U_{thickness}$), equivalent hydraulic conductivity of unsaturated zone ($K_{equivalent}$), Drainage density ($D_{density}$) and Land use (L_{use}).

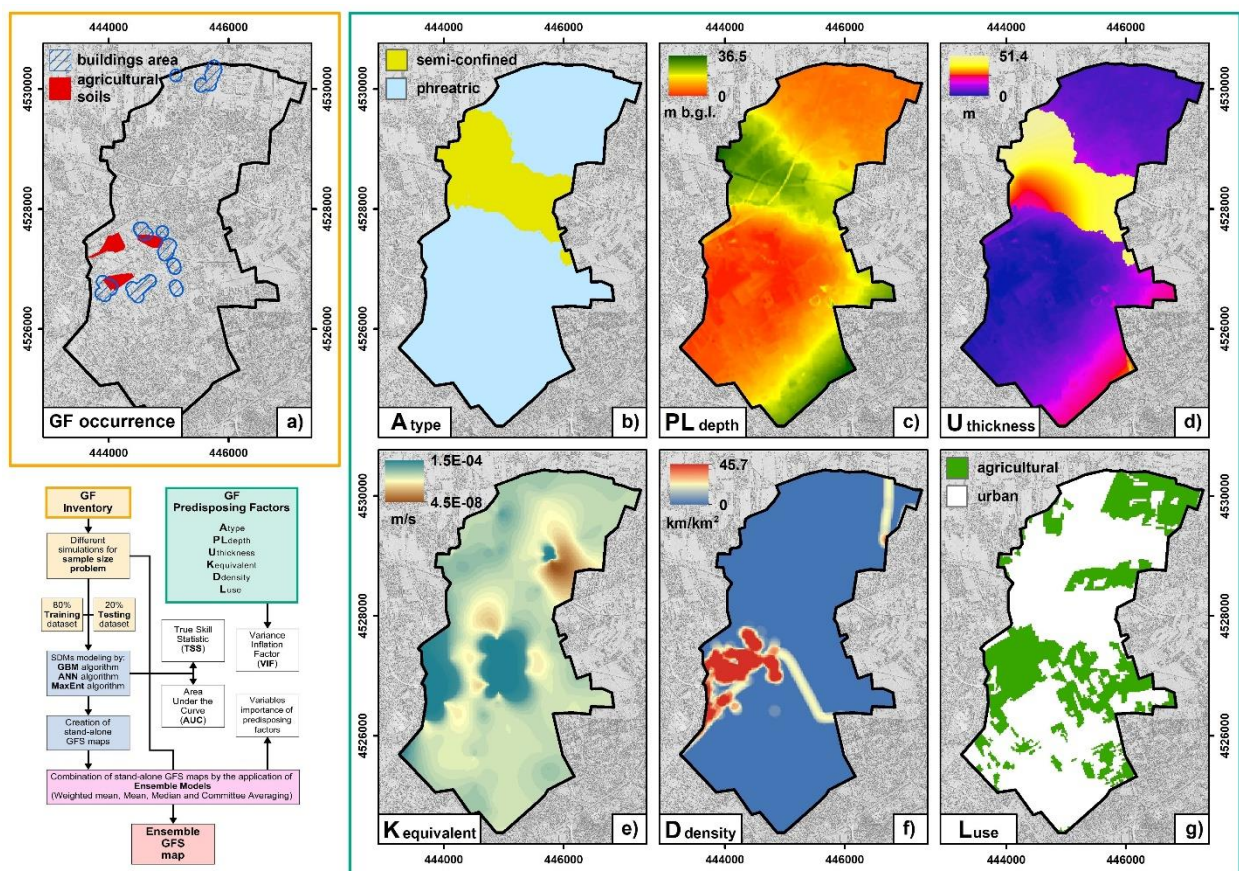


Figure 5.5 - Groundwater flooding occurrences (a) and Predisposing factors maps: b) Aquifer type (A_{type}); c) Piezometric Level depth (PL_{depth}); d) Unsaturated zone thickness ($U_{thickness}$); e) Equivalent hydraulic conductivity of unsaturated zone ($K_{equivalent}$); f) Drainage density ($D_{density}$); g) Land use (L_{use}).

Using LiDAR dataset (<http://sit.cittametropolitana.na.it/lidar.html>), a Digital Elevation Model (DEM) with 1×1 m cells has been implemented in a GIS environment and it has been employed in order to obtain the PFs. Most of the variables have been realized from

the DEM layer resampled to 20 × 20 m resolution, and all the hydrogeological and environmental variables have been defined exactly to the same grid.

A_{type} is a categorical predisposing factor that expresses the groundwater flow condition within an aquifer (Fig. 5.5b). It was derived from a high-resolution 2D hydro-stratigraphic model of the pyroclastic-alluvial aquifer, based on a database of 149 boreholes and 127 wells (Figs. 5.2a and 5.2b; Table S4 in supplementary materials; Allocca et al., 2021). As reported in Section 2 and shown in Figure 5.5b, phreatic and semi-confined aquifers have been recognized in the study area.

PL_{depth} and $U_{thickness}$ are continuously distributing PFs (Figs. 5.5c and 5.5d), variable between 0 and 36.5 m b.g.l., and 0 and 51.4 m, respectively. The first one has been elaborated selecting maximum historical piezometric data for the 1924-2017 period (Allocca and Celico, 2008; Allocca et al., 2021), in which GF impacts have been registered, corresponding to the piezometry of March 2015 (Fig. 5.3a). The Inverse Distance Weighted (IDW) technique to interpolate point values at the municipality scale has been used. PL_{depth} has been obtained subtracting the maximum piezometry to DEM layer. Where the aquifer is phreatic, PL_{depth} corresponds to the unsaturated zone thickness. Where the aquifer is semi-confined or confined, $U_{thickness}$ extends from ground surface down to bottom of aquitard or aquiclude layer.

The $K_{equivalent}$ factor (Fig. 5.5e) has been obtained from the hydrostratigraphic database and applying the method reported in Fusco et al. (2020). In detail, vertical logs of hydraulic conductivity of the unsaturated zone have been elaborated for each borehole, according to Freeze and Cherry (1979) classification. Equivalent hydraulic conductivity has been calculated for each log by the following formula:

$$K_{equivalent} = \frac{D}{\sum_{i=1}^n \frac{h_i}{K_{sat.i}}} \quad (1)$$

where D (m) is the depth to water table, n is the number of hydro-stratigraphic horizons, h_i is the thickness (m) of the i^{th} hydro-stratigraphic horizon, and $K_{sat.i}$ is the saturated hydraulic conductivity (m/s) of the i^{th} hydro-stratigraphic horizon. The calculated $K_{equivalent}$ have been interpolated by IDW method to obtain a map at the distributed scale with values comprised between 4.5×10^{-8} and 1.5×10^{-4} m/s.

The presence of surface water bodies, whether these are hydraulically connected to the aquifer or not, can play a major role in GF occurrence (Macdonald et al., 2008; Korkmaz

et al., 2009). Therefore, D_{density} factor (Fig. 5.5f), ranging from 0 and 45.7 km/km², has been obtained by following the approach used in Allocca et al. (2021).

Lastly, L_{use} factor (Fig. 5.5g) has been provided from Corine Land Cover (EEA, 2018), at the 1:100,000 scale, integrated with high-resolution Google Earth satellite imagery, dividing the study area in urban and agricultural land use.

QGIS, version 3.10 'A Coruña', has been used to implement the corresponding thematic layers and analyze groundwater spatial dataset in a GIS.

Selection of predisposing variables should be evaluated to avoid multicollinearity issues during modelling. For this purpose, before the modeling, a selection process is essential to detect the correct variables. The Variance Inflation Factor (VIF) has been chosen as multi-collinearity analysis and to evaluate the possible correlations among the predisposing factors. VIF measures how much the variance of an independent variable is influenced by its interaction with the other independent variables. A high VIF indicates that an independent variable is highly collinear with the other variables (Cama et al., 2017). Predisposing factors with VIF values greater than 10 should be considered affected by multicollinearity issues (Dormann et al., 2013; Guns and Vanacker, 2012). In this study, two different strategies were employed to exclude highly correlated variables: one that computes the correlation matrix between the variables and excludes one in the pair having a correlation higher than a pre-set threshold value ($VIF_{\text{COR}} = 0.7$, in this study) and another one that calculates the VIF considering all the variables and excludes all those variables increasing the total VIF over a pre-set VIF threshold ($VIF_{\text{STEP}} = 3$, in this study) (Guisan et al., 2017). Both the strategies were performed using the functions provided in the package *usdm* (Naimi et al. 2014).

3.3 Models' calibration and evaluation

All statistical calculations have been executed using the free statistical programming language "R" (R Core Team, 2020). All models have been performed by applying of R library "biomod2" (Thuiller et al., 2016). Artificial Neural Network (ANN), Generalized Boosting Model (GBM) and Maximum Entropy (MaxEnt) algorithms have been employed, recognized for their high predictive performance (Elith et al., 2006) (see the following sections for a brief description of the MLAs employed in this study). Models were calibrated and evaluated by means of a 5-fold Cross-Validation procedure. This methodology consists in randomly dividing the original dataset into 5 portions and by using 4 portions of data (training data, 80%) for models' calibration, whereas the

remaining set (testing data, 20%) is used as an independent record to measure model's predictive performance. The overall procedure is then reproduced several times (50 in this study) for any of the considered algorithms and the average predictive accuracy is finally reported (Naimi and Araújo, 2016). During the 5-fold cross validation, the models' predictive performances were measured by means of specific indices (see below for a detailed description of the indices). Once the models have been evaluated by the 5-fold cross validation, for any of the employed MLAs, a single model with the complete dataset (the full model), was trained and this one was finally used to the final ensemble procedures (described in Section 3.4). As regards the measures of the models' predictive performance, two indices have been employed: the Area Under the Curve (AUC; Hanley and McNeil, 1982) and the True Skill Statistics (TSS; Allouche et al., 2006). In details, AUC is the measure of the area under the curve of sensitivity (i.e. the proportion of accurately predicted true presences) plotted against 1-specificity (the proportion of accurately predicted true absences) for the range of all the possible thresholds to discretise the probability values assigned to either predicted presences and absences, and hence it is "threshold independent" (Raes and Aguirre Gutierrez, 2018; Shabani et al., 2018). One of the main advantages of the AUC is its ability to be insensitive of prevalence (i.e. the proportion of observed sites in which the species were recorded as present) (McPherson et al., 2004; Somodi et al., 2017). AUC values range from 0 to 1, where values < 0.6 indicates weak modeling accuracy, $0.6 - 0.7$ shows moderate accuracy, $0.7 - 0.8$ exhibits good accuracy, and > 0.8 indicates very good accuracy (Corsini and Mulas, 2017; Peterson et al., 2008; Yesilnacar and Topal, 2005). TSS is another widely used measure of model's performance with the property of being independent of prevalence (Allouche et al., 2006). TSS is defined as "sensitivity + specificity - 1" and ranges from -1 to $+1$ (Allouche et al., 2006). A TSS equal to -1 indicates that the model provides no better results than a random score to observed presences and absences. A TSS equal to 0 indicates model unable to discriminate between presences and absences. Values ranging from 0.2 to 0.5 are considered poor; scores higher than 0.5 but lower than 0.8 are useful; values larger than 0.8 are considered good to excellent (Coetzee et al., 2009).

3.3.1 Generalized Boosting Model

Gradient Boosting Models (GBMs) are a family of powerful Machine Learning algorithms for continuous and categorical response variables and rely on decision trees. Given X as the matrix of some predictor variables and Y as the values of a response variable, a simple

decision tree starts from its root to splitting dichotomously the values of some randomly-chosen predictor variables into subsequent nested-smaller clusters. This splitting produces some branches, and it continues until identifying a combinations of X values resembling those characterizing the observed Y . The X values are not to be splitted, until perfectly identifying the predictor values associated to the observed Y values, in order to avoid overfitting (i.e. a model standing too much on observations) and to create a model with predictive ability. A single decision tree is called “a weak learner” and a GMB algorithm is based on the idea that a combination of many “weak learners” has a higher predictive performance than a single “strong learner”. Indeed, a GMB algorithm starts by building a first decision tree relying on a random subset of X variables and then by measuring its performance in predicting the observed Y values. The algorithm carries on new different subsequent decision trees and a new tree is added to the previous one only if improving the predictive performance of the ensemble model. In order to reduce the overfitting issue, the best trees’ ensemble model is the one minimizing a “loss function”, which is represented by a combination of model’s prediction errors and complexity (i.e. number of trees) (Knoll et al., 2019). To sum up, a GBM consists of three simple steps (Natekin and Knoll, 2013):

- an initial model F_0 is defined to predict the target variable y . This model will be associated with a loss function L :

$$L = \sum_i l(\hat{y}_i - y_i) + \sum_k \Omega(f_k) \quad (2)$$

where the first term (training loss) measures the difference between a predicted value achieved by the score at the terminal node (\hat{y}_i) and its corresponding observed value (y_i) in the training dataset;

while, the second one (regularization) represent the complexity of the model;

- a new tree h_1 is fit to the residuals from the previous step;
- F_0 and h_1 are combined to give F_1 , the boosted version of F_0 and its loss function evaluated.

This algorithm runs “ n ” times (iterations) until the loss function has been minimized as much as possible.

3.3.2 Artificial Neural Network

Artificial Neural Network (ANN) is an attempt to simulate the network of biological neurons that make up a human brain so that the computer will be able to learn things and to process information (Zurada, 1992). ANN algorithm uses different layers of mathematical processing to find relationships between response and predictor variables. Typically, a neural network has dozens of artificial neurons, called units, organized in sequences of layers. The input layer contains the predictor data. From the input, data go through one or more hidden layers containing several unit neurons. The hidden unit's job is to transform the input into something the output unit can use. On the other side of the network, there are the output units, i.e., the response variable. Connections between nodes and hidden layers may be characterized by specific weights that can be randomly assigned at the beginning of the process (the higher the weight, the greater influence one unit has on another), and later updated for algorithm optimization employing back-propagation processes (Pijanowski et al., 2002). The neurons in each hidden layer represent different combinations of the environmental variables weighted by the weights' sum of the previous neurons (Peh et al., 2000):

$$c_j = \sum_{i=1}^p w_{ij}x_i \quad (3)$$

where w_{ij} is the weight from neuron i in the input layer to neuron j in the hidden layer, x_i is the i -th input element and p is the number of neurons in the input layer. This calculation is performed for each neuron in the hidden layer. At each neuron, if the weighted sums coming from the previous layer neurons is higher enough for a so-called "activation function", then that specific neuron, i.e. a specific combination of the input variables, is turned on and the signal passes to the following layer neurons up to the output layer. There are many different forms of activation functions and a commonly used one is the logistic function, which produces a sigmoid curve with an outcome between 0 and 1 (Peh et al., 2000):

$$o_j = \frac{1}{1+\exp(-c_j)} \quad (4)$$

where o_j is the output of the j -th node in the hidden layer. The outcome of the activation function is then passed to the output layer.

3.3.3 Maximum Entropy

MaxEnt is a presence-only Machine Learning method (Phillips et al., 2006), currently one of the most popular algorithms for presence-only datasets. MaxEnt starts from the assumption that observed event's occurrences are a restricted random sample of the actual event spatial distribution. This algorithm compares the observed probability density functions (PDFs) of environmental factors at the event's occurrence sites with the PDFs of the same variables of a remaining landscape's random sample (Elith et al., 2011). MaxEnt algorithm assesses the predicted (actual) PDFs of environmental variables characterizing the events that approximate the PDFs on the landscape, i.e. by maximizing the entropy of information. This maximized-entropy model produces information to predict the event occurrence probability at unsampled locations. MaxEnt then calculates the ratio between these two probability densities, which gives the relative "environmental suitability" for the presence of an event for each location in the study area (the landscape) (Eq. 5) (Elith et al., 2011):

$$\Pr(y = 1 | z) = f_1(z) \Pr(y = 1) / f(z) \quad (5)$$

Equation 5 shows that if the PDF of the environmental variables at the presence locations is known, $f_1(z)$, along with the density of the same variables across the study area $f(z)$, it then only needs knowledge of the prevalence (proportion of occupied sites) $\Pr(y = 1)$ to compute the event's occurrence probability at unknown locations.

3.4 Ensemble methods and variables' importance

Ensemble techniques have been adopted for the first time by Burnham and Anderson (2002), who performed a simple average of several regression models. Ensemble models (EMs) approach, which produces a predictions integration of every stand-alone model, provides a solid contribution to minimize uncertainty and to improve the prediction accuracy (key parameter indispensable when working with susceptibility). Such EMs often result in better classification than individual ones (Di Napoli et al., 2021; Pourghasemi et al., 2017). In predictive modeling, a single model can have biases, high variability or inaccuracies that influence the reliability of its outcomes and modeling variability in SDM outputs has been widely described (Araújo and New, 2007; Elith and Graham, 2009; Pourghasemi et al., 2017). EMs help to minimize these issues as long as single-algorithms are different and independent.

In this research, the EM procedure consisted in firstly performing the stand-alone SDMs, considering the above mentioned algorithms. After this step, since all the performed models can have different prediction's performances, only those models with AUC scores higher than 0.8 have been selected in the final ensembled model to produce GFS' occurrence probability map. Then, the following ensemble procedures have been considered: mean, median, weighted mean and the committee averaging of the models. In the very special case of the weighted mean strategy, the models' predictions are weighted by their respective AUC score before averaging.

Both the stand-alone and ensemble GFS maps have been employed identifying five value ranges to discriminate the groundwater flood susceptibilities classes from very low to very high, using Natural Breaks classification (Jenks, 1967). Natural Breaks aims at defining the best data distribution in significant classes, taking advantage of the intervals naturally present in the data distribution and attempting to reduce the variance within each class and maximizing that between the classes themselves.

For the committee averaging, the Natural Breaks subdivision was not applied, because this ensemble forecasting method is based on the binary classification of occurrence probability maps. The committee averaging method transforms any probability map coming from the stand-alone models (i.e. MaxEnt, GBM and Neural Network, separately) into binary maps using a threshold (the one maximizing both sensitivity and specificity). These binary maps are, then, overlaid and a cell-wise scores sum is performed. The final committee averaging map is the one in which any single map's cell score is divided by the number of the original models. The interesting feature of this measure is that it gives both a prediction and a measure of prediction's variation (Gallien et al., 2012). When the prediction is close to 0 or 1, it means that all models agree to predict 0 and 1, respectively. If the prediction is around 0.5, it means that half the models predict 1 and the other half 0 (Thuiller et al., 2016). The best ensemble model has been chosen by comparing the validation performance (i.e. AUC and TSS) of each ensemble procedures.

Lastly, to assess the contribution of each predictor variable in explaining the response variable's variance, a variables' importance measure has been applied. Variable importance is defined as 1 minus the Pearson's correlation coefficient between the model's prediction standing on all the predictor variables and the prediction made by randomly ruling out one single variable at time. The higher the correlation, the lowest the importance of the excluded variable. This variables' importance index ranges between 0 (no importance) and 1 (high importance) (Lomba et al., 2010; Thuiller et al.,

2016). The variables importance measure was computed by using the specific functions provided in the "biomod2" package. In addition, a further analysis about the spatial distribution of PFs have been carried out, to detect the value range of each PFs that determine the highest GFS class.

4. Results

4.1 Optimal sample size

The performance analysis outcomes for different sample sizes are illustrated in Figure 6. The analyses highlighted that for all the algorithms used (i.e., GBM, ANN and MaxEnt), both with the AUC curves and with the TSS method, 500 occurrences are the minimum number of sampled observations that maximise the models' accuracy. In Figure 5.6, magenta dotted line divides the trend into two subgroups: on the left the AUC and TSS values have a variable behavior, while on the right it is possible to observe a constant trend of accuracy values. Therefore, all the analysis carried out subsequently has been undertaken starting with a dataset composed of 500 points, generated randomly in the phenomenon occurrence area.

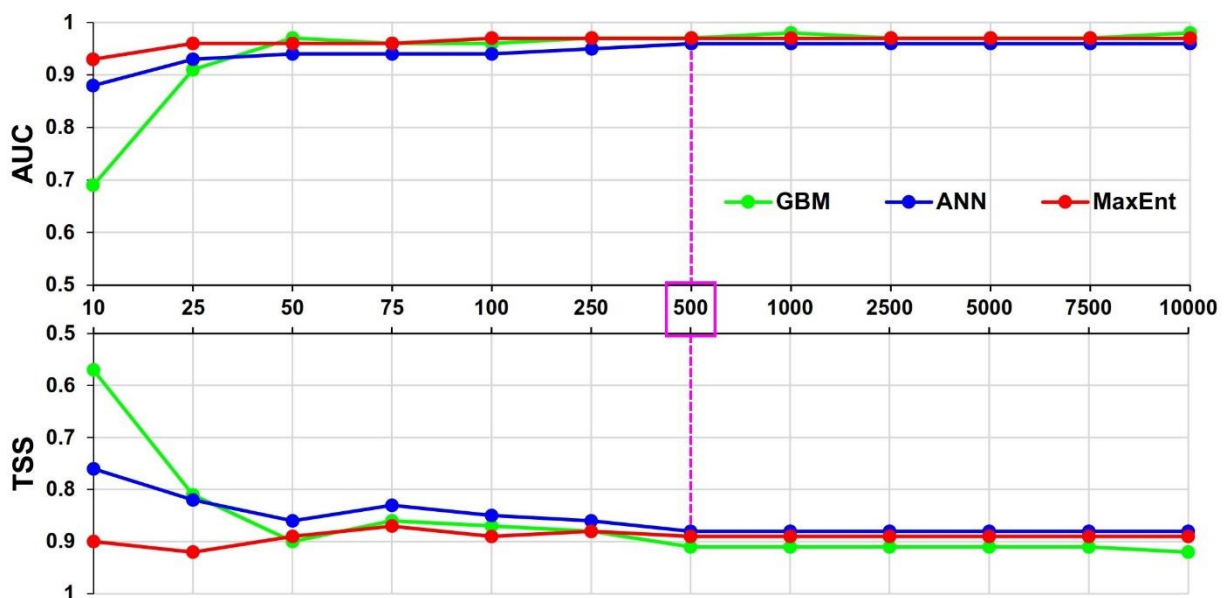


Figure 5.6 - Optimal sample size identification (box in magenta) comparing AUC and TSS parameters for the stand-alone models.

4.2 Multi-collinearity analysis of PFs

VIF has been adopted to evaluate the possible correlations among each factor and this method helps to improve the models' prediction performance (Arabameri et al., 2020). There is no well-defined and accepted threshold in the literature, the general rule of thumb is that VIFs exceeding 4 need more analysis, while VIFs exceeding 5 or 10 denotes serious multicollinearity issue, requiring revision (Hair et al., 2010). The calculated VIF are reported in Table 1. Both the VIF correlation strategies values of each PFs are smaller than 4. The highest VIF is 2.10 and the highest correlation is 2.16 (both associated to the $U_{\text{thickness}}$), thereby no multicollinearity problem was detected between independent factors in the current study.

Table 5.1 - Multicollinearity analysis indices for all the predisposing factors used in the work; such scores represent the average of the various models obtained.

Predisposing factors	VIF_{STEP}	VIF_{COR}
A_{type}	1.77	1.80
PL_{depth}	1.85	1.80
U_{thickness}	2.10	2.16
K_{equivalent}	1.21	1.18
D_{density}	1.24	1.35
L_{use}	1.21	1.20

4.3 GFS modeling

4.3.1 Models validation

The validation of the models' predictions has been analyzed using AUC curves and TSS validation criterion, and the calculated values are reported in Table 5.2.

Both evaluation metrics show very high values. When considering stand-alone models, the AUC and TSS scores are the average values computed with the 5-fold cross validation procedure, since the ensemble models are an ensemble of the full models calibrated with the complete dataset, the AUC and TSS scores represent the ability of the ensemble models in reproducing the training dataset. Among the stand-alone models, both the GBM (AUC = 0.93, TSS = 0.89) and MaxEnt (AUC = 0.95, TSS = 0.89) have higher average

predictive accuracy, followed by the ANN model (AUC = 0.80, TSS = 0.86). On the other hand, in the case of EMs, Weighted mean probabilities (Wmean) (AUC = 0.96, TSS = 0.92) and mean of probabilities (mean) exhibit the highest values (AUC = 0.95, TSS = 0.91). They are followed by the median of probability (AUC = 0.94, TSS = 0.89) and, lastly, committee averaging (AUC = 0.92, TSS = 0.88). Despite small differences, all the ensemble models show high accuracy values.

Table 5.2 - In blue, the AUC and TSS average scores of the stand-alone models. In magenta, the scores represent the ability of the ensemble of the full models to reproduce the training dataset.

Models	AUC	TSS
GBM	0.93	0.89
ANN	0.80	0.86
MaxEnt	0.95	0.89
CA	0.92	0.88
Mean	0.95	0.91
Median	0.94	0.89
Wmean	0.96	0.92

4.3.2 Stand-alone and Ensemble models' GFS maps

Different GFS maps, as a result of Machine Learning algorithms (Fig. 5.7), have been generated by applying 50 different combinations between training (80%) and testing (20%) dataset, attempting to generate the best predicting models. Based on the Natural Break classification, the reconstructed susceptibility maps have been subdivided into very low, low, moderate, high and very high GFS classes.

The most prone areas have been identified in the northern and south-western sectors. The full stand-alone model-based maps (Figs. 5.7a, 5.7b and 5.7c), show a high prediction variability. In particular, as shown in Figure 5.8a, all the stand-alone models highlight elevated variability in the high and very high susceptibility classes. In detail, GBM (5.7a) detects 6% of the total area falling into high class and 11% in very high susceptibility class. ANN GFS map (5.7b) is characterized by 21% in the high class while 8% falling into very high susceptibility class. Percentage susceptibility classes in the MaxEnt map (Fig. 5.7c) are distributed as follows: 9% high and 5% very high susceptibility class. Such discrepancy helps to understand how the stand-alone models diverge from each other

and how the ensemble models are needed in order to obtain outcomes more reliable and accurate.

Such high variability is confirmed by Committee Averaging (CA) ensemble model (Fig. 5.7c), in which areas characterized by white and green colors represent sectors where all stand-alone models predict similar outcomes. On the other hand, the extreme models' variability is highlighted in the sectors with yellow and magenta colors.

The ensemble models have improved on the stand-alones' prediction variability, as shown in Figures 5.7e, 5.7f, 5.7g and 5.8b. In fact, by comparing the percentage of area falling into each GFS classes (Fig. 5.8b), maximum difference of 5% has been recognized, specifically in the lower susceptibility classes. Conversely, in the highest classes, this difference is reduced to a maximum of 2% in the high class and 1% in the very high one.

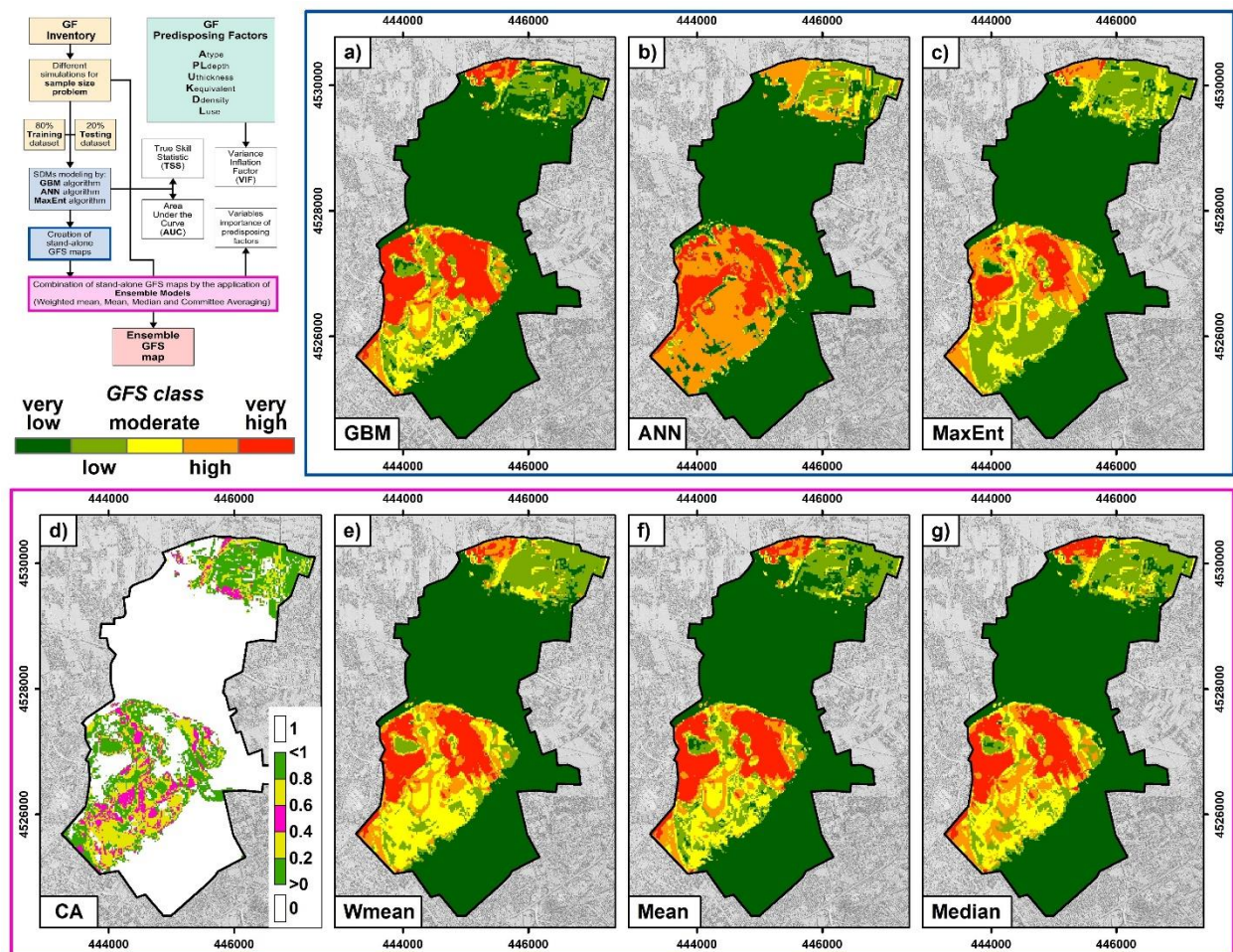


Figure 5.7 - Stand-alone (a-c) and Ensemble models (d-g) maps: a) Artificial Neural Network (ANN); b) Generalized Boosting Model (GBM); c) MaxEnt; d) Committee Averaging; e) Weighted mean (Wmean); f) Mean; g) Median.

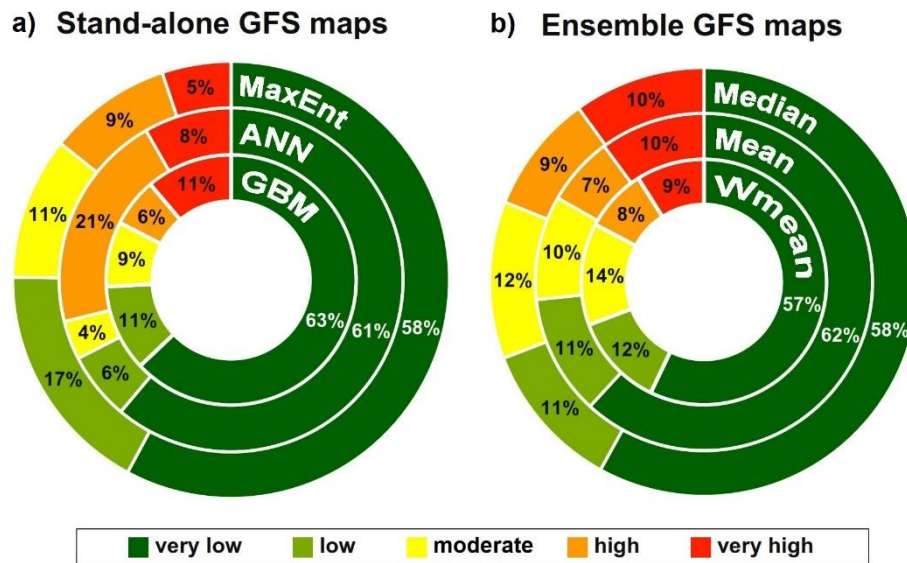


Figure 5.5 - Percentage of area attributed to each GFS class for the stand-alone (a) and ensemble models (b) after Natural Breaks classification.

4.4 GFS final map

Based on model validation, previously reported and commented in Section 4.3.1, Wmean ensemble model obtained the highest AUC and TSS scores (0.96 and 0.92 respectively), and it has been chosen for the final GFS map (Fig. 9a).

The areas characterized by high and very high susceptibility involve 8.3% and 9.0% of total study area, respectively (Fig. 10). As previously mentioned, these areas are located in the northern and south-western sectors. Very low class covers 57% of the study area, falling into the central and south-eastern sectors. The remaining portions are assigned the low (12.1%) and moderate (13.6%) classes.

Figures 9b and 9c show the spatial distribution of buildings and agricultural soils affected by GF. A good correspondence can be observed between the areas characterized by very high and high susceptibility and the location of impacted elements, both for buildings in the northern sector (Fig. 9b) and for buildings and agricultural soils in the south-western sector (Fig. 9c). An apparent anomaly is represented by CAAN (Agri-Food Centre of Naples) in the south-western sector (Fig. 9c), a large structure extending approximately over 362.000 m² used as a wholesale market, that partially falls into moderate class. To support the accuracy of the prediction, in Figure 10 the percentage of occurrence points falling into the susceptibility classes is reported. 92.8% of occurrences has been assigned to high and very high susceptibility, while 0.4% and 6.8% to low and moderate ones. No

occurrence point is classified as very low susceptibility. It is possible to observe an increasing trend of the occurrence points falling into the different susceptibility classes, from the lowest to the highest. Conversely, concerning the areal extension of each class, it is possible to notice a decreasing trend, i.e., the areal extension decreases as the susceptibility class increases.

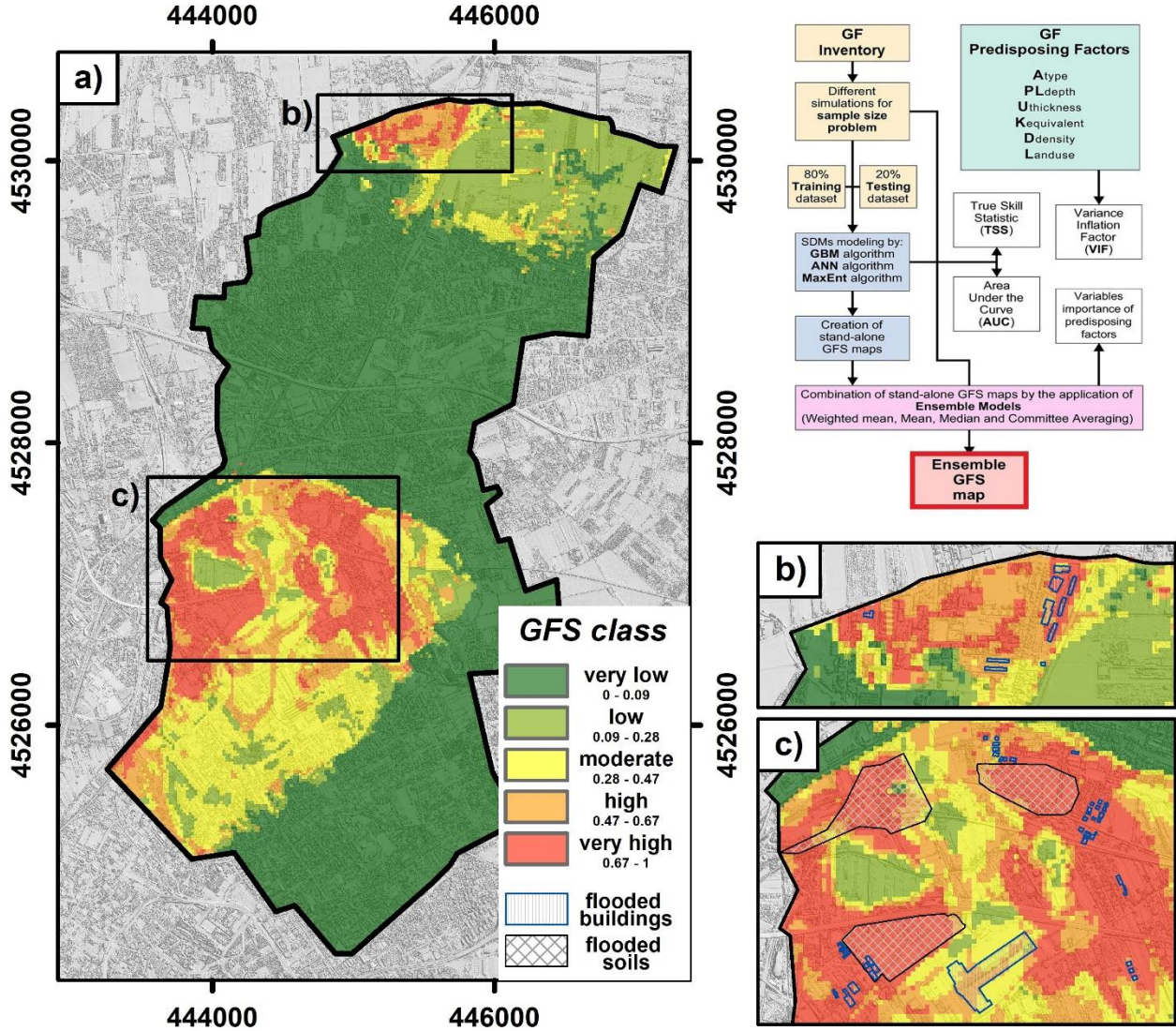


Figure 5.9 - Final Groundwater Flooding Susceptibility map (a) and focus on flooded buildings and agricultural soils in the impacted sectors of study area (b and c).

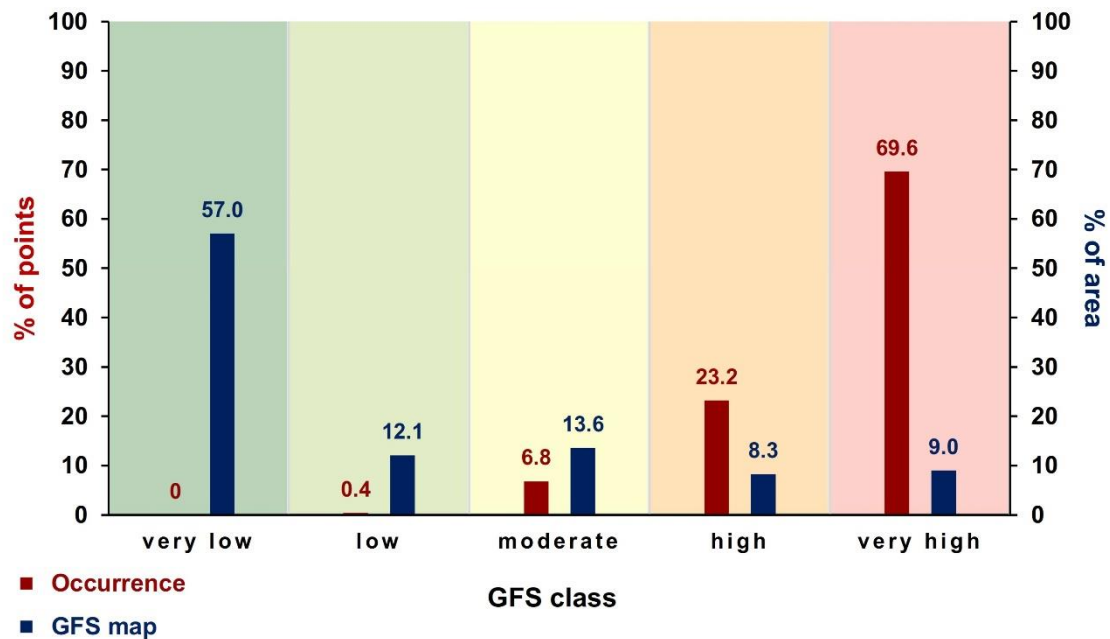


Figure 5.10 - Comparison between percentage of area (in blue) and percentage of occurrence points (in red) falling in each GFS class.

4.4.1 PFs analysis

It is always hard to compare predictions from different models as they do not rely on the same algorithms, techniques and assumptions about the expected relationship between the input data and the environmental variables. In biomod2 package, it has been possible to examine the importance of the variables in the models. Table 3 presents the importance of each variable, expressed in values ranging from 0 to 1 (no influence and maximum influence, respectively). In particular, the results reveal that the highest conditioning variable is D_{density} with an absolute value of 0.62, while A_{type} presents the smallest value (0.10). Values of the others PFs are listed in order of their diminishing importance: $U_{\text{thickness}}$ (0.39), PL_{depth} (0.32), $K_{\text{equivalent}}$ (0.25) and L_{use} (0.11).

Moreover, in the right column of Table 3 the values of each PFs in the areas attributed to high and very high GFS are reported. Therefore, it has been observed that the maximum GFS is reached, for the categorical variables (A_{type} and L_{use}), in condition of phreatic aquifer and both for urban and agricultural land use. In addition, thickness of unsaturated zone, as well as the piezometric level depth, can vary between 0 and 5.2 m, with an equivalent hydraulic conductivity ranging from 4.5×10^{-8} and 1.6×10^{-4} m/s. Lastly, density drainage assumes values between 0 and 26.5 km/km².

Table 5.3 - Variables' importance and their variability in high and very high classes.

Predisposing factors	Variables importance	Range values in high and very high classes
A_{type}	0.10	Only phreatic aquifer
PL_{depth}	0.32	0 – 5.2 [m b.g.l.]
U_{thickness}	0.39	0 – 5.2 [m]
K_{equivalent}	0.25	$4.5 \times 10^{-8} - 1.6 \times 10^{-4}$ [m/s]
D_{density}	0.62	0 – 26.5 [km/km ²]
L_{use}	0.11	Both urban and agricultural

5. Discussion

GFS mapping could constitute an important tool for GF risk mitigation, particularly if executed rigorously and supported by an accurate dataset. Hence, statistical techniques represent an ideal synthesis, especially if applied to large areas. However, the uncertainty associated with every process greatly affects statistical techniques and a percentage of unpredictability is always closely linked to statistical modeling. In this work, stand-alone models (i.e. GBM, ANN, MaxEnt; Fig. 7) have been adopted for a GFS assessment. Results showed an elevated predictive variability (Fig. 8a). To reduce these effects, Ensemble models (i.e. Wmean, Mean, Median and CA; Fig. 7) have been accomplished, which are based on the assumption that running two or more related but different models and then merging the results into a single model, improves the accuracy of predictive analytics (Guisan et al. 2017). In particular, CA ensemble model (Fig. 7d) allowed to estimate the general variation (and thus uncertainty) of stand-alone models. This last ensemble methodology is widely adopted for its double functionalities of predictivity and uncertainty measurement (Hao et al., 2019; Thuiller et al., 2016). All EMs results appear

to be encouraging and perform better than stand-alone methods, with AUC and TSS values higher than 0.89, hence excellent according to the various classifications available in literature (Fressard et al., 2014; Hair et al., 2010). Wmean model obtained the best validation scores and it was chosen to the final GFS map (Fig. 9). Further validation analysis has been carried out intersecting the GFS map with flooding occurrences points (Figs. 9b, 9c and 10), the latter falling into high and very high classes of susceptibility in about 93% of the monitored points, notwithstanding the limited areal extension of these classes (17.3% of total area). The unique exception is found for the area where is located the CAAN (Fig. 9c), built in the period 2006-2008. This sector, affected by GF episodes before the period 2006-2008, is characterized, according to EMs results, by moderate susceptibility. This apparent discrepancy is related to the lifting of ground level surface realized to mitigate the GF, that changed the original ground elevation (Coda et al., 2019b). Exploring PFs spatial distribution in the sector characterized by high and very high GFS (Table 3), it is possible to observe some common features. Firstly, the alluvial plain aquifer is locally phreatic (i.e. $U_{thickness}$ is equivalent to PL_{depth}), and the alert piezometric threshold, i.e. the local surveillance level of water table below which GF of buildings occurs, is 5.2 m b.g.l.. Secondly, the $D_{density}$ is low, with values ranging from 0 to 26.5 km/km², according to local drainage channel network (Allocca et al., 2021). This finding is in line with the hydrogeological conceptual model and with the GF triggering mechanism locally observed. Actually, in the areas of southern sector characterized by highest values of $D_{density}$, low susceptibility has been recognised, proving the GF mitigation effect of Cozzone and Volla rivers and Reale Lufrano channel. However, other case studies available in literature are characterized by different GF scenarios (Macdonald et al., 2008), showing that GFS is greater near surface water-bodies or where values of drainage density are high. These differences are strongly related to the GF mechanism type, the latter having a key-role of MLA methodology. Hydro-geo-environmental predisposing factors have been selected: they are based on the specific hydrogeological conceptual model. Consistently with other susceptibility assessment methodologies, parameters for GFS assessment are not universally recognized, and, therefore, parameters must be determined based on the specific groundwater flooding phenomenon and its triggering mechanism. Furthermore, PFs computation represents a critical issue, such as the identification of the historical maximum level of water table, and knowledge about natural and anthropogenic factors that locally control GF occurrence and its spatio-temporal distribution. A robust hydrostratigraphic database, as

well as a long-period monitoring of piezometric levels and GF impacts, have been used to overcome this issue (Allocca et al., 2021). Poor data quality/quantity could invalidate the predictive performance of the models, requiring a refinement of input data.

6. Conclusions

In this paper a novel methodological procedure aimed at evaluating GFS associated with GWLr has been proposed. For the first-time, a combination and comparison of Ensemble methods based on different MLAs, including ANN, GBM and MaxEnt, has been employed for GFS mapping. The methodology proposed has been applied in a mixed land-use aquifer located in the Metropolitan City of Naples, affected by urban groundwater rebound since 1990 and groundwater flooding since 2007, where a considerable geological and groundwater database is available, as well as systematic hydrogeological monitoring of water table and flooding.

The first step to produce GFS modeling has been the identification of the optimal number of points to insert as inputs to run the models. Flood predisposing factors were chosen according to the hydrogeological conceptual model and the triggering mechanism of the observed GF. The initial dataset was randomly divided into 80% as training and 20% as testing, the latter used for validation purpose, and for each model spatial maps were derived. The main results of this study can be listed as follows:

1. according to Ensemble Modeling results, drainage density, unsaturated zone thickness, and depth of piezometric level are the most important conditioning factors, followed by equivalent hydraulic conductivity of unsaturated zone, land use, and saturated aquifer type;
2. although the high variability and uncertainty characterizing the different stand-alone models, the Ensemble models allowed to detect groundwater flooding susceptible areas with highest occurrence probability;
3. the comparison between GFS map and groundwater flooding inventory data is encouraging, since most of the recorded flood events (about 93%) were located in the high and very high susceptibility classes.

The application of this method can be extended to other urban and rural areas affected by GWLr-induced GF, at the basin as well as local scale, to investigate Groundwater

Flooding Susceptibility. The methodology here developed represents a first step to GF hazard and risk assessment and to forecast the spatial and temporal distribution of flooding prone areas, as required by Italian and European legislation. In addition, GFS maps provide a new tool to assist local government authorities, planners and water decision-makers in addressing the problems deriving from GF, supporting the design of measures to mitigate the risks and damages caused by GF, facilitating the construction of safe man-made underground structures.

Supplementary Material

Table S4 - Hydrogeological, hydrological, stratigraphic dataset and GF inventory for the study area. U.D. unavailable data; A, Agricultural; I, Industrial; D, Drinking.

Hydrogeological and hydrological data						
Monitoring period	Type	Total number	Density (No./Km ²)	Use	Depth range (m)	Reference
August, 1924	Well	85	6.07	A and D	4-12	Fiorelli (1926)
February-September, 1978	Well	U.D.	U.D.	A, I, D and D	U.D.	Celico (1983)
March, 1989	Well	28	1.95	A, I, D and D	10-60	Celico and De Paola (1992)
January, 1993	Well	24	1.67	A, I and D	10-70	Esposito (1998)
February, 1994	Well	24	1.67	A, I and D	10-70	Celico et al. (1995)
February, 2002	Well	30	2.09	A, I and D	10-70	Basin Authority of the North-Western Campania Region (2004)
November, 2013	Well	127	9.07	A, I and D	10-60	Field campaign
November, 2013	River head	28	1.95	\	\	Field campaign
March, 2015	Well	127	9.07	A, I and D	10-60	Field campaign
March, 2015 - ongoing	Piezometer	9	0.64	\	10-30	Field campaign
March, 2015	River head	28	1.95	\	\	Field campaign
February, 2017	Well	127	9.07	A, I and D	10-60	Field campaign
February, 2017	River head	28	1.95	\	\	Field campaign
1924 - ongoing (annual rainfall) 2013 - ongoing (monthly rainfall)	Meteorological station	1	\	\	\	San Marcellino Meteorological Observatory

Stratigraphic data						
Monitoring period	Type	Total number	Density (No./Km²)	Use	Depth range (m)	Reference
1980-2015	Borehole	148	10.34	Urban planning	10-60	Casalnuovo di Napoli and Volla municipalities unpublished database
\	Borehole	1	0.07	Scientific issues	430	Torrente et al. (2010)
GF inventory						
Monitoring period	Type	Total number	Density (No./Km²)	Use	Max Extension (m² or ha)	Reference
November, 2013 - ongoing	Private building	55	3.84	Private	65916.85 m ²	Unpublished online questionnaire and field survey
November, 2013 - ongoing	Agricultural soil	3	0.21	Private	25.36 ha	Unpublished online questionnaire and field survey

6

Conclusions and prospects for research

This multi-disciplinary study allowed to characterize a complex phenomenon as the rise of groundwater levels (GWLr) and its effects in some representative areas of the Metropolitan City of Naples.

In the eastern plain of Naples, causes and dynamics of the phenomenon were detected by reconstructing a comprehensive hydrogeological conceptual model of the aquifer and the evolution of piezometric levels, groundwater use and land use in the last 100 years. This made it possible to attribute piezometric rise to the groundwater rebound (GR) process, occurred since 1990 and caused by the drastic reduction of groundwater abstraction after a period of aquifer over-exploitation. The pyroclastic alluvial aquifer of the eastern plain of Naples can be considered as a representative example of mismanagement. At the end of the 80s, the withdrawals for drinking, industrial and agricultural purposes reached a maximum value of about 6 m³/s, exceeding the mean annual water budget of the aquifer of approximately 2,65 m³/s. The overexploitation caused the progressive decline of piezometric levels and extraction of highly mineralized waters coming from deeper parts of the aquifer. As a result of this, an increase in Fe, Mn and fluoride concentrations of natural origin occurred. In addition, high NO₃ values were found in water, coming from the use of nitrogen fertilizers in agricultural activity as well as from urban and industrial waste. High contamination values of groundwater led to drastic reduction of drinking water abstractions and groundwater pumping for industrial and agricultural use, the latter favoured also by deindustrialization processes and land use changes (from industrial and rural to semiurban).

In Casalnuovo di Napoli and Volla municipalities, the rise of piezometric levels occurred in the whole area reaching, in some sectors, a magnitude up to 16.54 m for the period 1990-2015 with an almost total recovery of piezometric levels of early 1900s. No relationship between GWLr and rainfall has been recognised for that period. Conversely, the current piezometric oscillation is mostly influenced by the hydrologic regime, as observed in the period 2015-2017; a decrease of piezometric levels has been registered in 2017 after the period 2016-2017 characterized by scarce precipitation. A rising trend is currently occurring due to precipitation increasing in the period 2017-2020, as emerges

from data of the piezometric monitoring stations, installed in March 2015 and still working today (data only partially published).

A thorough analysis of the effects of GWLr was carried out and, for the first time in the Metropolitan City of Naples, it was demonstrated that ground deformation and groundwater's hydrochemical variations can be GWLr-induced phenomena. However, the most impactful GWLr-induced process turned out to be the groundwater flooding (GF), with severe environmental and economic damage/costs for inhabitants and the cultural heritage. A first inventory of GF episodes has been created including detailed information about the impacted buildings and agricultural soils. It has been carried out through field survey and a citizen participatory approach. The flooding episodes showed inhomogeneous spatial distribution despite of a widely diffused GWLr. This aspect has been investigated to identify the natural and anthropogenic influencing factors of GF, based on the hydrogeological, hydrographic and hydraulic characteristics of the aquifer, as well as land use.

The findings about the characterization of GR and GF represented preparatory data for the implementation of a novel methodology for GF susceptibility (GFS) assessment through, for the first time in this research field, machine learning techniques. Applying Spatial Distribution Models (SDM), GF occurrence data, coming from the GF inventory, have been connected to predisposing factor (PFs) to estimate the most prone areas' distribution. Aquifer type, depth of piezometric level, thickness and hydraulic conductivity of unsaturated zone, drainage density and land use have been employed as PFs. The algorithms adopted to perform the analysis were Generalized Boosting Model, Artificial Neural Network and Maximum Entropy. Ensemble Models were carried out to reduce the uncertainty associated with each algorithm and increase its reliability. GFS has been mapped by choosing the ensemble model with the best predictivity performance and dividing occurrence probability values into five classes, from very low to very high susceptibility. The comparison between GFS map and groundwater flooding inventory data was encouraging, since most of the flood events recorded (about 93%) fell in the high and very high susceptibility classes.

A further aspect of GR and GF has been analysed in Casalnuovo di Napoli area, as the economic impact on property values and costs of dealing with GF problem. Several typologies of expenditures have been analysed, referred to a representative building of the study area, including geological and hydrogeological surveys reports, construction

and maintenance/substitution of micro-pumps plant, maintenance of damaged elevators, electricity consumption and expenditure for legal and technical support (solicitors, geologists, engineers). The expenditure ranged from a minimum of 2,748 euros in 2011 when the pumping system was installed, to a maximum of about 12,000 euros in 2015, when the full set of micro-pumping plants were working. In addition, a comparison between time series of piezometric levels and electricity bills has been employed for the period January 2015 - July 2018. From this analysis, an elasticity relationship of electricity expenditure to the piezometric level emerged, and it has been estimated to be of 6.2, meaning that for one point percentage increase in the piezometric level, electricity expenditure will grow by 6.2 per cent.

Regarding the vertical displacement, in both the two investigated areas of eastern plain of Naples (Casalnuovo di Napoli and Volla municipalities, Lufrano and Acerra well-fields), coupled analysis of piezometric variation and ground deformation allowed to identify cause-effect relationship between GWLr and uplift. DInSAR data of ERS-1/2 and ENVISAT satellites, processed by using the PS-InSAR technique, showed a general ground uplift with a magnitude up to 40-50 mm starting from the period of interruption of groundwater pumping. A comparison between trends of groundwater levels and ground displacement indicated that the ground uplift was linked to a poro-elastic rebound mechanism in the porous aquifer system, which was triggered by the increase of pore pressure. In addition, the rate of ground displacement was controlled by the hydrostratigraphic characteristics of the multi-layered aquifer system and the distance from the core of GR (Lufrano well-field area), with higher rate where the aquifer was phreatic and in proximity of pumping stations, respectively.

The last GWLr-induced phenomenon considered was the variation of groundwater contamination in Casalnuovo di Napoli and Volla municipalities. Trends of the concentration of natural and anthropogenic contaminants, as Fe, Mn, NO₃ and fluoride, have been reconstructed for the period 1992-2017. From the comparison between the variation of piezometric levels and the concentration of the chemical compounds, a relationship emerged. Piezometric and nitrates variations had a positive trend. The reduction of the water table depth increased the concentration of this pollutant produced by human activity coming from the surface (reducing the time travel). Conversely, a negative trend is observed in the natural contamination. The high concentration of fluorides, Fe and Mn in the pumping period, caused by the mobilization of highly

mineralized water and by anoxic environment, have suffered an average sharp reduction. The interruption of pumping, the increase of the aquifer thickness and the reactivation of less deep horizontal flows led to a greater oxygenation of groundwater, as well as to the lack of mobilization of deep fluids and the dilution of these natural pollutants.

The GWLr also occurred in some coastal areas of the Metropolitan City of Naples, as the western coast of Phlegraean Fields. The triggering mechanism has been attributed to natural subsidence of this sector due to volcano-tectonic deformation with relative increase of sea level and consequent lifting of groundwater levels. Consequences of GWLr have been recognised in the Cumae archaeological site, which has suffered from GF for the last decade. Flooding of the archaeological ruins led to a reduction of archaeological excavation activity and reburial of many of them. Another threat for the safeguarding of the cultural heritage from deterioration was represented by natural and anthropogenic contamination of groundwater. Therefore, the processes that influenced quality of groundwater have been investigated by means of a hydrological, hydrochemical and isotopic survey of the volcanic-sedimentary aquifer system. Results showed that the natural influencing factors were related to aquifer lithology and localized ascent of magmatic fluids along buried volcano-tectonic discontinuities, which explained high values and concentrations of EC, temperature, chloride, fluoride, boron, arsenic, and ^{222}Rn . In addition, in the drained retro-dunal area of the coastal plain, where groundwater flow slowed down and the aquifer lithology was rich in organic matter, a denitrification trend has been highlighted by means of $\delta^{18}\text{O}-\text{NO}_3$ and $\delta^{15}\text{N}-\text{NO}_3$ ratios. Anthropogenic contamination was attributed to an increment of concentration of the natural compounds during the pumping period, mobilizing and drawing more the highly mineralized deep fluids. Other anthropogenic sources of contamination come from agricultural activity, recognizing high concentrations of $\text{NO}_3 (>50 \text{ mg L}^{-1})$, which, as evidenced by isotopic ratios of N and O, were attributed to mineral fertilizers, as well as natural sources and, to a minor extent, manure and possible leaks from septic tanks or sewage systems.

The results of the PhD research project, reported in this thesis, provide new knowledge on the GWLr phenomenon that is impacting a large territory of the Metropolitan City of Naples, defining its extent and dynamics. The methodological approach used highlights the importance of combining different techniques to characterize GWLr and to deal with GF and others GWLr-induced phenomena, and it can be exported in similar, as such as

different, geographical and hydrogeological contexts. The study can be understood as a guideline in the management of this widespread phenomenon and its effects.

The topic of GF risk is currently developing, starting from the implemented GFS methodology. GFS maps already represent a new tool to assist local government authorities, planners and water decision-makers in addressing the problems deriving from GF. In particular, definition of the most prone areas provides support for designing of mitigation measures and new safe man-made underground structures. Furthermore, the hydrogeological monitoring of piezometric levels and GF impacted areas is still on going and enlarged at the whole basin. The development of a methodology for GF hazard assessment is underway, as well as the deepening of vulnerability and exposure factors, in order to obtain a complete evaluation of GF risk as required by Italian and European legislation. After that, the following step is going to individuate the best mitigation measures, both of passive and active defence (e.g., waterproofing or lifting of ground level and floor, surficial groundwater draining system, well-point systems), also simulating their effectiveness and sustainability by using numerical groundwater flow modelling.

7

Scientific production

PhD Program's publications

- Allocca V., Coda S., De Vita P., Di Rienzo B., Ferrara L., Giarra A., Mangoni O., Stellato L., Trifuoggi M., Arienzo M. (2018). *Hydrogeological and hydrogeochemical study of a volcanic-sedimentary coastal aquifer in the archaeological site of Cumae (Phlegraean Fields, southern Italy)*. *Journal of Geochemical Exploration*, 185, 105-115.
- Coda S., Tessitore S., Di Martire D., Calcaterra D., De Vita P., Allocca V. (2019). *Coupled ground uplift and groundwater rebound in the Metropolitan City of Naples (southern Italy)*. *Journal of Hydrology*, 569, 470-482.
- Coda S., Confuorto P., De Vita P., Di Martire D., Allocca V. (2019). *Uplift evidences related to the recession of groundwater abstraction in a pyroclastic-alluvial aquifer of southern Italy*. *Geosciences*, 9(5), 215.
- Coda S., Tessitore S., Di Martire D., De Vita P., Allocca V. (2019). *Environmental effects of the groundwater rebound in the eastern plain of Naples*. *Rendiconti Online Società Geologica Italiana*, 48, 35-40.
- Allocca V., Coda S., De Vita P., Di Rienzo B., Ferrara L., Giarra A., Mangoni O., Stellato L., Trifuoggi M., Arienzo M. (2019). *Hydrogeological and hydrogeochemical monitoring in the Cumae archaeological site (Phlegraean Fields, southern Italy)*. *Rendiconti Online Società Geologica Italiana*, 47, 18-23.
- Stellato L, Coda S, Arienzo M, De Vita P, Di Rienzo B, D'Onofrio A, Ferrara L, Marzaioli F, Trifuoggi M, Allocca V., 2020. *Natural and Anthropogenic Groundwater Contamination in a Coastal Volcanic-Sedimentary Aquifer: The Case of the Archaeological Site of Cumae (Phlegraean Fields, Southern Italy)*. *Water*, 12(12):3463.
- Allocca V. Coda S., Calcaterra D., De Vita P., 20XX. *Groundwater rebound and flooding in the Naples' periurban area (Italy)*. *Journal of Flood Risk Management*, submitted in February 2020.
- Allocca V., Di Napoli M., Coda S., Carotenuto F., Calcaterra D., Di Martire D., De Vita P., 20XX. *A novel methodology for Groundwater Flooding Susceptibility assessment through*

Machine Learning techniques in a mixed-land use aquifer. Science of The Total Environment, submitted in February 2021.

Allocca V., Castellucci L., Coda S., Caromaldi M., De Vita P., Marzano E., 20XX. *Integrating hydrogeological and economic analyses of groundwater flooding in an urban aquifer: the plain of Naples (Italy) as a case study.* Journal of Cleaner Production, submitted in April 2021.

Other topics

Fusco F., Allocca V., Coda S., Cusano D., Tufano R., De Vita P., 2020. *Quantitative Assessment of Specific Vulnerability to Nitrate Pollution of Shallow Alluvial Aquifers by Process-Based and Empirical Approaches.* Water, 12(1):269.

Tufano R., Allocca V., Coda S., Cusano D., Fusco F., Nicodemo F., Pizzolante A., De Vita P., 2020. *Groundwater vulnerability of principal aquifers of the Campania region (southern Italy).* Journal of Maps, 16:2, 565-576.

Massarotti N, Mauro A, Normino G, Vanoli L, Verde C, Allocca V, Calcaterra D, Coda S, De Vita P, Forzano C, Palombo A, Cosenza P., 2020. *Innovative Solutions to Use Ground-Coupled Heat Pumps in Historical Buildings: A Test Case in the City of Napoli, Southern Italy.* Energies, 14(2):296.

Petrosino P., Angrisani A.C., Barra D., Donadio C., Aiello G., Allocca V., Coda S., De Vita P., Jicha B.R., Calcaterra D., 2021. *Multiproxy approach to urban geology of the historical center of Naples, Italy.* Quaternary International, 577, 147-165.

Participation to international and national conferences

- “European Geosciences Union General Assembly 2018”, Wien 8-13 April 2018, promoted by EGU (European Geosciences Union). *Geochemical and isotopic characterization of a volcanic-sedimentary coastal aquifer in the Archaeological Site of Cumae (Phlegraean Fields, southern Italy).*
- “XIII Convegno Nazionale GIT-SI”, Sarzana 11-13 June 2018, promoted by SGI (Società Geologica Italiana). *Environmental effects of the groundwater rebound in the eastern plain of Naples (Italy).*
- “6° Convegno Nazionale AIGA”, Courmayeur 27-29 June 2018, promoted by AIGA (Associazione Italiana di Geologia Applicata e Ambientale). 1) *Advances in hydrogeology and vulnerability of the Terminio karst aquifer (southern Italy).* 2) *Assessment of vulnerability to agricultural nitrate pollution of shallow alluvial aquifers by a numerical modelling approach. A case study from Campanian Plain (southern Italy).*

- “89° Congresso della Società Geologica Italiana”, Catania 12-14 September 2018, promoted by SGI (Società Geologica Italiana). *Groundwater rebound problems in urban and rural areas in the eastern plain of Naples.*
- “XXVII Congresso Divisione di Chimica Analitica”, Bologna 16-20 September 2018, promoted by SCI (Società Chimica Italiana). *Adsorption of fluoride onto tuff varieties of the Neapolitan area.*
- “4th National Meeting on Hydrogeology” – Flowpath, Milan 12-14 June 2019, promoted by IAH (International Association of Hydrogeologist). *A preliminary method for the assessment of groundwater flooding susceptibility in urban and rural areas.*
- “XI Convegno Nazionale dei Giovani Ricercatori in Geologia Applicata”, Matera 19-21 September 2019, promoted by AIGA (Associazione Italiana di Geologia Applicata e Ambientale). *Variation of groundwater contamination related to groundwater rebound in the eastern plain of Naples.*

References

- Abboud, J.M., Ryan, M.C., & Osborn, G.D., 2018. *Groundwater flooding in a river-connected alluvial aquifer*. Journal of Flood Risk Management, 11(4), e12334.
- Abdalla, C.A., Roach, B.A., Epp, D.J., 1992. *Valuing Environmental Groundwater Changes Using Averting Expenditures: An Application to Groundwater Contamination*. Land Econ. 68, 163-169.
- Abdallah, I.M. & Abd El-Tawab, N.A., 2013. *Effects of the groundwater on deterioration of the catacombs of Kom El-Shoqafa, Alexandria, Egypt*. E Conserv., 168-181.
- Abidin H.Z., Djaja R., Darmawan D., Hadi S., Akbar A., Rajiyowiryono H., Sudibyo Y., Meilano I., Kasuma M.A., Kahar J., Subarya C., 2001. *Land subsidence of Jakarta (Indonesia) and its geodetic monitoring system*. Natural Hazards 23, 365-387.
- Abu Al Naeem, M.F., Yusoff, I., Ng, T.F., Maity, J.P., Alias, Y., May, R., Alborsh, H., 2019. *A study on the impact of anthropogenic and geogenic factors on groundwater salinization and seawater intrusion in Gaza coastal aquifer, Palestine: An integrated multi-techniques approach*. J. Afr. Earth Sci., 156, 75-93.
- Abu-Rizaiza, O.S., 1999. *Threats from Groundwater Table Rise in Urban Areas in Developing Countries*. Water International 24, 46-52.
- Adams, R., Younger, P.L., 2001. *A Strategy For Modeling Ground Water Rebound In Abandoned Deep Mine Systems*. Groundwater 39, 249-261.
- Aicha, O., Abdessamad, G., Hassane, J.O., 2020. *Groundwater Flooding in Urban Areas: Occurrence process, Potential Impacts and The Role Of Remote Sensing And GIS Techniques In Preventing It*. In: 2020 IEEE International Conference of Moroccan Geomatics (Morgeo), 1-5.
- Aiuppa, A., Avino, R., Brusca, L., Caliro, S., Chiodini, G., D'Alessandro, W., Favara, R., Federico, C., Ginevra, W., Inguaggiato, S. et al., 2006. *Mineral control of arsenic content in thermal waters from volcano-hosted hydrothermal systems: Insights from island of Ischia and Phlegrean Fields (Campanian Volcanic Province, Italy)*. Chem. Geol., 229, 313-330.
- Aldiss D., Burke H., Chacksfield B., Bingley R., Teferle N., Williams S., Blackman D., Burren R., Press N., 2014. *Geological interpretation of current subsidence and uplift in the London area, UK, as shown by high precision satellite-based surveying*. Proceedings of the Geologists' Association, 125, 1-13.
- Alekperov, A.B., Agamirzayev, R.C., Alekperov, R.A., 2006. *Geoenvironmental Problems in Azerbaijan*. Urban Groundwater Management and Sustainability 39-58.
- Allen D.R., Mayuga M.N., 1969. *The mechanics of compaction and rebound, Wilmington Oil Field, Long Beach, California, U.S.A.*. Proceedings of the Tokyo Symposium on Land Subsidence 2, 410-423, International Association of Scientific Hydrology and UNESCO, September 1969, Tokyo.
- Allocca V. & Celico P., 2010. *Le risorse dell'acquifero vulcanico a Nord-Ovest del Somma-Vesuvio (Napoli): idrodinamica, qualità e quantità*. Proceedings of International Conference "Montagne di Fuoco - Rischi e Risorse in Aree Vulcaniche: Vesuvio ed Etna", 109-124, ISBN 88-6026-118-2.
- Allocca, V., Coda, S., Calcaterra, D., De Vita, P., 2021. *Groundwater rebound and flooding in the Naples' periurban area (Italy)*. Journal of Flood Risk Management, in press.
- Allocca V., Coda S., De Vita P., Di Rienzo B., Ferrara L., Giarra A., Mangoni O., Stellato L., Trifuoggi M., Arienzo M., 2018. *Hydrogeological and hydrogeochemical study of a volcanic-sedimentary coastal aquifer in the*

- archaeological site of Cumae (Phlegraean Fields, southern Italy). *Journal of Geochemical Exploration* 185, 105–115.
- Allocca V., Marzano E., Coda S., De Vita P., Iorio A., Viola R., 2017. *Groundwater resource mismanagement in the plain of Naples (southern Italy): a hydrological and socio economic analysis*. Proceedings of the 4th Water Research Conference “The Role of Water Technology Innovation in the Blue Economy”. 10-13 September 2017, Waterloo, Ontario, Canada.
- Allocca, V., Celico, F., Celico, P., De Vita, P., Fabbrocino, S., Mattia, S., Monacelli, G., Musilli, I., Piscopo, V., Scalise, A.R., Summa, G., Tranfaglia, G., 2007. *Illustrative Notes of the Hydrogeological Map of Southern Italy*. Istituto Poligrafico e Zecca dello Stato, 1-211 (2007), Rome.
- Allocca, V., Celico, P., 2008. *Scenari idrodinamici nella piana ad Oriente di Napoli (Italia) nell'ultimo secolo: cause e problematiche idrogeologiche connesse*. *Giornale di Geologia Applicata, Special Issue*, 9 (2), 175-198.
- Allocca, V., Coda, S., De Vita, P., Di Rienzo, B., Ferrara, L., Giarra, A., Mangoni, O., Stellato, L., Trifuoggi, M., Arienzo, M., 2018. *Hydrogeological and hydrogeochemical study of a volcanic-sedimentary coastal aquifer in the archaeological site of Cumae (Phlegraean Fields, southern Italy)*. *Journal of Geochemical Exploration*, 185, 105–115.
- Allocca, V., Coda, S., De Vita, P., Iorio, A., Viola, R., 2016. *Rising groundwater levels and impacts in urban and semirural area around Naples (southern Italy)*. *Rend. Online Soc. Geol. It.*, 41 (2016), 14-17.
- Allocca, V., Manna, F., De Vita, P., 2014. *Estimating annual groundwater recharge coefficient for karst aquifers of the southern Apennines (Italy)*. *Hydrol. Earth Syst. Sci.*, 18, 803–817.
- Allouche, O., Tsoar, A., Kadmon, R., 2006. *Assessing the accuracy of species distribution models: prevalence, kappa and the true skill statistic (TSS)*. *Journal of Applied Ecology* 43, 1223–1232.
- Al-Rashed, M.F., Sherif, M.M., 2001. *Hydrogeological aspects of groundwater drainage of the urban areas in Kuwait City*. *Hydrological Processes* 15, 777–795.
- Al-Sefry, S.A., Şen, Z., 2006. *Groundwater Rise Problem and Risk Evaluation in Major Cities of Arid Lands – Jeddah Case in Kingdom of Saudi Arabia*. *Water Resour Manage* 20, 91–108.
- Amin, A., Bankher, K., 1997. *Causes of land subsidence in the Kingdom of Saudi Arabia*. *Nat. Hazards*, 16(1), 57-63.
- Amoruso A., Crescentini L., Martino S., Petitta M., Tallini M., 2014. *Correlation between groundwater flow and deformation in the fractured carbonate Gran Sasso aquifer (INFN underground laboratories, central Italy)*. *Water Resour. Res.*, 50, 4858–4876.
- Arabameri, A., Chen, W., Lombardo, L., Blaschke, T., Tien Bui, D., 2020. *Hybrid Computational Intelligence Models for Improvement Gully Erosion Assessment*. *Remote Sensing* 12, 140.
- Araújo, M.B., New, M., 2007. *Ensemble forecasting of species distributions*. *Trends in Ecology & Evolution* 22, 42–47.
- Aravena, R., Evans, M.L., Cherry, J.A., 1993. *Stable Isotopes of Oxygen and Nitrogen in Source Identification of Nitrate from Septic Systems*. *Groundwater*, 31, 180–186.
- Arnone, E., Francipane, A., Scarbaci, A., Puglisi, C., Noto, L.V., 2016. *Effect of raster resolution and polygon-conversion algorithm on landslide susceptibility mapping*. *Environmental Modelling & Software* 84, 467–481.
- Arora, A., Arabameri, A., Pandey, M., Siddiqui, M.A., Shukla, U.K., Bui, D.T., Mishra, V.N., Bhardwaj, A., 2021. *Optimization of state-of-the-art fuzzy-metaheuristic ANFIS-based machine learning models for flood*

- susceptibility prediction mapping in the Middle Ganga Plain, India. *Science of The Total Environment* 750, 141565.
- Attard, G., Winiarski, T., Rossier, Y., Eisenlohr, L., 2016. *Review: Impact of underground structures on the flow of urban groundwater*. *Hydrogeol Journal*, 24, 5–19.
- Baek, K.-W., Song, S.-H., Kang, S.-H., Rhee, Y.-W., Lee, C.-S., Lee, B.-J., Hudson, S., Hwang, T.-S., 2007. *Adsorption Kinetics of Boron by Anion Exchange Resin in Packed Column Bed*. *J. Ind. Eng. Chem.*, 13, 452–456.
- Bartik, T.J., 1988. *Evaluating the Benefits of Non-marginal Reductions in Pollution Using Information on Defensive Expenditures*. *Journal of Environ. Econ. Manag.* 15, 111–127.
- Barzegar, R., Moghaddam, A.A., Deo, R., Fijani, E., Tziritis, E., 2018. *Mapping groundwater contamination risk of multiple aquifers using multi-model ensemble of machine learning algorithms*. *Science of The Total Environment* 621, 697–712.
- Basin Authority of the North-Western Campania region (2004). *Il contributo al Piano di Tutela delle Acque della Regione Campania*, Grafica Montese snc. ed. Napoli.
- Bazzoffi, P., and Nieddu, S., 2011. *Effects of waterlogging on the soil structure of some Italian soils in relation to the GAEC cross-compliance standard Maintenance of farm channel networks and field convexity*. *Italian Journal of Agronomy* 2011, 6(s1):e9.
- Béjar-Pizarro M., Guardiola-Albert C., García-Cárdenas R.P., Herrera G., Barra A., López Molina A., Tessitore S., Staller A., Ortega-Becerril J.A., García-García R.P., 2016. *Interpolation of GPS and geological data using InSAR deformation maps: method and application to land subsidence in the alto guadalentin aquifer (SE Spain)*. *Remote Sens.*, 8, 965-982.
- Belloni, P., Cavaioli, M., Ingraio, G., Mancini, C., Notaro, M., Santaroni, P., Torri, G., Vasselli, R., 1995. *Optimization and comparison of three different methods for the determination of Rn-222 in water*. *Sci. Total Environ.*, 173–174, 61–67.
- Bellucci, F., 1994. *Nuove conoscenze stratigrafiche sui depositi vulcanici del sottosuolo del settore meridionale della Piana Campana*. *Boll. Soc. Geol. It.* 113, 395–420.
- Bellucci, F., 1998. *Nuove conoscenze stratigrafiche sui depositi effusivi ed esplosivi nel sottosuolo dell'area del Somma-Vesuvio*. *Boll. Soc. Geol. It.* 117, 385–405.
- Bellucci, F., Corniello, A., De Riso, R., Russo, D., 1990. *Idrogeologia della Piana a NE di Napoli*. *Mem. Soc. Geol. It* 45, 339–349.
- Beretta, G.P., Avanzini, M., Pagotto, A., 2004. *Managing groundwater rise: Experimental results and modelling of water pumping from a quarry lake in Milan urban area (Italy)*. *Environmental Geology* 45, 600–608.
- Bianco F., Castellano M., Milano G., Ventura G., Vilardo G., 1998. *The Somma-Vesuvius stress field induced by regional tectonics: evidences from seismological and mesostructural data*. *Journal of Volcanology and Geothermal Research*, 82, 199-218.
- Biot M. A., 1941. *General theory of three dimensional consolidation*. *Journal of Applied Physics*, 12(2), 155-164.
- Bitelli, G., Bonsignore, F., Carbognin, L., Ferretti, A., Strozzi, T., Teatini, P., Tosi, L., Vittuari, L., 2010. *Radar interferometry-based mapping of the present land subsidence along the low-lying northern Adriatic coast of Italy*. *Land Subsidence, Associated Hazards and the Role of Natural Resources Development, Proceedings of EISOLS* 279–286.

- Blower, T., 1987. *Potential consequences for surface structures of rising groundwater levels beneath London*. Structural Engineer Part A, 234–5.
- Bob, M., Rahman, N., Elamin, A., Taher, S., 2016. *Rising Groundwater Levels Problem in Urban Areas: A Case Study from the Central Area of Madinah City, Saudi Arabia*. Arab J Sci Eng 41, 1461–1472.
- Bonano M., Manunta M., Marsella M., Lanari R., 2012. *Long-term ERS/ENVISAT deformation time-series generation at full spatial resolution via the extended SBAS technique*. International Journal of Remote Sensing, 33(15), 4756–4783.
- Bonì, R., Bosino, A., Meisina, C., Novellino, A., Bateson, L., McCormack, H., 2018. *A methodology to detect and characterize uplift phenomena in urban areas using Sentinel-1 data*. Remote Sens-Basel, 10(4), 607.
- Boni R., Cigna F., Bricker S., Meisina C., McCormack H., 2016. *Characterization of hydraulic head changes and aquifer properties in the London Basin using Persistent Scatterer Interferometry ground motion data*. J. Hydrol., 540, 835–849.
- Brassington, F.C., & Rushton, K.R., 1987. *A rising water table in central Liverpool*. Quarterly Journal of Engineering Geology and Hydrogeology, 20(2), 151–158.
- Braun, E. & UNEP The Woods Hole Research Centre, 2007. *Reactive Nitrogen in the Environment: Too Much or Too Little of a Good Thing*; UNEP/Earthprint: Paris, France.
- Bravi, S., Fuscaldo, M., Guarino, P.M., Schiattarella, M., 1996. *Evoluzione sedimentaria olocenica dell'area dell'antico porto di Cumae (Campi Flegrei)*. In: *Variazioni Climatico-Ambientali ed Impatto Sull'uomo Nell'area Circum-Mediterranea Durante L'olocene*. Territorio Storico ed Ambiente; EdiPuglia: Bari, Italy, pp. 23–64.
- Bruno P. P. G., Cippitelli G., Rapolla A., 1998. *Seismic study of the Mesozoic carbonate basement around Mt. Somma-Vesuvius, Italy*. Journal of Volcanology and Geothermal Research, 84, 311–322.
- Bruno P. P. G., Rapolla A., Di Fiore V., 1998. *Structural setting of the Bay of Naples (Italy) seismic reflection data: implications for Campanian volcanism*. Tectonophysics, 372, 193–213.
- Burnham, K.P. & Anderson, D.R., 2002. *A practical information-theoretic approach*, 2nd ed, Model selection and multimodel inference. Springer, New York, 2.
- Caliro, S., Chiodini, G., Avino, R., Minopoli, C., Bocchino, B., 2011. *Long time-series of chemical and isotopic compositions of Vesuvius fumaroles: Evidence for deep and shallow processes*. Ann. Geophys., 54.
- Cama, M., Lombardo, L., Conoscenti, C., Rotigliano, E., 2017. *Improving transferability strategies for debris flow susceptibility assessment: Application to the Saponara and Itala catchments (Messina, Italy)*. Geomorphology 288, 52–65.
- Capano, M., Rescigno, C., Sirleto, R., Passariello, I., Marzaioli, F., D'Onofrio, A., Terrasi, F., 2015. *AMS 14C dating at CIRCE: The Major Temple in Cumae (NA–Italy)*. Nucl. Instrum. Methods Phys. Res. Sect. B Beam Interact. Mater. Atoms, 361, 654–658.
- Caputo, P., Morichi, R., Paone, R., 2010. *Cuma e il Suo Parco Archeologico. Un Territorio E le Sue Testimonianze*; Scienze e Lettere; Bardi Ed.: Rome, Italy.
- Caputo, V., Navarro, A., Storia, V., Tarantino, O., 2000. *Le paludi della "Civitas Neapolis": l'opera della bonifica nella trasformazione idrogeologica-urbanistica-antropica*, Associazione Onlus Casali. Napoli.
- Carminati, E. & Martinelli, G., 2002. *Subsidence rates in the Po Plain, northern Italy: the relative impact of natural and anthropogenic causation*. Eng. Geol., 66(3–4), 241–255.

- Carotenuto, F., Di Febbraro, M., Mondanaro, A., Castiglione, S., Serio, C., Melchionna, M., Rook, L., Raia, P., 2020. MInOSSE: A new method to reconstruct geographic ranges of fossil species. *Methods Ecol Evol* 11, 1121–1132.
- Carreira, P.M., Marques, J.M., Nunes, D., 2014. Source of groundwater salinity in coastline aquifers based on environmental isotopes (Portugal): Natural vs. human interference. A review and reinterpretation. *Appl. Geochem.*, 41, 163–175.
- Cartwright, I., Weaver, T., Tweed, S., Ahearne, D., Cooper, M., Czapnik, C., Tranter, J., 2000. O, H, C isotope geochemistry of carbonated mineral springs in central Victoria, Australia: Sources of gas and water–rock interaction during dying basaltic volcanism. *J. Geochem. Explor.*, 69–70, 257–261.
- Celico, F., Esposito, L., & Mancuso, M., 2001. *Complessità idrodinamica e idrochimica dell'area urbana di Napoli: scenari interpretativi*. *Geologia Tecnica & Ambientale*, 2 (2001), 35-54, Roma
- Celico, P., Dall'Aglio, M., Ghiara, M.R., Stanzione, D., Brondi, M., Prosperi, M., 1992. Geochemical monitoring of the thermal fluids in the Phlegraean Fields from 1970 to 1990. *Boll. Soc. Geol. Ital.*, 111, 409–422.
- Celico P., Stanzione D., Esposito L., Ghiara M. R., Piscopo V., Caliro S., La Gioia, P., 1998. *Caratterizzazione idrogeologica e idrogeochimica dell'area vesuviana*. *Bollettino della Società geologica italiana*, 117(1), 3-20.
- Celico, F., Celico, P., Esposito, L., Guadagno, F., Habetswallner, F.M.R., 1995. *Sull'evoluzione idrogeologica dell'area del Sebeto (Campania)*. *Geologia Applicata e Idrogeologia*, 30, 567–582.
- Celico, P., 1983. *Idrogeologia dei massicci carbonatici, delle piane quaternarie e delle aree vulcaniche dell'Italia centro-meridionale: Marche e Lazio meridionali, Abruzzo, Molise e Campania*, Quaderni della Cassa per il Mezzogiorno, 4/2, 1-225, Roma.
- Celico, P., De Gennaro, M., Esposito, L., Mastrangelo, E., 1994. *La falda ad oriente della città di Napoli: idrodinamica e qualità delle acque*. *Geologica Romana*, 30, 663–670.
- Celico, P., De Paola, P., 1992. *La falda dell'area napoletana: ipotesi sui meccanismi naturali di protezione e sulle modalità di inquinamento*. *Atti Giornata di Studio "Acque per Uso Potabile"; CI ESSE I Centro Scientifico Internazionale: Milan, Italy* 387C–412C.
- Celico, P., Esposito, L., Guadagno, F.M., 1997. *Sulla qualità delle acque sotterranee nell'acquifero del settore orientale della Piana Campana*. *Geologia Tecnica e Ambientale*, 4/97, 17-27, Roma.
- Champ P.A., Boyle, K.J., Brown, T.C. (Eds), 2017. *A Primer on Nonmarket Valuation*. Springer, Netherlands, 576.
- Chatton, E., Aquilina, L., Pételet-Giraud, E., Cary, L., Bertrand, G., Labasque, T., Hirata, R., Martins, V., Montenegro, S., Vergnaud, V., et al, 2016. *Glacial recharge, salinisation and anthropogenic contamination in the coastal aquifers of Recife (Brazil)*. *Sci. Total Environ.*, 569–570, 1114–1125.
- Chaudhary, M.T.A., 2012. *Implications of rising groundwater level on structural integrity of underground structures - investigations and retrofit of a large building complex*. *Structural Survey*, 30 Issue 2, 111-129.
- Chaussard E., Milillo P., Bürgmann R., Perissin D., Fielding E. J., Baker B., 2017. *Remote Sensing of Ground Deformation for Monitoring Groundwater Management Practices: Application to the Santa Clara Valley During the 2012–2015 California Drought*. *Journal of Geophysical Research: Solid Earth*, 122 (10), 8566-8582.
- Chebanov, O., Zadniprovska, A., 2011. *Zoning groundwater flooding risks in the cities and urban agglomeration areas of Ukraine*. In: *Proceedings of Symposium H03 Held during IUGG2011 in Melbourne, Australia*. Presented at the Risk in Water Resources Management, p. 7.

- Chen, C.-T., Hu, J.-C., Lu, C.-Y., Lee, J.-C., Chan, Y.-C., 2007. *Thirty-year land elevation change from subsidence to uplift following the termination of groundwater pumping and its geological implications in the Metropolitan Taipei Basin, Northern Taiwan*. *Engineering Geology*, 95, 30–47.
- Chini, M., Bignami, C., Stramondo, S., Pierdicca, N., 2008. *Uplift and subsidence due to the 26 December 2004 Indonesian earthquake detected by SAR data*. *Int. J. Remote Sens.*, 29(13), 3891–3910.
- Choubin, B., Moradi, E., Golshan, M., Adamowski, J., Sajedi-Hosseini, F., Mosavi, A., 2019. *An ensemble prediction of flood susceptibility using multivariate discriminant analysis, classification and regression trees, and support vector machines*. *Science of The Total Environment* 651, 2087–2096.
- Cigna, F., Osmanoglu, B., Cabral-Cano, E., Dixon, T. H., Ávila-Olivera, J.A., Garduño-Monroy, V.H., DeMets, C. & Wdowinski, S. (2012). *Monitoring land subsidence and its induced geological hazard with Synthetic Aperture Radar interferometry: A case study in Morelia, Mexico*. *Remote Sensing of Environment*, 117, 146–61.
- Cinque A., Ascione A., Caiazzo C., 2000. *Distribuzione spazio-temporale e caratterizzazione della fogliazione quaternaria in Appennino meridionale*. In: *Le ricerche del GNDT nel campo della pericolosità sismica* (F. Galadini, C. Meletti and A. Rebez, eds) CNR – Gruppo Nazionale per la Difesa dai Terremoti – Roma, 203–218.
- Cinque, A., Irollo, G., Romano, P., Ruello, M.R., Amato, L., Giampaola, D., 2011. *Ground movements and sea level changes in urban areas: 5000 years of geological and archaeological record from Naples (Southern Italy)*. *Quaternary International*, 232, 45–55.
- Città Metropolitana di Napoli—Telerilevamento Mediante Lidar. Available online: <http://sit.cittametropolitana.na.it/lidar.html> (accessed on 26 October 2020).
- Clark, I.D. & Fritz, P., 1997. *Environmental Isotopes in Hydrogeology*; Lewis Publishers: Boca Raton, NY, USA.
- Cobby, D., Morris, S., Parkes, A., & Robinson, V., 2009. *Groundwater flood risk management: Advances towards meeting the requirements of the EU floods directive*. *Journal of Flood Risk Management*, 2(2), 111–119.
- Coda, S., Confuorto, P., De Vita, P., Di Martire, D., Allocca, V., 2019b. *Uplift Evidences Related to the Recession of Groundwater Abstraction in a Pyroclastic-Alluvial Aquifer of Southern Italy*. *Geosciences* 9, 215.
- Coda, S., De Tommaso, G., Iuliano, M., Jantáková, N., Villani, R., Allocca, V., 2019d. *Variation of groundwater contamination related to groundwater rebound in the eastern plain of Naples*. *Proceedings of the XI Convegno Nazionale Dei Giovani Ricercatori in Geologia Applicata*. 19–21 September 2019, Matera (Italy).
- Coda, S., Tessitore, S., Di Martire, D., Calcaterra, D., De Vita, P., Allocca, V., 2019a. *Coupled ground uplift and groundwater rebound in the metropolitan city of Naples (southern Italy)*. *Journal of Hydrology*, 569, 470–482.
- Coda, S., Tessitore, S., Di Martire, D., De Vita, P., Allocca, V., 2019c. *Environmental effects of the groundwater rebound in the eastern plain of Naples (Italy)*. *Rendiconti Online Soc. Geol. It.*, 48 (2019), 35–40.
- Colombani, N., Osti, A., Volta, G., Mastrocicco, M., 2016. *Impact of Climate Change on Salinization of Coastal Water Resources*. *Water Resour. Manag.*, 30, 2483–2496.
- Coetsee, B.W.T., Robertson, M.P., Erasmus, B.F.N., Rensburg, B.J.V., Thuiller, W., 2009. *Ensemble models predict Important Bird Areas in southern Africa will become less effective for conserving endemic birds under climate change*. *Global Ecology and Biogeography* 18, 701–710.

- Colombo L., Gattinoni P., Scesi L., 2017. *Influence of underground structures and infrastructures on the groundwater level in the urban area of Milan, Italy*. International Journal of Sustainable Development and Planning, 12 (1), 176-184.
- Coplen, T.B., Herczeg, A.L., Barnes, C., 2000. *Isotope Engineering—Using Stable Isotopes of the Water Molecule to Solve Practical Problems*. In: Environmental Tracers in Subsurface Hydrology; Cook, P.G., Herczeg, A.L., Eds.; Springer: Boston, MA, USA; pp. 79–110.
- Corine Land Cover, 2012. <https://land.copernicus.eu/pan-european/corine-land-cover/clc-2012>.
- Corniello, A., Ducci, D., Catapano, O., Monti, G.M., 2003. *Variazioni piezometriche nella zona orientale della città di Napoli*. Quaderni Geologia Applicata, 10, 43–57.
- Corsini, A., Mulas, M., 2017. *Use of ROC curves for early warning of landslide displacement rates in response to precipitation (Piagneto landslide, Northern Apennines, Italy)*. Landslides 14, 1241–1252.
- Costabile S., 2010. *The national geoportal: the not-ordinary plan of environmental remote sensing* (In Italian). GEOmedia 14 (3).
- Costantini, M.; Falco, S.; Malvarosa, F.; Minati, F., 2008. *A new method for identification and analysis of persistent scatterers in series of SAR images*. In IGARSS 2008-2008 IEEE International Geoscience and Remote Sensing Symposium, IEEE; Volume 2, pp. II-449.
- Costanzo, M.R., Nunziata, C., 2014. *Lithospheric Vs models in the Campanian Plain (Italy) by integrating Rayleigh wave dispersion data from noise cross-correlation functions and earthquake recordings*. Phys. Earth. Planet., 234, 45-59.
- Cox, M.E. & Thomas, D.M., 1979. *Cl/Mg ratio of Hawaiian groundwaters as a regional geothermal indicator*. Geotherm. Resour. Counc. Trans., 3, 145–148.
- Custodio, E., 2010. *Coastal aquifers of Europe: An overview*. Hydrogeol. J., 18, 269–280.
- Custodio, E., 1987. *Effects of human activities on salt–fresh water relationships in coastal aquifers*. In: Groundwater Problems in Coastal Areas; Custodio, E., Bruggeman, G.A., Eds.; Studies and Reports in Hydrology; UNESCO: Paris, France.
- D’Amore, F., Fancelli, R., Panichi, C., 1987. *Stable isotope study of reinjection processes in the Larderello geothermal field*. Geochim. Cosmochim. Acta, 51, 857–867.
- Dansgaard, W., 1964. *Stable isotopes in precipitation*. Tellus, 16, 436–468.
- Dati, F., 2006. *Emungimenti e subsidenza nell’area nord-orientale di Napoli*. Master's degree thesis, Università degli Studi di Napoli Federico II, Napoli.
- de Beer, H. & Matthiesen, H., 2008. *Groundwater monitoring and modelling from an archaeological perspective: Possibilities and challenges*. In: Geology for Society; Slagstad, T., Ed.; Geological Survey of Norway Special Publication; Geological Survey of Norway: Trondheim, Norway; pp. 67–81.
- De Caro, M., Crosta, G.B., Previati A., 2020. *Modelling the interference of underground structures with groundwater flow and remedial solutions in Milan*. Engineering Geology 272 (2020) 105652.
- De Giorgio, G., Chieco, M., Zuffianò, L.E., Limoni, P.P., Sottani, A., Pedron, R., Vettorello, L., Stellato, L., Di Rienzo, B., Polemio, M., 2018. *The Compatibility of Geothermal Power Plants with Groundwater Dependent Ecosystems: The Case of the Cesine Wetland (Southern Italy)*. Sustainability, 10, 303.
- De Vita, P., Allocca, V., Celico, F., Fabbrocino, S., Mattia, C., Monacelli, G., Musilli, I., Piscopo, V., Scalise, A.R., Summa, G., 2018. *Hydrogeology of continental southern Italy*. Journal of Maps 14, 230–241.

- De Vita, P., Allocca, V., Manna, F., Fabbrocino, S., 2012. *Coupled decadal variability of the North Atlantic Oscillation, regional rainfall and karst spring discharges in the Campania region (southern Italy)*. Hydrology and Earth System Sciences 16, 1389–1399.
- De Vivo, B., Rolandi, G., Gans, P.B., Calvert, A., Bohrsen, W.A., Spera, F.J., Belkin, H.E., 2001. *New constraints on the pyroclastic eruptive history of the Campanian volcanic Plain (Italy)*. Mineralogy and Petrology 73, 47–65.
- Dean, J.L., Sholley, M.G., 2006. *Groundwater basin recovery in urban areas and the implications for engineering projects*. In: Culshaw, M. G., Reeves, H. J., Jefferson, I. & Spink, T. W. (eds) Engineering Geology for Tomorrow's Cities. Geological Society, London, Engineering Geology Special Publications, 22.
- Di Martire, D., Paci, M., Confuorto, P., Costabile, S., Guastaferro, F., Verta, A., Calcaterra, D., 2017. *A nationwide system for landslide mapping and risk management in Italy: The second Not-ordinary Plan of Environmental Remote Sensing*. Int. J. Appl. Earth. Obs., 63, 143-157.
- Di Napoli, M., Di Martire, D., Bausilio, G., Calcaterra, D., Confuorto, P., Firpo, M., Pepe, G., Cevasco, A., 2021. *Rainfall-Induced Shallow Landslide Detachment, Transit and Runout Susceptibility Mapping by Integrating Machine Learning Techniques and GIS-Based Approaches*. Water 13, 488.
- Di Napoli, M., Carotenuto, F., Cevasco, A., Confuorto, P., Di Martire, D., Firpo, M., Pepe, G., Raso, E., Calcaterra, D., 2020a. *Machine learning ensemble modelling as a tool to improve landslide susceptibility mapping reliability*. Landslides 17, 1897–1914.
- Di Napoli, M., Marsiglia, P., Di Martire, D., Ramondini, M., Ullo, S.L., Calcaterra, D., 2020b. *Landslide Susceptibility Assessment of Wildfire Burnt Areas through Earth-Observation Techniques and a Machine Learning-Based Approach*. Remote Sensing 12, 2505.
- Dickey, D.A., Fuller, W.A., 1981. *Likelihood ratio statistics for autoregressive time series with a unit root*. Econometrica, 49, 1057-1072.
- Dickie, M., 2017. *Defensive Behaviour and Damage Costs Methods*. In: Champ P.A., Boyle K.J., Brown T.C. (Eds), A Primer on Nonmarket Valuation. Springer, Netherlands, 293-346.
- Dodangeh, E., Choubin, B., Eigdir, A.N., Nabipour, N., Panahi, M., Shamshirband, S., Mosavi, A., 2020. *Integrated machine learning methods with resampling algorithms for flood susceptibility prediction*. Science of The Total Environment 705, 135983.
- Donnelly, L.J., 2009. *A review of international cases of fault reactivation during mining, subsidence and fluid abstraction*. Q. J. Eng. Geol. Hydroge., 42, 73– 94.
- Dormann, C.F., Elith, J., Bacher, S., Buchmann, C., Carl, G., Carré, G., Marquéz, J.R.G., Gruber, B., Lafourcade, B., Leitão, P.J., Münkemüller, T., McClean, C., Osborne, P.E., Reineking, B., Schröder, B., Skidmore, A.K., Zurell, D., Lautenbach, S., 2013. *Collinearity: a review of methods to deal with it and a simulation study evaluating their performance*. Ecography 36, 27–46.
- Doulati, A.F., 2003. *Hydrogeological investigations of backfilled surface coal mine sites*. Doctor of Philosophy thesis, Faculty of Engineering, University of Wollongong, 2003. <https://ro.uow.edu.au/theses/1829>.
- Ducci, D., Del Gaudio, E., Sellerino, M., Stellato, L., Corniello, A., 2019. *Hydrochemical and isotopic analyses to identify groundwater nitrate contamination. The alluvial-pyroclastic aquifer of the Campanian plain (southern Italy)*. Geoinf. Ambient. Min., 156, 4–12.
- EEA, 2018. *Corine Land Cover (CLC) 2018, Version 20b2*. Release Date: 21-12-2018. European Environment Agency. <https://land.copernicus.eu/pan-european/corine-land-cover/clc2018>

- Eggleston, J., & Pope, J., 2013. *Land subsidence and relative sea-level rise in the southern Chesapeake Bay region*. US Geological Survey Circular 1392, 30.
- Elith, J., Graham, C.H., 2009. *Do They? How Do They? Why Do They Differ? On Finding Reasons for Differing Performances of Species Distribution Models*. *Ecography* 32, 66–77.
- Elith, J., Graham, C.H., Anderson, R.P., Dudík, M., Ferrier, S., Guisan, A., Hijmans, R.J., Huettmann, F., Leathwick, J.R., Lehmann, A., Li, J., Lohmann, L.G., Loiselle, B.A., Manion, G., Moritz, C., Nakamura, M., Nakazawa, Y., Overton, J.M.M., Peterson, A.T., Phillips, S.J., Richardson, K., Scachetti-Pereira, R., Schapire, R.E., Soberón, J., Williams, S., Wisz, M.S., Zimmermann, N.E., 2006. *Novel methods improve prediction of species' distributions from occurrence data*. *Ecography* 29, 129–151.
- Elith, J., Leathwick, J.R., 2009. *Species Distribution Models: Ecological Explanation and Prediction Across Space and Time*. *Annual Review of Ecology, Evolution, and Systematics* 40, 677–697.
- Elith, J., Phillips, S.J., Hastie, T., Dudík, M., Chee, Y.E., Yates, C.J., 2011. *A statistical explanation of MaxEnt for ecologists*. *Diversity and Distributions* 17, 43–57.
- Eppich, G.R., Wimpenny, J.B., Yin, Q.-Y., Esser, B.K., 2011. *California GAMA Special Study: Stable Isotopic Composition of Boron in Groundwater—Analytical Method Development—Tech. Rep. LLNL-TR-498360*; Lawrence Livermore National Laboratory: Livermore, CA, USA; p. 29.
- ESI, 2016. *The Role of Groundwater in Risk from Flooding in England: Methodologies, analysis and preliminary findings*. Bryan Lovell Meeting 2016: Water, hazards and risk: Managing uncertainty in a changing world. The Geological Society, 24-25 November 2016, London.
- Esposito, L., 1998. *Nuove conoscenze sulle caratteristiche idrogeochimiche della falda ad Oriente della città di Napoli (Campania)*. *Quaderni di Geologia Applicata*, 5 - 1/98, Pitagora Editrice, Bologna.
- Ezquerro P., Herrera G., Marchamalo M., Tomás R., Béjar-Pizarro M., Martínez R., 2014. *A quasi-elastic aquifer deformational behavior: Madrid aquifer case study*. *J Hydrol* 519:1192–1204.
- Ferguson, G. & Gleeson, T., 2012. *Vulnerability of coastal aquifers to groundwater use and climate change*. *Nat. Clim. Chang*, 2, 342–345.
- Ferretti A., Prati C., Rocca F., 2000. *Nonlinear Subsidence Rate Estimation Using Permanent Scatterers in Differential SAR Interferometry*. *IEEE Trans. Geoscience And Remote Sensing*, 38(5), 2202–2212.
- Fiaschi S., Tessitore S., Bonì R., Di Martire D., Achilli V., Borgstrom S., Ibrahim A., Floris M., Meisina C., Ramondini M., Calcaterra D., 2017. *From ERS-1/2 to Sentinel-1: two decades of subsidence monitored through A-DInSAR techniques in the Ravenna area (Italy)*. *GIScience & Remote Sensing*.
- Fiorelli, T., 1926. *Cenni sull'andamento della falda acquifera nel sottosuolo della zona tra Napoli e Pomigliano d'Arco in relazione colla costituzione geologica e la topografia e idrologia superficiale del territorio medesimo*. *Annali del Genio Civile*, Fascicolo VII, 613-626, Roma.
- Font-Capo, J., Pujades, E., Vázquez-Suñé, E., Carrera, J., Velasco, V., Montfort, D., 2015. *Assessment of the barrier effect caused by underground constructions on porous aquifers with low hydraulic gradient: A case study of the metro construction in Barcelona, Spain*. *Engineering Geology* 196, 238–250.
- Fourcade, Y., Engler, J.O., Rödder, D., Secondi, J., 2014. *Mapping Species Distributions with MAXENT Using a Geographically Biased Sample of Presence Data: A Performance Assessment of Methods for Correcting Sampling Bias*. *PLoS ONE* 9, e97122.
- Freeze, R.A., Cherry, J.A., 1979. *Groundwater*. Prentice-Hall, Englewood Cliffs, New Jersey.

- Fressard, M., Thiery, Y., Maquaire, O., 2014. *Which data for quantitative landslide susceptibility mapping at operational scale? Case study of the Pays d'Auge plateau hillslopes (Normandy, France)*. *Natural Hazards and Earth System Sciences* 14, 569–588.
- Froehlich, K., Gibson, J.J., Aggarwal, P.K., 2002. *Deuterium excess in precipitation and its climatological significance*. In: *Study of Environmental Change Using Isotope Techniques; C&S Paper Series; IAEA: Vienna, Austria*; pp. 54–65.
- Fürst, J., Bichler, A., Konecny, F., 2015. *Regional Frequency Analysis of Extreme Groundwater Levels*. *Groundwater* 53, 414–423.
- Fusco, F., Allocca, V., Coda, S., Cusano, D., Tufano, R., De Vita, P., 2020. *Quantitative Assessment of Specific Vulnerability to Nitrate Pollution of Shallow Alluvial Aquifers by Process-Based and Empirical Approaches*. *Water*, 2020, 12, 269.
- Fukada, T., Hiscock, K.M., Dennis, P.F., Grischek, T., 2003. *A dual isotope approach to identify denitrification in groundwater at a river-bank infiltration site*. *Water Res.*, 37, 3070–3078.
- Gallien, L., Douzet, R., Pratte, S., Zimmermann, N.E., Thuiller, W., 2012. *Invasive species distribution models – how violating the equilibrium assumption can create new insights*. *Global Ecology and Biogeography* 21, 1126–1136.
- Galloway, D. L., Jones, D. R., Ingebritsen, S. E., 1999. *Land subsidence in the United States*. US Geological Survey (Vol. 1182).
- Galloway D.L., Erkens G., Kuniandy E.L., Rowland J.C., 2016. *Land subsidence processes*. *Hydrogeol J.* 24, 547-550.
- Galloway D.L., Hoffmann J., 2007. *The application of satellite differential SAR interferometry-derived ground displacements in hydrogeology*. *Hydrogeol J* 15:133–154.
- Gambolati G., Teatini P., Baù D., Ferronato M., 2000. *Importance of poroelastic coupling in dynamically active aquifers of the Po river basin, Italy*. *Water Resources Research*, 36, No.9, 2443-2459.
- Gambolati G., Teatini P., Ferronato M., 2005. *Anthropogenic land subsidence*. In 720 Anderson, M.G., (Ed.), *The Encyclopedia of Hydrological Sciences*. John Wiley & Sons, London, 2443-2460.
- Gambolati, G., Giunta, G., Putti, M., Teatini, P., Tomasi, L., Betti, I., Morelli, M., Berlamont, J., De Backer, K., Decouttere, C., 1998. *Coastal evolution of the Upper Adriatic Sea due to sea level rise and natural and anthropic land subsidence*. In: Gambolati G. (eds) *CENAS. Water Science and Technology Library*, 28, 1-34. Springer, Dordrecht
- García-Gil, A., Vázquez-Suñé, E., Sánchez-Navarro, J.Á., Mateo Lázaro, J., Alcaraz, M., 2015. *The propagation of complex flood-induced head wavefronts through a heterogeneous alluvial aquifer and its applicability in groundwater flood risk management*. *Journal of Hydrology* 527, 402–419.
- Gat, J.R.; & Carmi, I., 1970. *Evolution of the isotopic composition of atmospheric waters in the Mediterranean Sea area*. *J. Geophys. Res.*, 75, 3039–3048.
- Gattinoni, P., Scesi, L., 2017. *The groundwater rise in the urban area of Milan (Italy) and its interactions with underground structures and infrastructures*. *Tunnelling and Underground Space Technology* 62, 103–114.
- Genereux, D.P., Wood, S.J., Pringle, C.M., 2002. *Chemical tracing of interbasin groundwater transfer in the lowland rainforest of Costa Rica*. *J. Hydrol.*, 258, 163–178.

- Geological Survey of Italy (SGI) database. Available online: <http://www.isprambiente.gov.it/en/databases/soil-and-territory>.
- George, D.J., 1992. *Rising groundwater: a problem of development in some urban areas of the Middle East*. In: McCall G.J.H., Laming D.J.C., Scott S.C. (eds), *Geohazards. Natural and man-made*. AGID Report Series (The Geosciences in International Development) Springer, Dordrecht, 171–182. ISBN 978-0-412-43930-8
- Giudici M., Foglia L., Parravicini G., Ponzini G., Sincich B., 2000. *A quasi three dimensional model of water flow in the subsurface of Milano (Italy): the stationary flow*. *Hydrol Earth Syst Sci*, 4:113–124.
- Gonfiantini, R., Fröhlich, K., Araguás-Araguás, L., Rozanski, K., 1998. *Isotopes in Groundwater Hydrology*. In: *Isotope Tracers in Catchment Hydrology*; Kendall, C., McDonnell, J.J., Eds.; Elsevier: Amsterdam, The Netherlands.
- González-Morán, T., Rodríguez, R., Cortes, S. A., 1999. *The Basin of Mexico and its metropolitan area: water abstraction and related environmental problems*. *J. S. Am. Earth Sci.*, 12(6), 607-613.
- Gotkowitz, M.B., Attig, J.W., & McDermott, T., 2014. *Groundwater flood of a river terrace in southwest Wisconsin, USA*. *Hydrogeology Journal*, 22(6), 1421–1432.
- Greswell, R.B., Lloyd, J.W., Lerner, D.N., & Knipe, C.V., 1994. *Rising groundwater in the Birmingham area*. In: *Groundwater Problems in Urban Areas*, Wilkinson, W.B. (ed.), Thomas Telford, London, 331–341.
- Griliches, Z., 1971. *Price Indexes and Quality Change*. Harvard University press, Cambridge, Massachusetts, 287.
- Guisan, A., Graham, C.H., Elith, J., Huettmann, F., 2007. *Sensitivity of predictive species distribution models to change in grain size*. *Diversity and Distributions* 13, 332–340.
- Guisan, A., Thuiller, W., Zimmermann, N.E., 2017. *Habitat Suitability and Distribution Models: with Applications in R*. Cambridge University Press.
- Guns, M., Vanacker, V., 2012. *Logistic regression applied to natural hazards: rare event logistic regression with replications*. *Natural Hazards and Earth System Sciences* 12, 1937–1947.
- Habel S., Fletcher C.H., Rotzoll K., El-Kadi A.I., 2017. *Development of a model to simulate groundwater inundation induced by sea-level rise and high tides in Honolulu, Hawaii*. *Water Research*, 114 (2017) 122-134.
- Hair, J.F., Black, W.C., Babin, B.J., Anderson, R.E., 2010. *Multivariate Data Analysis: A Global Perspective* (7th ed.). New Jersey: Pearson Education Inc.
- Hanley, J.A., McNeil, B.J., 1982. *The meaning and use of the area under a receiver operating characteristic (ROC) curve*. *Radiology* 143, 29–36.
- Hao, T., Elith, J., Guillera-Arroita, G., Lahoz-Monfort, J.J., 2019. *A review of evidence about use and performance of species distribution modelling ensembles like BIOMOD*. *Diversity and Distributions* 25, 839–852.
- Hayashi, T., Tokunaga, T., Aichi, M., Shimada, J., Taniguchi, M., 2009. *Effects of human activities and urbanization on groundwater environments: An example from the aquifer system of Tokyo and the surrounding area*. *Science of The Total Environment* 407, 3165–3172.
- Hecht, J.E., 2005. *National Environmental Accounting: Bridging the Gap Between Ecology and Economy*. Resources for the Future, Routledge, 272.
- Henton, M.P., 1981. *The problem of water table rebound after mining activity and its effect on ground and surface water quality*. *Studies in Environmental Science*. Elsevier, 17, 111-116.
- Herczeg, A.L. & Edmunds, W.M., 2000. *Inorganic Ions as Tracers*. In: *Environmental Tracers in Subsurface Hydrology*; Cook, P.G., Herczeg, A.L., Eds.; Springer: Boston, MA, USA; pp. 31–77.

- Hernández, M.A., González, N., 1997. *Impact of rising piezometric levels on Greater Buenos Aires due to partial changing of water services infrastructure*. Proceedings of the XXVII IAH Congress on Groundwater in the Urban Environment: Problems, Processes and Management. Nottingham/UK, 21-27 September 1997. John Chilton et al. (eds), Balkema, Rotterdam, Brookfield, 237–242.
- Herrera G., Fernández J.A., Tomás R., Cooksley G., Mulas J., 2009. *Advanced interpretation of subsidence in Murcia (SE Spain) using A-DInSAR data: modelling and validation*. Nat Hazards Earth Syst Sci, 9:647–661.
- Holden, J., West, L.J., Howard, A.J., Maxfield, E., Panter, I., Oxley, J., 2006. *Hydrological controls of in situ preservation of waterlogged archaeological deposits*. Earth Sci. Rev., 78, 59–83.
- Hoover, D.J., Odigie, K.O., Swarzenski, P.W., & Barnard P., 2017. *Sea-level rise and coastal groundwater inundation and shoaling at select sites in California, USA*. Journal of Hydrology: Regional Studies 11 (2017) 234–249.
- Hosseini, F.S., Choubin, B., Mosavi, A., Nabipour, N., Shamshirband, S., Darabi, H., Haghghi, A.T., 2020. *Flash-flood hazard assessment using ensembles and Bayesian-based machine learning models: Application of the simulated annealing feature selection method*. Science of The Total Environment 711, 135161.
- Howard, K.W.F., Israfilov, R.G., 2002. *Current Problems of Hydrogeology in Urban Areas, Urban Agglomerates and Industrial Centres*. NATO Science Series. 4, Earth and Environmental Sciences, 8, 1-500, Kluwer Academic Pub, Springer, Dordrecht.
- Hughes, A.G., Vounaki, T., Peach, D.W., Ireson, A.M., Jackson, C.R., Butler, A.P., Bloomfield, J.P., Finch, J., & Wheeler, H.S., 2011. *Flood risk from groundwater: Examples from a Chalk catchment in southern England: Flood risk from groundwater*. Journal of Flood Risk Management, 4(3), 143–155.
- IPCC, 2007. 2007: Climate Change 2007: The Physical Science Basis. Contribution of Working Group I to the Fourth Assessment Report of the Intergovernmental Panel on Climate Change; Solomon, S., Qin, D., Manning, M., Chen, Z., Marquis, M., Averyt, K.B., Tignor, M., Miller, H.L., Eds.; Cambridge University Press: Cambridge, UK; New York, NY, USA.
- Ishitsuka K., Fukushima Y., Tsuji T., Yamada Y., Matsuoka T., Giao P.H., 2014. *Natural surface rebound of the Bangkok plain and aquifer characterization by persistent scatterer interferometry*. Geochem. Geophys. Geosyst., 15, 965–974.
- Ishitsuka K., Matsuoka T., Nishimura T., Tsuji T., ElGharbawi T., 2017. *Ground uplift related to permeability enhancement following the 2011 Tohoku earthquake in the Kanto Plain, Japan*. Earth, Planets and Space, (2017) 69:81.
- ISPRA, 2019. Geological maps of Italy, scale 1:50.000, Sheets No. 446-447 and No. 448. Retrieved from <http://www.isprambiente.gov.it/Media/carg/campania.html>.
- Jacob T., Chéry J., Boudin F., Bayer R., 2010. *Monitoring deformation from hydrologic processes in a karst aquifer using long-baseline tiltmeters*. Water Resour. Res., 46, W09542.
- Jakovljević, V.V., Svirenko, L.P., Chebanov, O.J., Spirin, O.I., 2002. *Rising groundwater levels in North-Eastern Ukraine: hazardous trends in urban areas*. In: Current Problems of Hydrogeology in Urban Areas, Urban Agglomerates and Industrial Centres, Nato Science Series. Springer, Dordrecht, 221–241.
- Jenks, G.F., 1967. The data model concept in statistical mapping. Israel National Center Registry. International Yearbook of Cartography 7, International Cartographic Association. University of Ulm, ULMGermany 1967 186–190.

- Jerome Morrissey, P., McCormack, T., Naughton, O., Meredith Johnston, P., William Gill, L., 2020. *Modelling groundwater flooding in a lowland karst catchment*. Journal of Hydrology 580, 124361.
- Jiménez-Valverde, A., Lobo, J.M., Hortal, J., 2009. *The effect of prevalence and its interaction with sample size on the reliability of species distribution models*. COMMUNITY ECOLOGY 10, 196–205.
- Johnson, S.T., 1994. *Rising groundwater levels: engineering and environmental implications*. In: Groundwater Problems in Urban Areas, Wilkinson, W.B. (ed.), Thomas Telford, London, 285–298.
- Julínek, T., Duchan, D., & Říha, J., 2020. *Mapping of uplift hazard due to rising groundwater level during floods*. Journal of Flood Risk Management, n/a(n/a), e12601.
- Karolytè, R., Serno, S., Johnson, G., Gilfillan, S.M.V., 2017. *The influence of oxygen isotope exchange between CO₂ and H₂O in natural CO₂-rich spring waters: Implications for geothermometry*. Appl. Geochem., 84, 173–186.
- Kendall, C., 1998. *Tracing Nitrogen Sources and Cycling in Catchments*. In: Isotope Tracers in Catchment Hydrology; Kendall, C., McDonnell, J.J., Eds.; Elsevier: Amsterdam, The Netherlands; pp. 519–576.
- Kim, Y., Lee, K.-S., Koh, D.-C., Lee, D.-H., Lee, S.-G., Park, W.-B., Koh, G.-W., Woo, N.-C., 2003. *Hydrogeochemical and isotopic evidence of groundwater salinization in a coastal aquifer: A case study in Jeju volcanic island, Korea*. J. Hydrol., 270, 282–294.
- King N. E., Argus D., Langbein J., Agnew D. C., Bawden G., Dollar R. S., Liu Z., Galloway D., Reichard E., Yong A., Webb F. H., Bock Y., Stark K., Barseghian D., 2007. *Space geodetic observation of expansion of the San Gabriel Valley, California, aquifer system, during heavy rainfall in winter 2004–2005*. J. Geophys. Res., 112, B03409.
- Kitsiou, D. & Karydis, M., 2011. *Coastal marine eutrophication assessment: A review on data analysis*. Environ. Int., 37, 778–801.
- Knoll, L., Breuer, L., Bach, M., 2019. *Large scale prediction of groundwater nitrate concentrations from spatial data using machine learning*. Science of The Total Environment 668, 1317–1327.
- Korkmaz, S., Ledoux, E., Önder, H., 2009. *Application of the coupled model to the Somme river basin*. Journal of Hydrology 366, 21–34.
- Koundouri, P., 2004. *Current issues in the economics of groundwater resource management*. J. Econ. Surv., 18(5), 703–740.
- Koundouri, P., Roseta-Palma, C., Englezos, N., 2017. *Out of Sight, Not Out of Mind: Developments in Economic Models of Groundwater Management*. Int. Rev. Environ. Resour. Econ., 11 (1), 55–96.
- Kreibich, H., Thielen, A.H., 2008. *Assessment of damage caused by high groundwater inundation*. Water Resources Research, 44, Issue 9, W09409.
- Kreibich, H., Thielen, A.H., 2009. *Coping with floods in the city of Dresden, Germany*. Natural Hazards 51, 423.
- Kreyns, P., Geng, X., Michael, H.A., 2020. *The influence of connected heterogeneity on groundwater flow and salinity distributions in coastal volcanic aquifers*. J. Hydrol., 586, 124863.
- Kusaka, T., Sreng, S., Tanaka, H., Sugiyama, H., Ito, T., Kobayashi, K., 2016. *Experimental study on influence of ground rebound on tunnels caused by groundwater restoration*. Japanese Geotechnical Society Special Publication 2, Issue 45, 1578–1582.
- La Licata, I., Colombo, L., Francani, V., Alberti, L., 2018. *Hydrogeological Study of the Glacial-Fluvioglacial Territory of Grandate (Como, Italy) and Stochastic Modeling of Groundwater Rising*. Applied Sciences 2018, 8, 1456.

- Lambeck, K., Anzidei, M., Antonioli, F., Benini, A., Esposito, A., 2004. *Sea level in Roman time in the Central Mediterranean and implications for recent change*. Earth and Planetary Science Letters 224, 563–575.
- Lamé, A., 2013. *Modélisation hydrogéologique des aquifères de Paris et impacts des aménagements du sous-sol sur les écoulements souterrains* [PhD Thesis, Ecole Nationale Supérieure des Mines de Paris]. pastel-00973861.
- Lanari R., De Natale G., Berardino P., Sansosti E., Ricciardi G.P., Borgstrom S., Capuano P., Pingue P., Troise C., 2002. *Evidence for a peculiar style of ground deformation inferred at Vesuvius volcano*. Geophysical Research Letters, 29, No., 9, 1292.
- Langelier, W.F. & Ludwig, H.F., 1942. *Graphical Methods for Indicating the Mineral Character of Natural Waters*. J. Am. Water Work. Assoc., 34, 335–352.
- Le Mouélic S., Raucoules D., Carnec C., King C., 2002. *A ground uplift in the city of Paris (France) detected by satellite radar interferometry*. Geophysical Research Letters, 29, No. 17, 1853.
- Lin, J.K., 1990. *Nitrosamines as potential environmental carcinogens in man*. Clin. Biochem., 23, 67–71.
- Liu, M., Guo, Q., Wu, G., Guo, W., She, W., Yan, W., 2019. *Boron geochemistry of the geothermal waters from two typical hydrothermal systems in Southern Tibet (China): Daggyai and Quzhuomu*. Geothermics, 82, 190–202.
- Lofgren, B. E., Klausning, R. L., 1969. *Land subsidence due to ground-water withdrawal, Tulare-Wasco area, California*. US Government Printing Office (Vol. 437).
- Lomba, A., Pellissier, L., Randin, C., Vicente, J., Moreira, F., Honrado, J., Guisan, A., 2010. *Overcoming the rare species modelling paradox: A novel hierarchical framework applied to an Iberian endemic plant*. Biological Conservation 143, 2647–2657.
- Lombardo, L., Bachofer, F., Cama, M., Märker, M., Rotigliano, E., 2016. *Exploiting Maximum Entropy method and ASTER data for assessing debris flow and debris slide susceptibility for the Giampileri catchment (north-eastern Sicily, Italy)*. Earth Surface Processes and Landforms 41, 1776–1789.
- MacDonald, A.M., Lapworth, D.J., Hughes, A.G., Auton, C.A., Maurice, L., Finlayson, A., Gooddy, D.C., 2014. *Groundwater, flooding and hydrological functioning in the Findhorn floodplain, Scotland*. Hydrology Research 45, 755–773.
- Macdonald, D., Dixon, A., Newell, A., Hallaways, A., 2012. *Groundwater flooding within an urbanised flood plain*. Journal of Flood Risk Management 5, 68–80.
- Macdonald, D.M.J., Bloomfield, J.P., Hughes, A.G., Macdonald, A.M., Adams, B., McKenzie, A.A., 2008. *Improving the understanding of the risk from groundwater flooding in the UK*, in: FLOODrisk 2008, European Conference on Flood Risk Management, Oxford, UK. CRC Press, The Netherlands.
- Madonia, P., Federico, C., Favara, R., 2014. *Isotopic composition of rain- and groundwater at Mt. Vesuvius: Environmental and volcanological implications*. Environ. Earth Sci., 72, 2009–2018.
- Mancini, C.P., Lollai, S., Volpi, E., & Fiori, A., 2020. *Flood Modeling and Groundwater Flooding in Urbanized Reclamation Areas: The Case of Rome (Italy)*. Water, 12(7), 2030.
- Marinos, P., Kavvas, M., 1997. *Rise of the groundwater table when the flow is obstructed by tunnels*. In: Groundwater in the Urban Environment: Problems, Processes and Management. Balkema, Rotterdam, pp. 49–54.
- Mariotti, A., Landreau, A., Simon, B., 1988. *¹⁵N isotope biogeochemistry and natural denitrification process in groundwater: Application to the chalk aquifer of northern France*. Geochim. Cosmochim. Acta, 52, 1869–1878

- Martinelli, G., Dadomo, A., De Luca, D.A., Mazzola, M., Lasagna, M., Pennisi, M., Pilla, G., Sacchi, E., Saccon, P., 2018. Nitrate sources, accumulation and reduction in groundwater from Northern Italy: Insights provided by a nitrate and boron isotopic database. *Appl. Geochem.*, 91, 23–35.
- Marturano A., Aiello G., Barra D., 2013. *Somma-Vesuvius ground deformation over the last glacial cycle*. *Journal of Volcanology and Geothermal Research*, 255, 90-97.
- Mateos R.M., Ezquerro P., Luque-Espinar J. A., Béjar-Pizarro M., Notti D., Azañón J. M., Montserrat O., Herrera G., Fernández-Chacón F., Peinado T., Pedro Galve J., Pérez-Peña V., Fernández-Merodo J. A., Jiménez J., 2017. *Multiband PSInSAR and long-period monitoring of land subsidence in a strategic detrital aquifer (Vega de Granada, SE Spain): An approach to support management decisions*. *J. Hydrology*, 553, 71-87.
- Mazzeo, G., 2009. *Naples*. *Cities* 26, 363–376.
- McKenzie, A.A., Rutter, H.K., Hulbert, A.G., 2010. *The use of elevation models to predict areas at risk of groundwater flooding*. Geological Society, London, Special Publications 345, 75.
- McPherson, J.M., Jetz, W., Rogers, D.J., 2004. *The effects of species' range sizes on the accuracy of distribution models: ecological phenomenon or statistical artefact?* *Journal of Applied Ecology* 41, 811–823.
- Meltzner, A. J., Sieh, K., Abrams, M., Agnew, D. C., Hudnut, K. W., Avouac, J. P., Natawidjaja, D. H., 2006. *Uplift and subsidence associated with the great Aceh-Andaman earthquake of 2004*. *J. Geophys. Res-Sol. Ea.*, 111(B2).
- Merlivat, L. & Jouzel, J., 1979. *Global climatic interpretation of the deuterium-oxygen 18 relationship for precipitation*. *J. Geophys. Res. Ocean.*, 84, 5029–5033.
- Milillo, P., Giardina, G., DeJong, M., Perissin, D., Milillo, G., 2018. *Multi-temporal InSAR structural damage assessment: The London crossrail case study*. *Remote Sens-Basel*, 10(2), 287.
- Modoni G., Darini G., Spacagna R.L., Saroli M., Russo G., Croce P., 2013. *Spatial analysis of land subsidence induced by groundwater withdrawal*. *Eng Geol*, 167, 59–71.
- Naimi, B., Araújo, M.B., 2016. *sdm: a reproducible and extensible R platform for species distribution modelling*. *Ecography* 39, 368–375.
- Natekin, A., Knoll, A., 2013. *Gradient boosting machines, a tutorial*. *Front. Neurobot.* 7.
- Naughton, O., Johnston, P.M., & Gill, L.W., 2012. *Groundwater flooding in Irish karst: The hydrological characterization of ephemeral lakes (turloughs)*. *Journal of Hydrology* 470–471, 82–97
- Naughton, O., Johnston, P.M., McCormack, T., Gill, L.W., 2017. *Groundwater flood risk mapping and management: examples from a lowland karst catchment in Ireland: Groundwater flood risk mapping in lowland karst*. *J Flood Risk Management* 10, 53–64.
- Nelson, G.L., 1978. *Hydrologic information for land-use planning; Fairbanks vicinity, Alaska (Report No. 78-959)*, Open-File Report.
- Nord, A.G., Tronner, K., Mattsson, E., Borg, G.C., Ullén, I., 2005. *Environmental Threats to Buried Archaeological Remains*. *Ambio*, 34, 256–262.
- Notti D., Mateos R.M., Oriol M., Devanthery N., Peinado T., Roldán F.J., Fernández-Chacón F., Galve J.P., Lamas F., Azañón J.M., 2016. *Lithological control of land subsidence induced by groundwater withdrawal in new urban areas (Granada Basin, SE Spain) Multiband DInSAR monitoring*. *Hydrol. Processes*, 30, 2317-2331.

- Ogasawara, H., Fujimori, K., Koizumi, N., Hirano, N., Fujiwara, S., Otsuka, S., Nakao, S., Nishigami, K., Taniguchi, K., Iio, Y., Nishida, R., Oike, K., & Tanaka, Y., 2002. *Microseismicity Induced by Heavy Rainfall Around Flooded Vertical Ore Veins*. The Mechanism of Induced Seismicity, 91–109.
- Oliver M., Webster R., 1990. *Kriging: a method of interpolation for geographical information systems*. International Journal of Geographical Information Systems, 4, Issue 3, 313-332.
- Orsi G., Di Vito M., de Vita S., 1996. *The restless, resurgent Campi Flegrei Nested Caldera (Italy): constraints on its evolution and configuration*. J Volcanol Geotherm Res 74:179-214.
- Ortolani, F. & Aprile, F., 1985. *Principali caratteristiche stratigrafiche e strutturali dei depositi superficiali della Piana Campana*. Boll. Soc. Geol. It., 104, 195-206.
- Osmanoğlu, B., Dixon, T. H., Wdowinski, S., Cabral-Cano, E., Jiang, Y., 2011. *Mexico City subsidence observed with persistent scatterer InSAR*. Int. J. Appl. Earth Obs., 13(1), 1-12.
- Oyedele, K.F., Ayolabi, E.A., Adeoti, L., Adegbola, R.B., 2009. *Geophysical and hydrogeological evaluation of rising groundwater level in the coastal areas of Lagos, Nigeria*. Bull Eng Geol Environ 68, 137–143.
- Pastén-Zapata, E., Ledesma-Ruiz, R., Harter, T., Ramírez, A.I., Mahlknecht, J., 2014. *Assessment of sources and fate of nitrate in shallow groundwater of an agricultural area by using a multi-tracer approach*. Sci. Total Environ., 470–471, 855–864.
- Patacca, E., Sartori, R., Scandone, P., 1990. *Tyrrhenian basin and Apenninic arcs: Kinematic relations since Late Tortonian times*. Mem. Soc. Geol. It 45 (1990), 425–451.
- Pauwels, H., Gaus, I., le Nindre, Y.M., Pearce, J., Czernichowski-Lauriol, I., 2007. *Chemistry of fluids from a natural analogue for a geological CO₂ storage site (Montmiral, France): Lessons for CO₂–water–rock interaction assessment and monitoring*. Appl. Geochem., 22, 2817–2833.
- Peh, K.K., Lim, C.P., Quek, S.S., Khoh, K.H., 2000. *Use of Artificial Neural Networks to Predict Drug Dissolution Profiles and Evaluation of Network Performance Using Similarity Factor*. Pharm Res 17, 1384–1389.
- Perrone, G., Morelli, M., Piana, F., Fioraso, G., Nicolò, G., Mallen, L., Cadoppi, P., Balestro, G., Tallone, S., 2013. *Current tectonic activity and differential uplift along the Cottian Alps/Po Plain boundary (NW Italy) as derived by PS-InSAR data*. J. Geodyn., 66, 65-78.
- Petelet-Giraud, E., Négrel, P., Aunay, B., Ladouche, B., Bailly-Comte, V., Guerrot, C., Flehoc, C., Pezard, P., Lofi, J., Dörfliger, N., 2016. *Coastal groundwater salinization: Focus on the vertical variability in a multi-layered aquifer through a multi-isotope fingerprinting (Roussillon Basin, France)*. Sci. Total Environ., 566–567, 398–415.
- Peterson, A.T., Papeş, M., Soberón, J., 2008. *Rethinking receiver operating characteristic analysis applications in ecological niche modeling*. Ecological Modelling 213, 63–72.
- Pfahl, S. & Sodemann, H., 2014. *What controls deuterium excess in global precipitation?* Clim. Past **2014**, 10, 771–781.
- Phien-wej N., Giao P.H., Nutalaya P., 2006. *Land subsidence in Bangkok, Thailand*. Engineering Geology, 82, 187–201.
- Phillips, S.J., Anderson, R.P., Schapire, R.E., 2006. *Maximum entropy modeling of species geographic distributions*. Ecological Modelling 190, 231–259.
- Pijanowski, B.C., Brown, D.G., Shellito, B.A., Manik, G.A., 2002. *Using neural networks and GIS to forecast land use changes: a Land Transformation Model*. Computers, Environment and Urban Systems 26, 553–575.

- Pinault, J.-L., Amraoui, N., Golaz, C., 2005. *Groundwater-induced flooding in macropore-dominated hydrological system in the context of climate changes*. *Water Resources Research* 41.
- Plane, E., Hill, K., May, C., 2019. *A Rapid Assessment Method to Identify Potential Groundwater Flooding Hotspots as Sea Levels Rise in Coastal Cities*. *Water*, 2019, 11, 2228.
- Pollicino, L.C., Colombo, L., Alberti, L., Masetti, M., 2021. PCE point source apportionment using a GIS-based statistical technique combined with stochastic modelling. *Science of The Total Environment* 750, 142366.
- Pourghasemi, H.R., Yousefi, S., Kornejady, A., Cerdà, A., 2017. *Performance assessment of individual and ensemble data-mining techniques for gully erosion modeling*. *Science of The Total Environment* 609, 764–775.
- Pujades E., De Simone S., Carrera J., Vázquez-Suñé E., Jurado A., 2017. *Settlements around pumping wells: Analysis of influential factors and a simple calculation procedure*. *Journal of Hydrology*, 548, 225-236.
- Pujades, E., López, A., Carrera, J., Vázquez-Suñé, E., Jurado, A., 2012. *Barrier effect of underground structures on aquifers*. *Engineering Geology* 145–146, 41–49.
- R Core Team, 2020. *R: a language and environment for statistical computing*. R Foundation for Statistical Computing, Vienna, Austria. Available from: <https://www.R-project.org/>
- Raes, N. & Aguirre Gutierrez, J., 2018. *A Modeling Framework to Estimate and Project Species Distributions in Space and Time*. Wiley.
- Rahmati, O., Pourghasemi, H.R., Melesse, A.M., 2016. *Application of GIS-based data driven random forest and maximum entropy models for groundwater potential mapping: A case study at Mehran Region, Iran*. *CATENA* 137, 360–372.
- Renau-Pruñonosa, A., Morell, I., Pulido-Velazquez, D., 2016. *A Methodology to Analyse and Assess Pumping Management Strategies in Coastal Aquifers to Avoid Degradation Due to Seawater Intrusion Problems*. *Water Resour. Manag.*, 30.
- Richter, B.C. & Kreitler, C.W., 1993. *Geochemical Techniques for Identifying Sources of Ground-Water Salinization*; Smoley, C.K., Ed.; CRC press: Austin, Texas, USA.
- Robinson, R., 2000. *Mine gas hazards in the surface environment*. *Mining Technology*, 109(3), 228–236.
- Robinson, V.K, Solomon, J, Morris, S., 2001. *Groundwater Flooding in the Thames Region, winter 2000/01*. Environment Agency Report, Thames region, Reading.
- Rolandi, G., Bellucci, F., Heizler, M.T., Belkin, H.E., De Vivo, B., 2003. *Tectonic controls on the genesis of ignimbrites from the Campanian Volcanic Zone, southern Italy*. *Mineralogy and Petrology* 79, 3–31.
- Rolandi, G., Petrosino, P., Mc Geehin, J., 1998. *The interplinian activity at Somma–Vesuvius in the last 3500 years*. *Journal of Volcanology and Geothermal Research* 82, 19–52.
- Rosen, S., 1974. *Hedonic prices and implicit markets: product differentiation in pure competition*. *J. Polit. Econ.*, 82, 34-55.
- Rozanski, K., Araguas-Araguas, L., Gonfiantini, R., 1993. *Isotope patterns in modern global precipitation*. *Am. Geophys. Union Monogr.*, 78, 1–36.
- Rushton, K.R., Al-Othman, A.A.R., 1994. *Control of rising groundwater levels in Riyadh, Saudi Arabia*. In: *Groundwater Problems in Urban Areas*. Thomas Telford, London, pp. 299–309.
- Russak, A. & Sivan, O., 2010. *Hydrogeochemical Tool to Identify Salinization or Freshening of Coastal Aquifers Determined from Combined Field Work, Experiments, and Modeling*. *Environ. Sci. Technol.*, 44, 4096–4102.

- Sacchi, M., Molisso, F., Pacifico, A., Vigliotti, M., Sabbarese, C., Ruberti, D., 2014. *Late-Holocene to recent evolution of Lake Patria, South Italy: An example of a coastal lagoon within a Mediterranean delta system*. *Glob. Planet. Chang.*, 117, 9–27.
- Sajedi-Hosseini, F., Malekian, A., Choubin, B., Rahmati, O., Cipullo, S., Coulon, F., Pradhan, B., 2018. *A novel machine learning-based approach for the risk assessment of nitrate groundwater contamination*. *Science of The Total Environment* 644, 954–962.
- Salvati, L., 2014. *Population distribution and urban growth in Southern Italy, 1871–2011: emergent polycentrism or path-dependent monocentricity?* *Urban Geography* 35, 440–453.
- Santangelo, N., Romano, P., Ascione, A., Ermolli, E. R., 2017. *Quaternary evolution of the Southern Apennines coastal plains: a review*. *Geol. Carpath*, 68(1), 43–56.
- Schirmer, M., Leschik, S., Musolff, A., 2013. *Current research in urban hydrogeology – A review*. *Advances in Water Resources* 51 (2013) 280–291.
- Schneiderbauer, S., Ehrlich, D., 2006. *Risk, Hazard and People's Vulnerability to Natural Hazards: A Review of Definitions, Concepts and Data*. European Commission-Joint Research Centre (EC-JRC), Brussels.
- Schoff, S.L., Sayán, J.L.M., 1969. *Ground-water resources of the Lambayeque Valley, Department of Lambayeque, northern Peru*, Geological Survey Water-Supply Paper 1663-F. US Government Printing Office, Washington.
- Schwaninger, M., Groesser, S., 2020. *System Dynamics Modeling: Validation for Quality Assurance*. In: Dangerfield, B. (Ed.), *System Dynamics: Theory and Applications*, Encyclopedia of Complexity and Systems Science Series. Springer US, New York, NY, 119–138.
- Selim, S.A., Hamdan, A.M., Rady, A.A., 2014. *Groundwater rising as environmental problem, causes and solutions: case study from Aswan city, Upper Egypt*. *Open Journal of Geology* 4, 324–341.
- Sereni, E., 1997. *History of the Italian agricultural landscape*. Princeton University Press, 41 William Street, Princeton New Jersey 08540.
- Shabani, F., Kumar, L., Ahmadi, M., 2018. *Assessing Accuracy Methods of Species Distribution Models: AUC, Specificity, Sensitivity and the True Skill Statistic* 13.
- Shafizadeh-Moghadam, H., Valavi, R., Shahabi, H., Chapi, K., Shirzadi, A., 2018. *Novel forecasting approaches using combination of machine learning and statistical models for flood susceptibility mapping*. *Journal of Environmental Management* 217, 1–11.
- Shamsudduha, M., Chandler, R.E., Taylor, R.G., Ahmed, K.M., 2009. *Recent trends in groundwater levels in a highly seasonal hydrological system: the Ganges-Brahmaputra-Meghna Delta*. *Hydrol Earth Syst Sc* 13, 2373–2385.
- Shaw, W.D., 2016. *Environmental and Natural Resource Economics Decisions Under Risk and Uncertainty: A Survey*. *Int. Rev. Environ. Resour. Econ.*, 9 (1–2), 1–130.
- Shirzadi, A., Solaimani, K., Roshan, M.H., Kaviani, A., Chapi, K., Shahabi, H., Keesstra, S., Ahmad, B.B., Bui, D.T., 2019. *Uncertainties of prediction accuracy in shallow landslide modeling: Sample size and raster resolution*. *CATENA* 178, 172–188.
- Silva, S.R., Kendall, C., Wilkison, D.H., Ziegler, A.C., Chang, C.C.Y., Avanzino, R.J., 2000. *A new method for collection of nitrate from fresh water and the analysis of nitrogen and oxygen isotope ratios*. *J. Hydrol.*, 228, 22–36.

- Singh, A., Krause, P., Panda, S.N., Flugel, W.A., 2010. *Rising water table: A threat to sustainable agriculture in an irrigated semi-arid region of Haryana, India*. *Agricultural Water Management* 97, 1443–1451.
- Sommer, T., Karpf, C., Ettrich, N., Haase, D., Weichel, T., Peetz, J.-V., Steckel, B., Eulitz, K., Ullrich, K., 2009. *Coupled modelling of subsurface water flux for an integrated flood risk management*. *Nat. Hazards Earth Syst. Sci.* 9, 1277–1290.
- Somodi, I., Lepesi, N., Botta-Dukát, Z., 2017. *Prevalence dependence in model goodness measures with special emphasis on true skill statistics*. *Ecology and Evolution* 7, 863–872.
- Soren, J., 1976. *Basement flooding and foundation damage from water table rise in the East New York section of Brooklyn*. USGS Water-Resources Investigation, Long Island 76–95.
- Stellato, L., 2010. *Isotopic Methodologies: A Valuable Tool to Study Stream Water-Groundwater Interactions*. In: *Horizons in Earth Science Research*; Veress, B., Szigethy, J., Eds.; Nova Science Publishers: New York, NY, USA; Volume 1, pp. 239–260.
- Stellato, L., Coda, S., Arienzo, M., De Vita, P., Di Rienzo, B., D’Onofrio, A., Ferrara, L., Marzaioli, F., Trifuoggi, M., Allocca, V., 2020. *Natural and Anthropogenic Groundwater Contamination in a Coastal Volcanic-Sedimentary Aquifer: The Case of the Archaeological Site of Cumae (Phlegraean Fields, Southern Italy)*. *Water* 12, 3463.
- Stellato, L., Petrella, E., Terrasi, F., Belloni, P., Belli, M., Sansone, U., Celico, F., 2008. *Some limitations in using ^{222}Rn to assess river-groundwater interactions: The case of Castel di Sangro alluvial plain (central Italy)*. *Hydrogeol. J.*, 16, 701–712.
- Stellato, L., Terrasi, F., Marzaioli, F., Belli, M., Sansone, U., Celico, F., 2013. *Is ^{222}Rn a suitable tracer of stream-groundwater interactions? A case study in central Italy*. *Appl. Geochem.*, 32, 108–117.
- Stipho, A.S., 1993. *The Impact of Rising Ground Water Level on the Geotechnical Behavior of Soil in Hot Climate Regions*. *International Conference on Case Histories in Geotechnical Engineering* 11.
- Stocchi, P., Spada, G., 2009. *Influence of glacial isostatic adjustment upon current sea level variations in the Mediterranean*. *Tectonophysics* 474, 56–68.
- Stockwell, D.R.B., Peterson, A.T., 2002. *Effects of sample size on accuracy of species distribution models*. *Ecological Modelling* 148, 1–13.
- Strozzi, T. & Wegmuller, U., 1999. *Land subsidence in Mexico City mapped by ERS differential SAR interferometry*. In: *IEEE 1999 Int. Geosci. Remote Se. IGARSS’99 (Cat. No. 99CH36293)*; Volume 4, pp. 1940–1942.
- Swets, J.A., 1988. *Measuring the accuracy of diagnostic systems*. *Science* 240, 1285–1293.
- Szostak-Chrzanowski A., Chrzanowski A., 2014. *Study of natural and man-induced ground deformation in Machezie Delta Region*. *Acta Geodyn. Geomater.*, 11, No.2 (174), 117–123.
- Teatini P., Ferronato M., Gambolati G., Bertoni W., Gonella M., 2005. *A century of land subsidence in Ravenna, Italy*. *Environmental Geology* 47, 831–846.
- Teatini P., Gambolati G., Ferronato M., Settari A., Walters D., 2011. *Land uplift due to subsurface fluid injection*. *Journal of Geodynamics*, 51, Issue 1, 1–16.
- Terada T., 1929. *On the form of volcanoes*. *Bull. Earthq. Res. Inst., Univ. Tokyo*, 7, 207–221.
- Terranova C., Ventura G., [Vilardo G.](#), 2015. *Multiple causes of ground deformation in the Napoli metropolitan area (Italy) from integrated Persistent Scatterers DinSAR , geological, hydrological, and urban infrastructure data*. [Earth-Science Reviews](#), 146, 105–119.

- Tessitore S., Fernández-Merodo J. A., Herrera G., Tomás R., Ramondini M., Sanabria M., Duro J., Mulas J., Calcaterra D., 2015. [*Regional subsidence modelling in Murcia city \(SE Spain\) using 1-D vertical finite element analysis and 2-D interpolation of ground surface displacements*](#). Proc. IAHS, 372, 425-429.
- Tessitore S., Fernández-Merodo J.A., Herrera G., Tomás R., Ramondini M., Sanabria M., Duro J., Mulas J., Calcaterra D., 2016. *Comparison of water-level, extensometric, DInSAR and simulation data for quantification of subsidence in Murcia (SE Spain)*. Hydrogeol. J., 24, 727-747.
- Thibaud, E., Petitpierre, B., Broennimann, O., Davison, A.C., Guisan, A., 2014. *Measuring the relative effect of factors affecting species distribution model predictions*. Methods in Ecology and Evolution 5, 947-955.
- Thuiller, W., Georges, D., Engler, R., Breiner, F., 2016. Biomod2: ensemble platform for species distribution modeling.
- Thuiller, W., Lafourcade, B., Engler, R., Araújo, M.B., 2009. BIOMOD – a platform for ensemble forecasting of species distributions. Ecography 32, 369-373.
- Thyne, G.D., Gillespie, J.M., Ostidick, J.R., 1999. *Evidence for interbasin flow through bedrock in the southeastern Sierra Nevada*. GSA Bull., 111, 1600-1616.
- Todesco, M., Costa, A., Comastri, A., Colleoni, F., Spada, G., Quarenì, F., 2014. *Vertical ground displacement at Campi Flegrei (Italy) in the fifth century: Rapid subsidence driven by pore pressure drop*. Geophysical Research Letters 41, 1471-1478.
- Tomás R., Herrera G., Cooksley G., Mulas J., 2011. *Persistent Scatterer Interferometry subsidence data exploitation using spatial tools: the Vega Media of the Segura River Basin case study*. J. Hydrol., 400, 411-428.
- Tomás, R., Herrera, G., Delgado, J., Lopez-Sanchez, J. M., Mallorquí, J. J., Mulas, J., 2010. *A ground subsidence study based on DInSAR data: Calibration of soil parameters and subsidence prediction in Murcia City (Spain)*. Eng. Geol., 111(1-4), 19-30.
- Tomás R., Romero R., Mulas J., Marturià J.J., Mallorquí J.J., López-Sánchez J.M., Blanco P., 2014. *Radar interferometry techniques for the study of ground subsidence phenomena: a review of practical issues through cases in Spain Environ. Earth Sci.*, 71, 163-181.
- Torrente, M.M., Milia, A., Bellucci, F., Rolandi, G., 2010. *Extensional tectonics in the Campania Volcanic Zone (eastern Tyrrhenian Sea, Italy): new insights into the relationship between faulting and ignimbrite eruptions*. Italian Journal of Geosciences 129, 2, 297-315.
- Townsend Peterson, A., Cohoon, K.P., 1999. *Sensitivity of distributional prediction algorithms to geographic data completeness*. Ecological Modelling 117, 159-164.
- Tricker, A.R. & Preussmann, R., 1991. *Carcinogenic N-nitrosamines in the diet: Occurrence, formation, mechanisms and carcinogenic potential*. Mutat. Res. Genet. Toxicol., 259, 277-289
- Tsur, Y., Zemel, A., 2004. *Endangered aquifers: Groundwater management under threats of catastrophic events*. Water Resour. Res., 40 (6), W06S20.
- Tsur, Y., Zemel, A., 2014. *Dynamic and Stochastic Analysis of Environmental and Natural Resources*. In : Fischer, M.M., Nijkamp, P. (Eds.), Handbook of Regional Science, Springer, Berlin, Heidelberg, 929-949.
- Tufano, R., Allocca, V., Coda, S., Cusano, D., Fusco, F., Nicodemo, F., Pizzolante, A., De Vita, P., 2020. *Groundwater vulnerability of principal aquifers of the Campania region (southern Italy)*. J. Maps, 16, 565-576.
- U.S. Environmental Protection Agency, 1978. Radon in Water Sampling Program; EPA/EERF Manual 78-1; U.S. Environmental Protection Agency: Washington, DC, USA; p. 11.

- Unsal, B., Yagbasan, O., Yazicigil, H., 2014. *Assessing the impacts of climate change on sustainable management of coastal aquifers*. Environ. Earth Sci., 72, 2183–2193.
- Upton, K.A., Jackson, C.R., 2011. *Simulation of the spatio-temporal extent of groundwater flooding using statistical methods of hydrograph classification and lumped parameter models*. Hydrological Processes 25, 1949–1963.
- Van De Noort, R., Chapman, H.P., Cheetham, J.L., 2001. *In situ preservation as a dynamic process: The example of Sutton Common, UK*. Antiquity, 75, 94–100.
- Van der Noort, R., 1996. *Assessment and management of sites in wetland landscapes: Four case studies from the Humber wetlands*. In: Preserving Archaeological Remains in Situ; Corfield, M., Hinton, P., Nixon, T., Pollard, M., Eds.; Museum of London Archaeology Service: London, UK; pp. 133–143.
- van Westen, C.J., Castellanos, E., Kuriakose, S.L., 2008. *Spatial data for landslide susceptibility, hazard, and vulnerability assessment: An overview*. Engineering Geology, Landslide Susceptibility, Hazard and Risk Zoning for Land Use Planning 102, 112–131.
- Vázquez-Suñé, E., Sánchez-Vila, X., Carrera, J., Marizza, M., Arandes, R., Gutierrez, L.A., Chilton, J., 1997. *Rising groundwater levels in Barcelona: evolution and effects on urban structures*. In: John Chilton et al. (Eds.), Groundwater in the Urban Environment: Problems, Processes and Management. Balkema, Rotterdam, Brookfield, 267-271.
- Vázquez-Suñé, E., Sánchez-Vila, X., Carrera, J., 2005. *Introductory review of specific factors influencing urban groundwater, an emerging branch of hydrogeology, with reference to Barcelona, Spain*. Hydrogeol J 13, 522–533.
- Vekerdy Z., & Meijerink A.M.J., 1998. *Statistical and analytical study of the propagation of flood-induced groundwater rise in an alluvial aquifer*. J Hydrol, 205, (1–2), 112–125.
- Vengosh, A., 2003. *Salinization and Saline Environments*. In: Treatise on Geochemistry; Holland, H.D., Turekian, K.K., Eds.; Pergamon: Oxford, UK; pp. 1–35.
- Vengosh, A., Heumann, K.G., Juraske, S., Kasher, R., 1994. *Boron Isotope Application for Tracing Sources of Contamination in Groundwater*. Environ. Sci. Technol., 28, 1968–1974.
- Vengosh, A., Spivack, A.J., Artzi, Y., Ayalon, A., 1999. *Geochemical and boron, strontium, and oxygen isotopic constraints on the origin of the salinity in groundwater from the Mediterranean Coast of Israel*. Water Resour. Res., 35, 1877–1894.
- Vilardo G., Ventura G., Terranova C., Matano F., Nardò S., 2009. *Ground deformation due to tectonic, hydrothermal, gravity, hydrogeological, and anthropic processes in the Campania Region (Southern Italy) from Permanent Scatterers Synthetic Aperture Radar Interferometry*. Remote Sensing of Environment, 113, 197–212.
- Vink, A., Steffen, H., Reinhardt, L., Kaufmann, G., 2007. *Holocene relative sea-level change, isostatic subsidence and the radial viscosity structure of the mantle of northwest Europe (Belgium, the Netherlands, Germany, southern North Sea)*. Quaternary Science Reviews 26, 3249–3275.
- Viparelli, M., 1978. *Le acque sotterranee ad oriente di Napoli*. Fondazione Politecnica per il Mezzogiorno d'Italia, Napoli, 111, 1-48, Napoli.
- Waltham T. 2002. *Sinking cities - Feature*. Geology Today, 18(3), 95-100.
- Werner, A.D., Bakker, M., Post, V.E.A., Vandenbohede, A., Lu, C., Ataie-Ashtiani, B., Simmons, C.T., Barry, D.A., 2013. *Seawater intrusion processes, investigation and management: Recent advances and future challenges*. Adv. Water Resour., 51, 3–26.

- Wett, B., Jarosch, H., Ingerle, K., 2002. *Flood induced infiltration affecting a bank filtrate well at the River Enns, Austria*. Journal of Hydrology, Attenuation of Groundwater Pollution by Bank Filtration 266, 222–234.
- Whitesides, D.V., Faust, R.J., Zettwoch, D.D., 1983. Problems of rising ground-water levels in urban areas with special reference to the Louisville, Kentucky area. US Geological Survey, Water Resources Investigations Report 83-4233, Louisville, Kentucky 1983.
- Wilkinson, W.B., 1985. *Rising groundwater levels in London and possible effects on engineering structures*. Hydrogeology in the Service of Man. Mémoires of the 18th Congress of the International Association of Hydrogeologists, Cambridge, 145–157, 1985
- Wilkinson, W.B., 1994. Groundwater Problems in Urban Areas. Proceedings of the International Conference organised by the Institution of Civil Engineers and held in London, 2–3 June 1993. Thomas Telford, London.
- Widory, D., Kloppmann, W., Chery, L., Bonnin, J., Rochdi, H., Guinamant, J.-L., 2004. *Nitrate in groundwater: An isotopic multi-tracer approach*. J. Contam. Hydrol., 72, 165–188.
- Wisz, M.S., Hijmans, R.J., Li, J., Peterson, A.T., Graham, C.H., Guisan, A., 2008. *Effects of sample size on the performance of species distribution models*. Diversity and Distributions 14, 763–773.
- Wood, W.W. & Sanford, W.E., 1995. *Chemical and isotopic methods for quantifying ground-water recharge in a regional, semiarid environment*. Ground Water, 33, 458–469.
- Wu, S.-F., You, C.-F., Lin, Y.-P., Valsami-Jones, E., Baltatzis, E., 2016. *New boron isotopic evidence for sedimentary and magmatic fluid influence in the shallow hydrothermal vent system of Milos Island (Aegean Sea, Greece)*. J. Volcanol. Geotherm. Res., 310.
- Xue, D., Botte, J., De Baets, B., Accoe, F., Nestler, A., Taylor, P., Van Cleemput, O., Berglund, M., Boeckx, P., 2009. *Present limitations and future prospects of stable isotope methods for nitrate source identification in surface- and groundwater*. Water Res., 43, 1159–1170.
- Yang, J., Cao, G., Han, D., Yuan, H., Hu, Y., Shi, P., Chen, Y., 2019. *Deformation of the aquifer system under groundwater level fluctuations and its implication for land subsidence control in the Tianjin coastal region*. Environ Monit Assess (2019) 191: 162.
- Yasuhara, K., Murakami, S., Mimura, N., Komine, H., & Recio, J., 2007. *Influence of global warming on coastal infrastructural instability*. Sustainability Science, 2, 13–25.
- Ying-Kai, X., Bu-Yong, L., Wei-Guo, L., Yun, X., H, S.G., 2003. *Ion Exchange Extraction of Boron from Aqueous Fluids by Amber-lite IRA 743 Resin*. Chin. J. Chem., 21, 1073–1079.
- Yesilnacar, E., Topal, T., 2005. *Landslide susceptibility mapping: A comparison of logistic regression and neural networks methods in a medium scale study, Hendek region (Turkey)*. Engineering Geology 79, 251–266.
- Yu, M.-H., Jefferson, I., Culshaw, M., 2006. Geohazards caused by rising groundwater in the Durham Coalfield, UK. IAEG2006 Paper number 367, The Geological Society of London 2006.
- Yu, X., Moraetis, D., Nikolaidis, N.P., Li, B., Duffy, C., Liu, B., 2019. *A coupled surface-subsurface hydrologic model to assess groundwater flood risk spatially and temporally*. Environmental Modelling & Software 114, 129–139.
- Zeni, G., Bonano, M., Casu, F., Manunta, M., Manzo, M., Marsella, M., Pepe, A., Lanari, R., 2011. *Long-term deformation analysis of historical buildings through the advanced SBAS-DInSAR technique: The case study of the city of Rome, Italy*. J. Geophys. Eng., 8(3), S1-S12.

- Zepeda Quintana, D.S., Loeza Rentería, C.M., Munguía Vega, N.E., Peralta, J.E., Velazquez Contreras, L.E., 2018. *Sustainability strategies for coastal aquifers: A case study of the Hermosillo Coast aquifer*. J. Clean. Prod., 195, 1170–1182.
- Zhang, Q., Wang, H., Wang, L., 2018. *Tracing nitrate pollution sources and transformations in the over-exploited groundwater region of north China using stable isotopes*. J. Contam. Hydrol., 218, 1–9.
- Zhang Y., Wu¹ J., Xue¹ Y., Wang Z., Yao¹ Y., Yan X., Wang H., 2015. *Land subsidence and uplift due to long-term groundwater extraction and artificial recharge in Shanghai, China*. Hydrogeology Journal, 23, 1851–1866.
- Zhao, Q., Su, X., Kang, B., Zhang, Y., Wu, X., Liu, M., 2017. *A hydrogeochemistry and multi-isotope (Sr, O, H, and C) study of groundwater salinity origin and hydrogeochemical processes in the shallow confined aquifer of northern Yangtze River downstream coastal plain, China*. Appl. Geochem., 86, 49–58.
- Zhou, Y., Wang, L., Zhou, Y., Mao, X., 2020. *Eutrophication control strategies for highly anthropogenic influenced coastal waters*. Sci. Total Environ., 705, 135760.
- Zurada, J.M., 1992. *Introduction to artificial neural network systems* West Publishing Company 58.